Study and design of reconfigurable antennas using plasma medium

Mohd Taufik Jusoh Tajudin

THÈSE / UNIVERSITÉ DE RENNES 1
sous le sceau de l'Université Européenne de Bretagne

pour le grade de

DOCTEUR DE L'UNIVERSITÉ DE RENNES 1

Mention : Traitement du Signal et Télécommunications

Ecole doctorale MATISSE

présentée par

Mohd Taufik JUSOH TAJUDIN

préparée à l'unité de recherche I.E.T.R – UMR 6164
Institut d'Electronique et de Télécommunications de Rennes
Université de Rennes 1

Study and Design of Reconfigurable Antennas Using Plasma Medium

**Thèse soutenue à Rennes
le 04 avril 2014**

devant le jury composé de :

Mme. Paola RUSSO
Professeur, Università Politecnica delle Marche, Ancona, Italy / *rapporteur*

M. Olivier PASCAL
Professeur, Université de Toulouse, Toulouse, France / *rapporteur*

M. Christian PERSON
Professeur, Institut Telecom/Télécom Bretagne, Rennes, France / e*xaminateur*

M. Philippe POULIGUEN
HDR, Ingénieur DGA-MI, Bruz, France / e*xaminateur*

M. Olivier LAFOND
Maitre de Conférences HDR, IETR, Université de Rennes 1, Rennes, France / *co-directeur de thèse*

M. Franck COLOMBEL
Maitre de Conférences HDR, IETR, Université de Rennes 1, Rennes, France / *co-directeur de thèse*

M. Mohamed HIMDI
Professeur, IETR, Université de Rennes 1, Rennes, France / *directeur de thèse*

Acknowlegement

........specially dedicated to my beloved wife, Dr Fariha Hanim, our gifted sons, Abdullah Aqil, Fawwaz Zaki and to my honorable family

Résumé en français

Table des matières

1.0   Introduction

Le plasma est le 4ème état de la matière qui est naturellement disponible. Le plasma diffère des métamatériaux qui ont une permittivité et une perméabilité négative. En effet, le plasma conserve une perméabilité positive alors que sa perméabilité est négative. C'est la principale caractéristique du plasma qui présente un intérêt pour la conception des antennes. De manière générale, le plasma se comporte comme un matériau conducteur et cette caractéristique peut disparaître lorsque le plasma n'est plus excité. Ce caractère reconfigurable du plasma est utilisé dans ces travaux pour la conception d'antennes. La caractéristique conducteur/non-conducteur du plasma est contrôlée électriquement et le plasma est utilisé soit comme un élément rayonnant, soit comme un réflecteur ou bien comme un absorbant. Dans certains cas, le plasma peut alors remplacer avantageusement des matériaux métalliques.

La notion de plasma a été introduite en physique au début des années 20. Dans un premier temps, le plasma a été utilisé comme un élément rayonnant pour transmettre des signaux électromagnétiques. En 1919, le concept d'antenne plasma a été breveté par J. Hettinger. Les développements significatifs des plasmas ont démarré dans les années 60 lorsque ces derniers ont été introduits dans des systèmes de communication.

2.0   Modélisation du plasma

L'une des principales tâches de ces travaux concerne la caractérisation du plasma. Si la fréquence plasma et la fréquence de collision peuvent être estimées alors différentes zones de fonctionnement des antennes plasmas peuvent être identifiées. Dans ces travaux, le modèle du plasma a été défini en ce basant sur des mesures. La première mesure permet de déterminer la fréquence du plasma et la deuxième permet d'évaluer la fréquence de collision.

Pour déterminer ces caractéristiques, nous avons utilisé le dispositif suivant : Nous avons placé entre deux cornets suffisamment éloignés l'un de l'autre, d'une part un mur de plasma réalisé à l'aide de tubes néon et d'autre part une feuille de métal. On note que la feuille de métal est soit pleine, soit munie de fentes représentant l'espacement présent entre deux tubes néon adjacents (figure 1).

(a)   *(b)*
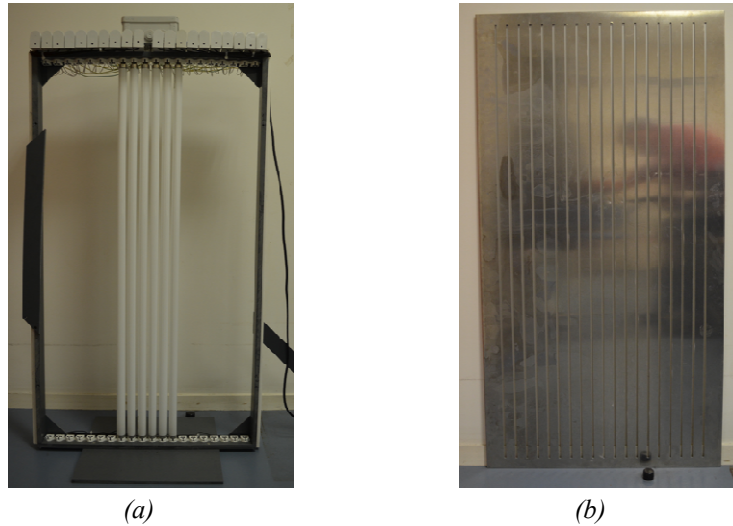
Figure 1 – Photographie du mur de plasma (a) Plasma réalisé à l'aide de 6 lampes fluorescentes en parallèles (la mesure a été faite avec 20 lampes fluorescentes) et le mur métallique (b) muni de fentes.

La figure 2 montre le dispositif de caractérisation du plasma. La mesure du coefficient de transmission entre les deux cornets a été effectuée dans cinq cas :

- En espace libre (pas d'obstacle situé entre les cornets).
- Avec un mur métallique plein entre les deux cornets.
- Avec un mur métallique muni de fentes entre les deux cornets.
- Avec un mur de tubes fluorescents (plasma) excités entre les deux cornets.
- Avec un mur de tubes fluorescents (plasma) non-excités entre les deux cornets.

La mesure a commencé avec aucun obstacle situé entre les deux cornets. Ceci sert de référence. Dans les autres cas, un des obstacles décrits précédemment est disposé entre les deux cornets. La mesure du coefficient de transmission permet de comprendre les caractéristiques du plasma.
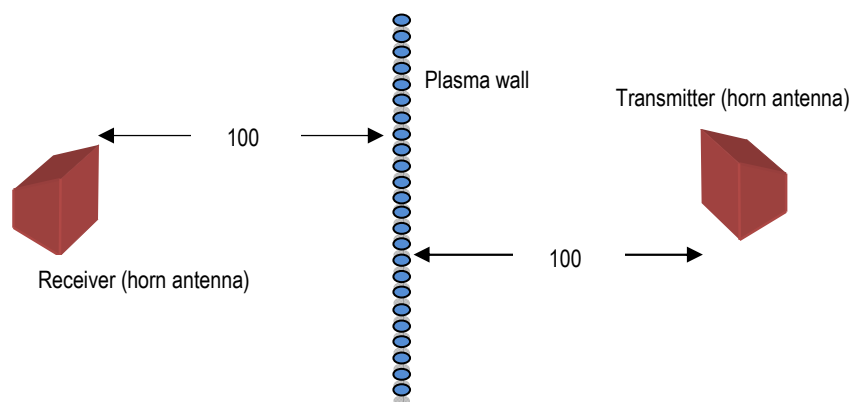
Figure 2 – Dispositif de mesure avec un mur de tubes fluorescents disposé entre deux cornets. La distance entre les deux cornets est de 100 cm.

Les résultats expérimentaux sont décrits sur la figure 3. Sur la figure 3a, on remarque qu'en dessous de 8 GHz, le coefficient de transmission est similaire lorsque qu'il n'y a pas d'obstacle (espace libre) ou lorsque l'on place un mur de tubes fluorescents non-excités. On estime que la propagation des ondes est atténuée à partir de 7 GHz lorsque le mur de tubes fluorescents est excité (figure 3b). On en déduit que le plasma passe alors d'un état non conducteur à un état conducteur. Ce travail se focalise en dessous de cette fréquence caractéristique, où le plasma possède alors une permittivité négative et se comporte comme un métal avec une conductivité faible.
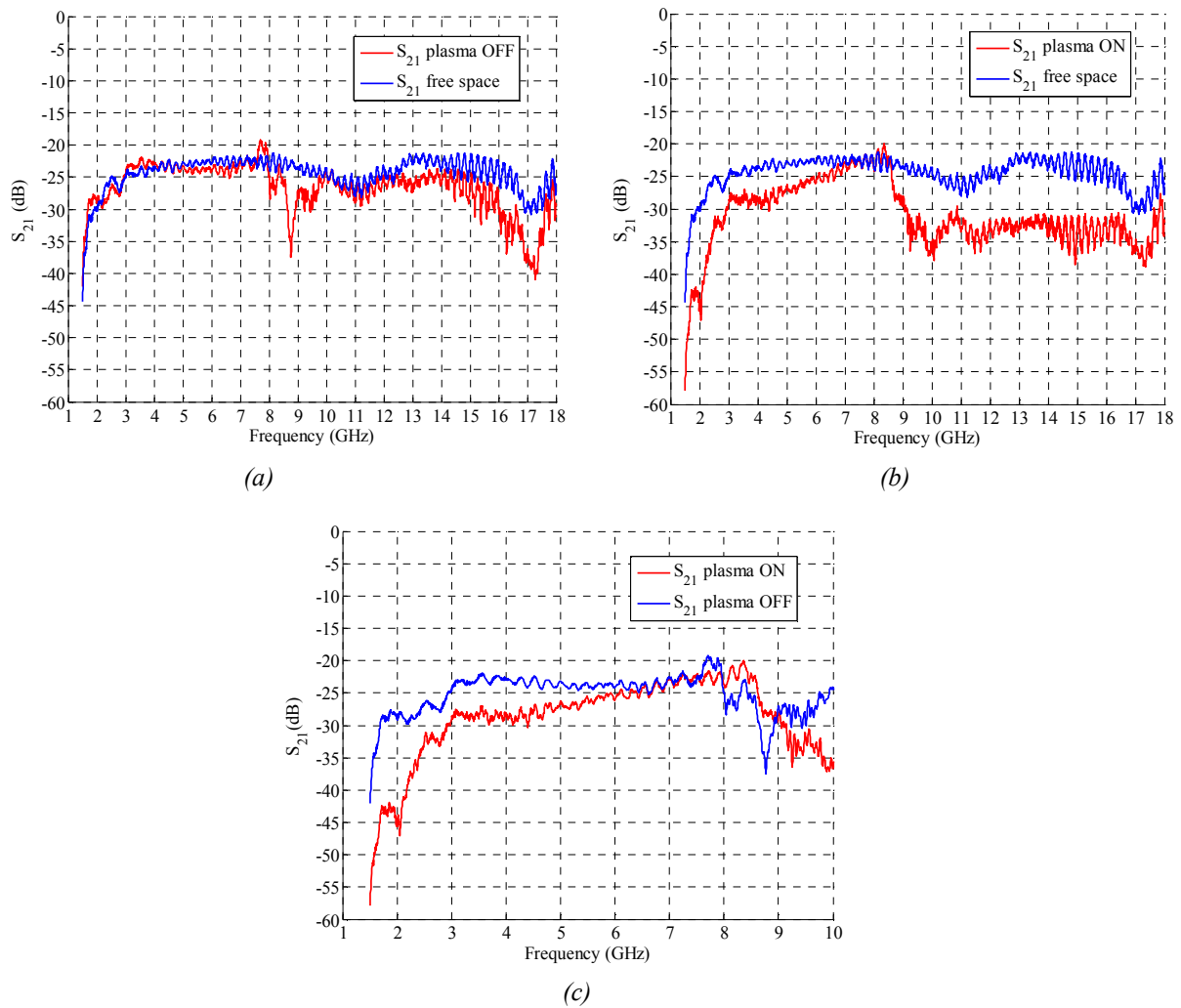
Figure 3 – Coefficients de transmission mesurés. (a) mur de tubes fluorescents non excités (Plasma OFF) et espace libre, (b) mur de tubes fluorescents excités (Plasma ON) et espace libre, (c) mur de tubes fluorescents excités (Plasma ON) et mur de tubes fluorescents non excités (Plasma OFF).

La figure 3c montre les résultats du coefficient de transmission sur une bande plus étroite lorsque le mur de tubes fluorescents est excité ou non excité. Ceci permet de représenter les états ON et OFF du plasma. Entre 2 et 2,5 GHz, la différence entre ces deux états varie entre 8 et 15 dB avec un maximum à 2 GHz. En se référant à cette

dernière mesure, on déduit que la fréquence du plasma se situe entre 7 et 9 GHz. Pour la suite du travail, on prendra 7 GHz.

En se basant sur cette fréquence plasma, une étude paramétrique sur la fréquence de collision du plasma est conduite sous CST entre 0,1 et 3 GHz. Les résultats simulés ont été comparés aux résultats expérimentaux et ont permis de conclure que la fréquence de collision du plasma considéré (tubes fluorescents) est de 900 MHz.

3.0   Réflecteur d'antenne reconfigurable

Dans ce travail, deux types d'antennes munies de réflecteurs réalisés avec des tubes fluorescents (Plasma) ont été étudiées :

- Antenne à réflecteur circulaire (RRA)
- Antenne à réflecteur triangulaire (CRA)

Ces antennes fonctionnant à 2,4 GHz ont toutes été conçues, simulées, réalisées et mesurées.

a. Antenne à réflecteur circulaire

Sur la figure 4, on montre une antenne à réflecteur circulaire (RRA). L'antenne est constituée d'un monopole métallique résonnant à 2,4 GHz situé au centre d'un réflecteur circulaire réalisé à l'aide de 15 tubes fluorescents (CFLs). Les performances de cette antenne ont été mesurées et ont montrés qu'il était possible de former le diagramme de rayonnement de l'antenne en excitant ou non une partie des tubes fluorescents. On note également que l'accord entre la théorie et la mesure est satisfaisant.

(a)   *(b)*

(c)   *(d)*

Figure 4 – Antenne à réflecteur circulaire (RRA). (a) 15 CFLs avec un plan de masse de 300 mm de coté, (b) Switches et ballasts permettant la commande des tubes fluorescents, (c) dispositif de commande, (d) Antenne à réflecteur circulaire (RRA) avec un quart des tubes fluorescents excités.

Une telle antenne permet de réaliser un nombre important de configurations de réflecteur en excitant ou non une partie des tubes fluorescents. Dans ce travail, trois configurations ont été testées en excitant 7, 9 ou 11 tubes fluorescents. Dans le cas où 9 tubes sont excités à 2,4 GHz, l'ouverture mesurée du diagramme de rayonnement dans le plan H est de 52° et le gain mesuré est de 9 dBi. Dans la littérature, on trouve des résultats obtenus à 2,8 GHz pour un réseau similaire réalisé avec des tubes métalliques analogues à ceux trouvés pour un réflecteur fait avec des tubes fluorescents (Plasma).

La mesure montre également la capacité d'une telle antenne à balayer son diagramme de rayonnement sur 360° d'azimut. Le pas de balayage du diagramme horizontal peut être diminué en utilisant des tubes fluorescents de plus faible rayon.

b.   Antenne à réflecteur triangulaire

Au cours de ces travaux, un autre type d'antenne à réflecteur a été étudié. Il s'agit d'une antenne à plan réflecteur triangulaire (figure 5a) appelée CRA.

(a)   *(b)*

Figure 5 – Antenne CRA. (a) plan de masse 500 mm x 500 mm. (b) antenne à réflecteur triangulaire réalisée avec deux arrangements de tubes fluorescents (24 éléments). Un monopole métallique résonant à 2,4 GHz est placé au cœur du dispositif.

L'antenne présentée sur la figure 5a été simulée et optimisée à 2,4 GHz. L'influence de l'arrangement des tubes fluorescents disposés en V sur le diagramme de rayonnement a été étudiée.

Pour l'antenne constituée d'un réflecteur en V à une seule rangée (CRA1), le gain mesuré est de 10,9 dBi et le gain simulé est de 11,8 dBi. On peut comparer ce gain à celui obtenu par l'antenne constituée du monopole et des tubes fluorescents non excités. Dans ce cas, le gain est logiquement voisin de celui d'un monopole puisqu'il vaut 5,4 dBi.

4.0   Antenna plasma

Toujours en utilisant les tubes fluorescents (CFLs), ces travaux se sont également intéressés aux antennes plasma. Dans ce contexte, deux antennes plasma ont été réalisées et leurs performances radioélectriques ont été évaluées à 450 et 900 MHz.

Les prototypes ont été fabriqués avec un tube fluorescent (CFLs) couplé électromagnétiquement avec une boucle réalisée en métal. Ceci permet de transférer le signal du connecteur de l'antenne vers le tube fluorescent (plasma). Le dispositif est présenté sur la figure 6.

(a)
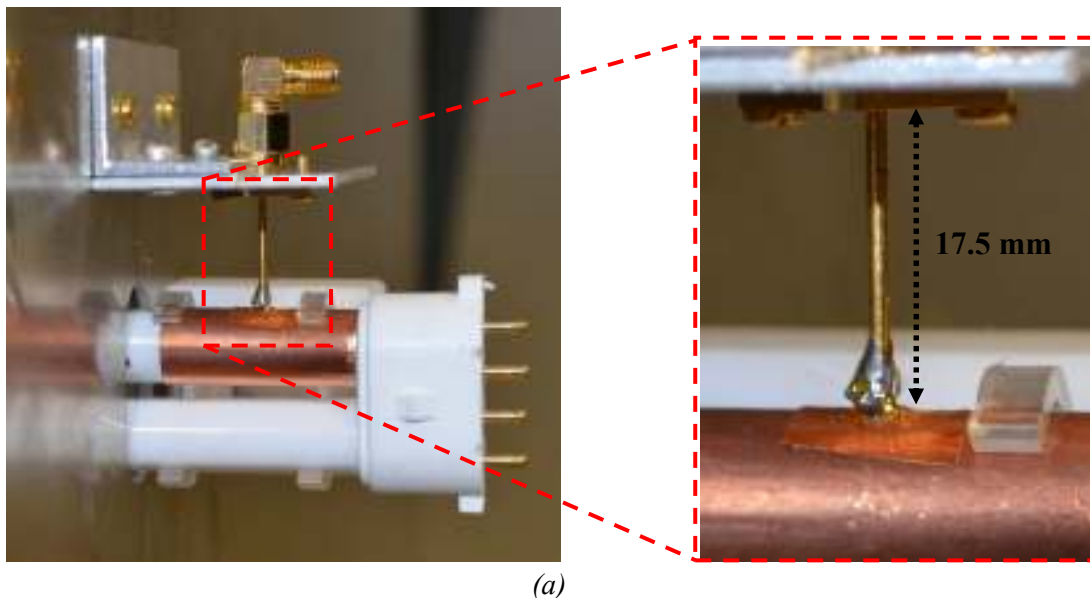
(b)

Figure 6 – Photographies des parties basses de l'antenne plasma fabriquée. (a) Antenne plasma avec $H_{rayonnante}$ = 77 mm. Une tige en cuivre de longueur 17,5 mm relie le connetceur SMA à la boucle métallique. (b) Antenne plasma avec $H_{rayonnante}$ = 35,7 mm.

Sur la figure 7 sont présentées plusieurs photographies de l'antenne plasma lors des mesures dans la base compacte SATIMO. L'antenne est alors placée sur un support (figure 7a). La figure 7b montre l'antenne lorsque le plasma est ionisé (allumé).

(a)

(b)

Figure 7 – Photo de l'antenne plasma dans la base compacte SATIMO ($H_{rayonnante}$ = 77 mm). (a) L'antenne est éteinte (plasma non ionisé). (b) L'antenne est allumée –plasma ionisé)

Sur la base des mesures effectuées durant ces travaux, il est possible de conclure que les tubes fluorescents peuvent être utilisés comme éléments rayonnants. Desantennes plasma avec des hauteurs rayonnantes différentes ont été fabriquées et mesurées à 900 et 450 MHz. A 900 MHz, les deux antennes présentent des diagrammes différents entre les états éteints et allumés, ce qui démontre bien le fonctionnement. A l'inverse, à 450 MHz, seul le tube fluorescent avec la plus petite longueur rayonnante présente un meilleur rayonnement lorsqu'il est allumé. Ceci peut s'expliquer par la très faible distance qu'il existe entre l'alimentation AC du tube et la partie de couplage électromagnétique ce qui induit des perturbations dans le fonctionnement.

Un rayonnement arrière important a été mesuré à 900 MHz pour ces antennes plasma en dépit de la présence d'un plan réflecteur. Ce rayonnement parasite est dû

vraisemblablement à la partie alimentation de l'antenne, ce rayonnement arrière étant beaucoup plus atténué (-15 dB) à 450 MHz quand le tube est éteint.

5.0 Surface Equivalente Radar des antennes plasma reconfigurables

Des simulations (CST Microwave Studio) de la SER de l'antenne à réflecteur circulaire (RRA) ont été effectuées pour deux configurations avec respectivement 7 et 9 tubes fluorescents excités (Chapitre 3). A cet effet, le réflecteur est illuminé par une onde plane selon l'axe x comme montré sur la figure 8.
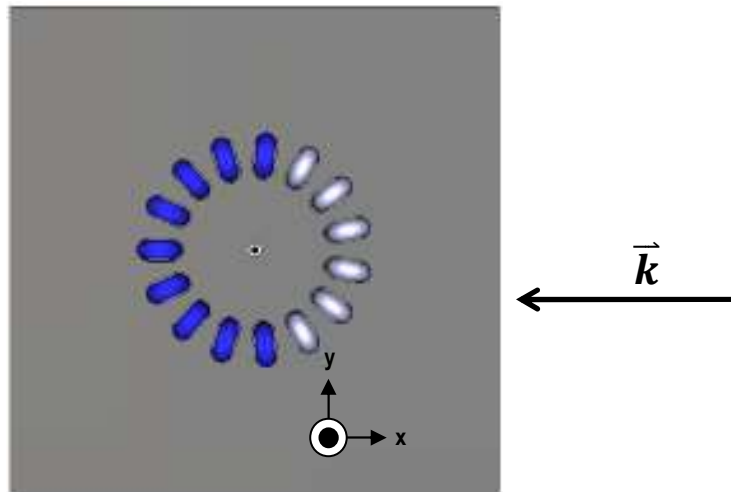
Figure 8 – La simulation de la SER du réflecteur circulaire avec 9 tubes actifs. L'illumination se fait par une onde plane selon l'axe x et polarisée selon l'axe z. (En bleu sont représentés les tubes allumés).

Pour mieux appréhender les simulations de SER des réflecteurs circulaires, 3 cas distincts ont été étudiés : Tous les tubes éteints, les 7 ou 9 tubes allumés, et un design identique en remplaçant les tubes par des éléments métalliques en cuivre.

A 2.4 GHz, la SER du RR4 avec 7 tubes allumés est 5 dB plus forte (-10 dBsm) que pour le RRA avec 9 tubes (-14,5 dBsm). La SER globale est due à la sommation (amplitude et phase) des différentes contributions des tubes fluorescents, ceci expliquant les différences de SER pour les deux cas. Pour les deux configurations, la SER du réflecteur avec tubes en cuivre donne un résultat proche de son équivalent en tubes fluorescents. Par contre, lorsque le plasma est dé-ionisé, la SER de l'antenne réflecteur est au maximum de -22,5 dBsm ce qui la rend beaucoup plus discrète d'un point de vue radar que l'antenne équivalente métallique.

A 8 GHz, que les tubes soient ionisés ou pas, la SER des RRAs sont comparables et proches de -10 dBsm mais de nouveau beaucoup plus faibles (10 dB) que les antennes

équivalentes avec des tubes métalliques. Ceci démontre un grand avantage des antennes plasma puisqu'elles sont beaucoup plus furtives à cette fréquence.

Des simulations de SER ont également été effectuées pour l'antenne à réflecteur triangulaire (CRA) et ceci pour différentes configurations, CRA1 allumé, CRA2 allumé et CRA1 et CRA2 allumés simultanément. Comme précédemment, ces réflecteurs sont illuminés par une onde plane selon X et un champ électrique polarisé selon z comme présenté figure 9.
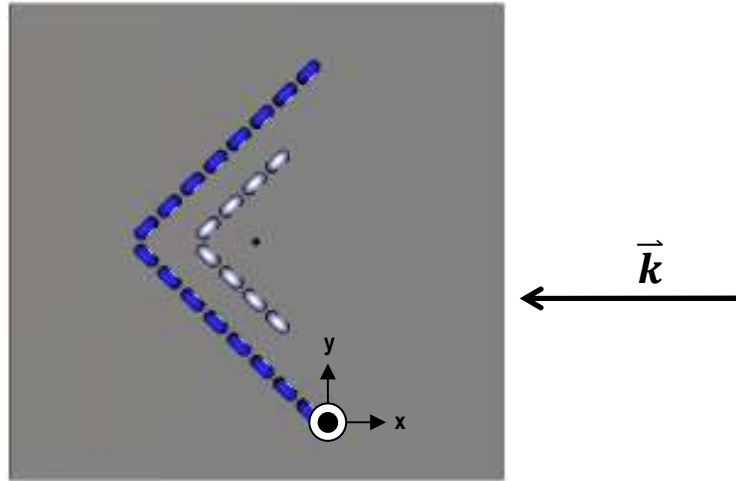
Figure 9 – Le CRA2 est activé et illuminé par une onde plane selon x avec un champ électrique polarisé selon z (en bleu sont représentés les tubes allumés).

A la fréquence de 2,4 GHz, et pour les 3 configurations, les SER des CRA sont équivalentes à celles des antennes avec tubes métalliques et les niveaux maximums de SER sont globalement situés entre -1 et -10 dBsm. Lorsque les tubes fluorescents sont éteints, la SER se réduit de 20 dB.

Si un radar illumine ces antennes à 8 GHz, les CRA activés (CRA1 ou CRA2) seront très difficilement détectables puisque leurs SER sont très faibles (-5 dBsm) si on les compare aux SER des antennes métalliques équivalentes (autour de 10 dBsm).

6.0   Conclusion

L'utilisation de milieux plasma est très intéressante dans les systèmes de communications, car ils présentent l'avantage de pouvoir être activés et désactivés en quelques millisecondes et donnent donc l'accès à une possibilité de reconfigurabilité. Si l'état de l'art concernant la physique des plasmas est large, c'est beaucoup moins le cas concernant les plasmas utilisés comme réflecteurs ou comme antennes et particulièrement dans les bandes ISM. En outre, les aspects validations expérimentales y sont encore moins décrits.

Deux types d'antennes réflecteurs à plasma ont été simulés, fabriqués et mesurés, respectivement un réflecteur circulaire (RRA) et un réflecteur triangulaire (CRA). Le RRA permet d'obtenir une antenne à balayage électronique mais également de changer la forme du faisceau. Les mesures sont en bon accord avec les simulations. Le gain mesuré est 5 dB plus élevé que celui d'un monopole seul pour une taille identique de plan de masse. Les niveaux de polarisation croisée restent faibles et le rapport avant arrière supérieur à 10 dB. La capacité de balayage de cette antenne est remarquable puisqu'elle permet de dépointer le faisceau sur 360° avec des diagrammes de rayonnement identiques pour les différentes directions.

Le réflecteur triangulaire (CRA) développé durant ces travaux de thèse est un nouveau concept puisqu'il intègre en fait deux réflecteurs triangulaires sur un même plan de masse ce qui offre la possibilité d'obtenir 3 formes de faisceau différentes et commutables. L'antenne CRA a été simulée, fabriquée et mesurée. Les résultats de simulation et de mesure sont en bon accord et un gain supérieur de 5 dB à celui d'un monopole classique a été obtenu. Les niveaux de polarisation croisée et de rapport avant arrière sont également très satisfaisants.

La hauteur des tubes fluorescents utilisés comme éléments réflecteurs reconfigurables a été modifiée (3 hauteurs) afin de voir s'il était possible de compacter ces réflecteurs reconfigurables (RRA ou CRA). Les performances obtenues sont satisfaisantes avec des tubes plus courts (54 mm) ce qui démontre qu'il est possible de compacter ces antennes et de les réaliser avec des tubes fluorescents commerciaux de faible taille.

En utilisant le même type de tube fluorescent, une étude de faisabilité de conception d'antenne rayonnante a également été engagée. Les tubes choisis ont des hauteurs respectives de 77 et 35,7 mm et les réalisations ont été mesurées à 900 et 450 MHz. Cette étude a prouvé qu'il était possible d'utiliser ces tubes fluorescents compactes comme éléments rayonnants cependant la technique d'alimentation du plasma et du couplage du signal électromagnétique ont un impact important sur les performances en rayonnement de l'antenne. Cette étude devrait donc être suivie d'une optimisation dans des travaux futurs.

Comme il est précisé dans la littérature, les antennes plasma permettent de réduire l'utilisation de matériaux métalliques et donc d'accéder à des antennes plus furtives présentant une SER plus faible que leur équivalent métallique. Durant ces travaux de thèse, des simulations de SER des antennes réflecteurs reconfigurables (RRA et CRA) ont été menées et démontrent bien que ces antennes sont plus furtives et donc plus difficilement détectables d'un point de vue radar que des antennes métalliques équivalentes.

Contents

Chapter 4

Chapter 5

Chapter 1

General introduction

1.1   Context and motivation of the study

Today's communication technologies have endured rapid and vast evolution. Therefore the necessity of the communication systems to become flexible in performance and reliable with time is very crucial. Moreover the wireless communications have become complex and even more severe due to the co-existence of the similar systems. Hence many research works have been conducted since then or even still in progress to ensure these communication systems remain steadfast. Ability to be reconfigured mechanically or electrically, capability to scan signals, capability to control beam patterns and or even to remain low cost continue to be part of the main quests in designing antennas.

Other than metamaterials which is not naturally exist, plasma is the fourth state of matter which is naturally available. Differ from metamaterials which have both negative values for its permittivity and permeability, plasma keeps its permeability in positive region while its permittivity is negative. This is the main feature offers by plasma so that it could be one of the beneficial materials in designing antenna. In general, plasma will act like a conductor and can be made disappear if it is de-energized. The reconfigurable behaviors offered by plasma are the factor why plasma antenna concepts are studied here.

In military applications, scanning capability can be used to jam undesired signals from hostiles. Ability to be dynamically tuned and reconfigured for frequency, direction, bandwidth, gain and beamwidth could help the system to suite its requirement variation and to stay dependable. In other words, the employment of plasma could reduce the number of multiples antennas.

In the IETR, this research is one of the earliest works that deals with plasma antenna. Therefore, at this moment, this study is very important since it would become a starting point in IETR so that other works will benefit from the output of this work. In France, one laboratory named as LAPLACE located at the University of Toulouse is active in plasma research. However the different between this study and theirs is that, this study utilizes low cost plasma elements which are commercially available. Thus a process to create homemade plasma which requires complex physic apparatus can be avoided.

The name of 'plasma' was first introduced in physic research in early 1920s [1]. Prior to that, plasma was first invented as radiator to transmit electromagnetic signals just after World War 1. In 1919, the concept of plasma antenna was patented and the patent was awarded to J. Hettinger with the name of "Aerial conductor for wireless signaling and other purposes" [2]. But even though plasma antenna had its beginnings in early 20 century, its significant development only starts in 1960s when the plasma began to be introduced in communication systems [3]. Since then, there is a considerable amount of inventions made by many research institutions and groups to exploit plasma as antenna [4-9]. Plasma can be controlled electrically to act like a radiator, reflector or even as an absorber and because of these factors, the research activities in plasma field are kept active and vibrant.

Plasma antennas are having more degree of freedom than metal antennas and hence making their applications have huge possibilities. Plasma will behave as a conductor regardless of it was fully ionized or partially ionized. The advantages of plasma antenna can be viewed in two perspectives. The first one is in the military point of view which plasma antenna could provide enormous flexibility in military applications. Ability of communication antennas to be invisible in the eyes of radar is essential in military applications. The stealth ability is the advantage of plasma which is unable to be done by metallic materials [5]. Plasma is also a good candidate to create confusion in warfare communication since it can disappear within microseconds. The unenergized plasma elements are hardly to be detected by hostile radar since there are no metallic antenna takes place when the plasma is switched off. In other words, the radar cross section (RCS) of the plasma antenna is low [5].

Plasma can also be applied as antenna elements for conventional communication systems. Since plasma is highly reconfigurable, the unused elements do not cause any unwanted effect to the whole systems. Implementation of plasma antenna enables the communication system to adjust its radio performances in order to suite and meet the changing of system requirement due to the system itself or due to environmental requirement. Today's communication systems become more complex especially to cope with the increasing number of users. Therefore with plasma ability, the communication systems are capable to remain reliable over the time.

1.2   Objectives and research contributions

Basically this research study is based on four main objectives.

The first objective of this study is to characterize plasma medium so that it corresponds to the commercially available plasma source in the market. The characterization is made based on dispersion model with the CST software [10] as a platform. Prior to this characterization, estimation and definition of plasma frequency is

required. For that reason, an experimental approach that employs an isolation technique or wave propagation experiment using a set of transmitting and receiving antennas is firstly identified. The experiments were aimed to be conducted without any aid of physic apparatus which are complex, expensive and bulky.

The second objective is to design and realize plasma antennas based on plasma medium for several specific purposes such as reconfigurable antennas with capabilities of beam scanning and beam shaping. Two types of reflector antennas that use plasma as its elements were constructed. These reflector antennas were designed to work within ISM band frequency. This objective only can be realized once the defined plasma characterization is finalized. Their performances such as reflection coefficient, gain and radiation patterns are compared with regard to their configuration styles.

The third objective is to analyze the performances of plasma as radiating element. The available U-shaped compact fluorescent lamp (CFL) is used as radiator and this lamp is excited using domestic AC supply. Since the plasma can be used to radiate radio signal, it is also can be called as plasma antenna. For further investigations, the plasma antennas were measured using our laboratory facilities and their performances between ON and OFF states are used to validate the ability of plasma antenna to effectively radiate radio signal.

The final objective of this work is to simulate and measure the radar cross section (RCS) performances of plasma reflector antennas. Prior to that, comparisons between simulated and calculated RCS of metallic sphere and metallic flat plate are performed to ensure a correct simulation setup has been made. Once the simulation setup is validated, the RCS performances of plasma reflector antennas can be compared to their twin metallic structures with similar configuration and arrangement. To further enhance the research's findings, the plasma reflector antennas (RRA and CRA) are measured for their actual RCS level for on and off state of plasma.

1.3   Thesis structure

This thesis consists of four main chapters.

The second chapter is dedicated to recall plasma as the fourth state of matter which is less exploited in communication systems. State of the arts of plasma is explained in this chapter for better understanding of plasma existence, generation and how it benefits to the communication systems. This chapter also elaborates plasma formulation using liquid model where in this part, the plasma parameters are linked to microwave variables commonly used in communication systems. Measurements setup and results which lead to selection of plasma parameters are also explained in this chapter.

The third chapter presents the realization of plasma reflector antennas. Two plasma reflector antennas have been constructed in this research work which are round and corner reflector antennas, RRA and CRA respectively. The design and optimization are thoroughly explained within the chapter. Realization of both reflectors which is involving mechanical works are explained step by step. The theoretical and experimental results for several configurations that have been realized in this research work are also compared. The final part will discuss about performances of the reflector antennas that used plasma as elements.

The fourth chapter deals with plasma as radio waves radiator. Prior to the realization, a state of the art of the plasma antenna is explained in this chapter. Reviews on coupling techniques are also explained in the subsequence topic. This is followed by the fabrication of two plasma antennas using commercially available U-shaped compact fluorescent lamp (CFL). Next, the antennas performances are discussed based on plasma ON and OFF states. Finally, conclusions are drawn with regard to the performances of the plasma antennas.

Chapter five discusses about radar cross section performances of the plasma reflector antennas. Two plasma reflector antennas (RRA and CRA) are simulated and measured for their RCS performances. The comparison between theoretical and simulation RCS for metallic shapes (sphere and flat plate) to validate simulation setup is also explained in the beginning of this chapter. In the end of this chapter, the performances of plasma reflectors are summarized with regard to their metallic counterparts.

References

[1]   Umran S. Inan, Marek Golkowski, "Introduction", in Principles of Plasma Physics for Engineers and Scientists, Cambridge University Press, NY: New York, 2011, pp. 1-19.

[2]   J. Hettinger, "Aerial conductor for wireless signaling and other purposes", Patent No. 1309031, 8 July 1919.

[3]   C. Y. Ting, B. R. Roa, W. A. Saxton, "Theoretical and experimental study of a finite cylindrical antenna in a plasma column", IEEE Trans., Antennas Propag., vol. AP-16, no. 2, pp. 246-255, Mar. 1968.

[4]   G. Borg, J. H. Harris, "Application of plasma columns to radiofrequency antennas," Appl., Phys., Lett., vol. 74, no. 22, May 1999.

[5]   J. P. Rayner, A. P. Whichello, A. D. Cheetham, "Physically Characteristics of Plasma Antennas", IEEE Trans., Plasma Sci., vol. 32, no. 1, pp. 269-281, Feb. 2004.

[6]   I. Alexeff, T. Anderson, S. Parameswaran, E. P. Pradeep, J. Hulloli, P. Hulloli, "Experimental and theoritical results with plasma antennas," IEEE Trans., Plasma Sci., vol. 34, no. 2, pp. 166-172, April 2006.

[7]   T. Anderson, I. Alexeff, N. Karnam, E. P. Pradeep, N. R. Pulasani, J. Peck, "An operating intelligent plasma antenna," IEEE 34th International Conference on Plasma Science (ICOPS 2007), pp. 353-356, 2007.

[8]   G. Cerri, R. De Leo, V. Mariani Primiani, P. Russo, "Measurement of the properties of a plasma column used as a radiating element," IEEE Trans., Instrum., Meas., vol. 57, no. 2, pp. 242-247, Feb. 2008.

[9]   P. Russo, G. Cerri, R. De Leo, E. Vecchioni, "Self-consistent analysis of cylindrical plasma antenna," IEEE Trans., Antennas Propag., vol. 59, no. 5, pp. 1503-1511, May 2011.

[10] 3D EM field simulation-CST computer simulation technology, Available at: http://www.cst.com. Accessed October 1, 2010.

Chapter 2

Plasmas and fundamentals

The objective of this chapter is to give a brief view of the fourth state of matter that can be classified into two types which are collisional and collision-less plasma. The state of the art of plasma is described in the first part of this chapter. In which the explanation covers on type of plasma, its generation, its modelization and its important parameters. The second part of this chapter is focusing on the theory that is affiliated with plasma especially its electrical conductivity, critical frequency and permittivity. The derivations of the theory explained in this chapter are based on a single particle motion that obeys momentum conservation equation. A theoretical estimation of electron-neutral collision frequency of plasma is also discussed. The third part of this chapter explains on measurements that have been carried out to estimate plasma working region. The measurement setup and results are explained in details. The determination of plasma electron-neutral collision frequency with regard to the experimental results is also discussed. Finally, a conclusion is drawn based on the works done and the defined plasma model is finalized.

2.1   State of the art

Plasma medium is often referred to as the fourth state of matter, since it has properties very much different from those of the gaseous, liquid, and solid states. In 1920s, a group of scientists headed by I. Langmuir has shown that the characteristic electrical oscillations of very high frequency can exist in an ionized gas that is neutral or quasi-neutral, and they introduced the terms plasma and plasma oscillations [1]. All states of matter represent different degrees of organization, corresponding to certain values of binding energy [1]. In the solid state, the important quantity is the binding energy of molecules in crystal lattice. If the average kinetic energy of a molecule exceeds the binding energy; typically a fraction of an electron volt, the crystal structure breaks up, either into a liquid or directly into a gas (for example: iodine). Similarly, a certain minimum kinetic energy is required to break the bonds of the van der Waals forces in order to change a liquid into a gas. For matter to make the transition to its fourth state and exist as plasma, the kinetic energy per plasma particle must exceed the ionizing potential of atoms (typically a few electron volts). Thus, the state of matter is basically determined by the average kinetic energy per particle [1].

11

An example to show transformation towards the fourth state of matter is best described by taking water (H_2O) as an example. Ice represents the solid state of H_2O in which the molecules of ice is fixed in lattice. The kinetic energy of each ice molecule is very weak therefore the ice remains in solid state unless extra energy is applied. If adequate energy is applied to the ice, the molecules will have more kinetic energy that allows them to agitate. The extra energy also will cause some of them to move freely. This condition turns the ice into water (liquid state). If more energy applied to liquid, for example by boiling the water, the molecules will have more energy and get excited. As a result, the molecules are free to move and change into steam (gaseous phase). In this case, the spacing between each molecule is large enough compared to its previous states of matter. Since each molecule moves in random manner, the kinetic energy for each molecule is different. If the steam is subjected to thermal heating, illuminated by UV or X-rays or bombardment by energetic particles, it becomes ionized. Table 1.1 shows the transformation of ice into plasma.

The plasma will exist when the electron and nucleus that formed the atom no longer can stay together due to high kinetic energy where the electrons are stripped out from the atoms. Plasmas are conductive, and respond to electric and magnetic fields moreover it also can be an efficient source of radiation. If there is insufficient sustaining energy, plasma will recombine into gas.

Table 1.1 – Transformation from solid state to plasma state.
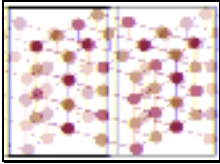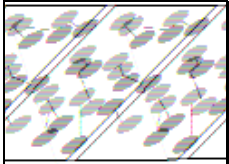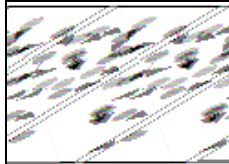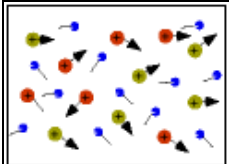
Solid	Liquid	Gas	Plasma
Example: Ice	Example: Water	Example: Steam	Example: Ionized Gas
H_2O	H_2O	H_2O	$H_2 => H^+ + H^+ + 2e^-$
Cold	Warm	Hot	Hotter
$T < 0°$ C	$0° < T < 100°$ C	$T > 100°$ C	$T > 100000°$ C
Molecules arranged in well-organized grid (lattice)	The grid arrangement is broken but the bonds between molecules maintained	Molecules are free to move and there are large spacing between them	Ions and electrons move independently and there are large spacing between them

Figure 2.1 shows the range of temperature, electron density and Debye length for typical plasma found in nature and in technological applications [1].
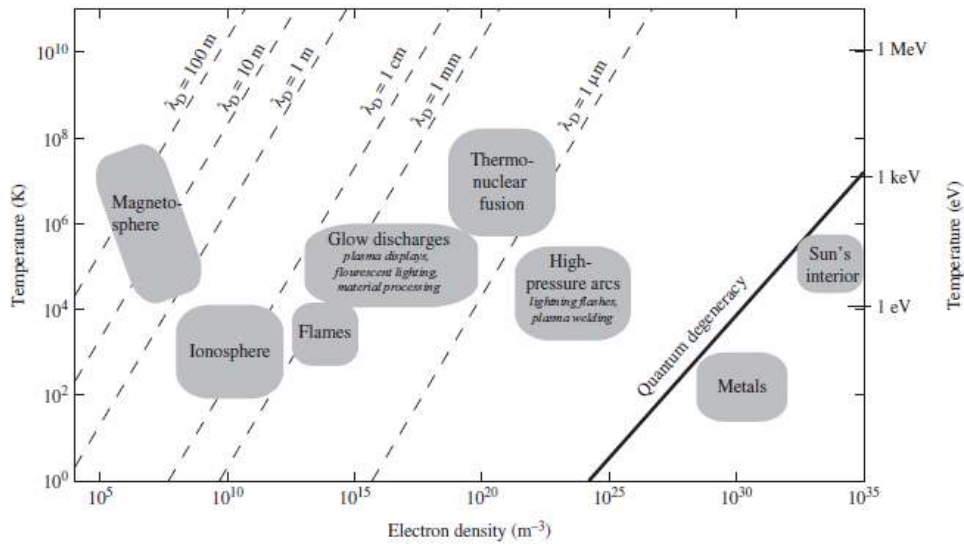
Figure 2.1 – Range of temperature, electron density and Debye length for typical plasma found in nature and in technological applications [1]. (1eV = 11600K).

2.1.1 Gaseous plasma

Plasma could exist in a glass tube if the encapsulated gas gets ionized. The typical gases that are used as plasma sources are the noble gases such as helium (He), neon (Ne), argon (Ar) and krypton (Kr). These gases are considered as low level reactivity thus they are safe to be used as a light source. Each of the gases mention here is having its own plasma characteristic. This can be discussed in terms of their plasma parameters. Since each of the gas atoms has different number of energy level, the total energy needed for each atom to be excited is also diverse. In other words, the required energy for the gas atom to transform into plasma state is also different.

Most of the plasma sources contain not only the ionized gas but also other chemical quantities to accelerate or to surge the process of ionizing. The well known quantity added along the encapsulated gas is mercury vapor. Other than domestic fluorescent lamps, mercury is also added in the high intensity discharge (HID) lamps. In standard fluorescent lamps, mercury vapor pressure plays one of the key roles to define electron density [2]. In view of the fact that, electrical conductivity of plasma depends on electron density and electron-neutral collision, the vapor pressure plays important role in determining plasma electrical conductivity too, which is important properties in determining the performance of plasma medium if they are used to radiate microwave signals. The low pressure gas usually encapsulated in insulating tube made of glass as shown in Figure 2.2.

13
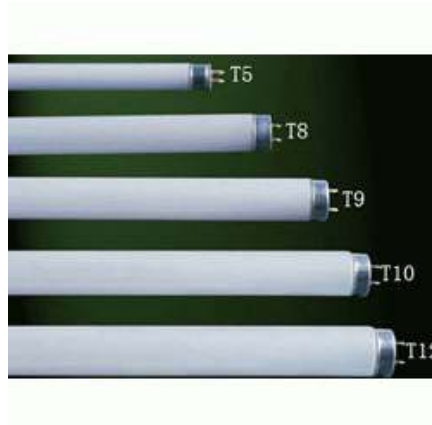
Figure 2.2 – Commercially available plasma column ; the fluorescent lamps.

The physical geometry of fluorescent lamps is depending on its applications. Because of that, they are available in many shapes and sizes. As shown in Figure 2.2, there are 5 common sizes of fluorescent lamps usually used for domestic usage. The technology of fluorescent lamp is expending year by year with the quest to provide variety of options for users to select. One of its options is the compact fluorescent lamp (CFL). The compact fluorescent lamps are also available in many sizes and shapes. Due to its high efficiency and compact in size, the CFL becomes most popular light source for energy saving.

2.1.2 Solid state plasma

Solid state plasma is a system of positive and negative carriers (electrons and holes) in solids [3]. The solid state can be charged such as electron plasma of metals, electron or hole-plasma of semiconductors, plasma with unequal electron or hole concentration in alloys [3]. It can also be neutral for example the electron-hole plasma of semiconductors and semimetals. The plasma particle density varies in different solids over a wide range, from 0 to 10^{22} cm^{-3} for a charged plasma and to 10^{17} cm^{-3} for a neutral plasma. Some properties of solid state plasma such as thermodynamic properties and kinetic coefficients are related to the type and peculiarities of the lattice of the solid and to the interaction between the carriers and the lattice; on the other hand, in many cases solid state plasma can be regarded as an almost isolated subsystem of the solid (which interacts weakly with the lattice), and the properties of this subsystem can be studied separately [3].

The solid state phenomenon has been studied in [4] and the review on the similarities and differences between gaseous and solid state plasmas was also reported. One of the differences that need to be highlighted between gaseous and solid state plasma is the much lower activation energy for ionization in solid state plasma. This advantage explains the low cost implementation of solid state plasma in various up-to-

date technologies typically for high frequency applications (60 GHz). Dense solid plasmas are much more easily established at reasonable temperatures and plasma phenomenons are observable in some solids even at liquid helium temperatures. Besides, the implementation of solid state microwave device at room temperature was reported in [5]. The other most important characteristic of solid state plasma is the presence of crystal lattice which is capable to support acoustic vibrations [4]. The existence of lattice means the presence of polarization ability which leads to a lattice dielectric constant, ε that is not unity.

However, if the implementation of solid state plasma is discussed in terms of its deployment as antenna element for lower frequency applications, solid state plasma is not a good candidate. This is because the size of typical solid state device (PIN diode etc.) is too small compared to the electrical length of antennas used in lower frequencies range. Thus, if the solid state plasma is meant for 2.4 GHz applications, the antenna will require several solid state devices. Due to its nature, the solid state devices need to be excited individually as a result the circuit becomes complex and not viable to be constructed.

2.1.3   Plasma generation

In general, generation of plasma in a gas container usually a dielectric tube or a discharge tube can be divided into two categories; electrode discharge tube and electrode-less discharge tube. However, the ionization process occurs in the gas container remains the same regardless how the gas is being excited. This section aims to focus on plasma excitation techniques that are intended to be used in communication systems. This includes the excitation of fluorescent lamps which falls under electrode discharges tube since it uses electrodes to ionize the gas in order for plasma to exist.

2.1.3.1   Electrode lamps

Usually a gas-filled dielectric tube used with electrode is operated on an AC supply which is known as fluorescent lamp. Differ to incandescent bulb, the fluorescent lamp has no heating filament but it has been replaced with a set of cathodes. The cathode is made of coiled tungtens filaments that coated with an electron-emitting substance and located at each end. When there is AC supply, the cathode will cause the electron flow due to the charge imbalance occurs at one end. This electron will flow through mercury vapor and collides with mercury atom and causes its electrons out of their natural orbit. The energy released from collision phenomenon is in the form of ultraviolet radiation. The ultraviolet radiation is turn into visible light when it strikes the phosphors coating.

This process will continue to occur since the AC supply causes the cathode pair to alternate as anode and cathode, therefore the imbalance charge is sustained. By having this condition, the encapsulated gas gets ionized and exhibits conducting behaviors. There are many research works on plasma antenna that have used this kind of excitation technique including those reported in [6-12].

2.1.3.2   Electrode-less lamps

One of the main advantages of electrode-less lamps is its longer life span compared to the electroded lamps. Since there is no direct connection between the gas and electrodes, a gas contamination could not occur. However the main obstacles of this excitation technique can be view in terms of technical aspects. There are four distinct types of excitation for electrode-less lamps which are inductive (H discharges), capacitive (E discharges), microwave discharges and traveling wave discharges [2].

2.1.3.2.1   Capacitive discharges

Capacitive discharges or also known as E discharges is the simplest technique to excite plasma in dielectric tube. A gas-filled container can be placed in between two capacitor plates. The electric field between capacitors will transfer extra energy to the gas container resulting plasma to exist. Another capacitive coupling is using a sheath of conductor to wrap a small part of the discharge tube and as a result a strong dependence on the E discharges. Figure 2.3 shows an example of a schematic of capacitive discharges in an excitation box [13-15].

 A domestic fluorescent lamp was used to create the plasma column. The tube (fluorescent lamp) was placed inside a metallic box just under a ground plane. Two copper ring were employed; the first one (excitation ring) is used and soldered to an N-type connector to pump the excitation RF energy. As a result a strong electric field is created between the copper ring and the ground plane. The electric lines of the electric field penetrate inside the tube and exciting the plasma column. The second copper ring (signal ring) is used to apply information signal using the same capacitive coupling [14].
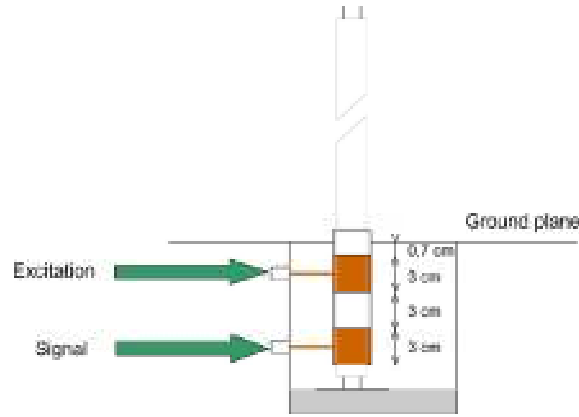
Figure 2.3 – Capacitive coupling in a excitation box [14]. Two copper rings are employed; the first one (Excitation) is to apply electric field for plasma excitation and the second one (Signal) is for transferring information signal.

2.1.3.2.2   Inductive discharges

Other name of inductive excitation is the **H** discharges. The discharges current is supplied to a coil that is placed around the dielectric tube. Sufficient power is applied will sustain the **H** discharges therefore the gas will get excited and gets ionized. An example of inductive excitation is shown in Figure 2.4 [16]. A coil of length L is used to winding around a discharges tube with the radius of R_2. The H_z is the axial magnetic field with time dependence $e^{j\omega t}$.
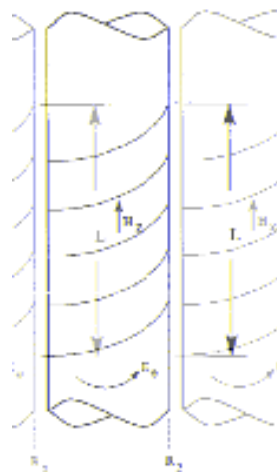
Figure 2.4 – Inductive coupling [16].

2.1.3.2.3   Microwaves discharges

Paola Russo et al., have actively studied the technique to ionize plasma in cylindrical tubes by using microwaves discharges [17], [18]. Numerical modeling and study of the similar approach to excite plasma has been presented in [19], [20]. A device known as "surfaguide" was firstly introduced by M. Moisan and Z. Zakrzewski in [21]. This device was actively developed by Paola Russo as to determine some important plasma antenna parameters such as effective length of antenna [17], conductivity [18] and density with respect to the power of electric field applied.

In particular, 2.45 GHz microwave pump signal is used for ignition. The advantage of this frequency is high power available with low cost [17]. By confining its electromagnetic field in a closed structure, it is simple to ionize plasma tube. The 430 MHz signal is used as radiated signal since the usage of this frequency is permitted without any restriction. Figure 2.5 (a) reports the longitudinal section of the surfaguide. It consists of two trunks L_0 of a standard waveguide WR340, two transitions L_1, and a waveguide L_2 with a reduced height. The guide is terminated by a moving short, whose length L_s can be varied for matching when the plasma column is turned on. Figure 2.5 (b) shows a sketch of the surfaguide launcher with a horizontal plasma tube.

(a)

(b)
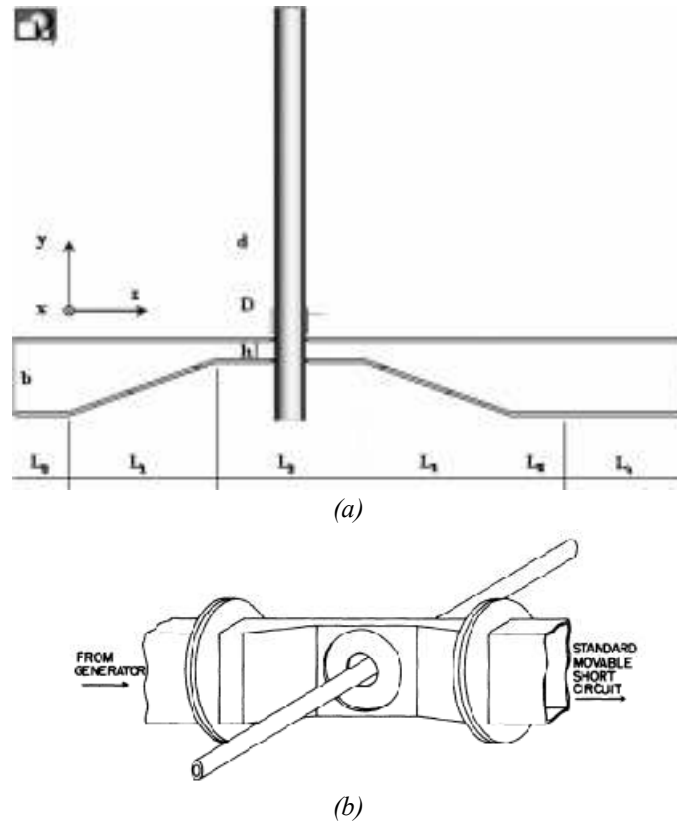
Figure 2.5 – (a) Longitudial section of the surfaguide. Vertical tube contains plasma to be ignited [17]. (b) Sketch of the surfaguide launcher with a horizontal plasma tube [21].

2.1.3.2.4   Laser

One example of plasma created by a laser in communication system is a plasma wire works as antenna proposed in [22]. A virtual reconfigurable plasma antenna consisting of a set of laser plasma filament produced in air by the propagation of femtosecond laser pulses. The Figure 2.6 shows the schematic diagram of plasma wire used as antenna.
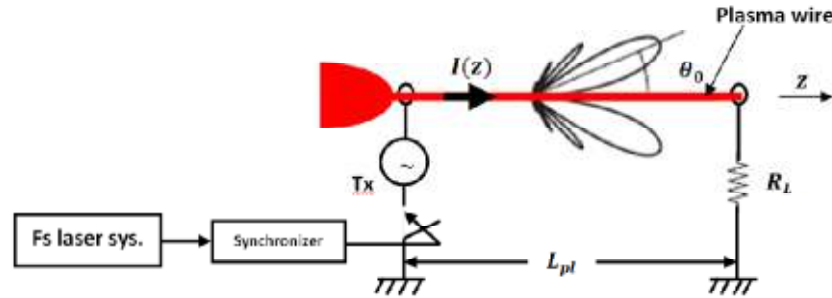
Figure 2.6 – Schematic diagram for a proposed Beverage or wave antenna [22].

The Beverage antenna is a horizontal, long-wire antennas designed for the transmission of lower frequency and it is vertically polarized ground waves. The antenna consists of a single plasma wire, two or more wavelengths long that is placed 3 to 6 meters above the ground plane. The antenna main lobe can be tilted with an angle of θ_o towards the traveling direction by changing the plasma wire length, L_{pl} [22].

2.1.4 Plasma model

As mentioned earlier, there are two types of plasma which are collision-less and collisional plasmas. In this research work, the plasma is modeled as a cold-plasma based on the Drude model. The effect of electron collision is associated with the model. The model is developed to represent the commercially available plasma source used in the experimental activities. The plasma source is assumed to have low pressure argon and mercury vapor encapsulated in pyrex glass tube. The model is developed in CST software [23] with an assumption that the isotropic plasma has uniform intensity in all direction. The material parameter setup window in CST software is shown in Figure 2.7.

19

Figure 2.7 – Material parameter definition window in CST [23].

With regard to the Drude model, the epsilon infinity is equal to 1 thus simplifying the permittivity equation as derived in Eq. 2.32.

2.1.5 Plasma parameters

Dealing with plasma it is necessary to consider some quantities that could change plasma properties. Generally the following are the quantities that could be altered to vary the plasma properties in order to benefit the purposes of applications:

- ❖ Excitation power or power injected to dielectric tube [24]
- ❖ Gas pressure (electron density depends on the mercury vapor pressure) [2]
- ❖ Type of gas and gas combination [25]

These three quantities if appropriately altered will able to change the following plasma parameters:

- ❖ Plasma frequency
- ❖ Conductivity
- ❖ Permittivity

Plasma frequency, conductivity and permittivity are the core parameters that must be comprehended when working with plasma. The subtopic 2.2 elaborates more about these parameters. Derivation is explained in details so that readers could understand important relations between plasma parameters.

2.2   Theoretical reminder

Plasma is a dispersive material which offers particular electrical properties when electromagnetic waves are applied to it. As a frequency dependent material it also has these properties; electrical conductivity, electrical permittivity, and magnetic permeability. These electrically controlled properties are allowing the exploration of plasma as one of material options in designing antennas. By understanding the relation between plasma medium and incoming electromagnetic waves, it may lead to a promising development of plasma antennas.

Plasma medium is formed by ions and electrons; therefore it is necessary to understand the interaction between plasma medium and electromagnetic waves. The following subtopics explain the plasma properties and its relation with electromagnetic waves. The explanation is started with consideration of a single particle motion model under the effect of electromagnetic field. The plasma derived in the following subtopic is with an assumption of homogenous plasma.

2.2.1 Plasma conductivity

In order to find plasma conductivity, it is easier to start the derivation with a single charge particle model. Let's consider this charge to be an electron, q where this particle must obey the Lorentz force (momentum conservation equation) [26-28].

$$m_e \frac{d\boldsymbol{v}}{dt} = q(\boldsymbol{E} + \boldsymbol{v} \times \boldsymbol{B}) \tag{2.1}$$

where the $\boldsymbol{v}$ is the velocity of the electron and the $\boldsymbol{E}$ and $\boldsymbol{B}$ are the electric and magnetic fields that effecting the electron.

To consider the most general cases, let's the $\boldsymbol{E}$ and $\boldsymbol{B}$ vary with time in free space with the factor of $e^{j\omega t}$ (AC cases, and the factor, $e^{j\omega t}$ (+ signs) result in waves travelling in the negative x, y or z direction). The $\boldsymbol{E}$ is in the x direction and the perpendicular $\boldsymbol{B}$ in the y direction. Hence, equations of both electric and magnetic fields are,

$$E = E_0 e^{j\omega t} a_x \tag{2.2}$$

$$B = \frac{E_0}{c} e^{j\omega t} a_y \tag{2.3}$$

where c is the speed of light in free space.

Since these fields have influence on the electron, the velocity of the electron can be determined by substituting Eq 2.2 and 2.3 into Eq 2.1. Thus,

$$a = \frac{dv}{dt} = \frac{q}{m_e}(E_0 e^{j\omega t} a_x + \left[v \times \frac{E_0}{c} e^{j\omega t} a_y\right]) \tag{2.4}$$

This equation is transformed into differential form to simplify the determination of electron acceleration.

$$\frac{d^2 x}{dt^2} a_x + \frac{d^2 y}{dt^2} a_y + \frac{d^2 z}{dt^2} a_z = \frac{q}{m_e}\left(E_0 e^{j\omega t} a_x + \left[v \times \frac{E_0}{c} e^{j\omega t} a_y\right]\right)$$
$$= \frac{q}{m_e}\left(E_0 e^{j\omega t} a_x - \frac{E_0}{c}\frac{dz}{dt} e^{j\omega t} a_x + \frac{E_0}{c}\frac{dx}{dt} e^{j\omega t} a_z\right) \tag{2.5}$$

Then, each of acceleration components can be written as

$$\frac{d^2 x}{dt^2} = \frac{q}{m_e}\left(1 - \frac{1}{c}\frac{dz}{dt}\right) E_0 e^{j\omega t} \tag{2.6}$$

$$\frac{d^2 y}{dt^2} = 0 \tag{2.7}$$

$$\frac{d^2 z}{dt^2} = \frac{q}{m_e}\frac{E_0}{c}\frac{dx}{dt} e^{j\omega t} \tag{2.8}$$

The velocity component of the single charge particle can be derived from above equations (the three equations). By only considering non-relativistic motion, so that the velocity in propagating direction is lesser than the speed of light in free space ($v \ll c$). Therefore the acceleration component in the x direction becomes

$$\frac{d^2 x}{dt^2} = \frac{q}{m_e} E_0 e^{j\omega t} \tag{2.9}$$

Then, the velocity and the displacement in the x direction is

$$\frac{dx}{dt} = \frac{q}{m_e} E_0 \frac{1}{j\omega} e^{j\omega t} \tag{2.10}$$

$$x = \frac{q}{m_e} E_0 \frac{1}{(j\omega)^2} e^{j\omega t} = -\frac{qE_0}{m_e \omega^2} e^{j\omega t} \tag{2.11}$$

Up to this point, the derived velocity and the displacement in the x direction is for single electron. Since the plasma is composed of many particles hence the collective effect electric and magnetic fields on the particles is essential. By considering electric current produced by all the particles, the collective current density vector is

$$\boldsymbol{J_E} = q n_e \boldsymbol{v} \, \boldsymbol{a_x} \tag{2.12}$$

Substituting Eq. 2.10 in (2.12)

$$\boldsymbol{J_E} = q n_e \left[\frac{q}{m_e} E_0 \frac{1}{j\omega} e^{j\omega t} \right] \boldsymbol{a_x} \tag{2.13}$$

The Eq. 2.13 assumes that the current flow is only in the x direction, since the velocity of particles in the z direction is negligible (Eq. 2.18). The volume current density (conduction current) can also be expressed in term of electric field as

$$\boldsymbol{J_E} = \sigma \boldsymbol{E} \tag{2.14}$$

and equating Eq. 2.14 and Eq. 2.13 the conductivity of plasma can be defined as

$$\sigma E_0 e^{j\omega t} = q n_e \left[\frac{q}{m_e} E_0 \frac{1}{j\omega} e^{j\omega t} \right] \tag{2.15}$$

$$\sigma = -j \frac{n_e q^2}{\omega m_e} \tag{2.16}$$

From the Eq. 2.16, it can be noticed that the conductivity is a scalar whenever there is no magnetic field ($\boldsymbol{B} = 0$).

Let's now apply the effect of collisional process with an assumption that the electrons loose all its energy during a collision. Since only a collision less single-particle model was assumed in the beginning of the derivation, with the effect of collision (the m_e in previous equations is now m to represent more than one particle involved in the collisional case), the Eq. 2.1 is now becomes

$$m \frac{d\boldsymbol{v}}{dt} + m \boldsymbol{v} v_{col} = q(\boldsymbol{E} + \boldsymbol{v} \times \boldsymbol{B}) \tag{2.17}$$

with an introduction of v_{col} (collision effect), and if time dependence $e^{j\omega t}$ is assumed, then the left-hand side of Eq. 2.17 turns out to be

$$j\omega m\boldsymbol{v}(1 + \frac{v_{col}}{j\omega}) = j\omega m\boldsymbol{v}(\frac{\omega - jv_{col}}{\omega}) \tag{2.18}$$

This result tells us that we could replace the m_e by $m(\frac{\omega-jv_{col}}{\omega})$ in Eq. 2.16 in order to include the effects of collisions. Therefore the conductivity turns into

$$\sigma = -j\frac{n_e q^2}{m(\omega - jv_{col})} \tag{2.19}$$

and if we assume there is only DC electric field and unmagnetized plasma (isotropic cases) [1], the conductivity suits the following

$$\sigma = \frac{n_e q^2}{m v_{col}} \tag{2.20}$$

2.2.2 Plasma critical frequency

Because of plasma is a medium of free charge carriers, therefore it exhibits natural oscillations that occur due to thermal and electrical disturbances. By focusing on the electron motion in plasma medium, the harmonic oscillation of electron around the ions is important to be analyzed. By assuming that, due to harmonic oscillation of electron around ions, the electron density can oscillate at angular frequency, ω_p and as a result the electric field intensity, $\boldsymbol{E}$ will also oscillate at the same frequency. In many reference books, the ω_p is always referred as plasma frequency, however in order to avoid confusion in this thesis, the ω_p will be referred as angular frequency of plasma and f_p will be referred as plasma critical or plasma frequency.

The density oscillations increase the total free charge density, ρ that related to volume current density, $\boldsymbol{J}$. The relation is known as Continuity Equation as shown as Eq. 2.21 [27].

$$\nabla \cdot \boldsymbol{J} = -\frac{d\rho}{dt} \neq 0 \tag{2.21}$$

Substituting Eq. 2.14 into Eq. 2.21, the equation will be

$$\nabla \cdot (\sigma \boldsymbol{E}) = \sigma(\nabla . \boldsymbol{E}) = -\frac{d\rho}{dt} \tag{2.22}$$

The relation between free charge density and electric field is defined in Eq. 2.23.

$$\nabla . \boldsymbol{E} = \frac{\rho}{\varepsilon_o} \tag{2.23}$$

In order to have free current charge density ρ with the influence of electric field, $\boldsymbol{E}$ the Eq. 2.16 and Eq. 2.23 substitute into Eq. 2.22.

$$-j \frac{n_e q^2}{\omega_p m_e} \frac{\rho}{\varepsilon_o} = -\frac{d\rho}{dt} \tag{2.24}$$

The ions are much heavier than the electrons, so its oscillation will not long last compare to electrons. Thus, the volume charge density in Eq. 2.24 is assumed to depend only on electron oscillation. Eq. 2.24 is solved using differential equation will yield,

$$\rho = \rho_o e^{j\frac{n_e q^2}{\omega_p m_e \varepsilon_o}} \tag{2.25}$$

The angular frequency of oscillation of the free charge density, ρ is also ω_p, and hence,

$$\omega_p = \sqrt{\frac{n_e q^2}{m_e \varepsilon_o}} \tag{2.26}$$

2.2.3   Plasma permittivity

The permittivity of plasma can be defined based on Maxwell equation as in Eq. 2.27 with an assumption of lossy medium and with the time factor of $e^{j\omega t}$.

$$\nabla \times \boldsymbol{H} = (j\omega\varepsilon_o + \sigma)\boldsymbol{E} \tag{2.27}$$

$$\nabla \times \boldsymbol{H} = j\omega\varepsilon_o(1 + \frac{\sigma}{j\omega\varepsilon_o})\boldsymbol{E} \tag{2.28}$$

Base on this equation, permittivity of plasma is derived for two cases, which are without and with the effect of collision process. By substituting Eq. 2.16 into the right hand side of Eq. 2.28, the equation become

$$j\omega\varepsilon_o(1 + \frac{\sigma}{j\omega\varepsilon_o})\boldsymbol{E} = j\omega\varepsilon_o(1 - \frac{n_e q^2}{\omega^2 \varepsilon_o m_e})\boldsymbol{E} \tag{2.29}$$

therefore the relative permittivity of plasma ($v = 0$) is

$$\varepsilon_r = (1 - \frac{n_e q^2}{\omega^2 \varepsilon_o m_e}) = (1 - \frac{\omega_p^2}{\omega^2}) \qquad (2.30)$$

and by substituting Eq. 2.19 into the right hand side of Eq. 2.28 the equation will be,

$$j\omega\varepsilon_o(1 + \frac{\sigma}{j\omega\varepsilon_o})E = j\omega\varepsilon_o(1 - \frac{n_e q^2}{\omega\varepsilon_o m_e(\omega - jv_{col})})E \qquad (2.31)$$

therefore the relative permittivity of plasma with collisional effect is

$$\varepsilon_r = (1 - \frac{n_e q^2}{\omega\varepsilon_o m_e(\omega - jv_{col})}) = (1 - \frac{\omega_p^2}{\omega(\omega - jv_{col})}) \qquad (2.32)$$

From Helmholtz equation, the contants k^2 is equal to $\omega^2 \mu\varepsilon$, and the wave number of propagation constants for the two cases (collision-less (Eq. 2.33) and collisional (Eq. 2.34)) are as follows

$$k = \sqrt{\omega^2 \mu\varepsilon_o(1 - \frac{\omega_p^2}{\omega^2})} \qquad (2.33)$$

$$k = \sqrt{\omega^2 \mu\varepsilon_o(1 - \frac{\omega_p^2}{\omega(\omega - jv_{col})})} \qquad (2.34)$$

As mention in [26], as long as Eq. 2.33 is positive, the k will be real number so does the velocity of propagation in plasma,v_p where $k = \omega/v_p$ and plane electromagnetic wave can propagate.

$$v_p = \frac{1}{(\mu_o \varepsilon_o \varepsilon_r)^{1/2}} \qquad (2.35)$$

As a conclusion, based on Eq. 2.30 and Eq. 2.32, if the radio frequency applied to plasma is higher than plasma frequency the resulting complex permittivity is less than unity, therefore plasma having dielectric properties. If the plasma frequency is higher enough with respect to radio frequency, the plasma will show conductor properties, and either it will reflect or absorb the incoming wave depending on the electron-neutral collision frequency.

Figure 2.8 shows plasma complex permittivity ($\varepsilon' - j\varepsilon''$) using Eq. 2.32 based on the Drude model in CST software [23]. Theoretically, the imaginary $-j\varepsilon''$ accounts for loss (heat) due to the damping of the vibrating of the dipole moment. Due to the energy

conservation, the imaginary part of complex permittivity must be negative value (ε'' positive). Therefore the highest in imaginary values means high loss in the medium. As for the case shown in Figure 2.8 (plasma frequency equals 7 GHz), as the incoming microwave frequency reduces from high to low, the loss in plasma start to increase.
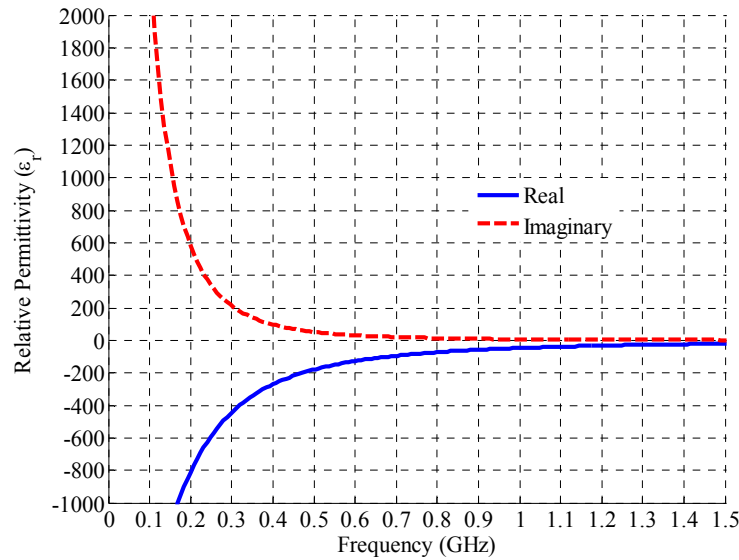
Figure 2.8 – Complex relative permittivity of plasma based on Drude model for plasma frequency equals 7 GHz and electron-collision frequency equals 900 MHz.

By looking into Eq. 2.32, the permittivity of plasma can be altered by varying the plasma frequency, electron-neutral collision frequency and microwave frequency. In other words, the behavior of plasma when reacting with impinged microwave frequency is depending on the microwave frequency itself. Here it comes the challenges when dealing with plasma medium.

2.2.4 Plasma collision frequency estimation

Knowledge of the dependence of the effective electron-neutral collision in noble gas such as argon is very important in order to understand many of plasma processes especially for its fundamental and applications. This type of collision frequency is often referred to evaluate the energy transfer between particles. The collision frequency occurs in gases is important in radio frequency field as highlighted in [29]. Collisional plasmas can be divided into two cases, which are partially ionized plasmas and fully ionized plasmas [1]. When discussing about partially ionized plasmas, the dominant collisional process is between electrons and neutrals. In general, as the partially ionized plasma is associated with low pressure plasma, collisions with neutral particles dominate all other elastic processes in low pressure discharge [29] [30].

In 1981, the effective collision frequency of electron in noble gases was studied in [31]. The Maxwellian distribution of electron particles was assumed to conduct the study. The group has compared their results with other previous published studies within the year of 1960 and 1978. The estimation was conducted for the noble gases such as helium, neon, argon, krypton and xenon. The following is the equation to estimate effective collision frequency between electrons and argon atoms [30].

$$v_{col} = N_{AR}\left(2.58 \times 10^{-12}T_e{}^{-0.96} + 2.25 \times 10^{-23}T_e{}^{2.29}\right) \qquad for\ (6 \times 10^2 K \ll T_e \ll 1.4 \times 10^4 K) \qquad (2.36)$$

or

$$v_{col} = N_{AR}\left(3.7 \times 10^{-8}T_e{}^{-0.315}\right) \qquad for\ (2.5 \times 10^2 K \ll T_e \ll 6 \times 10^2 K) \qquad (2.37)$$

where the T_e is electron temperature and N_{AR} is argon gas density.

For example, if the T_e of fluorescent lamp is known to be 11000K, and the argon gas density is 10^{23} m^{-3} at particular pressure, thus the estimated v_{col} will be 4000 x 10^6 Hz.

2.3   Experimental measurement

The goal of this measurement is to estimate plasma frequency for the commercially available plasma source. This step is essential prior to begin the research work because only by knowing plasma frequency, the working region can be estimated and the plasma model can be simulated. Once the model is developed, approximation of other parameters such as collision frequency can be made.

2.3.1 Technological preference

One of the main objectives of this research is to implement a low cost and a commercially available plasma source as antenna element. By choosing the compact fluorescent lamp which is normally use in domestic usage, the complexity to build a homemade plasma tube as presented in [8], [9], [32], [33] and [34] can be avoided.

The typical homemade plasma tube is having more flexibility to change the plasma parameters by controlling the excitation power, type of encapsulated gas, pressure of gas and also the density of the gas. However this method requires more complicated experimental apparatus therefore it will increase the complexity and the cost of realizing plasma antenna.

Therefore, in this research work, the fluorescent lamps (FL) are chosen as plasma source. By exploiting the FL and compact fluorescent lamps (CFL) [35], the complexity when dealing with plasma generation could be ignored. Figure 2.9 are the type of fluorescent lamps used during experimental activities.

Figure 2.9 – Compact fluorescent lamps used in the research [35].

The current technology of CFL only requires a simple electronic ballast to generate plasma in dielectric tube and a switch to control its state. Electronic ballast is known to have advantage over traditional magnetic ballast in term of noise control. The internal and external noises are reduced with the use of electronic ballast. Moreover, the bulk size of magnetic ballast and its heavy weight are not the problems if the electronic ballast is used as an alternative.

Other than its low cost and high availability, the FL and CFL allow fast and rapid experimental access. A simple plasma reflector and plasma antenna could be realized with less complexity and in easy way. Yet, optimizations of the design need to be done to give optimum performance. In this research work, the FLs and CFLs with a color temperature is equal to 4000K are used as plasma source [35].

2.3.2 Effect of plasma frequency on electromagnetic wave behaviors

In general, plasma frequency will define the margin of plasma operating region. Based on this region, the frequencies range where the plasma behaves as metal, absorber or even as a lossy dielectric could be estimated. As the electron density is directly related to plasma permittivity, the characteristic of plasma will also change as the density varies. Figure 2.10 shows the complex permittivity of plasma for several plasma frequencies in hertz. These plasma frequencies are represented by electron density of 1.5327×10^9 m^{-3}, 6.1310×10^{17} m^{-3} and 24.5234×10^{17} m^{-3} for the respective frequency of 3.5 GHz, 7 GHz and 14 GHz.

It is worth to remind that plasma is having complex permittivity, where the imaginary part represents losses in the medium and the real part related to energy store in the medium. As the plasma is having some conduction properties at region when the incoming wave frequency is lesser than plasma frequency, it can be used to radiate radio signal in which the signal propagates on a lossy conductor at which the plasma represents. The electrical conductivity of plasma will determine how good is the plasma if it meant to radiate radio signals. In other words, the electrical conductivity of plasma plays a major role whenever plasma is used as a radiator.
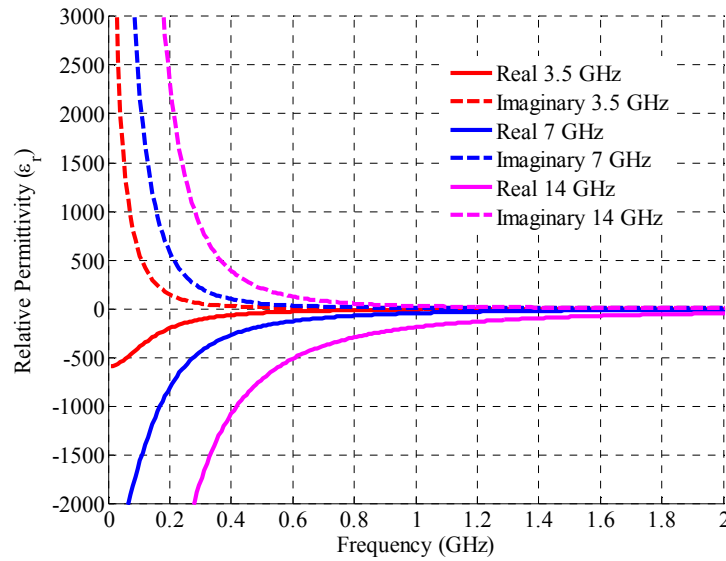
Figure 2.10 – Comparison of plasma complex relative permittivity when the plasma frequency varied and electron-neutral collision frequency is fixed at 900 MHz.

Back again to Figure 2.10, the value of imaginary part of the plasma complex permittivity increases when the operating frequency is decreased. For any case represented in Figure 2.10, as the real permittivity becoming more negative towards lower frequency range, the loss occur in plasma medium will also increase. Therefore it is important to know at what frequency to radiate or to reflect microwave signals. The knowledge of electromagnetic wave behavior towards plasma is very important as the plasma always remains as frequency dependent material. At a region where a transmitting wave interacts as intended with plasma is crucially related to the plasma's conduction properties.

In order to have a quick analysis, let's refer to Eq. 2.30. There are two conditions to better understand the electromagnetic wave propagation in plasma.

a) when the electromagnetic wave frequency is lower than plasma frequency ($\omega < \omega_p$), the relative permittivity is negative value. Thus, the propagation constant turns into imaginary as in Eq. 2.33. Therefore the electromagnetic wave will be reflected as the plasma behaves as conductor with low conductivity. If

considering the collisional plasma (Eq. 2.34), the electromagnetic wave could also be absorbed however it is depending on electron-neutral collision frequency.

b) when the plasma frequency is lower than electromagnetic wave frequency ($\omega > \omega_p$), the relative permittivity of plasma becomes positive and the propagation constant is real. Consequently, the plasma having dielectric properties that is electronically controlled. In this case, the electromagnetic waves will penetrate the plasma medium and suffer from losses.

2.3.3 Experimental estimation of plasma frequency

Because of the antenna element is made of the commercially available plasma source, there is no option to change the plasma parameters. In this work, the CFL is produced in the mass numbers and as a result the details about its technical raw data such as gas pressure, gas combination, and electron density are limited and kept confidential. Therefore, this research work has to begin with the characterization of the particular plasma source.

For that reason, experimental approach to estimate and identify plasma parameters such as plasma frequency is required. By knowing the plasma frequency, the other parameter such as electron-neutral collision frequency could be recognized by comparing parametric study and experimental results. Since plasma is frequency dependent material, its characteristics will also vary for every frequency changes.

There are several techniques to characterize plasma in dielectric tube such microwave interferometry [26], [36] that uses single FL tube as shown in Figure 2.11 or a conventional isolation measurement that uses several FL tubes which are arranged in parallel to create plasma wall or plasma slab [37], as illustrated in Figure 2.12 (a).
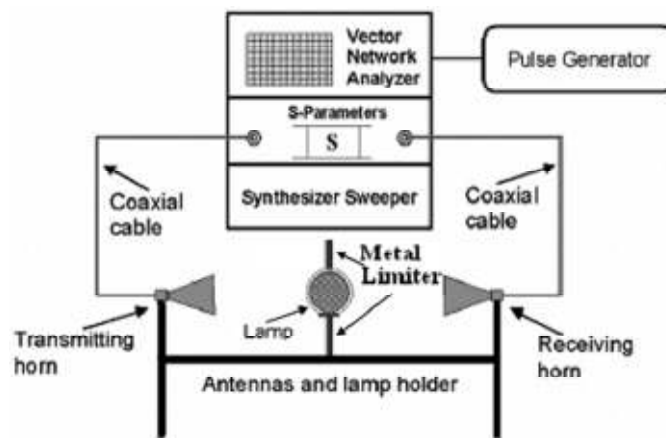
Figure 2.11 – Block diagram of interferometry measurement system [36].

The conventional isolation measurement is easy to conduct and able to give reasonably good and simple diagnostic technique. Therefore, the conventional isolation technique is chosen in this work in order to estimate the working region of plasma. However, the estimation of electron-neutral collision frequency cannot be done with this technique.

2.3.3.1   Measurement setup

In order to find the plasma's working region, isolation measurements were conducted in small anechoic chamber. The measurement equipments consists of a pair of wide band horn antennas (2 GHz -18 GHz), a network analyzer and the devices under test (DUT) that include plasma wall as shown in Figure 2.12 (a) and metal sheets. The technical details of the horn antennas are included in Appendix 2.1. There were two metal sheets used during measurement which are slotted metal sheet as shown in Figure 2.12 (b), and a complete metal sheet with the similar dimension.

(a) *(b)*
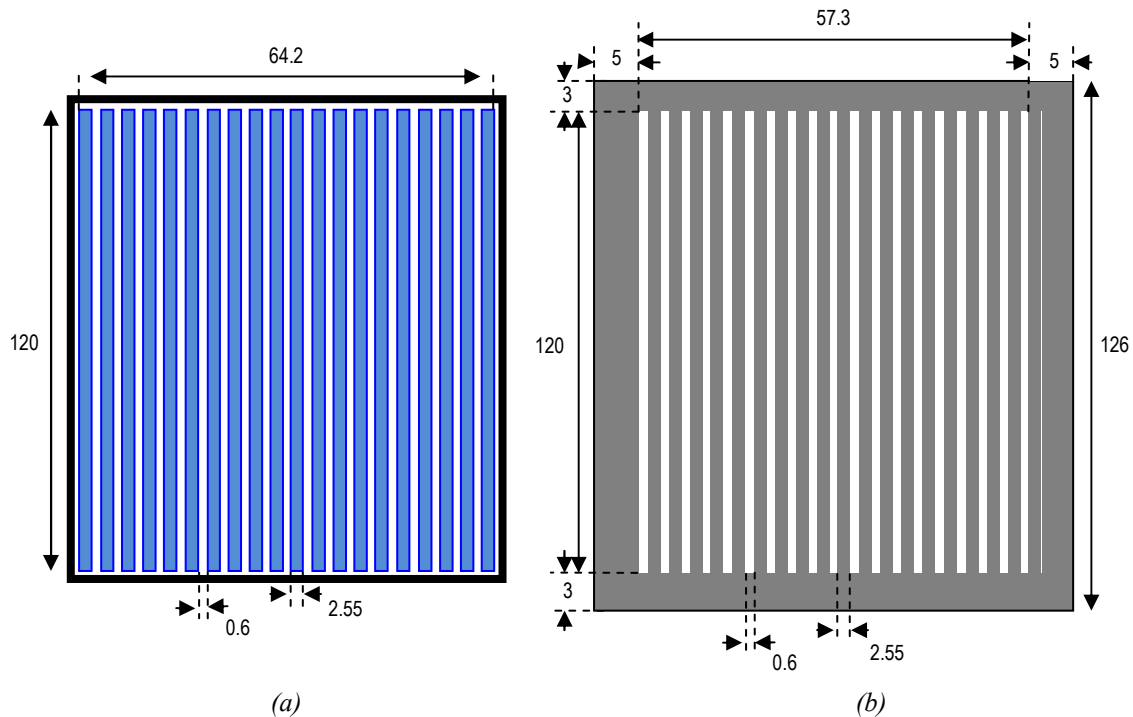
Figure 2.12 – Schematic diagrams of the devices under test (DUT). (a) Plasma wall made of 20 fluorescent lamps arranged in parallel (blue color represents fluorescent lamps). (b) Slotted metal sheet. (Unit in cm).

The complete metal and slotted metal sheets were fabricated using aluminum plate with a thickness of 3 cm. Plasma wall was build using fluorescent lamps (4000K color temperature) which are arranged in parallel. The lamp socket is bi-pin G13 and the

lamps are regulated by electronic ballasts. The photograph of the fabricated plasma wall and slotted metal are shown in Figure 2.13.

(a)   (b)
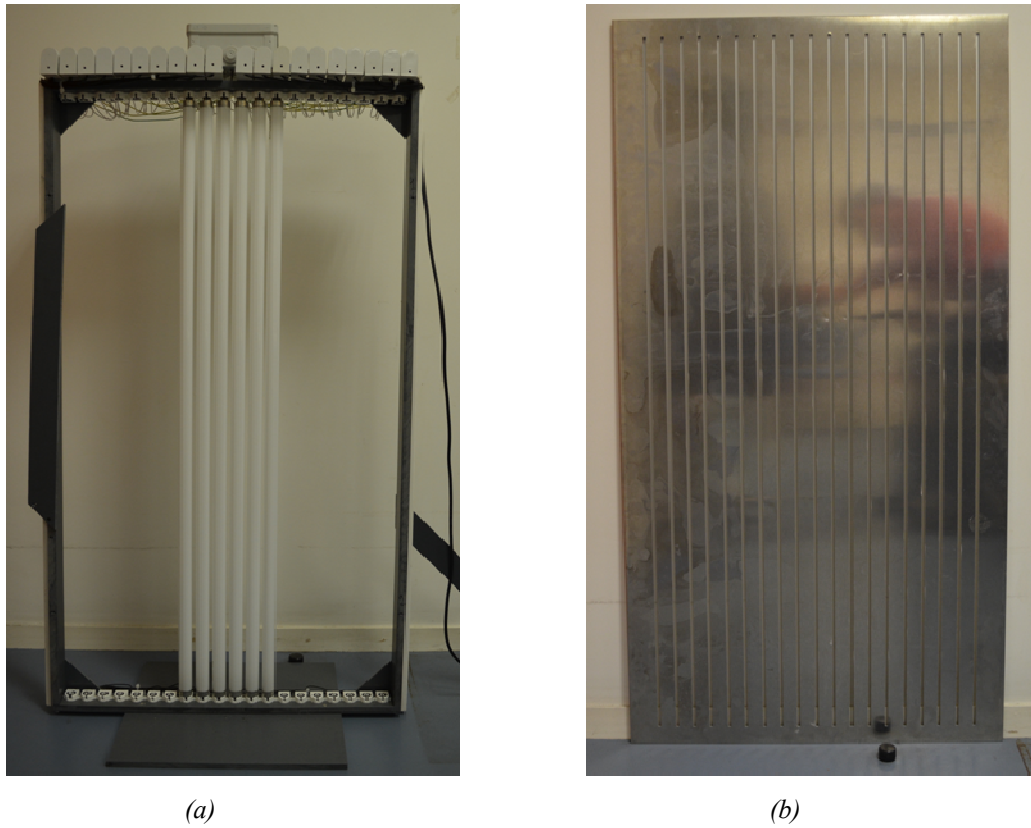
Figure 2.13 – Photographs of the devices under test (DUT). (a) Plasma wall made of 6 fluorescent lamps arranged in parallel (measurements are conducted with 20 fluorescent lamps). (b) Slotted metal sheet.

A similar technique of plasma characterization was conducted as those reported in [37]. The distance between DUT to each of the horn antennas is 1 meter as depicted in Figure 2.14. The horn antennas worked as transmitter and receiver antennas were arranged in vertical polarization. The measurements were conducted for five cases, which are free space, metal sheet, slotted metal sheet, plasma OFF and plasma ON. The slotted metal sheet in Figure 2.13 (b) was fabricated to mimic the plasma wall in Figure 2.13 (a) which is having an air gap between two adjacent fluorescent lamps. The measurements were started with the free space condition as a reference. The measurement results are then compared to understand the plasma characteristics with regard to metal walls, plasma wall and free space cases.
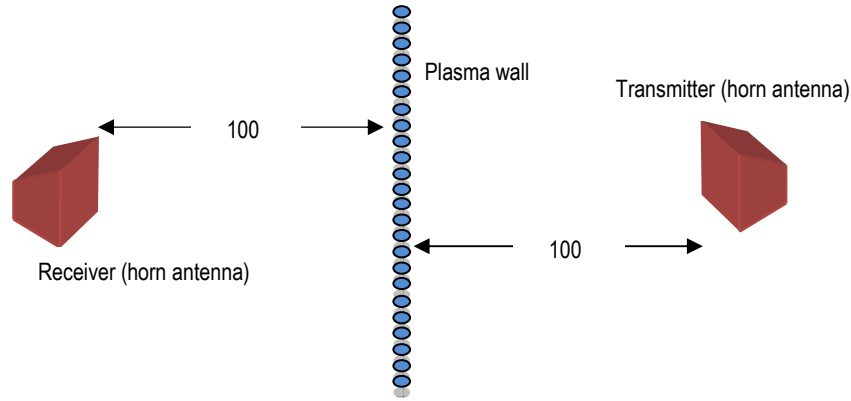
Figure 2.14 – Experiment arrangement with the plasma wall is placed at 100 cm from each of the linear polarized horn antennas. (Unit in cm).

2.3.3.2 Results analysis

The measurement results discussed in this section are based on the two selective cases which are performance of metal isolation and performance of plasma isolation.

Case 1: Metal sheet and metal slots isolation performance

The measurements were conducted for broadband frequency starting from 1.5 GHz up to 18 GHz. However, performances of the horn antennas are only valid from 2 GHz to 18 GHz. As the frequency shifts from low to high, the transmitted signal is suppressed by metal sheet from -45 dB to below -60 dB as depicted in Figure 2.15 (a). For the frequency from 2 GHz until 3 GHz, there are about 15 dB and 30 dB signal suppression with respect to free space case.

(a)

(b)

(c)
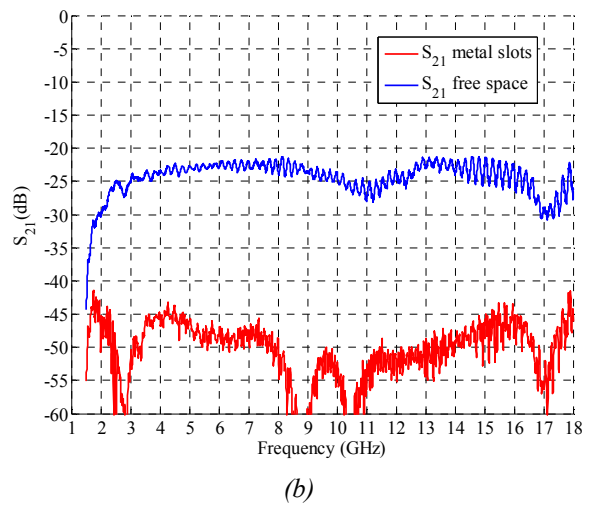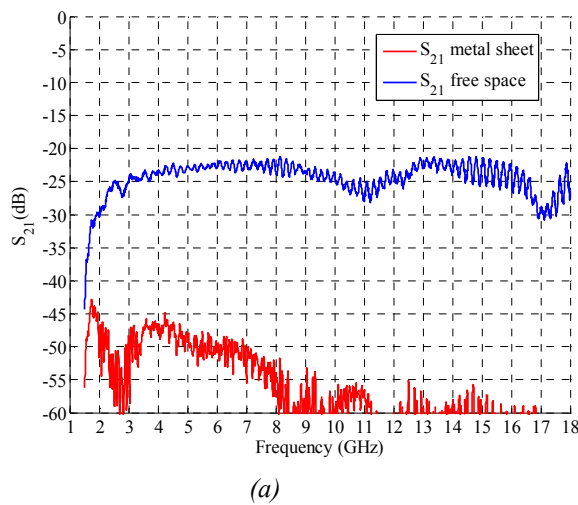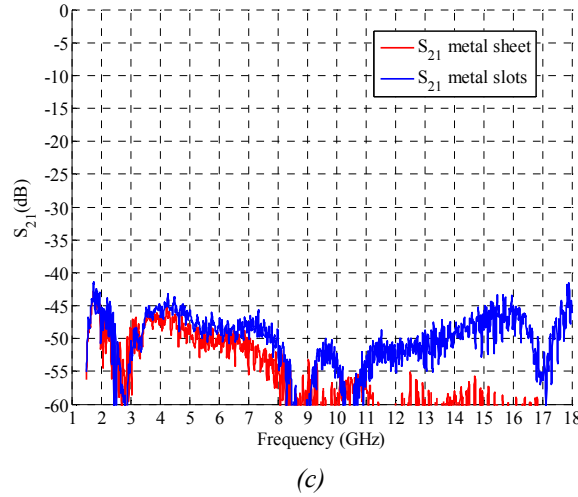
Figure 2.15 – Measured transmission coefficients. (a) Metal sheet versus the free space. (b) Metal slots versus the free space. (c) Metal sheet versus slotted metal sheet.

When the metal sheet is replaced by a slotted metal sheet, the similar pattern can be seen up to 9 GHz, as shown in Figure 2.15 (b). However when the frequency is exceeding 11 GHz, the metal slot seems to permit the signal to pass through its air gap therefore the magnitude of S_{21} starts to increase. This is due to the decreasing size of wavelength with the increment of frequency. Comparison between metal sheet and metal slot as shown in Figure 2.15 (c) also demonstrates that the transmitted signal is able to reach the receiving antenna with the aid of metal slot starting from 11 GHz.

Case 2: Plasma isolation performance

At each time the plasma is de-activated, its isolation performance have similar pattern with free space case as shown in Figure 2.16 (a). This similarity proves that the dielectric tubes used to encapsulate the noble gas has no major effect on electromagnetic waves when the frequency is increasing from 2 GHz to 18 GHz. However when the plasma is activated, there are attenuation effects at region below than 7 GHz and at region upper than 8.8 GHz as shown in Figure 2.16 (b).

Figure 2.16 (b) also shows a region where the behavior of plasma is changing from reflector to dielectric. This important transition occurs starting from 7 GHz to 8.8 GHz in which the transmitted signal can propagate through plasma when the frequency is exceeding 8.8 GHz. To prove that the plasma is exhibiting dielectric properties, it is good to compare Figure 2.16 (b) with Figure 2.15 (b). The S_{21} of plasma wall is higher than the S_{21} of slotted metal sheet, where the plasma wall is having S_{21} approximately higher than -35 dB from 9 GHz onwards, while below -50 dB for slotted metal sheet. The increment of S_{21} of slotted metal sheet more than -50 dB seen after 14 GHz (Figure 2.15 (b)) is mainly due to the wavelength's size relative to size of the air gap.

35
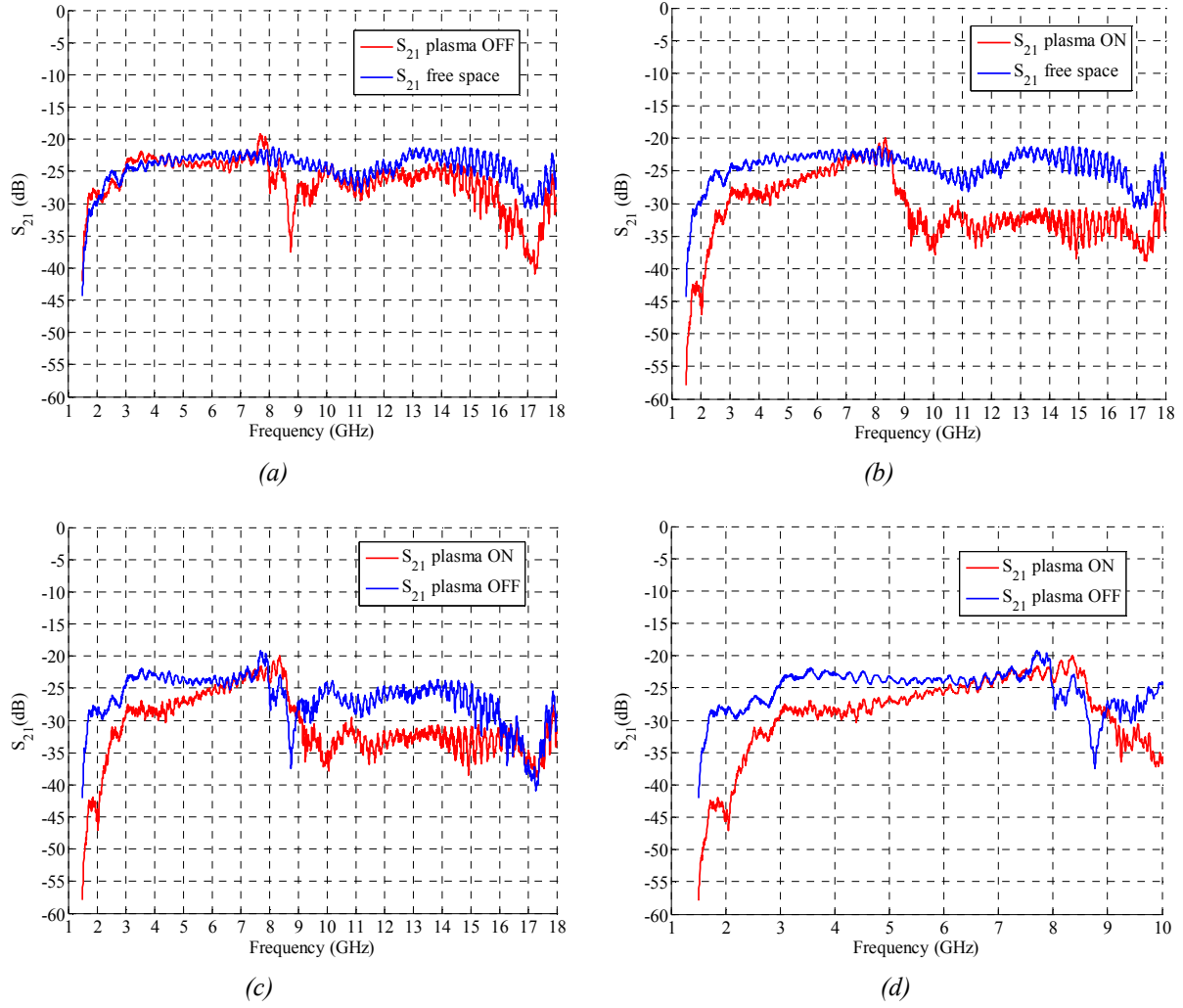
Figure 2.16 – Measured transmission coefficients. (a) Plasma OFF versus the free space. (b) Plasma ON versus the free space. (c) Plasma ON versus plasma OFF. (d) A close look for plasma ON versus plasma OFF.

As mentioned in [26], at the point where the transmitting frequency is higher than plasma frequency, the propagation is cutoff and something can be learned about the plasma. Since the transmitted frequency is known, the plasma density could be measured experimentally at the instant of cutoff. Region where the permittivity is below than unity, the plasma is presumed to have properties of metal.

In this work, we estimate the propagation is cutoff somewhere in the transition region (7 GHz to 9 GHz, Figure 2.16 (c)) where plasma changes it behavior from metal to dielectric. However, this work is focusing at the region where the plasma having negative permittivity as it behaves as metal with low conductivity. Figure 2.16 (d) shows the close look for the region below than 7 GHz which is more interesting to study. From 2 GHz to 2.5 GHz, the isolation between free space and activated plasma is between 8 dB and 15 dB, and with the maximum difference occur at 2 GHz.

To conclude, by referring to the experimental results, the plasma frequency is estimated occurring somewhere from 7 GHz to 9 GHz (Figure 2.16 (d)) and to get an approximation, the 7 GHz is estimated for the plasma frequency in this research work.

2.3.4 Estimation of electron-neutral collision frequency

In order to calculate approximated value of electron-neutral collision frequency, an experimental approach is needed. Complex permittivity that defines plasma characteristics varies with electron-neutral collision frequency. As an example, three values of electron-neutral collision frequency which having different complex permittivity graph curves are shown in Figure 2.17. The real permittivity is related to the energy stored in the medium while the imaginary permittivity is related to the dissipation or loss in the medium. For these particular cases, for a low collision frequency (100 MHz), the loss in plasma is negligible. However when the collision frequency is increased to 900 MHz, a vast loss occurs in plasma. As the collision frequency is amplified to 1700 MHz, there is no coherent difference in loss seen in the plasma. Therefore it is quite complex to define a model of plasma as its parameters are time and frequency dependent. However, since the loss in plasma is only manifest in the lower frequencies range as shown in Figure 2.17, the high frequencies range may have not be affected by the loss due to the electron-neutral phenomenon.
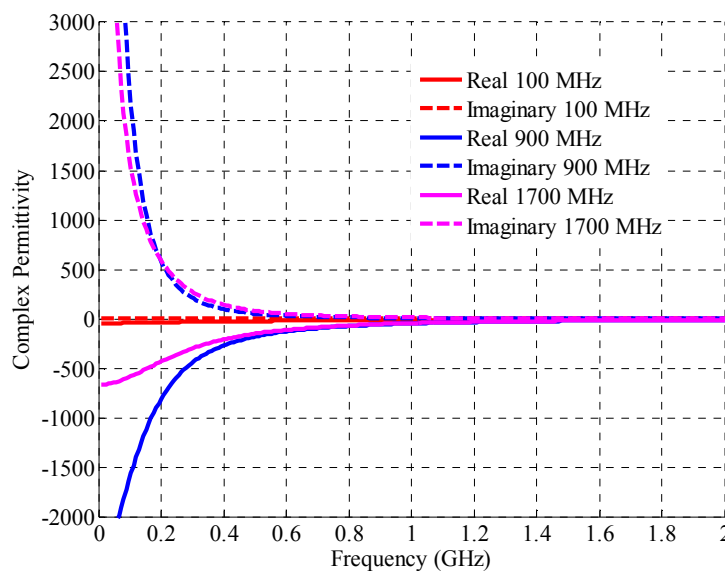
Figure 2.17 – Curve patterns of plasma complex permittivity for three different values of electron-neutral collision frequency (100 MHz, 900 MHz and 1700 MHz respectively). The plasma frequency is 7 GHz.

Yet, an experimental approach can be taken to start a process of estimating these parameters and to verify the loss sensitivity of the plasma throughout the frequency range seen in Figure 2.17. For that reason, in the beginning of this study, we aim to compare the measured and the simulated radiation patterns of the antenna as illustrated in Figure 2.18. By doing so, an estimation value of electron-neutral collision frequency can be made.

2.3.4.1   Measurement setup

A CFL with a physical height is equal to 40 mm from ground plane is expected to reflect electromagnetic wave radiated by a monopole antenna as illustrated in Figure 2.18. The distance between CFL's surface and central monopole antenna resonating at 4 GHz is 0.25λ.
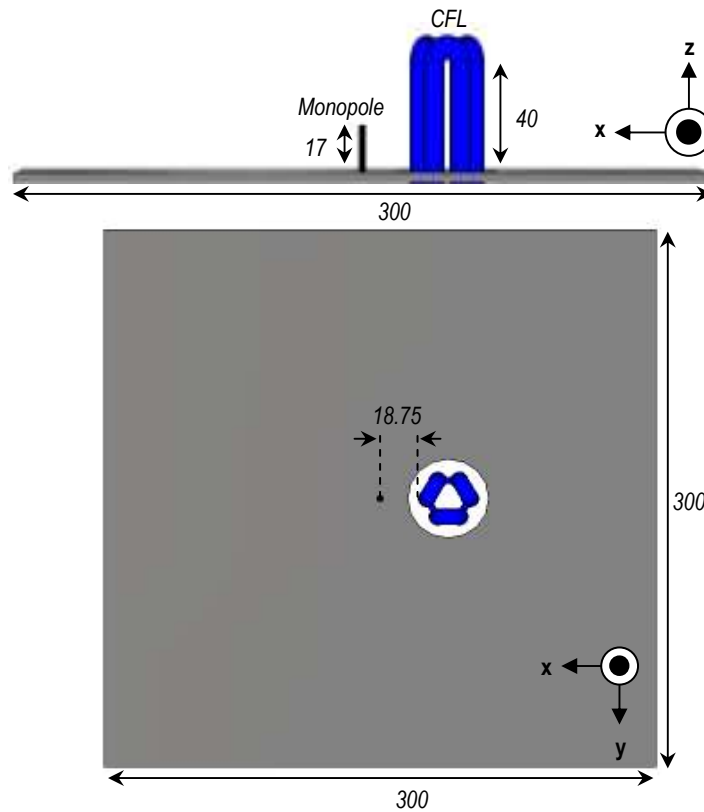
Figure 2.18 – Schematic diagram of antenna used for the radiation pattern measurement. (Unit in mm).

The monopole height is 17 mm and the ground plane dimension is 4λ x 4λ with a thickness of 3 mm. The frequency is swept from 1.5 GHz to 5.5 GHz to observe the evolution of radiation patterns. The measurements were conducted in Stargate 32 SATIMO anechoic chamber.

2.3.4.2 Result analysis

The radiation patterns are compared between measurement and simulation. The simulated model (CST software) is defined with plasma angular frequency equals 43.9823 $\times 10^9$ rad/s and electron-neutral-collision frequency is equivalent to 900 MHz. The first assumption of the collision frequency is made with regard to the work of G.G. Borg et al. in [38], [39].

The results for frequency 1.5 GHz, 2 GHz, 2.5 GHz and 3 GHz are shown in Figure 2.19, while the results for frequency from 3.5 GHz until 5.5 GHz are shown in Figure 2.20.
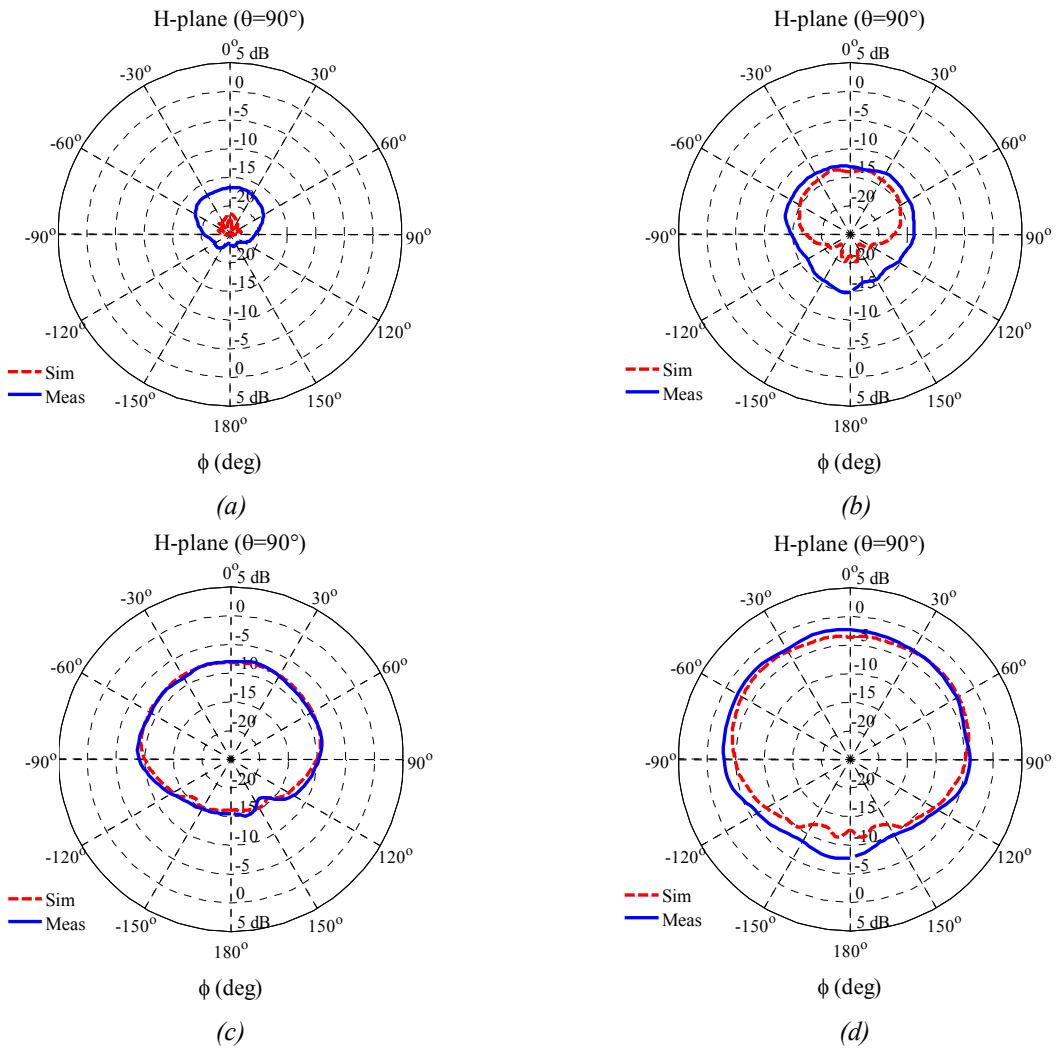
Figure 2.19 – Measured and simulated radiation patterns, E_θ components. (a) 1.5 GHz. (b) 2 GHz. (c) 2.5 GHz. (d) 3 GHz.

In Figure 2.19, the simulated and measured radiation patterns only start to have similar pattern at broadside direction from 2 GHz. The significant dissimilarity observed

in Figure 2.19 (a) is due the high sensitivity of loss in plasma in the lower frequencies range.
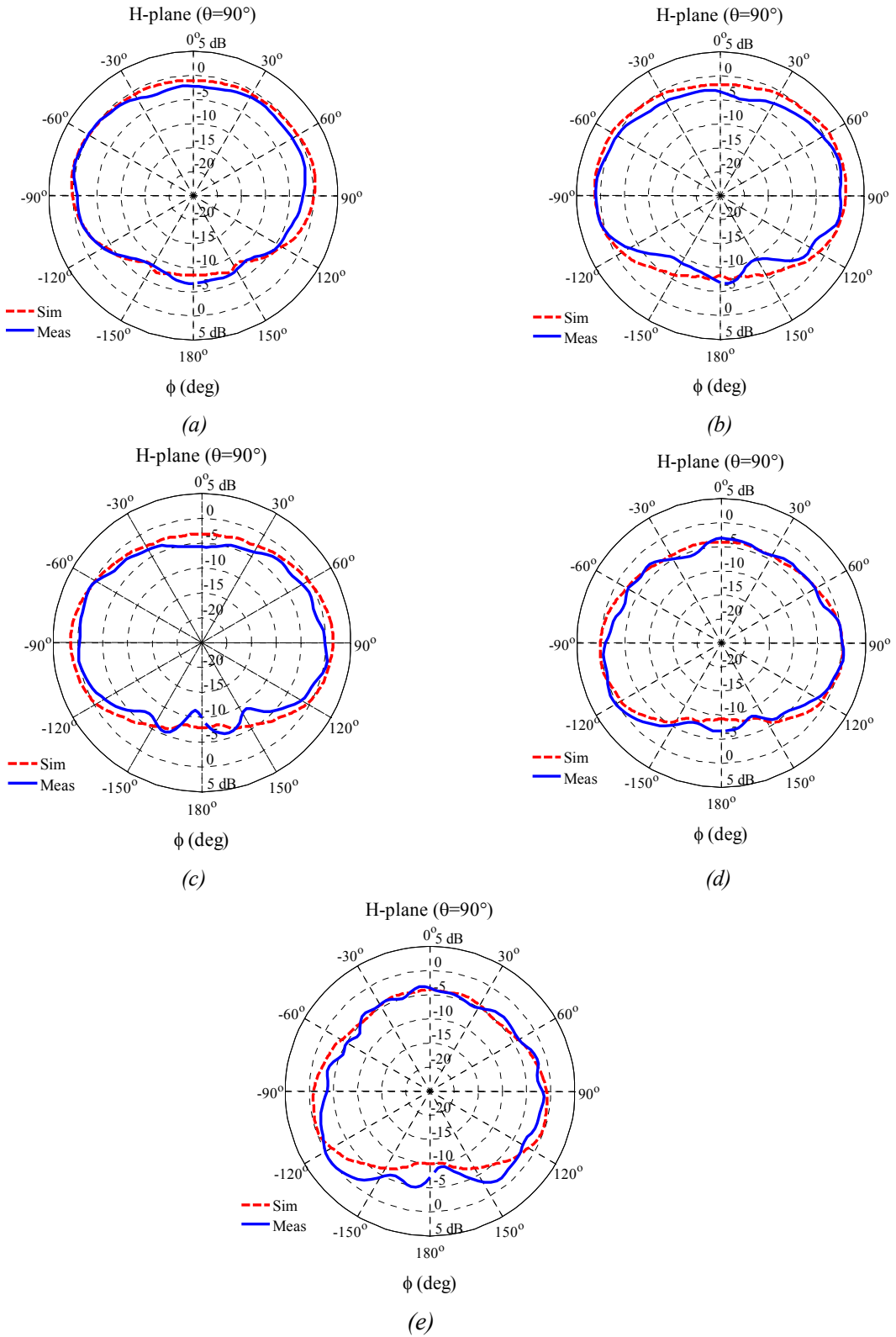
Figure 2.20 – Measured and simulated radiation patterns, E_θ components. (a) 3.5 GHz. (b) 4 GHz. (c) 4.5 GHz. (d) 5 GHz. (e) 5.5 GHz.

In Figure 2.20, the results are remain comparable between simulation and measurement and continue to have similar cardioids shapes until 5.5 GHz. The results also verify that at higher frequencies range (> 1.5 GHz), the loss due to the electron-neutral phenomenon is extremely low. The pattern evolution somehow validates that the plasma which has been modeled in simulation is corresponding to actual plasma source. This is satisfactory to characterize the CFLs in simulation for the frequency starting from 2.0 GHz until 5.5 GHz. The measured and simulated gains are depicted in Figure 2.21. The figure emphasizes that the defined plasma model gives similar gain curve if compared to the measured one.
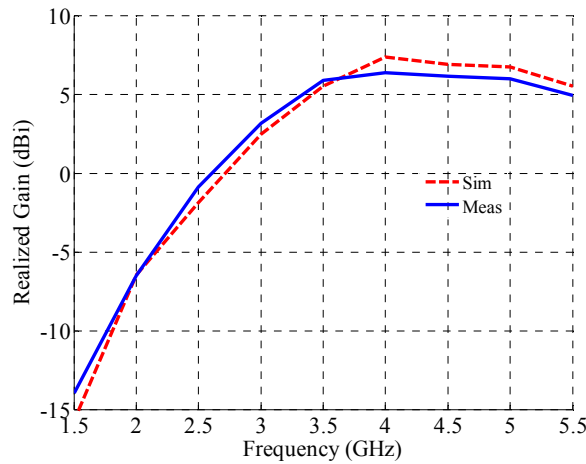
Figure 2.21 – The antenna gain in the maximum beam direction.

Again, as to reassure the correct estimation of electron-neutral collision frequency has been selected. A set of simulations was conducted by varying the value of electron-neutral collision frequency from 100 MHz until 3000 MHz. The results are depicted in Figure 2.22.
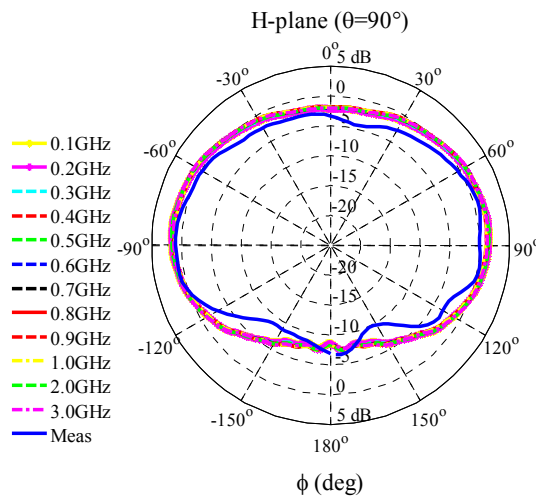
Figure 2.22 – Effect of electron-neutral collision frequency on radiation pattern, E_θ components at 4 GHz.

41

As illustrated in Figure 2.22, the effect of electron-neutral collision frequency on radiation pattern is negligible as the frequency increases from 100 MHz to 3000 MHz. Therefore the plasma model used in the simulations is adequate enough to represent actual plasma source in forecasting radiation pattern of plasma reflector antenna.

2.3.5 Summary of plasma parameters estimation

Based on the isolation experiments, the plasma frequency is anticipated to occur in the frequency region from 7 GHz and to 9 GHz. The transmission of electromagnetic wave in plasma medium is cutoff somewhere in this region and the estimation of the plasma frequency can be made. In order to conclude with one value of plasma frequency, the 7 GHz is estimated for the plasma frequency in this research work since at this frequency the plasma exhibits properties of metallic medium.

The measured and simulation results showed similar radiation patterns at the broadside direction starting from 2 GHz until 5.5 GHz when plasma source is placed near to central monopole antenna resonates at 4 GHz. Therefore, the experimental results have proven that the plasma model developed and used in the simulation is corresponding to actual plasma source when it works as reflector elements and having a good convergence between simulated and measured radiation patterns from 2 GHz up to 5.5 GHz. For the frequency of 1.5 GHz, the dissimilarity between simulated and measured radiation patterns is due to the high sensitivity of loss in plasma which is contributed by electron-collision phenomenon. Another plasma model has to be developed in order to characterize the particular plasma source for lower frequency antennas.

The variation of electron-collision frequency from 100 MHz up to 3000 MHz has no significant effect on reflector radiation patterns. Therefore, the initial value of electron-collision frequency (900 MHz) can be used to model the plasma.

2.4   Conclusion

A brief review of plasma as the fourth state of matters has been discussed in the beginning of this chapter. Series of plasma equations have been derived starting with the single particle motion. Elaboration of plasma equations for the two classifications of plasma which are collision and collisionless plasma was also explained. The cutoff frequency of plasma is very crucial to define plasma working region. As the plasma complex permittivity is also depending on the cutoff and transmitting radio frequencies, it is necessary to estimate the values of these two parameters. Experimental approach

has been taken to get an approximation of plasma cutoff frequency and finally the frequency of 7 GHz is chosen to be plasma frequency for this entire work. As the experiments were conducted with plasma worked as reflector, the model used in simulation can be used to represent the actual plasma source for any reflector configuration. The electron-neutral collision frequency is estimated to be 900 MHz and reassurance steps have been taken by varying its value from 100 MHz to 3000 MHz and the effect of reflector radiation patterns was observed. In conclusion, there is no significant effect occurred and hence the initial value is adequate to represent the actual plasma model. The performance of the defined plasma model for reflector antenna configurations will be explained in the following chapter. The similarity between measured and simulated results will again confirm the defined plasma model.

References

[1]　U. S. Inan, M. Golkowski, "Introduction", Principles of Plasma Physics for Engineers and Scientists, Cambridge University Press, NY: New York, 2011, pp. 1-19.

[2]　G. G. Lister, J. E. Lawler, W. P. Lapatovich, V. A. Godyak, "The physics of discharge lamps," Rev. Mod. Phys., vol. 76, no. 2, pp. 541-598, April 2004.

[3]　A. A. Vedenov, "Solid state plasma", Soviet Physics Uspekhi, vol. 7, no. 6, pp. 809-822, May-June 1965.

[4]　A. K. Jonscher, "Solid state plasma phenomena", Brit. Journal Applied Physics, vol. 15, pp. 365-377, 1964.

[5]　Kimio Suzuki, "Room temperature solid state plasma nonreciprocal microwave devices," IEEE Trans., Electron Devices, vol. ED-16, no. 12, pp. 1018-1021, December 1969.

[6]　I. Alexeff, T. Anderson, S. Parameswaran, E. P. Pradeep, J. Hulloli, P. Hulloli, "Experimental and theoritical results with plasma antennas," IEEE Trans., Plasma Sci., vol. 34, no. 2, pp. 166-172, April 2006.

[7]　T. Anderson, I. Alexeff, N. Karnam, E. P. Pradeep, N. R. Pulasani, J. Peck, "An operating intelligent plasma antenna," IEEE 34th International Conference on Plasma Science (ICOPS 2007), pp. 353-356, 2007.

[8]　M. Chung, W. Chen, B. Huang, C. Chang, K. Ku, Y. Yu, T. Suen, "Capacitive coupling return loss of a new pre-ionized monopole plasma antenna," IEEE Region 10 Conference (TENCON 2007), 2007.

[9]　M. Chung, W.Chen, Y.Yu, Z. Y. Liou, "Properties of DC-biased plasma antenna," International Conference on Microwave and Millimeter Wave Technology (ICMMT 2008), 2008.

[10]　I. Alexeff, T. Anderson, E. Farshi, N. Karnam, N. R. Pulasani, "Recent results of plasma antenna," Phys., Plasmas 15, 057104 (2008).

[11]　V. Kumar, M. Mishra, N. K. Joshi, "Study of a fluorescent tube as plasma antenna," Progress in Electromagnetics Research Letters, vol. 24, pp. 17-26, 2011

[12]　H. M. Zali , M. T. Ali, N. A. Halili, H. Jaafar, I. Pasya, "Study of monopole plasma antenna using fluorescent tube in wirelesss transmission Experiments," IEEE International Symposium on Telecommunication Technologies, pp. 52-55, 2012.

[13]　J. P. Rayner, A. P. Whichello, A. D. Cheetham, "Physically characteristics of plasma antennas," IEEE Trans., Plasma Sci., vol. 32, no. 1, pp. 269-281, Feb 2004.

[14]　G. Cerri, R. De Leo, V. Mariani Primiani, P. Russo, "Measurement of the properties of a plasma column used as a radiating element," IEEE Trans., Instrum., Meas., vol. 57, no. 2, pp. 242-247, Feb. 2008.

[15]　P. Russo, G. Cerri, R. De Leo, E. Vecchioni, "Self-consistent analysis of cylindrical plasma antenna," IEEE Trans., Antennas Propag., vol. 59, no. 5, pp. 1503-1511, May 2011.

[16]　G. G. Lister, M. Cox, "Modeling of inductively coupled discharges with internal and external coils," Plasma Sources Sci. Technol. 1, pp. 67-73, 1992.

[17]　G. Cerri, R. De Leo, V. M. Primiani, P. Russo, E. Vecchioni, "2.45 GHz waveguide plasma generation in cylindrical structures," The International Microwave Symposium Digest (IMS), pp. 1032-1035, 2010.

[18]　P. Russo, V. M. Primiani, G. Cerri, R. De Leo, E. Vecchioni, "Experimental characterization of a surfaguide fed plasma antenna," IEEE Trans. . Antennas Propag., vol. 59, no. 2, pp. 425-433, Feb. 2011.

[19] P. Russo, G. Cerri, E. Vecchioni, "Self-consistent model for the characterization of plasma ignition by propagation of an electromagnetic wave to be used for plasma antennas design," IET Micro., Antennas Propag., vol. 4, Iss. 12, pp. 2256-2264, 2010.

[20] P. Russo, G. Cerri, R. De Leo, E. Vecchioni, "Self-consistent analysis of cylindrical plasma antenna," IEEE Trans., Antennas Propag., vol. 59, no. 5, pp. 1503-1511, May 2011.

[21] M. Moisan, Z. Zakrzewski, R. Pantel, P. Leprince, "A waveguide-based launcher to sustain long plasma columns through the propagation of an electromagnetic surface wave," IEEE Trans., Plasma Sci., vol. no. 3, pp. 203-214, Sept. 1984.

[22] M. Alshershby, J. Lin, "Reconfigurable plasma antenna produced in air by laser-induced filaments: passive radar application," The International Conference on Optoelectronics and Microelectronics, pp. 364-370, Aug. 2012.

[23] 3D EM field simulation-CST computer simulation technology, Available at: http://www.cst.com. Accessed October 1, 2010.

[24] G. Cerri, R. De Leo, V. Mariani Primiani, P. Russo, "Measurement of the properties of a plasma column used as a radiating element," IEEE Trans., Instrum., Meas., vol. 57, no. 2, pp. 242-247, Feb. 2008.

[25] N. A. Halili, M. T. Ali, H. M. Zali, H. Jaafar, I. Pasya, "A study on plasma antenna characteristics with different gases," IEEE International Symposium on Telecommunication Technologies, pp. 56-59, 2012.

[26] J. L. Shohet, "The motion of isolated charged particles," in The Plasma State, Academic Press, Inc., NY: New York, 1971, pp. 39-66.

[27] Matthew N. O. Sadiku, "Magnetic forces, materials, and devices," in Elements of Electromagnetics 4th Edition, Oxford, NY: New York, 2007, pp.270-320.

[28] R. F. Tigrek, "An investigation on plasma antennas," Thesis Middle East Technical University, Ankara, Turkey, August 2005.

[29] G. G. Lister, "Low-pressure gas discharge modeling," J. Phys. D. Appl. Phys. 25 (1992) pp. 1649-1680, 1992.

[30] M. H. Elghazaly, S. Solyman, A. M. Abdel Baky, "Study of some basic transport coefficients in noble-gas discharges plasmas," Egypt. J. Solids, vol. 30, no. 1, pp. 137-149, 2007.

[31] P. Baille, J. Chang, A. Claude, R. M. Hobson, G. L. Ogram, A. W. Yau, "Effective collision frequency of electrons in noble gases," J. Phys. B. AT. Mol. Phys. 14 (1981), pp. 1485-1495, 1981.

[32] A. E. Robson, R. L. Morgan, R. A. Meger, "Demonstration of a plasma mirror for microwaves," IEEE Trans., Plasma Sci., vol. 20, no. 6, pp. 1036-1040, December 1992.

[33] R. Kumar, D. Bora, "Experimental investigation of different structures of a radio frequency produced plasma medium," Phys., Plasmas 17, 043503 (2010).

[34] R. Kumar, D. Bora, "Wireless communication capability of a reconfigurable plasma antenna," J., Appl., Phys. 109, 063303 (2011).

[35] Inspiring lighting solutions-Sylvania lighting solutions. Available at: http://www.havells-sylvania.com/en/products/0025902. Accessed December 1, 2011

[36] M. K. Howlader, Y. Yang, J. R. Roth, "Time-resolved measurement of electron number density and collision frequency for a fluorescent lamp plasma using microwave diagnostics," IEEE Trans. Plasma Sci., vol. 33, no. 3, pp. 1093-1099, June 2005.

[37] W. J. Vogel, H. Ling, G. W. Torrence, "Fluorescent light interaction with personal communication signals," IEEE Trans., Comm., vol. 43, no. 2/3/4, pp. 194-197, February, March, April 1995.

[38] G. Borg, J. H. Harris, "Application of plasma columns to radiofrequency antennas," Appl., Phys., Lett., vol. 74, no. 22, May 1999.

[39] G. G. Borg, J. H. Harris, N. M. Martin, D. Thorncraft, R. Miliken, D. G. Miljak, B. Kwan, T. Ng, J. Kircher, "An investigation of the properties and applications of plasma antennas," Switzerland-Millenium Conference on Antennas and Propagation Davos, April 2000.

Appendix 2.1

IDEAS ENGINEERED

Q-par Angus Ltd
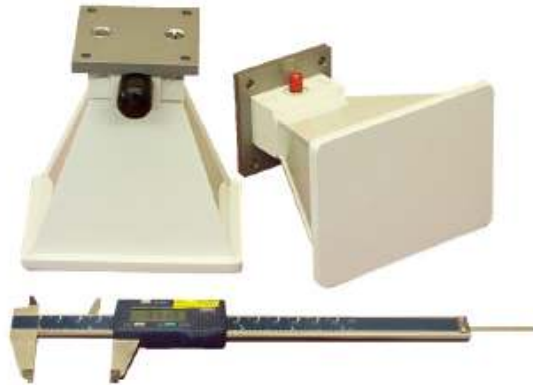
2 - 18 GHz Wide Band Antenna

Model Number WBH2-18N/S

This compact, high performance ridged waveguide horn model number WBH2-18N (Type N), or WBH2-18S (SMA) is ideal for EMI/RFI testing, EMC measurements, wide band surveillance, materials evaluation etc. The high gain and low VSWR over a wide frequency band make the antenna ideal for receiving low level signals or for transmitting moderate power levels.

Techniques have been incorporated to prevent higher order waveguide modes. The horn may be mounted in a parabolic reflector to increase directional resolution and gain.

Extended frequency range 2 to 24.5 GHz, Model Number WBH2-24S, & extra high gain, model number WBH2-18HN/S are also available, see pages 11 - 13, and 14 - 16 for further details.

Designed and Manufactured in England to the highest standards

Q-par Angus Ltd
Barons Cross Laboratories
Leominster
Herefordshire
HR6 8RS   UK

tel   +44 (0) 1568 612138
fax   +44 (0) 1568 616373
web   www.q-par.com
e-mail   sales@q-par.com

UKAS

INVESTOR IN PEOPLE

IDEAS ENGINEERED

Q-par Angus Ltd

SPECIFICATION
Model Number WBH2-18N/S

Frequency	2 - 18 GHz
Nominal Gain	7 - 13 dBi across the band
Nominal Beamwidth	19 - 86 degrees (3 dB)
VSWR	< 2.5 :1
Cross Polar	< -20 dB
Power Handling	50 Watts c.w. N, 20 Watts c.w. SMA
Construction	Metal/Glass-Resin composite
Dimensions	119 mm x 86 mm x 119 mm long
Connector	N Type or SMA (others available)
Weight	420g N, 370g SMA (including Mount Plate)
Temperature	-40 C - +70 C

GAIN TABLE

Frequency (GHz)	Gain (dBi)
2.0	7
4.0	10
6.0	10
8.0	10
10.0	11
12.0	13
14.0	13
16.0	13
18.0	10

Designed and Manufactured in England to the highest standards

Chapter 3

Reconfigurable reflector antenna

The chapter aims to discuss and explain the use of plasma as reflecting elements. The state of the art of reflector antennas is presented in the first part of this chapter. Mainly brief reviews cover on reflector antennas used for beam steering and shaping or even as a method for scanning. The reflector antennas were constructed by using metallic elements along with active devices. These active devices were employed to provide switching mechanism in order for the antennas to steer beam in particular directions. A review on corner reflector antennas which are meant to be used to reflect incoming beams in forward direction are given in details. The reflector antennas are very simple but can be used to replace other type of reflectors which are more complex in design to have comparable performance. The state of the art section is ended with a review of several works on plasma (naturally available material that comes with negative permittivity) used to reflect, to steer and to shape incoming beam such as plasma mirror. The second part of this presents a new design of plasma round reflector antenna (RRA) to steer, to shape and to do scanning beam in the ISM band. Prior to that, several RRA designs were proposed and their simulated performances were compared in order to select the final one. The final design has undergone optimization process prior to its fabrication. The measured results are presented along with its corresponding simulated ones. The optimized RRA exhibits good performances at 2.4 GHz and even better if compared to the wire circular monopole antenna array (as been reviewed in previous part of this chapter). A novel design of corner reflector antenna (CRA) using plasma medium is presented in the third part of this chapter. Two corner reflector antennas (CRA1 and CRA2) were fabricated on a single finite ground plane to offer extra flexibility that cannot or never been offered by any other classical CRA. Several configurations of CRA were measured and simulated in order to prove that the CRA is workable at 2.4 GHz. Finally, a conclusion is drawn based on the works done and the results of the fabricated RRA and CRA prototypes.

3.1 State of the art

In recent years, there has been an increasingly interest in plasma exploitation mainly in communication systems where the plasma is implemented as antenna element. The capability and flexibility of plasma have attracted many attentions thus accelerating the study of plasma as one of candidates in order to replace metal elements. A considerable amount of literature on plasma has been published since 1960s and to date; the number of publications has increased tremendously, especially within the five years back.

However, the literature only covers the usage of plasma as radiator to replace metallic radiator. Plasma is freely defined and can be developed to suite special purpose. Still this is only true for physics laboratories where the plasma characterization can be done and plasma parameters can be altered regarding their applications. Anybody can imagines how complex physics laboratory would be and as a result, many works were conducted since then by using the commercially available plasma source such as fluorescent lamps and its compact version. Since each of the existing plasma sources has their own parameters' values and the way plasma behaves is highly dependent on its parameters, it is quite difficult to model precisely plasma without first measuring the particular plasma source. Therefore the characterization of particular plasma source as mentioned and explained in previous chapter is extremely essential.

On the other hand, the hurdles to deal with plasma have not able to stop research interest on the plasma and yet has became a reason for other ideas to be expanded so as to enable implementation of plasma in communication systems which never been imagined before. To simplify, this section aims to review the use of plasma as reflecting elements to suite several applications such as beam steering, scanning and beam shaping. Prior to that, a brief review of other techniques using metallic elements to obtain the similar purposes is presented. Since the investigation work includes plasma corner reflector antenna, a review on corner reflector antennas using wire grid and metallic surfaces are also discussed.

3.1.1 Reviews of antennas for beam steering, beam scanning and beam shaping using metallic medium in printed technology

This part is focusing on the published works that used other than plasma medium in order to design antennas that are capable to steer, to shape incoming beams. On the whole, there are many design of antennas are meant for these capabilities, however this section is aimed to review only on the printed technology.

3.1.1.1   Beam steering and beam scanning antenna

In certain communication systems' applications, capability of the antennas to steer and to scan beam at particular direction has became essential nowadays. For example, the space communication systems that always working at higher frequencies such in the inter-satellite communications, close proximity data links, the indoor communications with high bit rates, or even the upcoming Wifi with data transfer rates of up to Gb/s may require antennas with diversity in their beam pattern characteristics. There are many techniques which can be adopted to realize this diversity. One of these techniques

is the printed antenna technology that uses either leaky wave [1], BSML [2] or even the double loop [3]. Lens antenna is also an option to have these capabilities as those reported in [4] and [5]. Recently, beam scanning antenna based on metamaterial planar lens was proposed in [6]. Other than the lens antennas, phase shifters along with MEMs switches are also an alternative to steer and scanning beam as presented in [7] and not to forget the advanced liquid crystal technology (LCD) has also been explored to steer beam and was presented in [8]. Even though the techniques in achieving diversity in communication systems becoming more advance and complex, occasionally, the conventional mechanical technique is enough to provide good output as those reported in [9]. Photograph of leaky wave antenna and microstrip crank-line antenna with moveable dielectric plate that have been proposed in literatures are shown in Figure 3.1 (a) and Figure 3.1 (b) respectively.

(a)   *(b)*
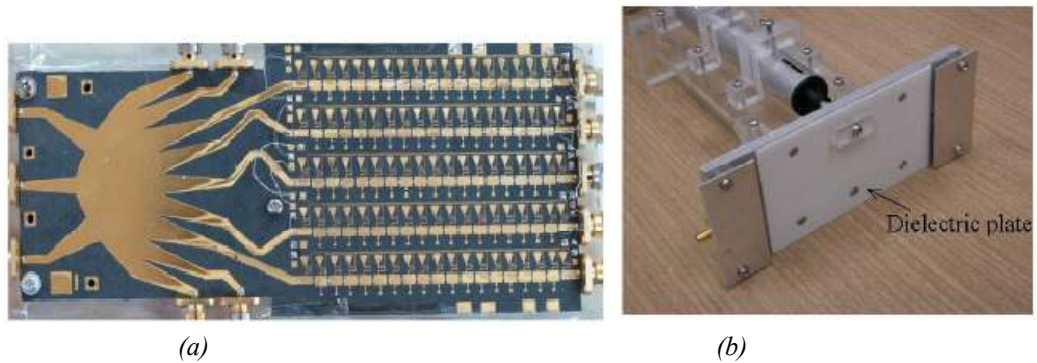
Figure 3.1– Photograph of fabricated antennas for beam steering and beam scanning. (a) Leaky wave antennas (LWA) with Rotman lens [1]. (b) Microstrip crank-line antennas covered with moveable dielectric plate at 20 GHz [9].
.

When it comes to low profile, low cost, low weight and easy to fabricate, microstrip based antennas are the ultimate choice for applications within low microwave frequencies such as the ISM band frequency, 5.85 GHz and 2.4 GHz. There are many antenna designs that use this technology to steer a beam or even to do beam scanning. This includes a novel beam steering leaky-wave antenna that uses reactive loading capacitor along the leaky line as presented in [10]. A prototype was constructed, tested and exhibited a beam scanning angle of 23°. This is obtained by periodically loading a leaky line with 0.06527 pF capacitors at 4 GHz. By replacing the capacitors with varactors diode, an angle of 13° of beam steering can be established.

For 5.8 GHz applications, active elements such varactor diode [11], PIN diode [12], variable reactance [13], or even the ESPAR that contains active and passive elements [14], [15] are among popular available choices to add extra functions on antenna to steer and scan beams or to shape the beam [12]. Figure 3.2 shows a long periodic slots loaded leaky wave antenna and its radiation pattern [14].

(a) *(b)*
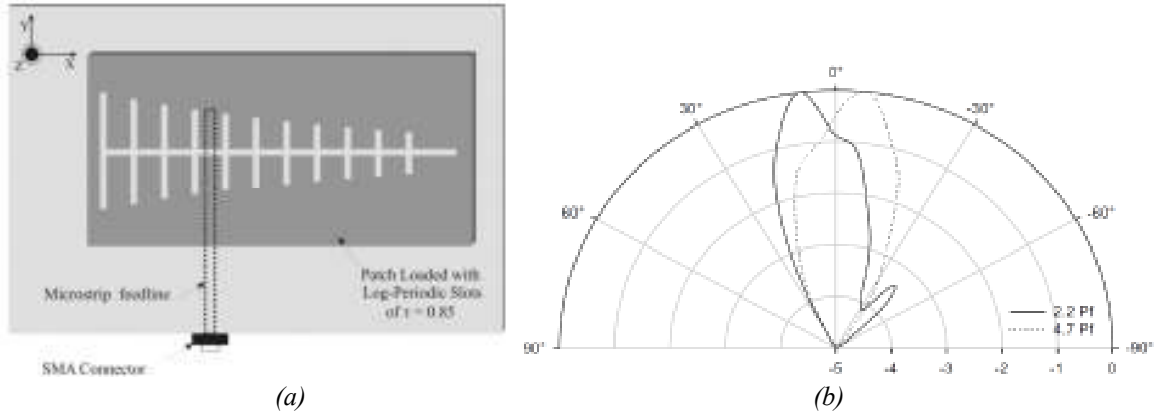
Figure 3.2– Beam steering antenna. (a) Geometry of proposed Log Periodic Slots loaded Leaky-wave antenna. (b) Experimental H-plane radiation pattern with metal-insulator-metal (MIM) capacitors (2.2 pF and 4.7 pF) at 5.4 GHz [14].

The design has been implemented and hence proving that, passive component can be modified with varactor diodes for beam steering by appropriate DC bias. The fabricated antenna exhibits a maximum scanning angle of 45° and beam steering of 15° at a fixed frequency (5.4 GHz) when the capacitor changes its value from 2.2 pF to 4.7 pF. Other microstrip based antennas that able to steer incoming beam for 2.4 GHz applications in the previous works including passive beam steering reported in [16], [17] and a miniature antenna that used RF switches reported in [18].

The use of parasitic elements to provide a sector beam steering was proposed in [19] for wireless ad-hoc communications. The details of the structure and dimension of quartered-beam switchable antenna are illustrated in Figure 3.3.
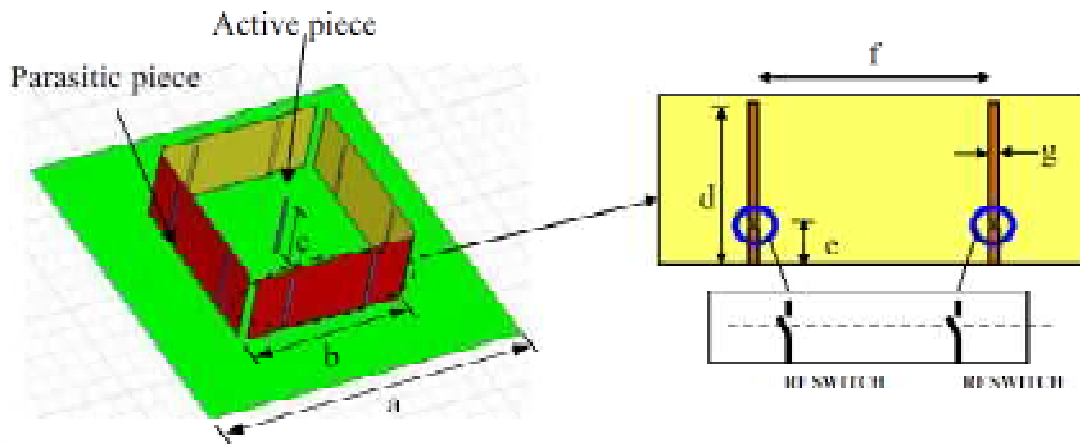
Figure 3.3 – Quartered-beam switchable antenna structure operating at 2.4 GHz. The dimensions are; a= 150, b = 80, c = 27.5, d = 28, e = 5, f = 40, and g = 2 (Unit in mm) [19].

The antenna consists of one active element surrounded by eight parasitic elements on a finite ground plane. These parasitic elements are switched to be short or open to act like a corner reflector for beam shaping and steering. The gain in the E-plane is 8.2 dBi

and gain in the H-plane is 5.6 dBi with HPBW equivalent to 82°. Figure 3.34 shows the radiation patterns of the antenna in the E- and H- planes.

(a)   *(b)*
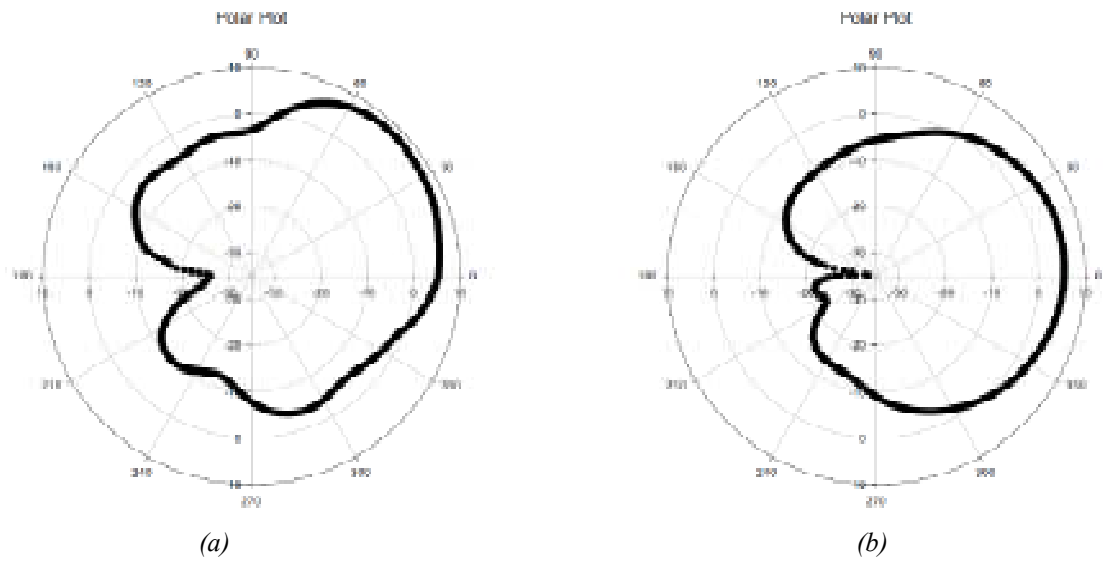
Figure 3.4 – Radiation pattern of the antenna at 2.4 GHz. (a) The E-plane radiation pattern reveals a gain of 8.2 dBi. (b) The E-plane radiation pattern reveals a gain of 5.6 dBi [19].

One way to achieve beam steering without the use of active devices was presented in [20]. The beam steering antenna was based on parasitic layer operating at 5.6 GHz. The schematic diagram of the antenna is depicted in Figure 3.5.
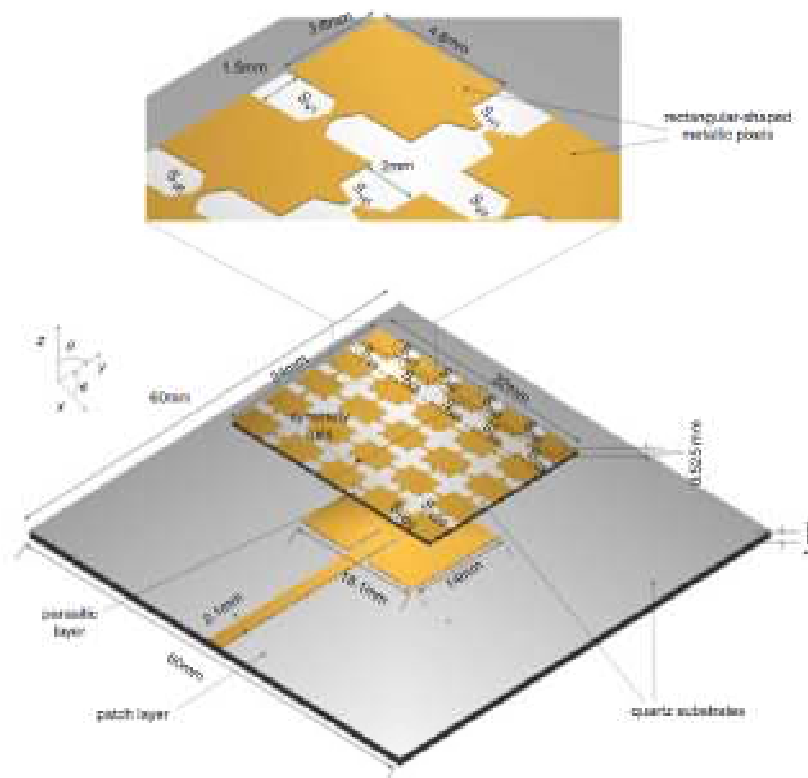
Figure 3.5 – 3D schematic of beam-steering antenna [20].

The steer ability of the antenna is within -30° to +30° with three main directions. The antenna structure consists of a driven microstrip-fed patch element and a parasitic layer located on top off the driven patch. The measured maximum azimuthal gain is around 8 dBi.

Other types of beam steering antennas have been reported for 900 MHz in [21] and 5.8 GHz applications in [22], [23]. These antennas were designed for wearable antenna applications. Figure 3.6 shows a wearable antenna with beam steering and its simulated radiation pattern at 900 MHz.

(a)   *(b)*
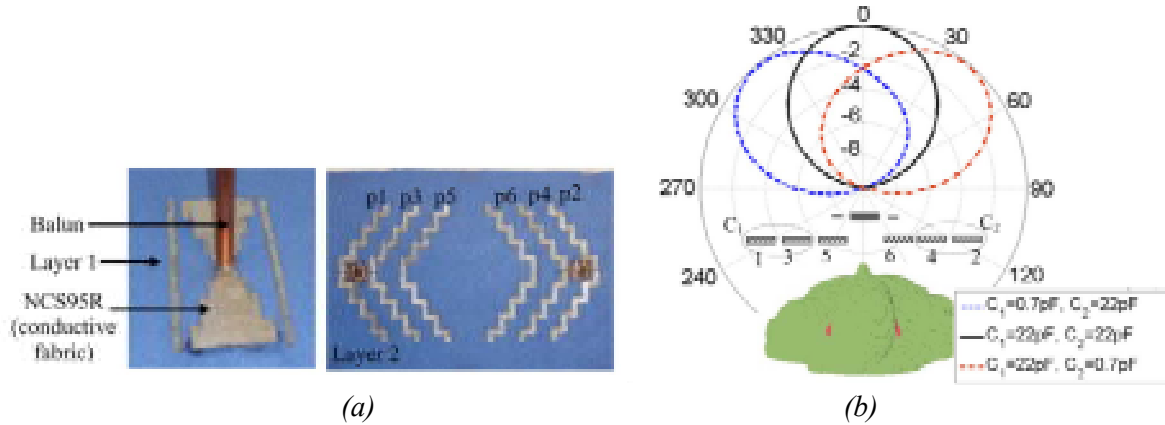
Figure 3.6 – Beam steering parasitic antenna. (a) Fabricated antenna on conductive fabric. (b) Simulated radiation patterns of the proposed parasitic array next to a human body model for several capacitance combinations [21].

The antenna consists of parasitic dipoles (p1 - p6) fabricated on the layer 2 and a driven dipole on the layer 1. The parasitic dipoles are connected to varactor diodes, C_1 (p1 and p3) and C_2 (p2 and p4) which provide variable capacitance. By controlling these capacitances and the distance between the driven and the parasitic dipoles, the induce current in the parasitic elements can be control thus controlling the beam direction. The shorted parasitic dipoles p5 and p6 can be used to improve array directivity.

3.1.1.2 Beam shaping antenna

An array of driven elements is one of several ways of achieving beam shaping. In 2005, this technique was proposed and presented in [24] using four-element dipole array. The antenna was proposed to work at 5.2 GHz. Another N-element monopole array was studied and presented in [25]. Instead of dipole, monopoles were employed thus reducing the physical size of the antenna. The 6-element monopole array was fabricated on a finite ground plane and the geometry of the antenna and its prototype are shown in Figure 3.7.

(a)

(b)
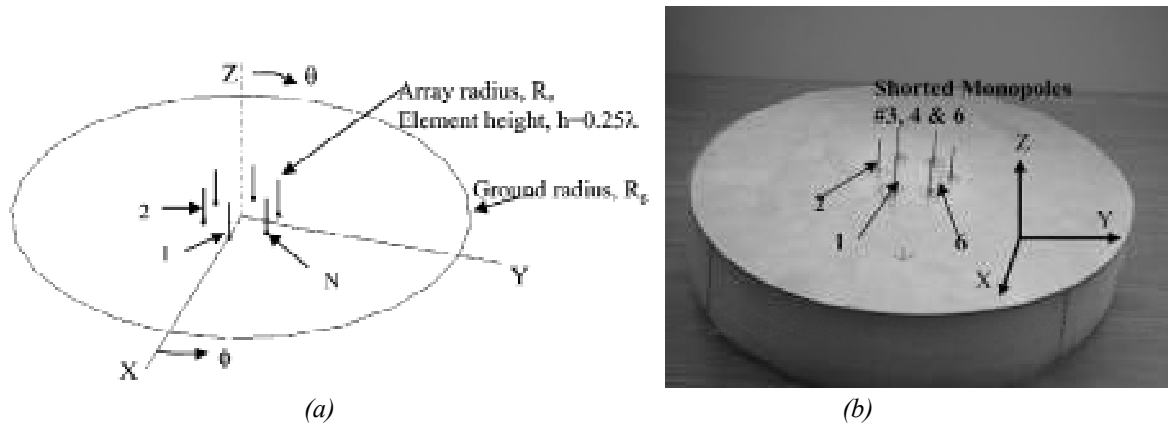
Figure 3.7 – Wire circular monopole array (CMA). (a) Geometry of an N - element CMA on a finite ground plane fed using a SMA probe. Its parameters are: R_a=0.25λ and R_g=1.50λ. (b) Photograph of 6 -element CMA designed for 2.8 GHz, the R_g = 1.40λ=15 cm, h=0.25λ=2.65 cm, R_a =0.234λ=2.5 cm, and the inter-element angle is 60° [25].

The antenna design was simulated for several configurations with various numbers of elements (4, 6, 8, and 10 elements) and their performances were then compared. For 6-elements array, the performance of the antenna is superior to other configurations. The excitation scheme of 2-0-6 (element 2 and 6 are excited, element 1 is open, and element 3, 4 and 5 is shorted to the ground plane) is chosen, since it has better directivity in the H-plane. Thus, this configuration is further optimized by observing the effect of the size of ground plane and array radius on antenna radiation pattern. Results tells that the array radius does not affect significantly on the radiation pattern but the size of the ground plane can help to suppress the side lobes with an appropriate size. The comparison between simulated and measured results is shown in Figure 3.8 for H- and E- planes. The measurement was conducted from 2 GHz to 3 GHz and the maximum gain only occurs at 2.8 GHz and the half power beamwidth in the H-plane is 67°.

(a)

(b)
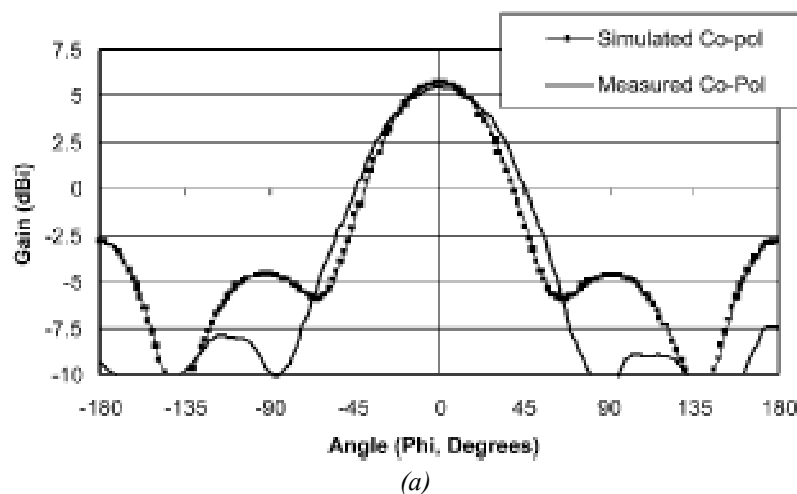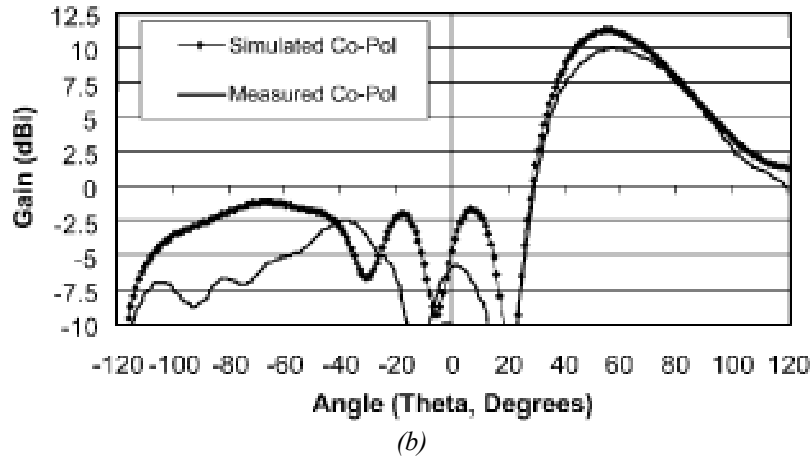
Figure 3.8 – Radiation pattern comparisons at 2.8 GHz. (a) H-plane, the maximum gain in the H-plane are 5.70 dBi (simulated) and 5.48 dBi (measured). (a) E-plane, the maximum gain in the E-plane are 11.20 dBi (simulated) and 10 dBi (measured)[25].

3.1.1.3   Large beam scanning antenna

Antennas are considered as large beam scanning antennas if the antennas are capable to steer a beam more than 180° or up to 360° direction without decreasing the antenna gain. Mainly active components such as diode are used to provide switching mechanism. In [26], a novel antenna structure known as reconfigurable orthogonal antenna array (ROAA) based on separated feeding network was proven to steer its main beam from 0° to 340° with 20° and 50° scanning steps. PIN diodes were employed as switches to steer the beam at desired directions. The ROAA consists of four vertical reconfigurable planar antenna array (RPAA) which was arranged as a box structure. The layout and fabricated antenna are shown in Figure 3.9.

(a)   *(b)*
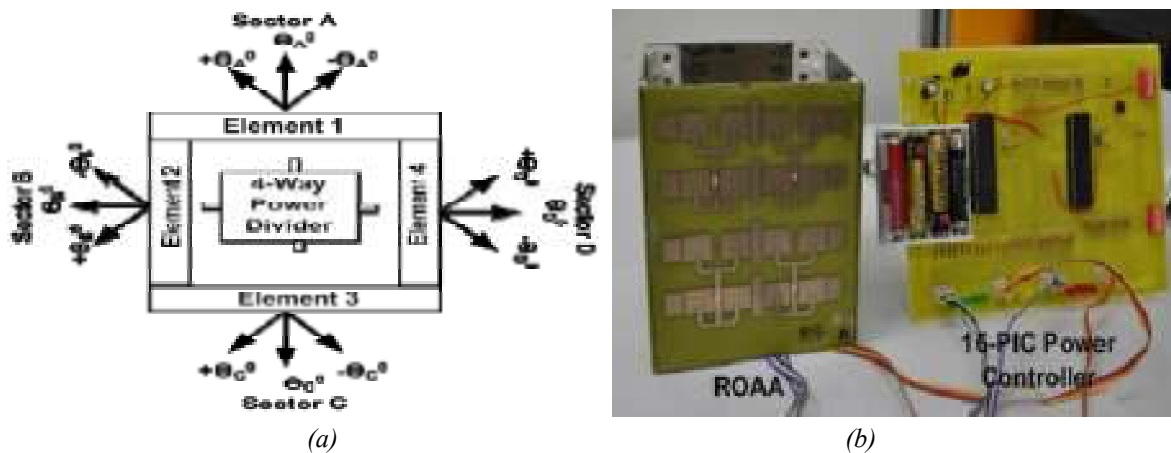
Figure 3.9 – Reconfigurable orthogonal antenna array (ROAA); (a) The layout diagram of the ROAA. (b) Fabricated antenna. [26].

The antenna was meant to work at 5.8 GHz and the fabricated antenna has been measured and was confirmed to steer in twelve directions (0°, 17°, 72°, 90°, 107°, 162°,

180°, 197°, 252°, 270°, 287°, and 342°). A 16 pins PIC power microcontroller was used to control the RPAA elements.

Another large beam steering antenna was proposed in [27]. The active antenna was designed for base station associates an omnidirectional antenna to a cylindrical controllable metallic Electromagnetic Band Gap (EBG). The omniditectional antenna is placed in the center of the active antenna. To control radiation over a 360° in the azimuth plane, the reconfigurable EBG structure is composed of a cylindrical lattice of discontinuous metallic wires along with PIN diodes. The diodes are used to control the size of the composite wire; long wires when the diodes are ON and   the EBG material is reflector, discontinuous wires when the diodes are OFF and the EBG is transparent. The antenna was measured at 950 MHz and its radiations intensity are shown Figure 3.10 for 90° of EBG aperture.
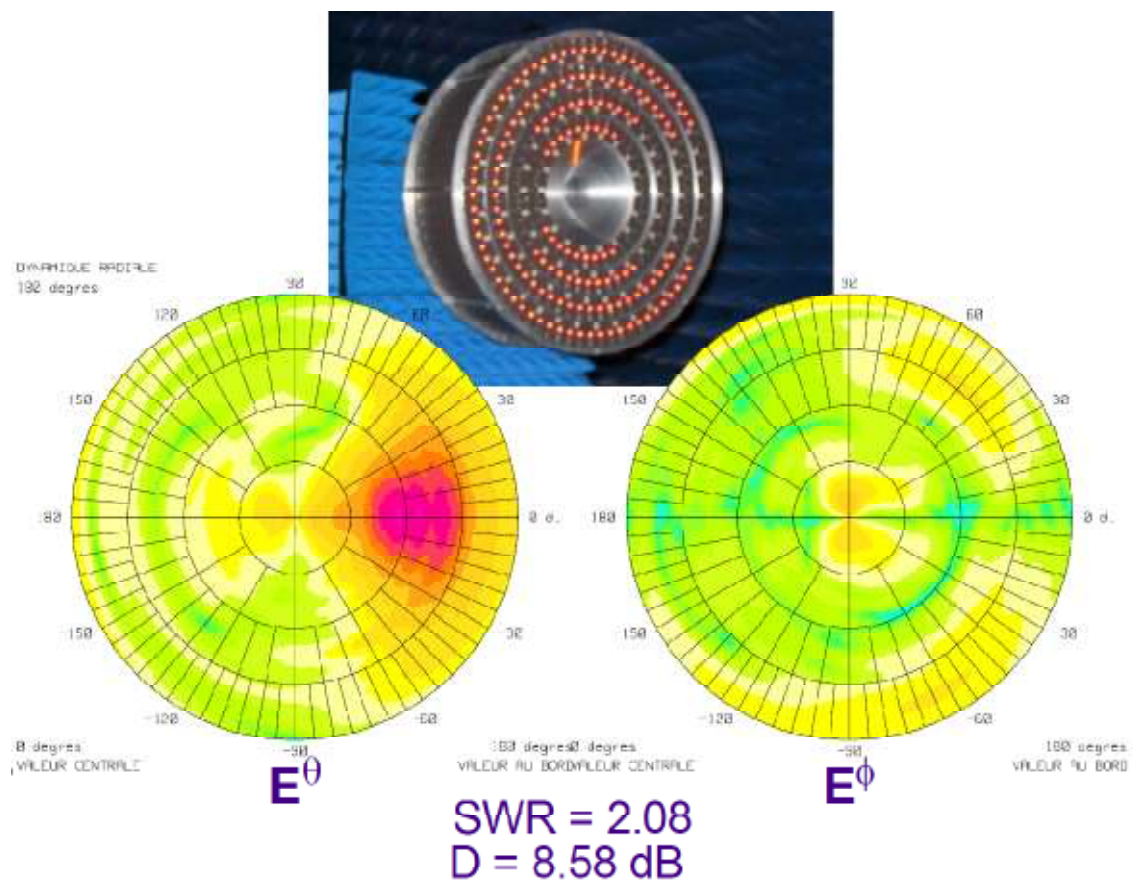
Figure 3.10 – Active antenna radiation intensity with 90° of EBG aperture at 950 MHz [27]. A photograph of the fabricated active antenna is shown in this figure (top).

3.1.1.4   Corner reflector antenna for beam shaping

A simple and yet effective technique to shape and to reflect a beam is by using corner reflector antenna. The corner reflector antenna (CRA) was first introduced by John D. Kraus and was known to have about 9-14 dBi gain [28]. The images theory is employed to run antenna analysis and also to give a useful guide in the antenna design [28-32]. Other than parabolic reflectors, CRA is a good candidate to steer and shape a beam in forward direction. Unlike, parabolic reflectors, CRAs are uncomplicated in design since they remove the crucial part of focal point for a driven dipole [28]. Figure 3.11 shows a single-flat sheet reflector and a parabolic reflector. As reported in [28], the parabolic reflectors provide slight or no improvement over CRA of a comparable size in terms of performance.
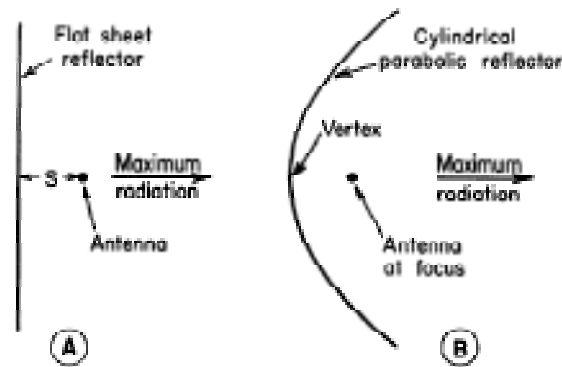
Figure 3.11 – A single-flat sheet reflector (labeled with A) and a parabolic reflector (labeled with B). The crucial part of focal point for a driven dipole is removed for the CRA [28].

By referring to Figure 3.12, John D. Kraus also claimed that by changing the feed-to-vertex spacing, *S* with the same included angle, *α* the beam can be varied from single beam into dual beams. However, with this approach, the *s* needs to be altered mechanically.
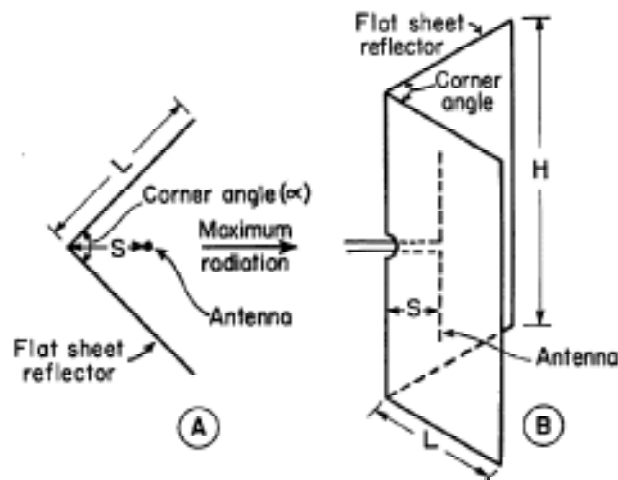
Figure 3.12 – Corner reflector in cross section (A) and in perspective (B) [28].

Various studies on CRAs were enlightened and conducted in many research papers including variation of radiation pattern due to the several varying included angles [32], [33], feed-to-vertex spacing [32], [33] and length of the reflecting surface [34]. A CRA with circular polarization was proposed and presented in [29] and in [30]. A tilted dipole is used to realize the circular polarization. The design details are illustrated in Figure 3.13. The dipole can be tilted 32° from origin and by doing so, in to and fro manner, a circular polarization will be produced.

(a)   *(b)*
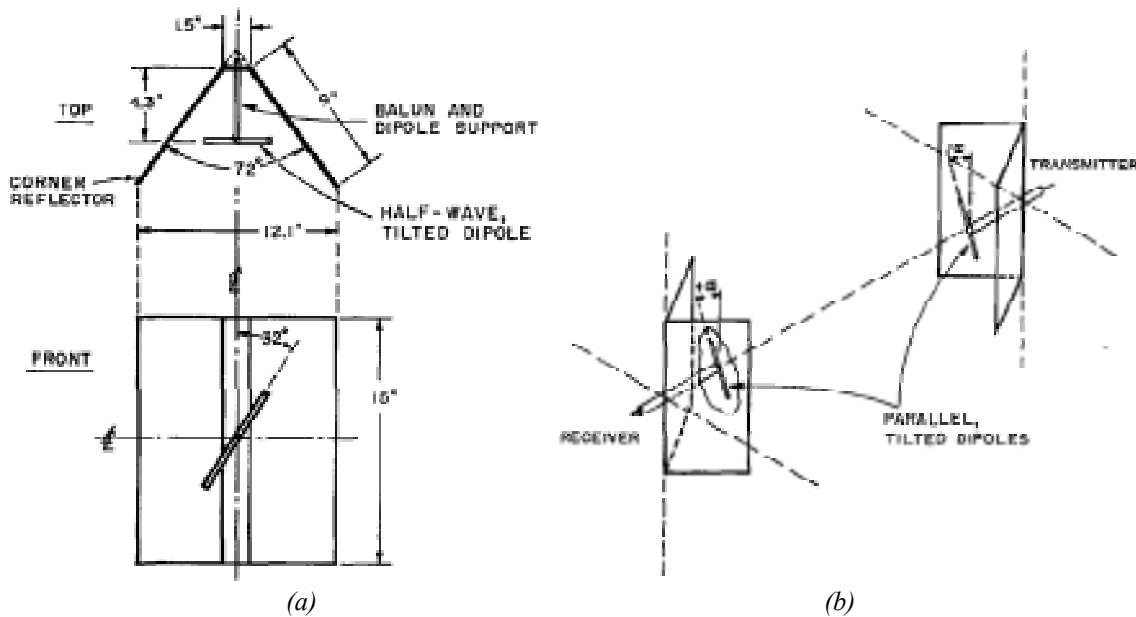
Figure 3.13 – Circular polarized CRA. (a) Geometry of antenna. (b) Field adjustment of CRA to produce circular polarization [29].

The earliest three-dimensional CRA was proposed by Naoki Inagi in [35]. This type of CRA employed three planar reflectors and a 3/4λ unipole radiator. Calculation analysis of antenna gain, input impedance and radiation pattern were made based on image and electromotive force (EMF) methods. Experiments conducted on the three-dimensional CRA and rectangular corners using finite reflecting surface have confirmed that type of CRA produced a gain of 5 dB greater than the two-dimensional CRA. Later in [36], with the same idea, two types of three-dimensional antenna were proposed and measured using finite reflecting sheet and a set of finite grids for VHF and UHF applications. Both designs are shown in Figure 3.14.

(a)   *(b)*
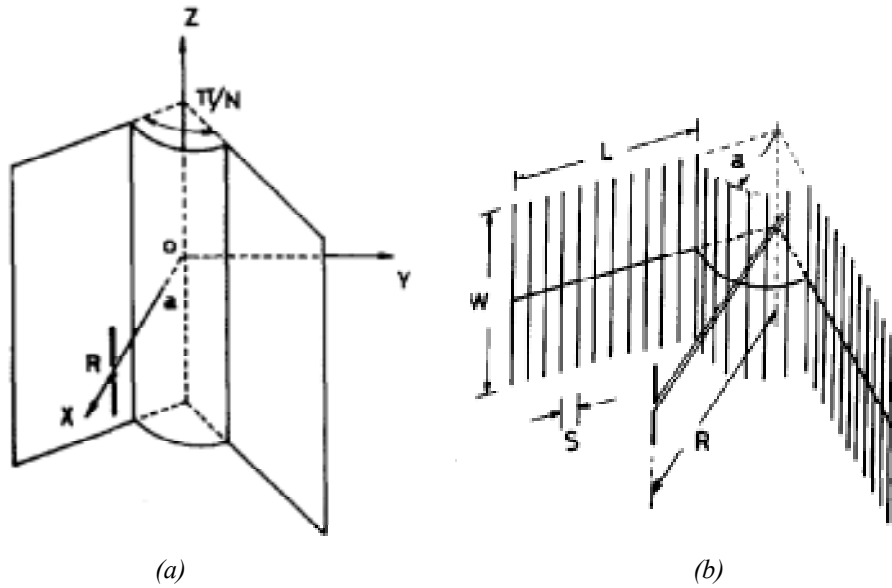
Figure 3.14 – A 60° CRA. (a) Constructed by using finite reflecting sheet. (b) Constructed by using finite grid [36].

The first type is constructed by adding a cylindrical reflecting surface of suitable radius to the V-shaped CRA and the second type is constructed by adding a cylindrical surface to the three dimensions CRA. Both designs offer 2 dBi and 6.5 dBi increments in the antenna gain. In following year, analysis of the three-dimensional CRAs in [36] was reiterated but this time by using method of moment (MoM) and was presented in [37]. The MoM was concluded to give higher values for the input resistance and lower values for the input reactance compared to image and EMF methods.

In terms of design robustness, a CRA made by a set of grids of reflecting surfaces has one coherent advantage over the finite reflecting sheet. The so called grid-ed CRA eliminates severe effect caused by the wind when the CRA is mounted in high and open air area such as on the top of buildings.

Other techniques of analysis of the radiation pattern were conducted in [38] using boundary elements method (BEM) and in [39] using finite difference time domain method (FDTD). Some CRA are designed with wide band capability and mainly for UHF and VHF applications [40], [41] with these techniques of analysis.

Many studies have been conducted to enhance the performances of the classical CRA. This includes by placing conducting object in front of the CRA, generally in the main lobe direction so that it can be configured to diffract and scatter incoming beam constructively. This technique was first introduced in [42] using ferrite cylinders and later by using metallic stripes as reported in [43]. Another proposed technique to improve the CRA performances is by using metamaterial cylinders or metal coated with metamaterial as the grid element [44]. Other than that, a novel design of CRA known as the triple corner reflector antenna (TCR) was proposed in [45]. The design was aimed to

60

improve antenna gain and to reduce the size of half power beamwidth. The schematic of the TCR and its performance are depicted in Figure 3.15.

(a)   (b)
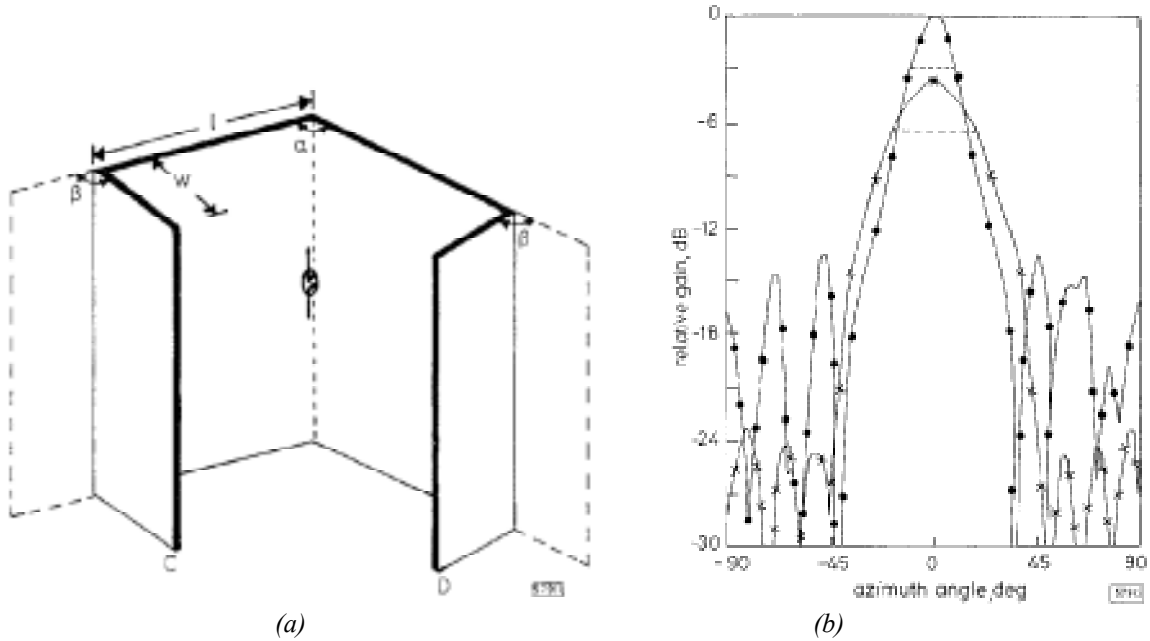
Figure 3.15 – A novel 120° triple corner reflector antenna (TCR) for X band applications. (a) Schematic diagram. (b) H-plane radiation pattern comparison (the TCR is represents by the dot, and the 90° classical CRA is represent by the cross) [45].

The experiment was repeated for several included angles, α which are 60°, 90° and 120° in the X band. Experiment iteration shows that optimum TCR with the highest gain occurs with the configuration α=120°, l=2λ, β=80° and w=1.5λ. The optimized TCR has 3 dB improvements in gain and the half power beamwidth is half of the value of the corresponding conventional CRA with 90° included angle. The side lobe level of the optimized TCR is below -13 dB.

For some applications, it is desirable to be able to adjust the beamwidth and the radiation pattern characteristics. For that reasons, a CRA with variable beamwidth was proposed in [46-48] with different techniques. In [46], a reconfigurable CRA was proposed with the use of mechanical movement as illustrated in Figure 3.16. The beamwidth characteristic is controlled by moving the reflector plates using a sliding ring that is connected to the plates by a hinge. The plates must be moved synchronously so that the dipole will always at the bisector line and this is where the main difficultly arise. The CRA was designed to work at 5 GHz and was fed by a half wave dipole separated by 30 mm (0.5λ) from the vertex, and the side length of the square plates was 120 mm (2λ).
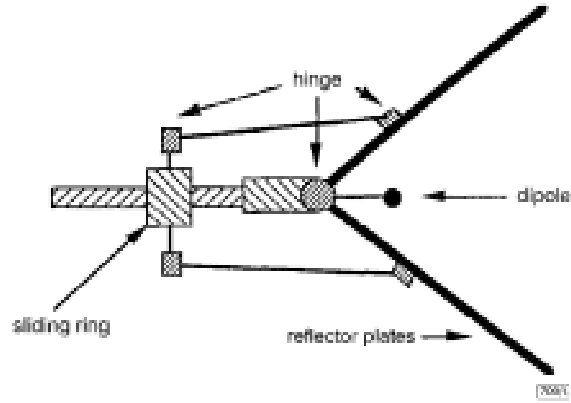
Figure 3.16 – Schematic of a variable beamwidth CRA simulated at 5 GHz [46].

The beamwidth characteristic is controlled by moving the reflector plates using a sliding ring that is connected to the plates by a hinge. The plates must be moved synchronously so that the dipole will always at the bisector line and this is where the main difficultly arise. The CRA was designed to work at 5 GHZ and was fed by a half wave dipole separated by 30 mm (0.5λ) from the vertex, and the side length of the square plates was 120 mm (2λ).

In [47], a novel quad corner reflector array was proposed and measured for 2.4 GHz applications. This antenna uses four identical dipoles placed at every 90° angle. The proposed and realized reflectors are depicted in Figure 3.17.

(a)   *(b)*
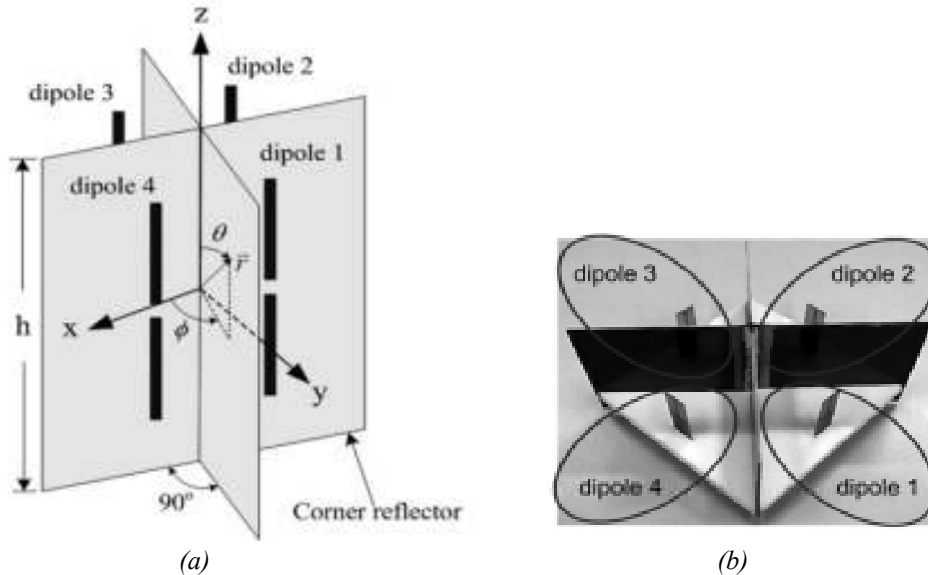
Figure 3.17 – A novel quad corner reflector array at 2.4 GHz. (a) Antenna configuration. (b) Prototyped model [47].

The measurements results are shown in Figure 3.18. The results are explained for three main cases; the first one is when the dipole antennas are in transmitting mode (Tx), the second and the last case are when the dipole 2 together with dipole 4 and dipole 1 together with dipole 3 are in receiving mode. The maximum gain for the case 1 is 8.8

dBi and the maximum gain for the case 2 and case 3 are the same with 11.8 dBi. All gains are measured at 2.45 GHz.

(a)   *(b)*
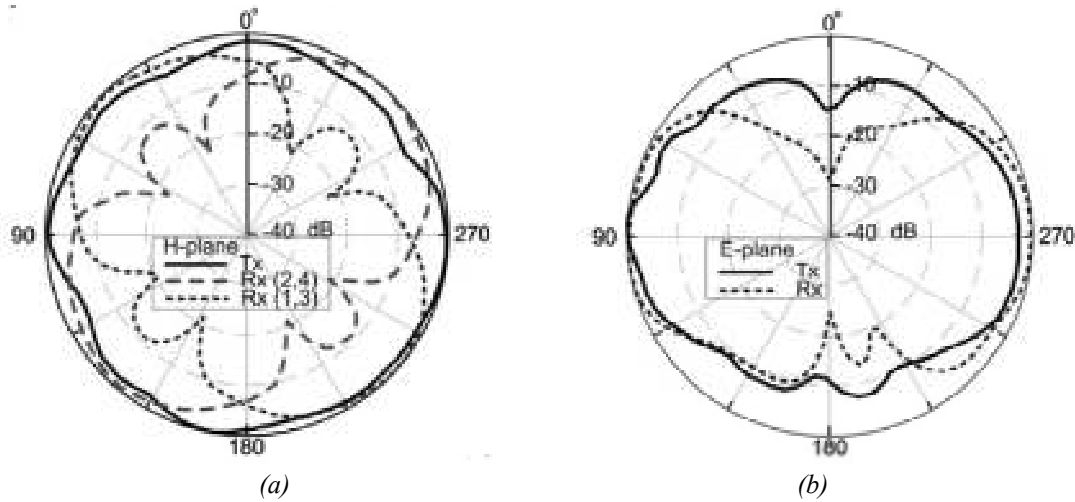
Figure 3.18 – Measured radiation patterns. (a) H-plane. (b) E-plane [47].

Another reconfigurable CRA for 2.4 GHz application is proposed in [48]. The CRA offers multiple beam forming capability since it incorporates electronic steerable passive radiator (ESPAR). The proposed corner reflector ESPAR is shown in Figure 3.19.
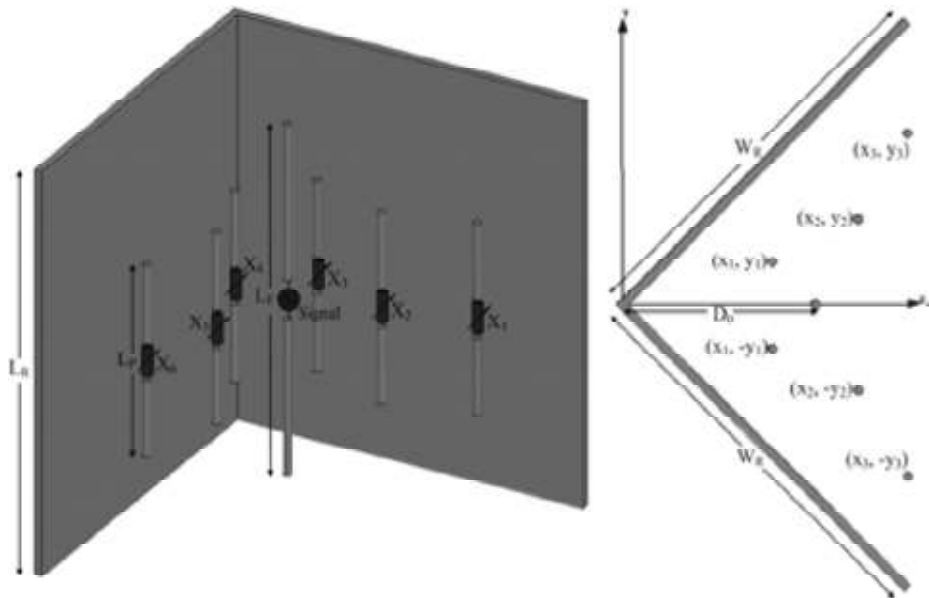
Figure 3.19 – The structure of the proposed CR-ESPAR antenna at 2.4 GHz for base station applications [48].

Beamforming in ESPAR antennas is performed by controlling the reactance loaded to a number of passive elements and for such design the ESPAR is integrated with CRA by placing these passive elements in front of the CRA. These passive elements are formed in symmetrical pairs around the bisector of the reflector and they can be loaded with different reactive load value. The optimization was conducted with respect to the

63

resonance frequency, input impedance, and multiple switched-beam pattern configuration. By using genetic algorithm (GA), the antenna was optimized and achieved maximum gain of 14 dBi for a 30° 3 dB beamwidth and 11 dBi for 45° 3 dB beamwidth. This is quite high compared to the research's literatures operating at the same frequency, which the maximum gain is 8 dBi. The author had claiming this is partially due to the size of the CR-ESPAR itself which is much bigger with those in the literatures.

Since the introduction of CRA in 1940s, most of the research works deal with low frequency bands including low microwave frequencies. However, in [49], a new milimeter wave corner reflector antenna array was designed and realized. The antenna was aimed to work at 26 GHz which is a popular for microwave communication network applications such as indoor and outdoor wireless LANs and point to point communications. Three CRAs were designed with different included angles, 127.5°, 180° and the new concept of included angle more than 180° which is equivalent to 255°. The sketch of the three different included angles and the realized antennas are shown in Figure 3.20. The simulated radiation pattern results are shown in Figure 3.21 revealing that the beamwidth in the H-plane changes corresponding to the included angle.

(a)

(b)
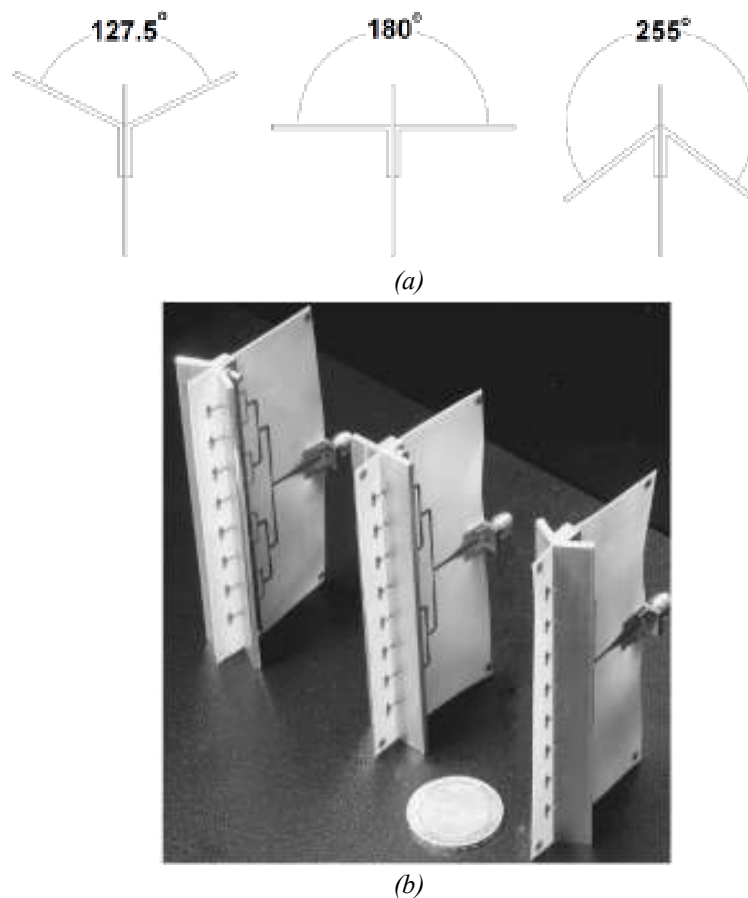
Figure 3.20 – (a) Sketch of three different included angles. (b) Realized antennas with three included angles (127.5°, 180°, 255°) [49].

(a)

(b)
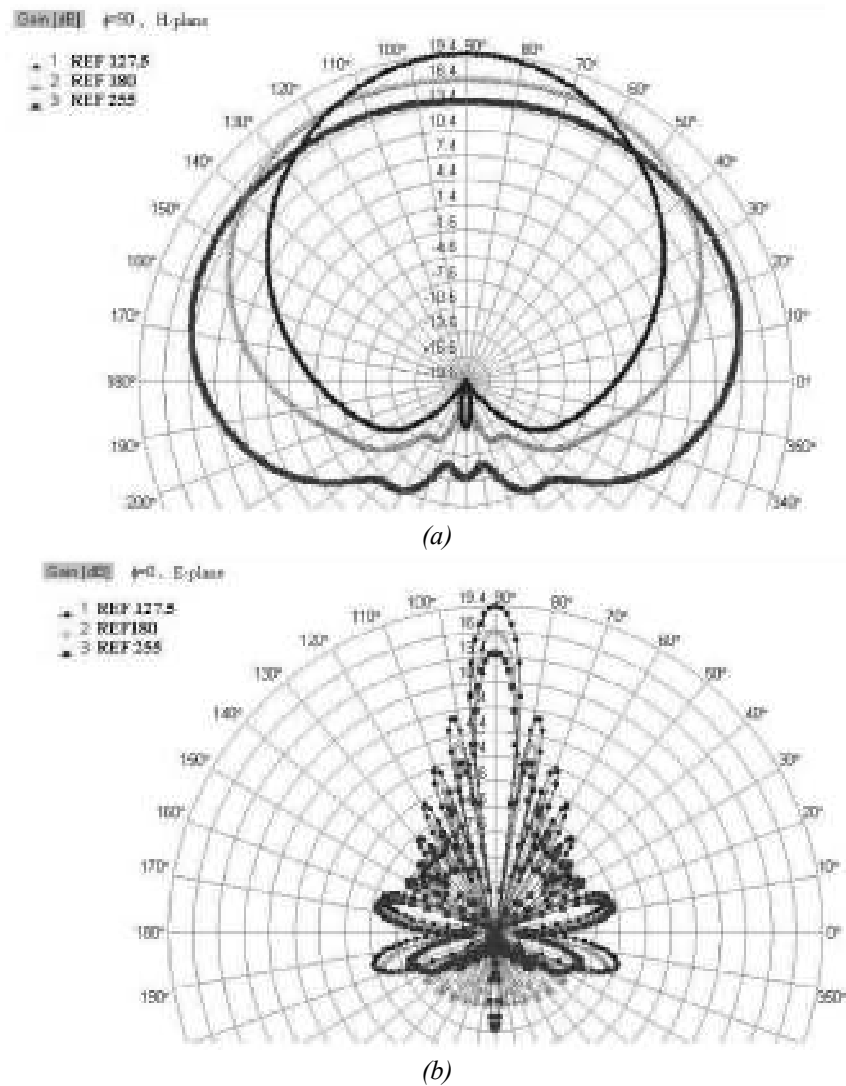
Figure 3.21 – Simulated radiation patterns. (a) H-plane. (b) E-plane [49].

The measured results are in a good agreement with the simulation ones. The measured antennas gain are 19.6 dBi, 16.5 dBi, and 13.8 dBi, for the respective included angles of 127.5°, 180° and 255°.

3.1.2 Reviews of antennas for beam steering, beam scanning and beam shaping using plasma medium

There are many shapes and configurations of reflector antennas that can be adopted to steer incoming signal to the intended direction. Reflector antennas are simpler in terms of design since it uses the free space as its feeding network. Beam steering by using plasma reflectors is very promising profile, especially ability of plasma to be

reconfigured electrically which is impossible to be done by metal elements. However, up to now, there are not many published works that have employed plasma as the medium to have beam steering and beam shaping capability. Thus, this section aims to provide brief review on the previous works so that an overview of plasma in designing reflector antennas can be comprehended easily.

3.1.2.1   Beam steering and beam scanning

In the earliest works, a type of reflectors known as plasma mirror has been used to steer electrical beam in particular direction especially in radar systems. The plasma mirror is designed to suite applications for space-based used in the X-band, 60 GHz and 94 GHz frequencies. This is because although the existing phased-array radar has tremendous response time advantage over other types of radars, yet it is generally restricted to low frequency [50] due to high insertion loss and easily affected by mutual coupling [51] in millimeter wave applications. The concept of the plasma mirror is shown in Figure 3.22.

(a)   *(b)*
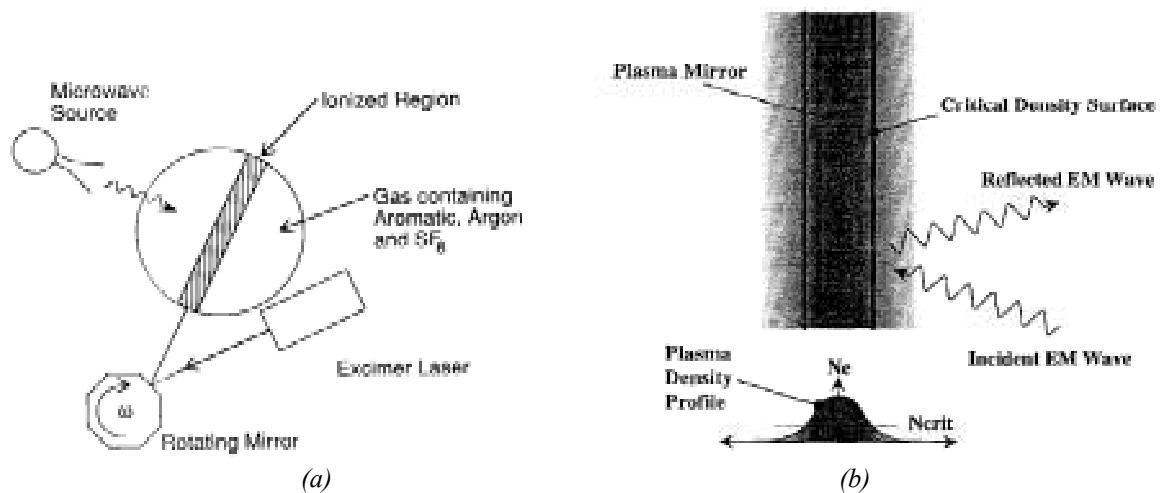
Figure 3.22 – (a) Agile mirror system [50]. (b) Geometry of microwave reflection from a plasma mirror [52].

In order to create an ionize region in the gas that contains Aromatic, Argon, and SF_6, a rotating mirror is use to maneuver a laser so that the laser will supply enough energy for the gas inside the container. The mirror could be rotated so that the ionized region can be relocated accordingly. The energy from the laser source is directed to the rotating mirror that would able to create an ionize region which is plasma.

Mirroring concept using plasma has been demonstrated in [53] in X band (10.5 GHz). A pulsed glow discharge is used to generate a plasma sheet with a linear, hollow cathode in an axial magnetic field. The plasma is experimentally tested and it can be established and extinguished on a time scale of 20 microseconds. The experiment

apparatus is shown in Figure 3.23 (a) and the measurement of the microwave layout to form plasma mirror is shown in Figure 3.23 (b).

(a)

(b)
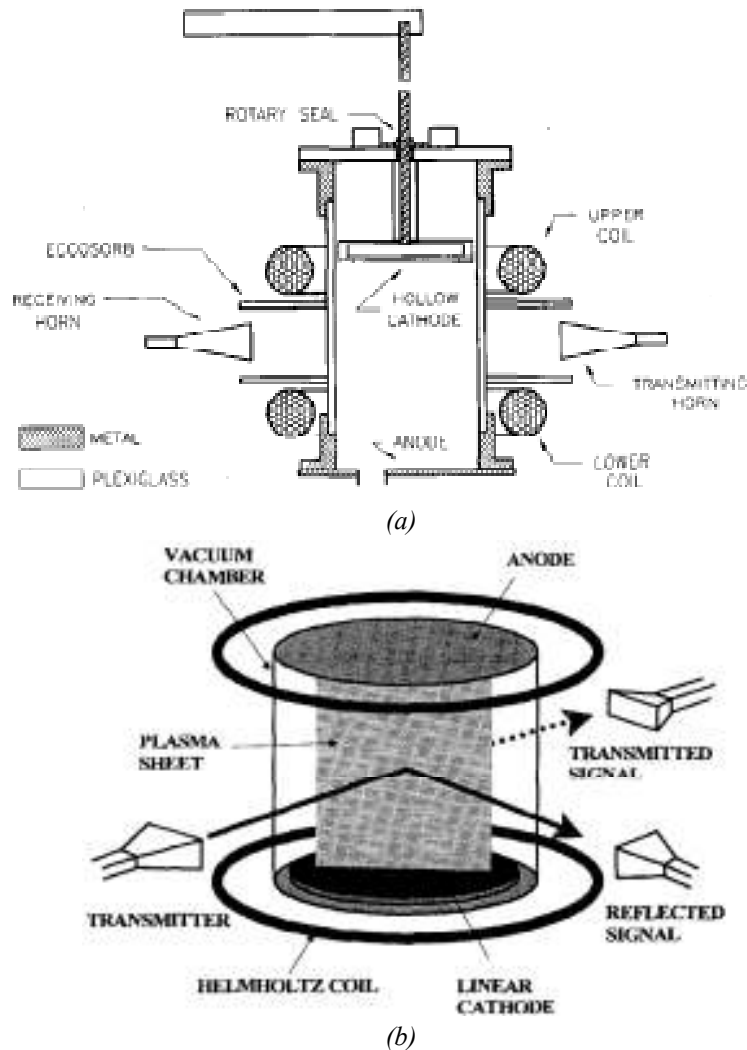
Figure 3.23 – (a) The experiment apparatus [53]. (b) The layout for microwave measurement [52].

The same technique which was presented in [53] is used to create a plasma mirror in [52], [54] and [55]. This time the performance of the plasma mirror is compared to it metal counterpart. A 50 cm wide, 1 cm thick and 60 cm long plasma sheet is formed between the cathode and the anode just after 10 microseconds when the voltage is applied. The plasma sheet is created by a 4 kV voltage pulse and 10^{13} cm^{-3} plasma is achieved within the plasma. The pressure of the discharge gas during the operating tile is 130 mTorr. A 30 cm diameter Cutler-feed antenna is used to illuminate the mirror at 10 GHz [52]. The comparison between plasma and metal mirrors in the same dimension is shown Figure 3.24.
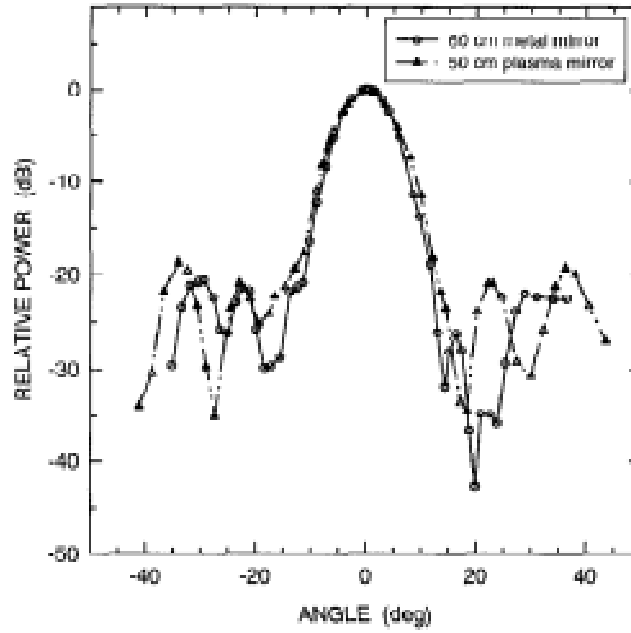
Figure 3.24 – Comparison of H-plane radiation patterns due to reflection from a metal mirror and a plasma mirror [52].

This pattern is obtained by rotating the plasma mirror while keeping the receiver horn fixed. The reflectivity of the plasma mirror is almost 100 percent and as a reflector the plasma mirror exhibits extremely low loss and the noise measurement result can be seen in Figure 3.25. The noise performance of the plasma mirror has been presented in [56]. The noise was measured at 10.5 GHz for an Argon plasma mirror with cutoff frequency of >12.5 GHz. The detector recorded the generated noise before, during and after the mirror pulse. During the 300 μs mirror pulse the noise power first increased when the mirror was turned ON then quieted down after ~50 μs. Thereafter the noise power settled down to a factor of 3 above the ambient noise level.
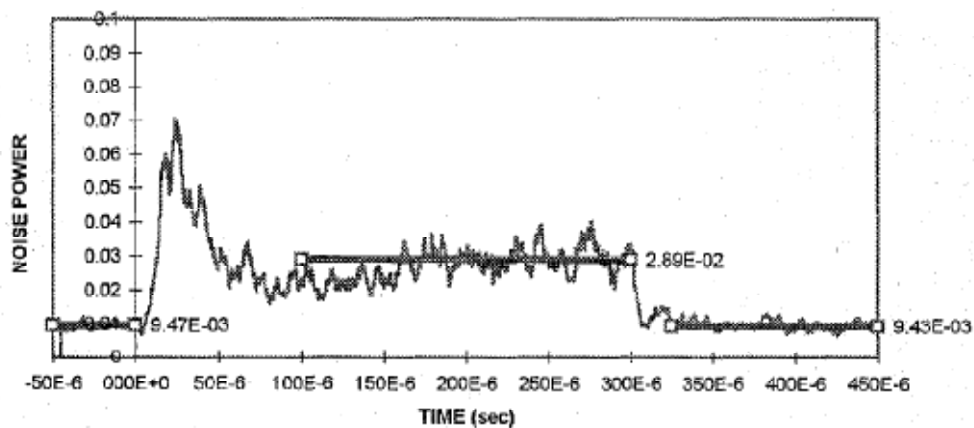
Figure 3.25 – Measurement of 10.5 GHz noise emission for an Argon plasma mirror [56].

Another way to steer a beam is by using microwave lens based on plasma medium as reported in [51]. Plasma lens can be formed when the ratio ω/ω_p falls within ~1-3 which allows the waves to propagate obliquely to a density gradient pass through a

region of gradient in the refractive index and thus deflected. The degree of deflection in plasma is depending on the plasma density. Interestingly in these conditions, the refractive index of plasma in less than unity and the wavelength is larger than in vacuum. This phenomenon is illustrated in Figure 3.26.
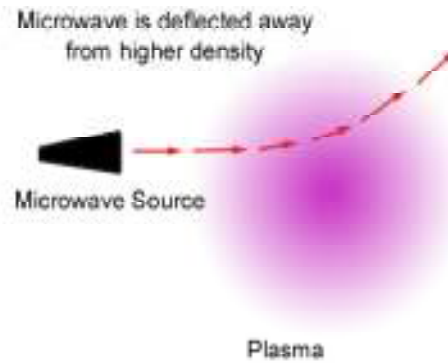
Figure 3.26 – The effect of a circular density gradient on the path of microwave beam [51].

The plasma lens experiment conducted in [51] is using special equipment known as basic ion laser (BASIL). The BASIL vacuum chamber is made of Pyrex tube with a transition from a 50 mm to 1000 mm diameter. The tube is surrounded by magnetic field coils to allow formation of the plasma by the excitation of helicon wave. The schematic of the BASIL is shown in Figure 3.27.

(a)   *(b)*
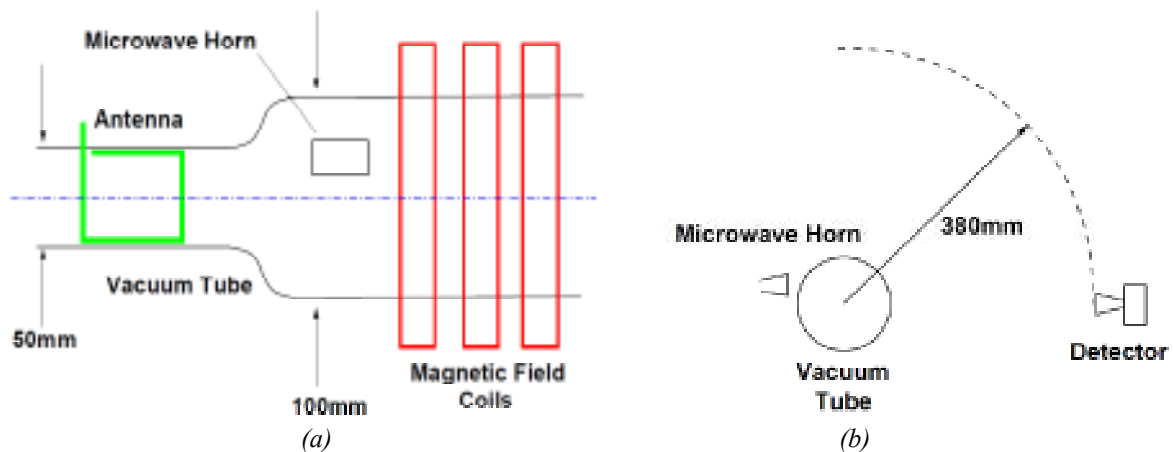
Figure 3.27 – Basic ion laser (BASIL). (a) Schematic showing setup of BASIL. (b) The arc swept out by detector to measure the radiation pattern of deflected and un deflected beams [51].

The microwave signal at 36 GHz is generated using IMPact ionization Avalanche Transit-Time (IMPATT) diode source and launched through a 25 x 32 mm, 3 dB horn antenna to an entry point at 22 mm from the tube axis. This offset ensures that microwave beam is directed through the plasma gradient at an angle. The detection of

microwaves signal is done using 20 x 35 mm horn feeding a point-contact diode with sensitivity of < 1 mW. The plasma frequency during the experiment was 20 – 30 GHz. The result is shown in Figure 3.28.
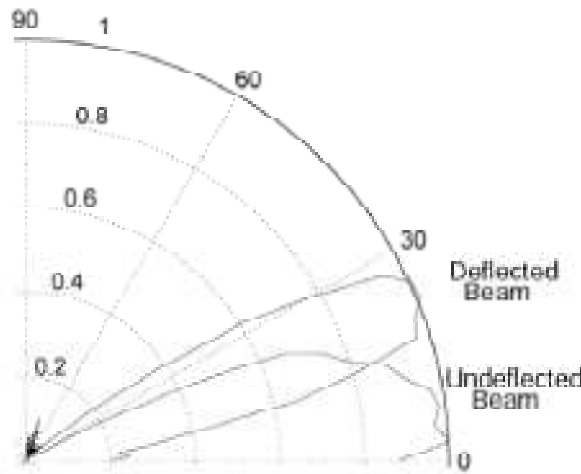
Figure 3.28 – Measured far-field radiation pattern of 36 GHz plasma lens [51].

It can be noted that there is good collimation of deflected beam. Therefore, the ability to steer beam has been proven and adequate to be used in practical applications. The plasma lens demonstrated in the paper can deflect about 25° without radically changing its shape or introducing significant side lobes. Insertion loss seemed to be controllable.

One of plasma reflector realizations to steer a beam was a parabolic plasma reflector operating at 3 GHz. This project has been realized by a group headed by Igor Alexeff and Ted Anderson in the middle of 2000 [57], [58]. Figure 3.29 shows one of their earliest designs of plasma reflector.

Figure 3.29 – Earliest design of plasma reflector [57].

The parabolic concept is furthermore enhanced with the use of commercially available fluorescent lamps and finally tested. Figure 3.30 shows plasma antenna installed in an anechoic chamber along with a metal antenna that was designed to be an identical twin to the plasma antenna.

(a)   *(b)*
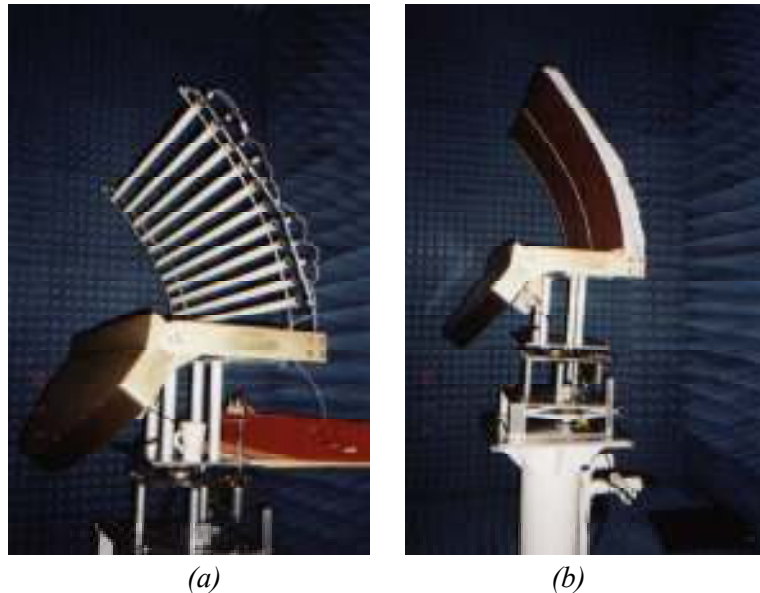
Figure 3.30 – Plasma (a) and metal (b) reflector antennas installed in an anechoic chamber. The metal antenna was designed to be an identical twin to the plasma antenna at 3 GHz [57], [58].

The plasma reflector has shown comparable performances with metal reflector in the same arrangement and the result is illustrated in Figure 3.31.
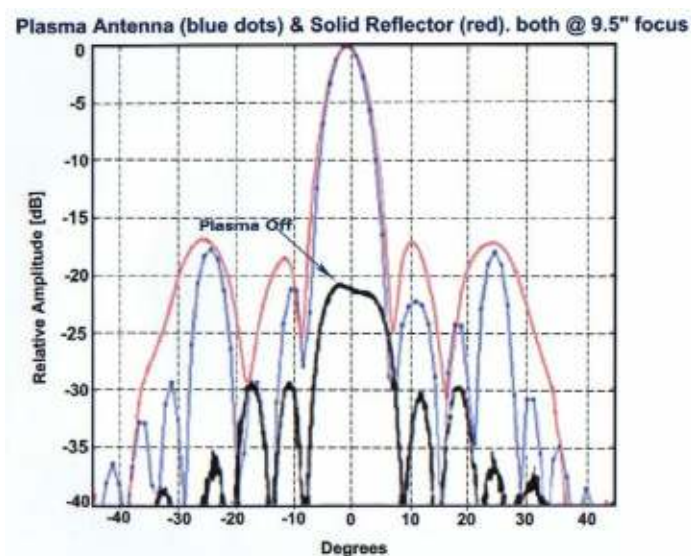
Figure 3.31 – Comparison of radiation pattern on plasma antenna (blue dots) and metal reflector (red solid line) [57], [58].

The radiation pattern of plasma is quite similar with its metal counterpart. It can be seen that when the plasma is de-activated, the reflected signal is dropped by over 20 dB. These two scenarios have confirmed that the plasma reflector antenna was able to give similar performances as metal reflector at 3 GHz and also the plasma can be destroyed to eliminate its existence.

3.1.2.2 Wide beam scanning and beam shaping

Igor Alexeff, Ted Anderson and their group have published several remarkable works in designing plasma using antenna medium such as smart plasma antenna in [59-61]. The plasma elements were arranged in circular coordination allowing extra possibility of beam steering, beam shaping and beam scanning. However, the large type fluorescent lamps were used as the plasma source and thus the resultant antenna is quite bulky. The schematic of the antenna is shown in Figure 3.32 (a). Any de-activated element will create a plasma window and allowing directional beam to emerge. The plasma window can be varied accordingly with number of elements are de-activated. The concept of smart antenna was realized at 2.5 GHz and the final antenna was fabricated as shown in Figure 3.32 (b).

(a)   *(b)*
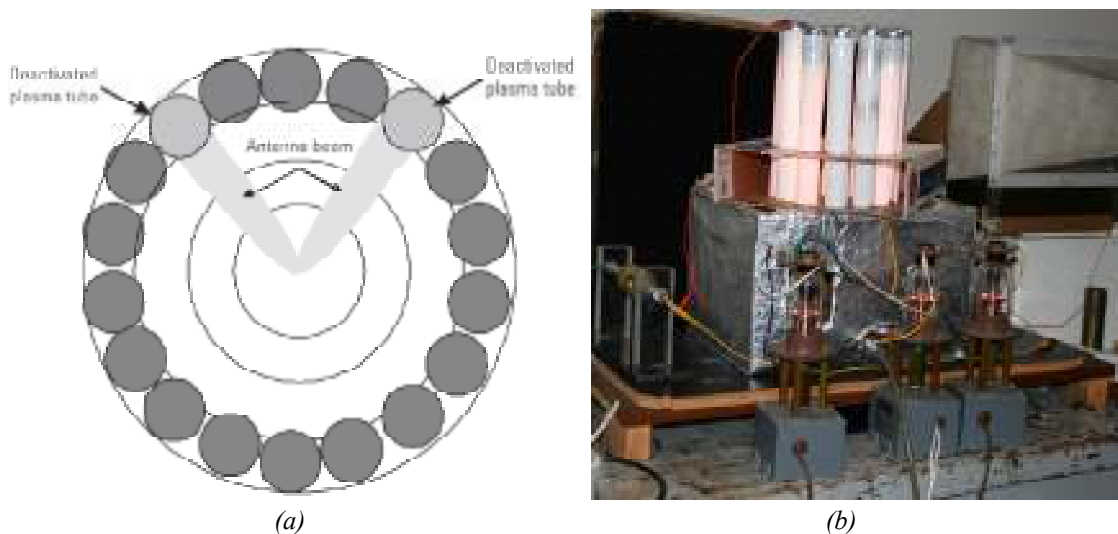
Figure 3.32 – (a) Schematic of beam forming for a plasma windowing directional antenna [60]. (b) Photograph of initial smart plasma antenna [61].

Generally, a reflector antenna operating at 2.5 GHz does not require physically tall reflecting elements. Therefore, it is sufficient to ensure that the reflecting elements are little bit taller than resonating element ($>\lambda/4$). For example, if the resonating element is a monopole antenna, the reflecting element must be a little bit taller than a quarter wavelengths so that the reflecting elements work as reflectors. Thus due to the size of plasma element used in [61], the plasma antenna has to be designed as such that the some part of fluorescent lamp (FL) need to be covered as shown in Figure 3.32 (b). This

is because the height of FL is too tall compared to the height of monopole antenna at 2.5 GHz (λ = 120 mm). The employment of big element radius also will increase scanning step and leads to the broader beamwidth. The used of cylindrical fluorescent lamp also requires both ends of the fluorescent lamp to be connected to power supply in order for the encapsulated gas to get ionized.

In [62], the similar arrangement of plasma cylindrical elements as introduced in [59-61] was applied in order to maneuver and steer incoming beams to certain direction. Because of plasma advantages, the arrangement allows a scanning beam to be realized. The plasma elements are arranged in circular form as illustrated in Figure 3.33. The results of a double beam and beam scanning are shown in Figure 3.34.

(a)   *(b)*
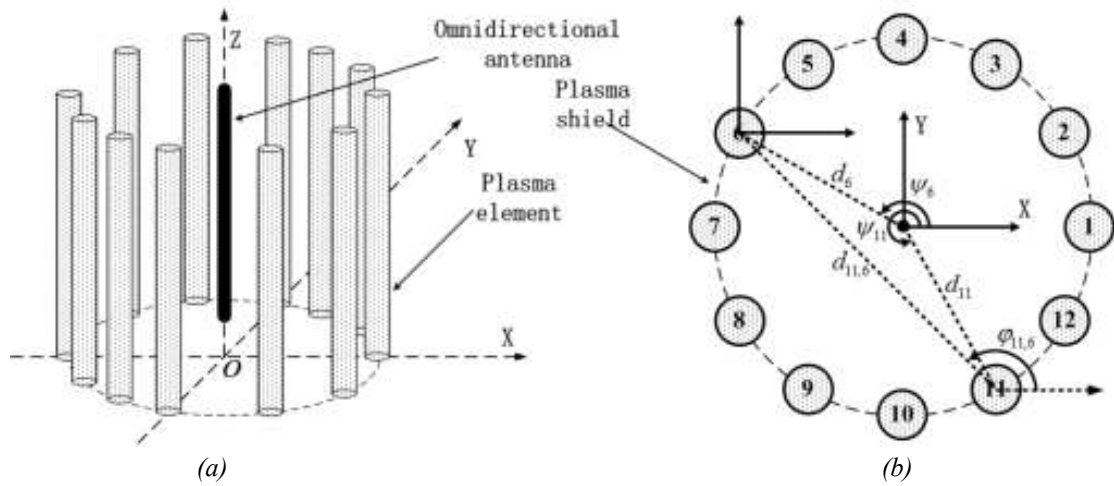
Figure 3.33 – Geometry of plasma antenna beam forming with 12 elements. (a) Side view. (b) Top view [62].

(a)   *(b)*
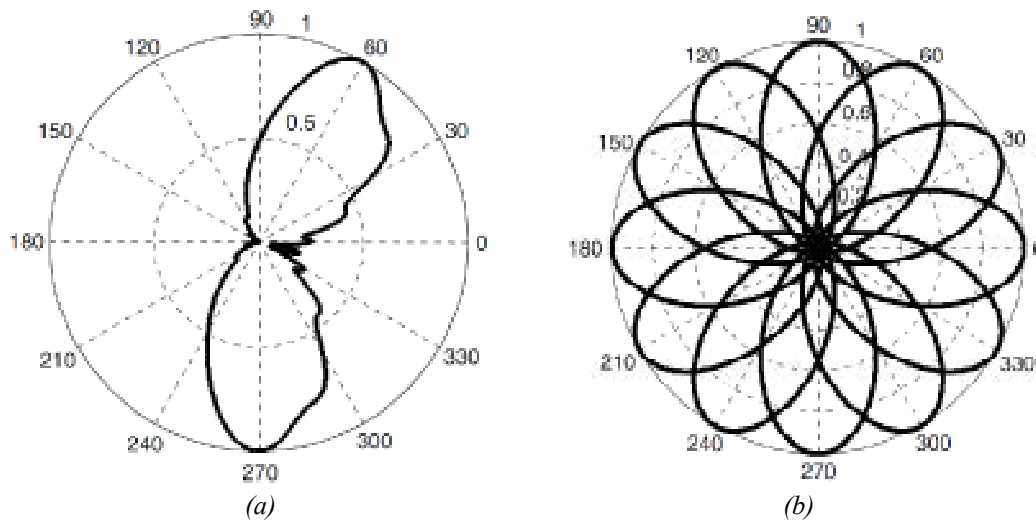
Figure 3.34 – (a) Double beams at 8.1GHz. (b) Single beam scanning at 8.1GHz. [62].

73

The signal is supplied by a classical monopole antenna that is located in the center of the circular-arranged reflecting elements. The theoretical result shows that with this arrangement, the beam can be steered at particular direction and the scanning beam can be done. The reflecting elements are assumed to be made by Argon gas encapsulated in T12 or T18 of the domestic fluorescent lamps. The assume pressure is from 1 to 5 Torr. The electron-neutral collision frequency and electron density are assumes as 6.83×10^7 Hz and 9.24×10^{17} m^{-3} respectively. The distance between plasma element and the central monopole is set to 0.0641 meter for 8.1 GHz operating frequency ($\lambda = 37$ mm).

Although the computed radiation patterns were presented in the paper seemed so satisfactory, the paper was lacked with some points. There was no confirmation of the proposed antenna performance such as antenna gain and reflection coefficient. Moreover the operating frequencies used in the simulation are rationally near to the plasma frequency which could lead to imprecision, refer to [57], [59]. Therefore, the only way to verify the results is through a concrete measurement.

3.1.3 Summary

By referring to the literatures, up to now, there are not many published working on plasma reflector antennas. Even though there are enormous works on designing antennas to steer, to shape and to scan beam have been published recently, these works mainly limited to the usage of metallic elements. Even more, active devices were often used in helping the antennas to switch from one configuration to another in order to redirect an incoming beam in particular directions.

Thus, plasma is another type of naturally available materials other than metallic material that can be exploited to give extra advantage in designing antennas. By implementing it, the requirement of non-linear active devices can be eliminated. Many type of plasma source have been used in the literatures. Some are complex in term of its excitation technique and some are not. However, there are many way to excite plasma and by using the commercially available CFL as plasma source, the complexity excitation can be reduced. Since plasma decays in microseconds, a round reflector antenna can be realized to steer, to shape and even to exhibit scanning beam.

3.2 Reconfigurable round reflector antenna (RRA)

To the best of our knowledge, only a few papers have reported about the scanning feasibility study of plasma reflector antennas [62], and none has reported about its verified performance except in [60], [61]. However, all of these reports have worked on specific size of plasma source which is large in size thus the performances and design may not be optimum at the specific operating frequency. For this reason, this section is aimed to present simulation and experimental results in order to verify the performance of a reconfigurable plasma reflector antenna with beam shaping and scanning capability in the ISM band. The reflector elements are made of series of compact fluorescent lamps (CFL) and are arranged in circular arrangement. Each of the elements is individually controlled by a single-pole electronic switch. Therefore, the change of beam profiles is effortless by narrowing or widening plasma window. As plasma only requires microseconds to decay [60], [63], the scanning beam can be maneuvered in split seconds too. Comparisons between simulated and measured results in the same configuration are discussed thoroughly in the following sections.

3.2.1 RRA antenna specifications

In the beginning of the study, there are four proposals to design a reflector antenna which incorporated beam scanning and beam shaping capability. The previous types of CFLs (Figure 2.9 in Chapter 2) were used in the simulations. These antennas are electrically reconfigurable so that once the plasma is de-activated, and with the presence of the dielectric tube, the antenna will radiate transmitting signal as the same as classical monopole antennas. In all four designs, the same ground plane size with a thickness of 3 mm was used. For the materials, the same dielectric tubes and metal were used in the simulation which are made from lossy glass pyrex with permittivity of 4.82 and ordinary annealed copper with conductivity of 5.8×10^7 S/m. The details of the proposed designs are explained in the following subtopics. Their simulated performances are also included. The optimization will only be done once the best design is selected based on the performance.

3.2.1.1 Round reflector antenna using Triple Biax compact fluorescent lamp

This is the first plasma reflector antenna that has been simulated after the plasma has been characterized. The design consists of five Triple Biax CFLs as shown in Figure 3.35. Details of the CFL are included in Appendix 3.1. The angle between the centers of

each element is 72° and the distance between reflector surface and central monopole antenna is 0.25λ at 4 GHz resonating frequency.
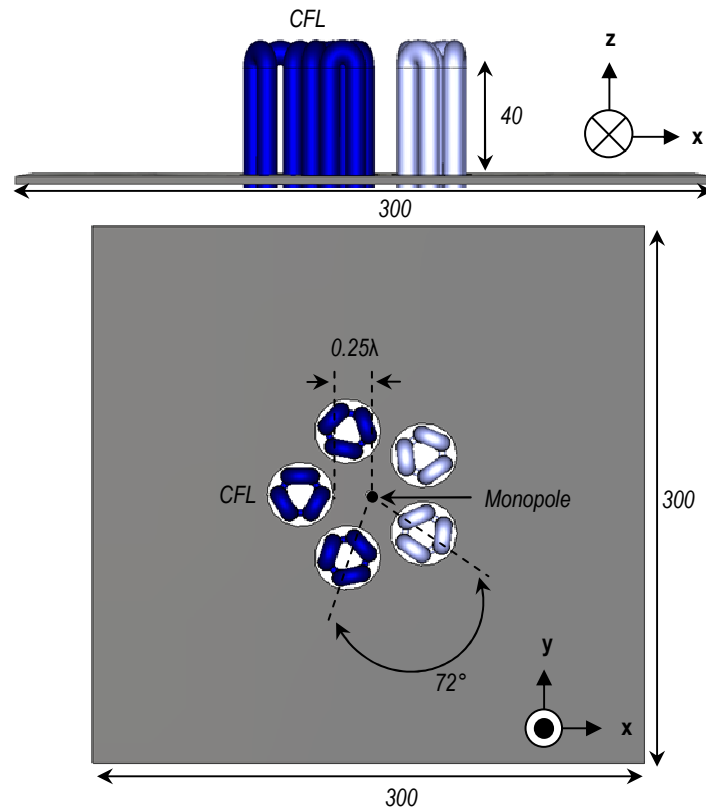
Figure 3.35 – Round reflector antenna using Triple Biax CFL consist of 5 elements. Only three elements are activated at the same time to reflect beam in forward direction.(Units in mm)

The height of CFL is measured 40 mm from the ground plane surface and its outer diameter is 10 mm. The height of the central monopole antenna is 17 mm with a diameter of 1 mm. Three elements are activated in order to shape the omnidirectional beam. The simulation results are shown in Figure 3.36.
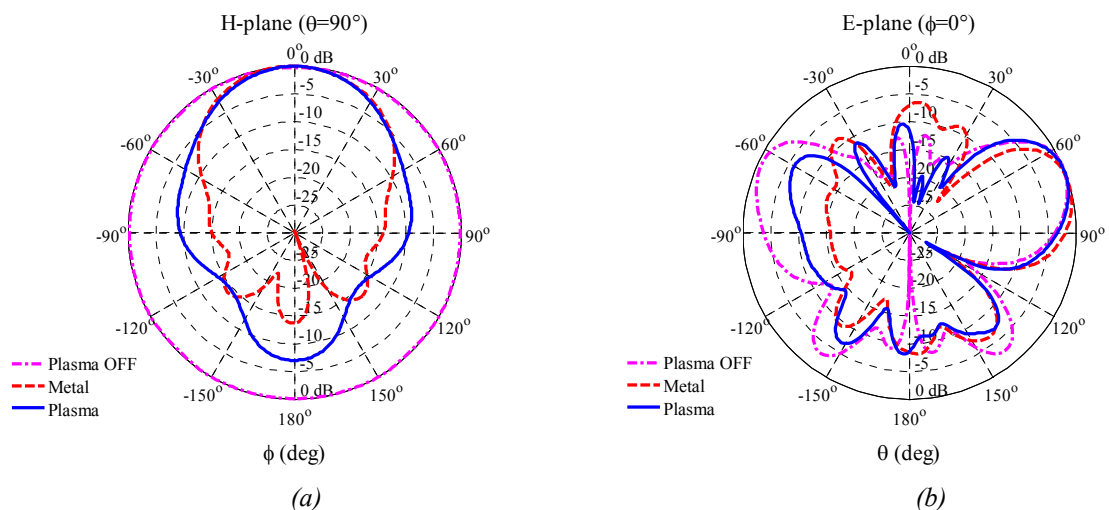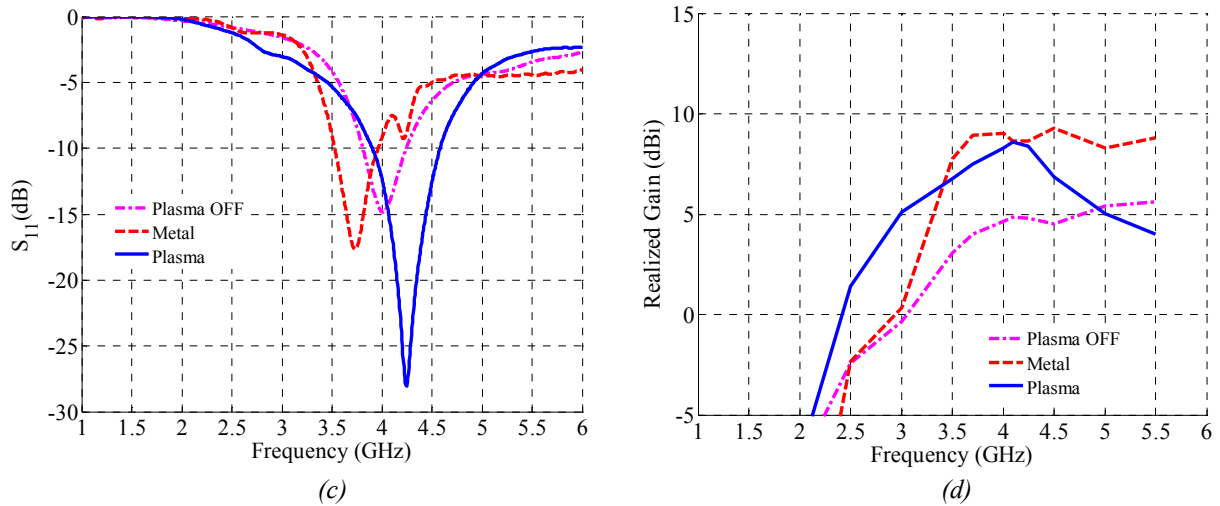
Figure 3.36 – Simulated performances of round reflector antenna using Triple Biax CFL. (a) Normalized H-plane radiation patterns, E_θ component at 4GHz. (b) Normalized E-plane radiation patterns, E_θ component at 4 GHz. (c) Magnitude of reflection coefficients, S_{11}. (d) Antenna gains.

Based on the design (Figure 3.35), three cases are simulated; plasma OFF, three metal elements, and three activated plasma elements (ON). From the results, radiation pattern of the two materials are corresponding to each other at the broadside direction as shown in Figure 3.36 (a), with -3 dB beamwidths are ± 35° and ± 30° for metal and plasma respectively. However the front to back ratio (f/b) of the plasma is less than 10 dB which is against its metal twin (13.5 dB) and this trend can be seen in Figure 3.36 (a) while Figure 3.36 (b) shows that the maximum beams are directed at θ equals 70°. In Figure 3.36 (c), all three cases are matched at 4 GHz, and yet metal and plasma having shifted reflection coefficients, S_{11} if compared to the case of glass tube. This is due to scattering effect caused by the surrounding elements that change the antenna input impedance. Both metal (9 dBi) and plasma (8.3 dBi) cases have shown almost 4 dB more in gain if compared to the plasma de-activated case as depicted in Figure 3.36 (d). In terms of scanning capability, the antenna main beam can be steered with 72° scanning step as illustrated in Figure 3.35.

3.2.1.2   Round reflector antenna using T5 fluorescent lamp

In the simulation of the second design of round reflector antenna, cylindrical-shaped fluorescent lamps (FL), type T5 are implemented as reflective elements and coordinated in circular arrangement. The total number of elements used in the simulation is 18. But not all elements are set as plasma or metal in every simulation. As the idea is to have sectoral beam shape, only half of the total elements are working as reflector at a time

and the rest remains as dielectric tubes. The geometry of this design is illustrated in Figure 3.37.
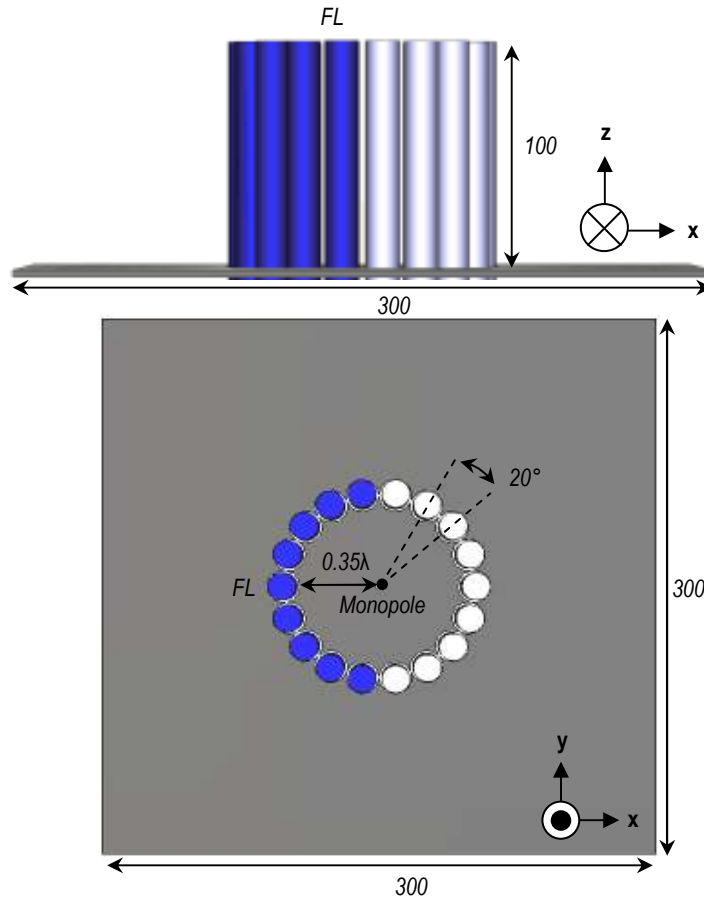
Figure 3.37 – Round reflector antenna using T5 fluorescent lamp consists of 18 elements. Only half of the total elements are activated at the same time. (Units in mm)

The height of each element from ground plane surface is 100 mm, the diameter of the lamp is 16 mm, and the central monopole height is 30 mm with a diameter of 1 mm. The angle between the centers of two adjacent elements is 20°, and it is depending on the distance between feeder and reflector surfaces. This angle will cause approximately 2 mm gap between two adjacent elements. In the simulations, the distance is set to 0.35λ at 2.4 GHz. The simulation performance results are given in Figure 3.38.
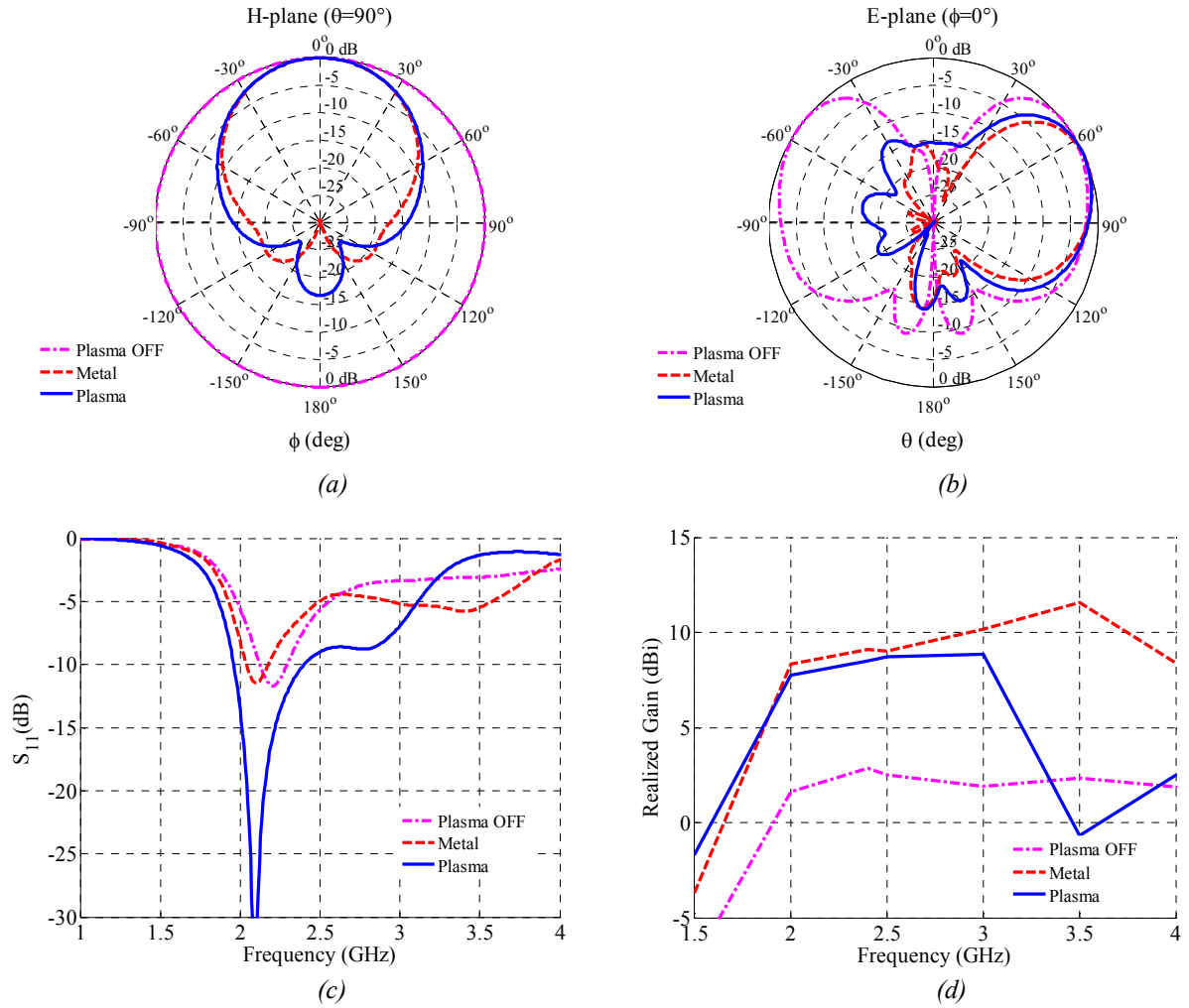
Figure 3.38 – Simulated performance of round reflector antenna using T5 fluorescent lamp antenna. (a) Normalized H-plane radiation patterns, E_θ component at 2.4 GHz. (b) Normalized E-plane radiation patterns, E_θ component at 2.4 GHz. (c) Magnitude of reflection coefficients, S_{11}. (d) Antenna gains.

By referring to Figure 3.37, only 9 elements are used to form plasma and metal reflectors in the simulations, while others remain as dielectric tubes. The gas inside the dielectric tubes is assumed to have ~1 permittivity since the noble gas (Argon) used in conventional FL is quite similar with the air in the room temperature. Therefore only the dielectric tube has effect on radiation patterns when the plasma and metal are absent. The simulated realized gains for plasma and metal elements are 8.5 dBi and 9.1 dBi respectively. The -3 dB angular widths is 66° for metal as well as plasma. The front to back ratio (f/b) are 19 dB (metal) and 16.5 dB (plasma). The main beam of this design can be steered with 20° step to complete 360° area as illustrated in Figure 3.37. Some drawbacks of this design in terms of its realization are; the reflecting elements (T5 FL) need to be excited on its both ends and the number of elements required for this design is high (18 elements).

3.2.1.3 Round reflector antenna using U-shaped compact fluorescent lamp arranged in series

The third design employs U-shaped compact fluorescent lamps (CFL) as its reflective elements. Because of its arrangement in series, this design employed less number of elements if compared to the round reflector antenna using T5 fluorescent lamp. Geometry of the simulated design is shown in Figure 3.39. A quarter wavelengths antenna is placed in the center of the ground plane having a diameter of 1 mm and a height of 30 mm. The height of each element from ground plane surface is 115 mm, and the diameter of the lamp is 13 mm. The geometric scale of the elements is based on the existing U-shaped CFL available in the market. The angles between the centers of two adjacent elements are 40° which is depending on the distance between feeder and reflector surfaces. The antenna performances are represented in Figure 3.40.
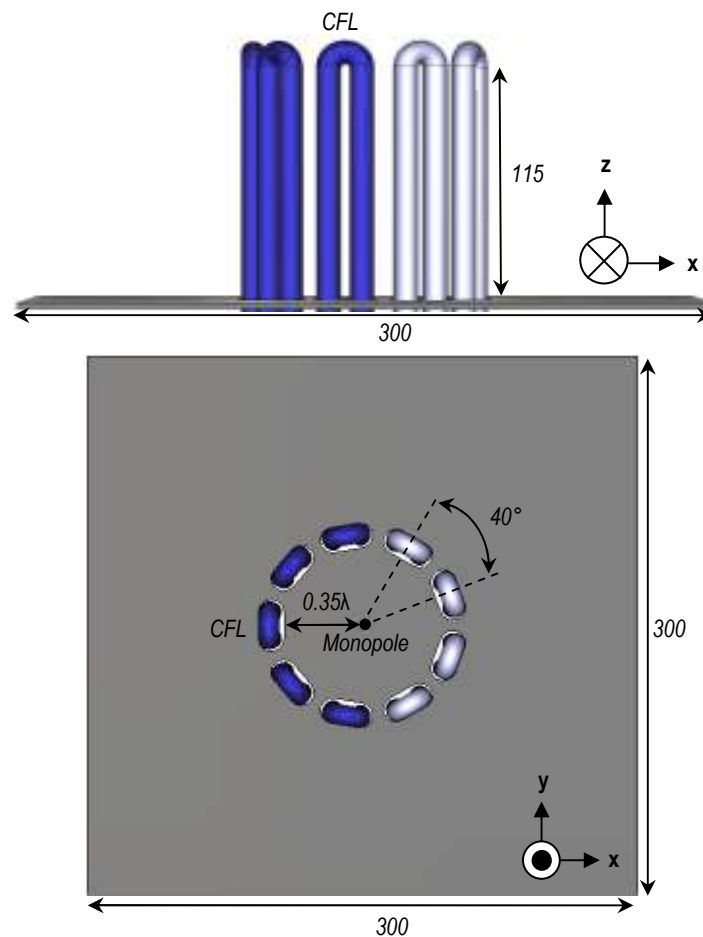
Figure 3.39 – Round reflector antenna using U-shaped CFL consists of 9 elements coordinated in series. Only five elements are activated at the same time. (Units in mm)
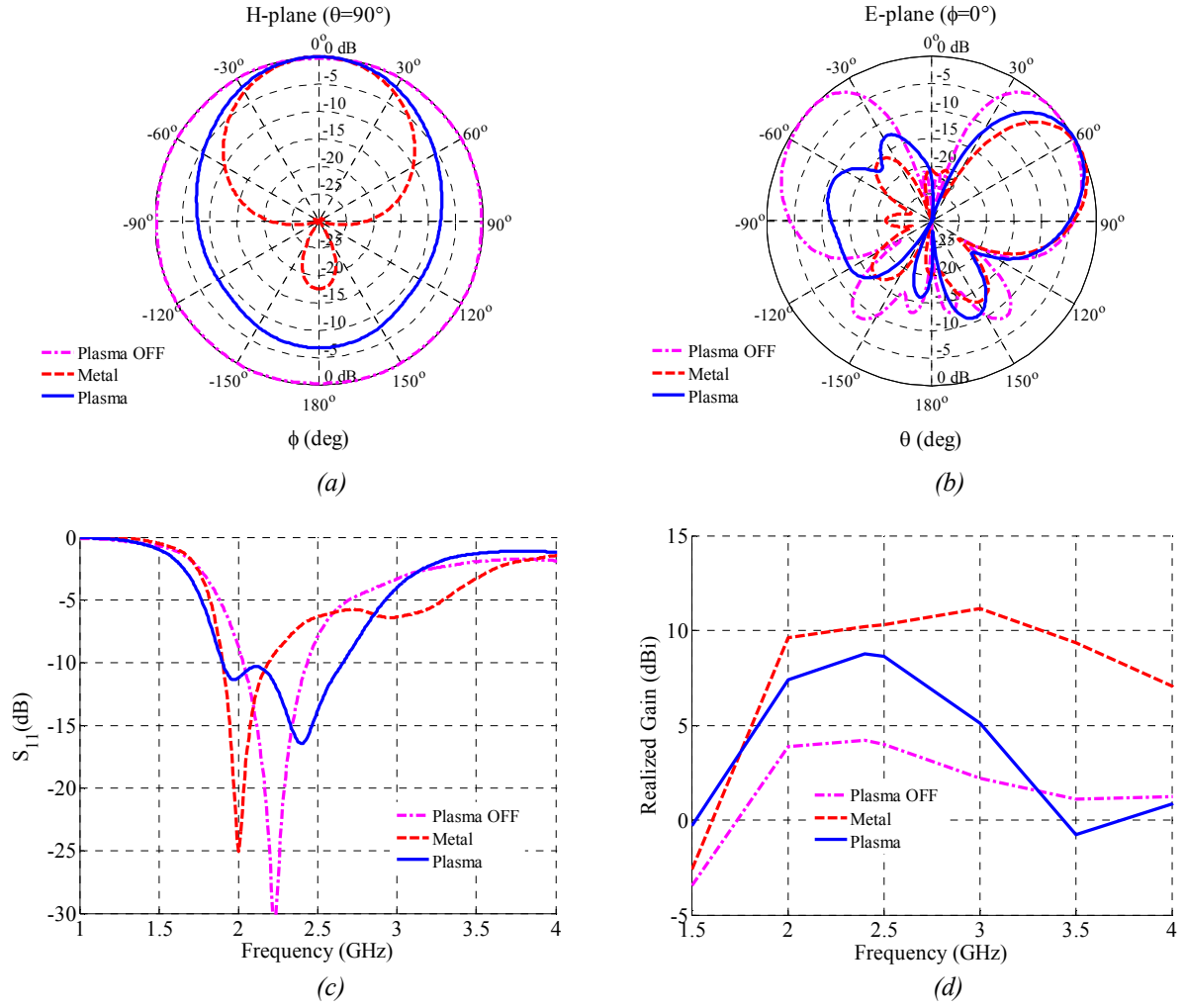
Figure 3.40 – Simulated performance of round reflector antenna using U-shaped CFL arranged in series. (a) Normalized H-plane radiation patterns, E_θ component at 2.4 GHz. (b) Normalized E-plane radiation patterns, E_θ component at 2.4 GHz. (c) Magnitude of reflection coefficients, S_{11}. (d) Antenna gains.

The radiation pattern shown in Figure 3.40 (a) and 3.40 (b) tell us that this plasma element arrangement does not provide good radiation pattern if compared to its metal counterpart. Even though, small degrees of broadside beam of the plasma (± 40°) and metal (± 30°) have a similarity, the front to back ratio of the plasma (7 dB) is not as good as the metal (17.5 dB). The refection coefficients and antenna simulated realized gains are depicted in Figure 3.40 (c) and 3.40 (d) respectively. Both cases (plasma and metal) have higher gains if compared to the gain of the monopole antenna (4.2 dBi at 2.4 GHz). The gain for metal case is 10.2 dBi while for the plasma is 8.9 dBi. For its scanning ability, the main beam of this design can be controlled to steer with 40° scanning step as depicted in Figure 3.39.

3.2.1.4 Round reflector antenna using U-shaped compact fluorescent lamp arranged in parallel

This design combines the best features of the second design (round reflector antenna using T5 FL, in Figure 3.37) and the third design (round reflector antenna using U-shaped CFL arranged in series, in Figure 3.39). The similar elements used in the third design are arranged in circular coordination as proposed in the second design. Therefore, this fourth design is assumed to have a good front to back ratio (f/b) as predicted in the second design. Since the U-shaped CFL is employed, the requirement of excitation at both ends for T5 FL as in the second design can be eliminated. Overall, this design requires 18 elements with only 11 elements activated at the same time while the rest remain de-activated. The height of each element is 115 mm with respect to the ground plane surface and the angle between the centers of two adjacent elements is 20°. The distance between central monopole and reflecting element is 0.35λ. The physical geometry of the antenna is shown in Figure 3.41 while its radiation patterns and antenna performances are depicted in Figure 3.42.
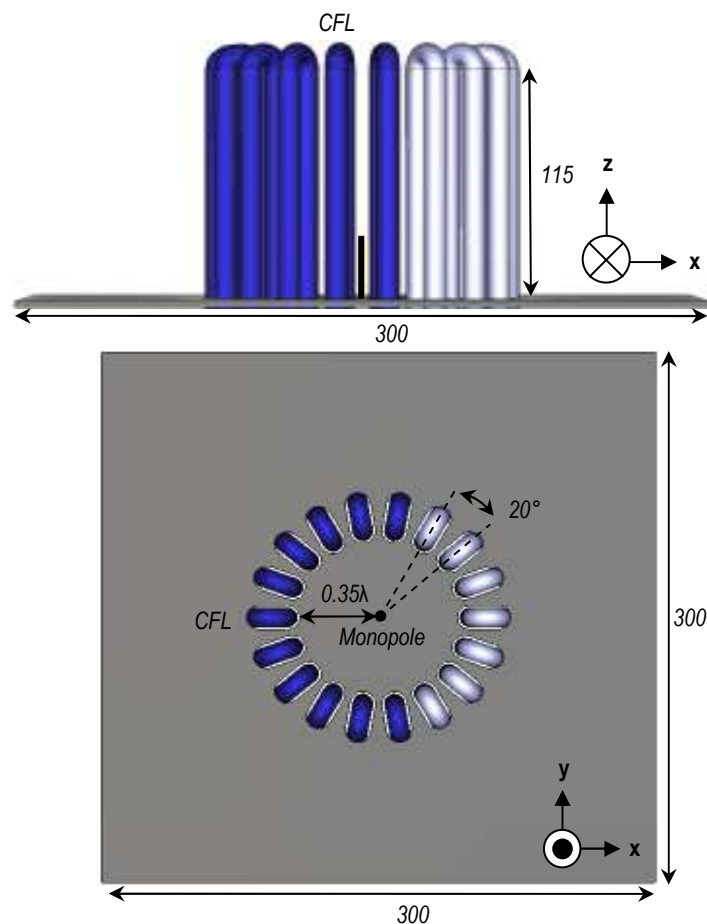
Figure 3.41 – Round reflector antenna using 18 U-shaped CFLs which are arranged in parallel. Only 11 elements are activated at a time to reflect an incoming wave. (Units in mm)
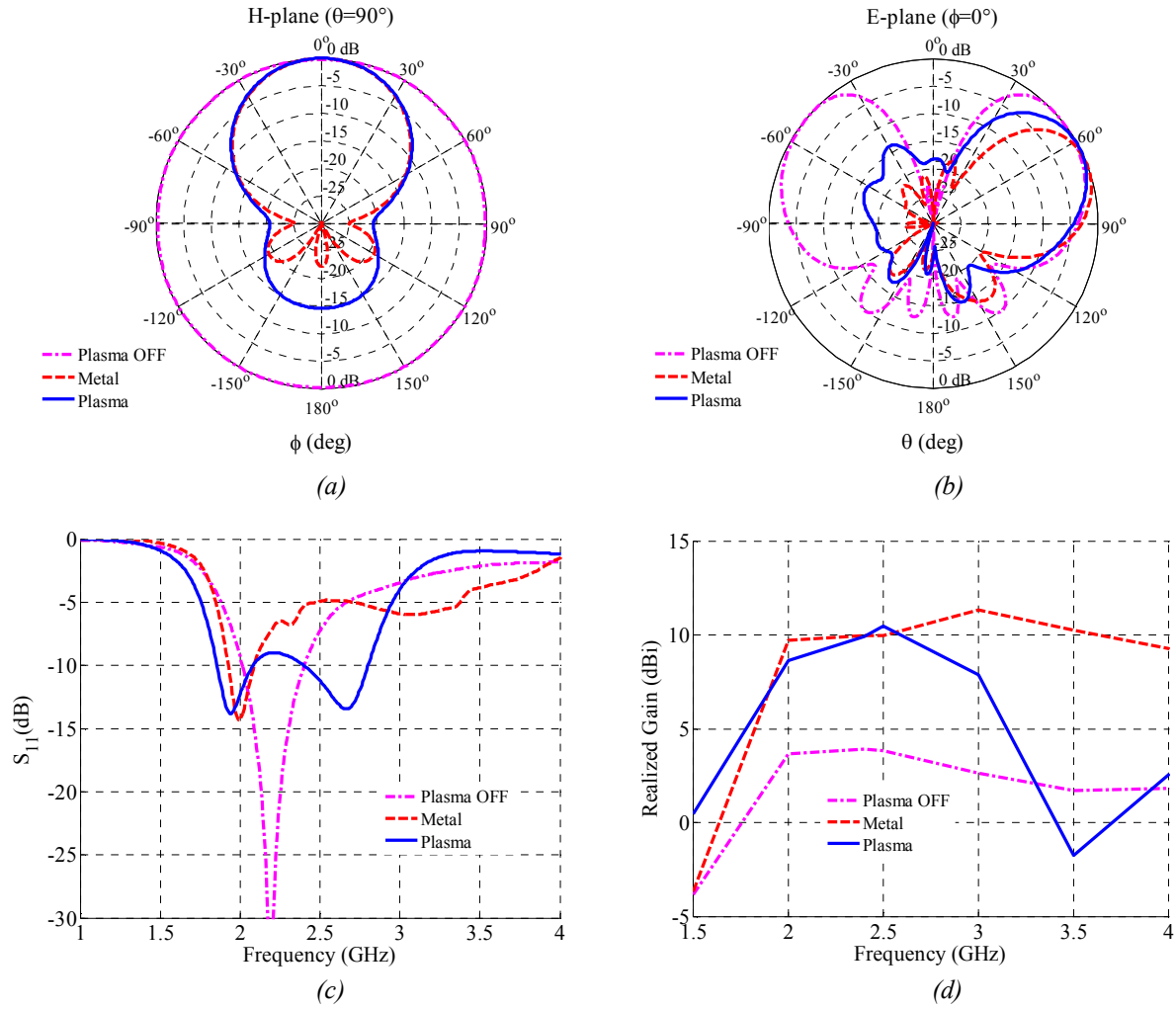
Figure 3.42 – Simulated performance of round reflector antenna using U-shaped CFL arranged in parallel. (a) Normalized H-plane radiation patterns, E_θ component at 2.4 GHz. (b) Normalized E-plane radiation patterns, E_θ component at 2.4 GHz. (c) Magnitude of reflection coefficients, S_{11}. (d) Antenna gains.

Figure 3.42 (a) tells that both plasma and metal cases have good agreement in terms of H-plane radiation pattern. The -3 dB beamwidth for plasma case is ± 30° as well as for the metal case. Plasma reflector antenna is exhibiting a good front to back ratio (f/b) which is 14.5 dB if compared to the first and the second designs which each of these designs produces f/b below than 10 dB. These two designs are previously shown in Figure 3.35 and Figure 3.37 respectively. An excellent agreement also can be seen in Figure 3.42 (b) for their elevation plane radiation patterns. The reflection coefficient of plasma is much better than metal case as represented in Figure 3.42 (c). Both plasma and metal provide good gains at 2.4 GHz (10 dBi for both cases) as shown in Figure 3.42 (d), which is more than the gain of its monopole antenna with surrounding dielectric tubes. This design has similar scanning capability as explained in the second design. The smallest possible scanning step is 20° and it can be realized by activating only 11 elements at the same time.

In general, this round reflector antenna using 18 U-shaped CFLs which are arranged in parallel has no significant drawback if compared to the three designs proposed in the previous sections.

3.2.1.5   Design summary

The round reflector antenna using Triple Biax CFL (first design) having the biggest separation angle which is due to its physical size. As a result, the finest scan step is only 72° which is higher than other proposed designs. For the round reflector antenna using T5 fluorescent lamp (second design), it has much better antenna performance than the first design in term of radiation pattern. However it requires excitation at its both ends therefore will lead to complexity when it comes to realization. For the round reflector antenna that uses 18 U-shaped CFLs arranged in series (third design), it reduces the complexity of the second design, however its circular arrangement with 40° separation angle is not good as those proposed by the second design. The back side radiation is broad and remains the biggest if compared to other designs.

Therefore, the round reflector antenna using 18 U-shaped CFLs arranged in parallel is the most favorable since it merges the best features proposed in Figure 3.35 and in Figure 3.37. Moreover this design shows a good similarity between metal and plasma in terms of their radiation patterns and gains. The reflection coefficient, S_{11} of plasma reflector is slightly lower than -10 dB at 2.4 GHz but it is a way better than its metal counterpart. However, this matching problem can be avoided with a right selection of the distance between reflector surface and an optimum angle between two adjacent elements. The summary for the proposed plasma reflector antennas are listed in Table 3.1

Table 3.1 – The performances summary of the proposed round reflector antennas using plasma as reflecting elements.

Components	Round reflector antenna using Triple Biax CFL	Round reflector antenna using T5 FL	Round reflector antenna using 18 U-shaped CFLs arranged in series	Round reflector antenna using 18 U-shaped CFLs arranged in parallel
Distance between central monopole antenna and reflector surface (mm)	0.25λ	0.35λ	0.35λ	0.35λ
Angle between centers of two adjacent elements (°)	72	20	40	20
No. of elements	5	18	9	18

No. of activated elements (required)	3	9	5	11
HPBW (°)	± 30	± 33	± 40	± 30
Gain (dBi)	8.3	8.5	8.9	10
Front to back ratio (f/b) (dB)	7	17	7	15

Based on this simulation results comparison, the round reflector antenna using 18 U-shaped CFLs arranged in parallel is chosen for the antenna optimization. The following topic will elaborate on the optimization process for the round reflector antenna using U-shaped CFL arranged in parallel.

3.2.2 Optimization of the round reflector antenna using U-shaped CFLs arranged in parallel

In the early work of optimization, several values of distances between central monopole antenna and reflecting element surface have been simulated. The parametric study has been conducted by varying the distance from 0.1λ up to 0.7λ. By doing so, the numbers of elements required to reflect omnidirectional beam into broadside direction will also vary accordingly. The evolution of distance and its required number of element is depicted in Figure 3.43.

<div align="center">
0.1λ   0.3λ   0.7λ
</div>
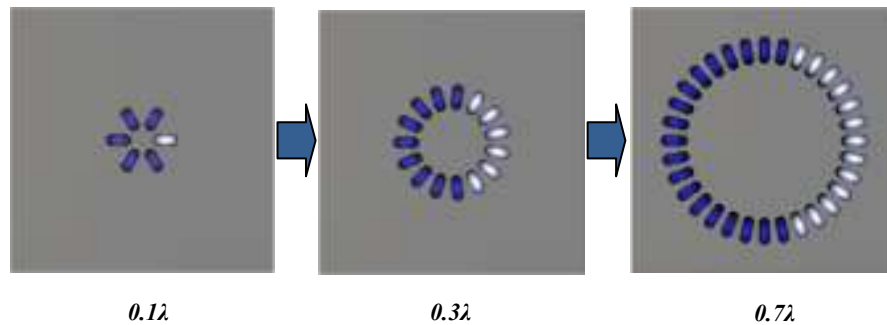
Figure 3.43 – Evolution of antenna arrangement for three different distances between central monopole antenna and reflector surface. The required activated elements are 5, 9 and 19 for the distances of 0.1λ, 0.3λ and 0.7λ respectively.

The figure shows only some of the simulated distances however it is enough to give an overview of the effect of the varying distance that changes the total number of required elements. The antenna parameters that have been used to optimize the antenna design in the following sections are depicted in Figure 3.44. D_{cc} is the distance between centers of two adjacent elements and D_{ms} is the distance between central monopole

antenna and reflector surface. The angle between centers of two adjacent elements is represented by θ_s.
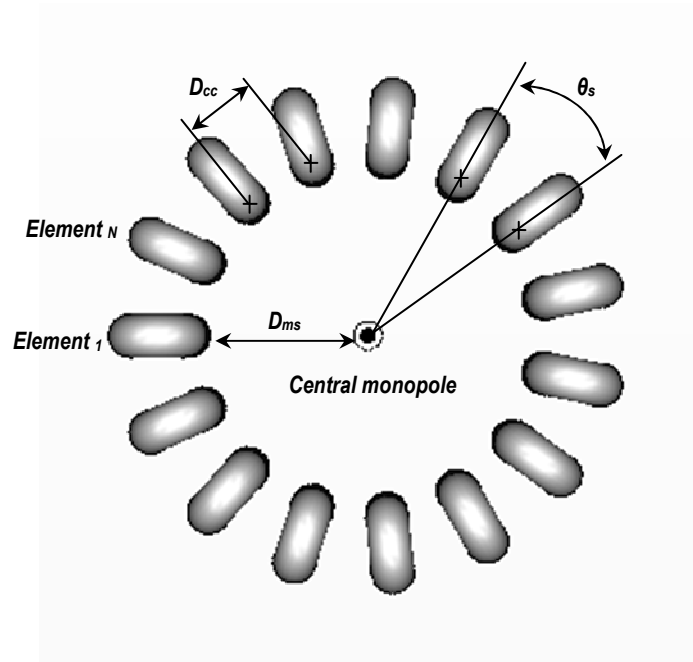
Figure 3.44 – Optimization parameters of the round reflector antenna. (D_{cc} is the distance between centers of adjacent elements, D_{ms} is the distance between central monopole antenna and reflector surface, θ_s is an angle between centers of two adjacent elements)

3.2.2.1 Optimization of distance between central monopole antenna and reflector surface, number of elements, and element separation angle based on physical arrangement

As mentioned earlier, by changing the distance between feeder (monopole antenna) and reflecting surface will also change the required number of total elements. This scenario is depicted for three different distances between central monopole antenna and reflector surface previously in Figure 3.43. However, the number of elements only can be finalized by respecting the actual physical gap between two adjacent elements (the lower part of the CFL). Hence, by verifying the actual CFL, the closest distance between two adjacent elements is measured to be 5 mm (inter-element spacing). As a consequence, if the lamp diameter is 13 mm (with 6.5 mm radius), the possible lower distance between centers of adjacent elements is 18 mm. By respecting this value, the results of the simulations are summarized in Table 3.2.

Table 3.2 – Summary of antenna optimization based on physical arrangement.

Distance between central monopole antenna and reflector surface, D_{ms} (mm)	Angle between centers of each element, θ_s (°)	No. of Elements	Distance between centers of adjacent elements, D_{cc} (mm)	No. of activated elements (required)
0.1λ	60	6	19.0	5
0.2λ	36	10	19.5	7
0.3λ	24	15	18.3	9
0.4λ	18.95	19	18.6	11
0.5λ	15	24	18.0	15
0.6λ	12.86	28	18.3	17
0.7λ	11.25	32	18.5	19

First of all, let's compare to the round reflector antenna using 18 U-shaped CFLs arranged in parallel. The separation angle between centers of two adjacent elements, θ_s is varied from 20° (refer to Figure 3.41) to 24° after optimization which corresponds to a reduction of 0.05λ on the distance between feeder and reflecting elements surface, D_{ms}. The total number of element is 15 (with 9 activated plasma elements) which is less 3 elements than the one proposed previously. Verification of this optimization will only be confirmed by comparing the antenna performance with respect to all distances.

3.2.2.2 Optimization of distance between central monopole antenna and reflector surface, and number of elements based on antenna performances

In the previous section, the best angle between centers of two adjacent CFLs is 24° in corresponds to the distance of 0.3λ (37.5 mm) between feeder and reflector surfaces. These two values are gained from a parametric study of the complete model by changing each value at one time, and with respect to the inter-element spacing limitation. The closer the distance, the less the number of elements used in the simulations. However, the space gap between elements might be higher when the number of elements is lesser. Thus, it can reduce the effectiveness of the overall reflector surface. For that reason, it is essential to select optimum configuration by taking into account the value of directivity, gain and number of required elements. Despite of the distances tabled in Table 3.2, a simulation with distance of 0.35λ (43.75 mm) was also conducted with regard to the distance proposed in the fourth design (round reflector antenna using 18 U-shaped CFLs arranged in parallel).

As shown in Figure 3.45 (a), the highest gain occurs at the distance of 0.4λ (50 mm). This is corresponding to 19 elements depicted in Figure 3.45 (b). However, it is worth to

look at a distance of 0.35λ, even though the gain is 0.8 dB lower, the number of elements is now reduced to 15. With this distance, the overall system gives optimum gain with respect to the directivity. Hence, the distance of 0.35λ is better than other distances that have been simulated. Even though with distance of 0.3λ, the number of required elements is the same as at 0.35λ (15 elements), the antenna is more efficient with the distance of 0.35λ. The gain takes into account all loss as well as the mismatch of the antenna, and it is related to the directivity by a coefficient that can be considered as the efficiency of the antenna. For that reason, the configuration with this distance (0.35λ) is chosen for simulations in this study and also for the model realization. The geometry of the finalized design is shown in Figure 3.46. The set of holes to insert the CFLs is also represented in the figure.

(a)   *(b)*
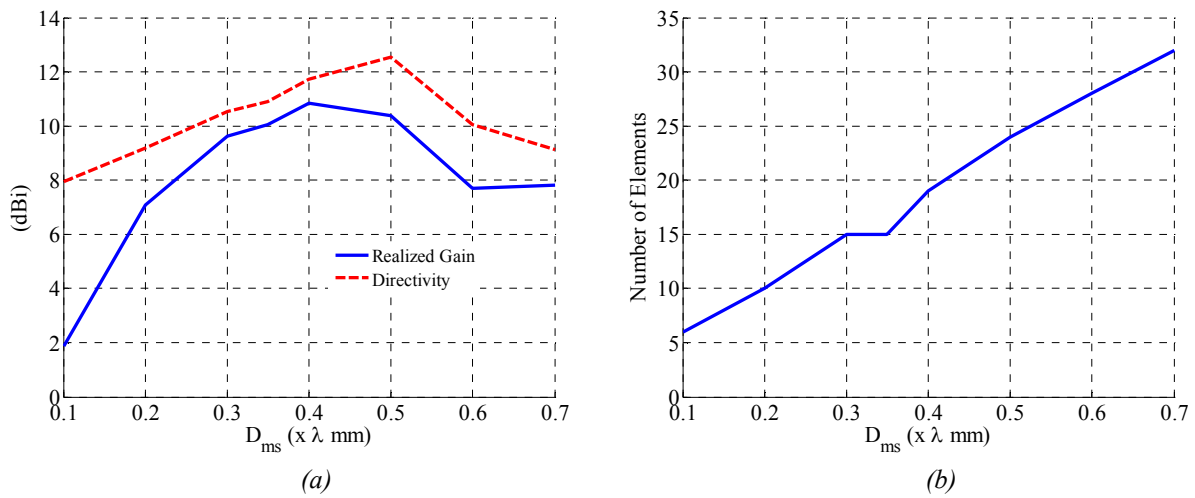
Figure 3.45 – Antenna performances and its number of element. (a) Simulated antenna gain and directivity with respect to distance, D_{ms} (gain-solid line, directivity-dotted line). (b) Number of elements versus distance, D_{ms}. Fifteen elements are required for the distances of 0.3λ and 0.35λ.
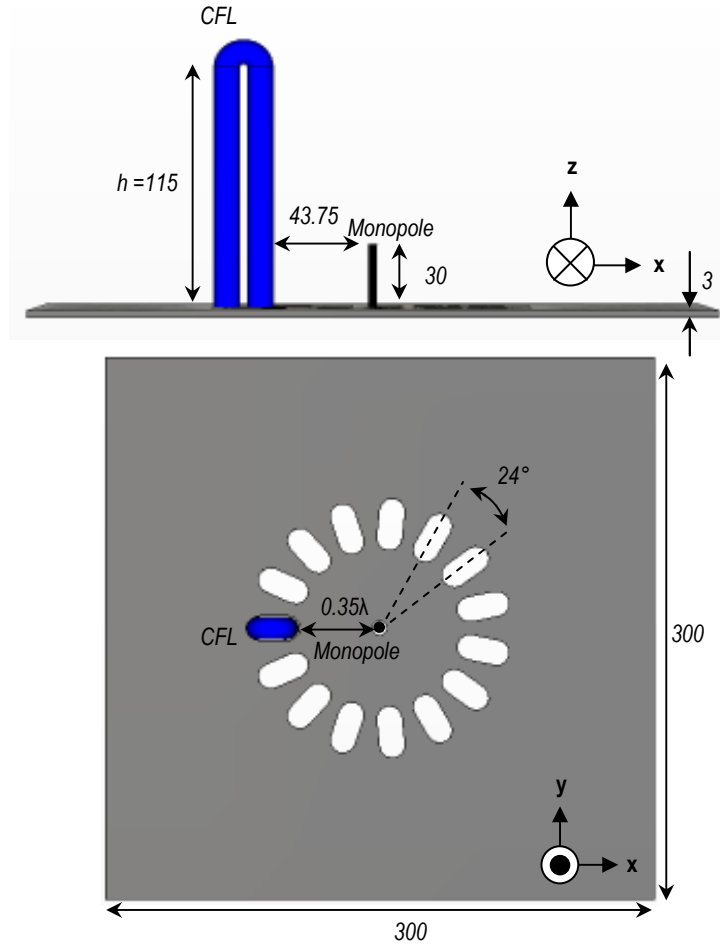
Figure 3.46 – Geometry of finalized round reflector antenna. Only 1 element out of 15 elements is illustrated in the figure along with a set of holes used to insert the CFLs.

3.2.3 Fabrication of round reflector antenna

The realized model was fabricated on 3 mm thick ground plane based on the geometry of the RRA given in Figure 3.46. The fabricated prototype and its supporting components are shown in Figure 3.47. Excitation power to energize the 9 Watts CFLs is supplied by a set of electronic ballasts with specification of 220-240 V, 50-60 Hz (Appendix 3.2). Each of the electronic ballast is controlled by a small single-pole switch and each of it required a set of four wires to be connected to each of the CFLs. Thus to come out with the prototype, 15 electric ballasts and 15 switches are needed as shown in Figure 3.47 (b).
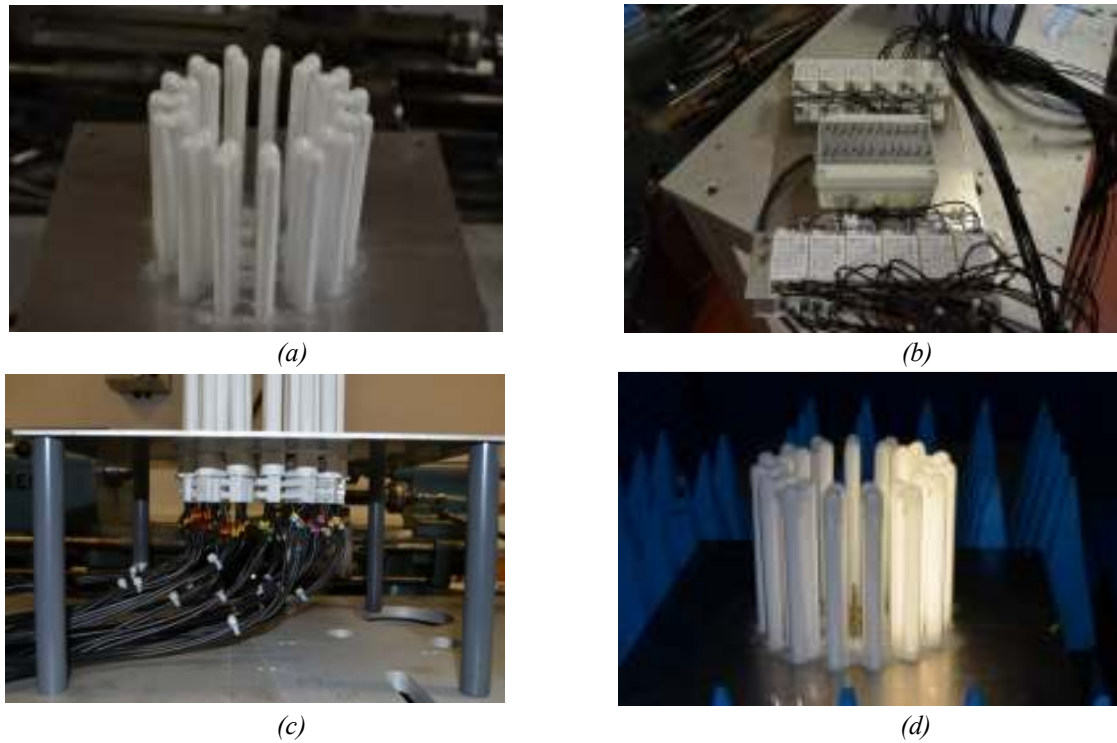
Figure 3.47 – Prototype of the round reflector antenna (RRA). (a) 15 CFLs with a 300 mm x 300 mm ground plane. (b) Switches and electronic ballasts. (c) Connectors box. (d) Quarter wave feeder in the center of the ground plane.

The electric ballast is chosen instead of magnetic ballast as an element to energize CFL because its simplicity, low noise and compact in size. However, a trade off exists in the increment numbers of connecting wires. The needs of CFL base type 2G7 was removed since the CFLs were inserted from the bottom of the ground plane and carefully glued to the ground plane. The gluing process need to be done one by one for the rest of CFLs. The CFLs must be vertically aligned with respect to the ground plane surface. Each of the wire is connected to CFL pins by using ordinary wire connecter box as shown in Figure 3.47 (c). There are 4 poly legs screwed to support the ground plane, and each of it having 160 mm length. The monopole antenna with diameter of 2 mm as shown in Figure 3.47 (d) is connected to the feeding line via a 50 Ohm SMA female connector.

3.2.4 Measurement setup of plasma round reflector antenna

This section explains on the measurements setup of the RRA and its apparatus. A switching scheme to steer, shape and to scan is also discussed.

3.2.4.1   Antenna performance measurement of round reflector antenna

The antenna performance measurements were conducted in two different anechoic chambers. The input impedance of the antenna was conducted in small anechoic chamber as shown in Figure 3.48 (a). A vector network analyzer was used to measure the input impedance. The measurements were conducted for all RRA configurations (beam shaping and beam scanning).

(a)   *(b)*

Figure 3.48 – Antenna input impedance measurement apparatus. (a) RRA with activated elements. (b) Vector network analyzer (Agilent N5242A).

The radiation pattern measurements were performed in a SATIMO 32 anechoic chamber with the peak gain accuracy of ± 0.8 dBi for 1 GHz up to 6 GHz operating frequencies. The SATIMO near-field chamber consists of 32 bipolarized receiving probe antennas located on an arch in circular-shaped arrangement with an internal diameter of 1.5 m. The SATIMO is shown in Figure 3.49 (a).

(a)

| (b) | (c) |

Figure 3.49 – The RRA radiation pattern and gain measurement apparatus. (a) SATIMO 32 anechoic chamber with 32 receiving probes. (b) A specially made support fixture used to place the AUT. (c) The specially made support fixture used during measurement.

The SATIMO measurement system consists of an amplification unit, a mixer unit, a probe array controller, an uninterruptible power supply, an antenna under test (AUT) positioner, a primary synthesizer, and an auxiliary synthesizer. The AUT is placed on a support fixture as can be seen in Figure 3.49 (b). The support fixture is specially made to be equipped with SATIMO. It has four legs and by varying the height of its legs, the placing height of AUT can be altered accordingly. The maximum height with respect to the flat surface is approximately 1 meter.

3.2.4.2   Switching scheme of RRA for beam scanning

The antenna prototype uses 15 single-pole electronic switches to control its element state (ON or OFF) in order to direct its main beam in particular directions. Since each of the elements can be controlled individually, the antenna has enormous possibility to shape and to steer its beam. Each of elements is represented by a dedicated switch as shown in Figure 3.50.
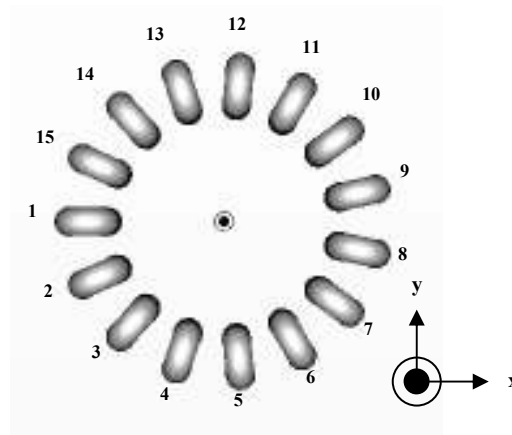
Figure 3.50 – There are 15 elements (CFL) for the fabricated RRA and the elements are numbered in anti-clockwise direction.

Generally, a number of activated elements (switched ON) will define the size of plasma window thus controlling the reflected beamwidth. In this investigation, with the optimized RRA, there are only 9 elements activated at the same time. By taking into account of an overlapping -3 dB beamwidth (HPBW), the RRA is controlled to steer its main beam with 48° step. Therefore, eight different main beam directions can be realized with this configuration. A switching setting scheme to steer the antenna beam is tabled out in Table 3.3, and it is based on the element numbering sequence as illustrated in Figure 3.50.

Table 3.3 – Switching setting for beam scanning (with 9 activated elements).

Beam Direction	Switched ON Elements	Switched OFF Elements
0°	5, 4, 3, 2, 1, 15, 14, 13, 12	11, 10, 9, 8, 7, 6
48°	7, 6, 5, 4, 3, 2, 1, 15, 14	13, 12, 11, 10, 9, 8
96°	9, 8, 7, 6, 5, 4, 3, 2, 1	15, 14, 13, 12, 11, 10
144°	11, 10, 9, 8, 7, 6, 5, 4, 3	2, 1, 15, 14, 13, 12
192°	13, 12, 11, 10, 9, 8, 7, 6, 5	4, 3, 2, 1, 15, 14
240°	15, 14, 13, 12, 11, 10, 9, 8, 7	6, 5, 4, 3, 2, 1
288°	2, 1, 15, 14, 13, 12, 11, 10, 9	8, 7, 6, 5, 4, 3
336°	4, 3, 2, 1, 15, 14, 13, 12, 11	10, 9, 8, 7, 6, 5

3.2.5 Design variety

Instead of having one element height for the fabricated RRA, the prototype is further enhanced with extra flexibility by varying its elements' height measured from ground plane surface. The design configurations with three different element heights are illustrated in Figure 3.51. An idea to change the antenna element height is originated from the availability of variety of CFL lengths in the market. Therefore, instead of

having one element's height, the antenna can be re-fabricated with a set of new CFLs with different heights and its performance can be measured and compared.

(a)   *(b)*

                                                         (c)
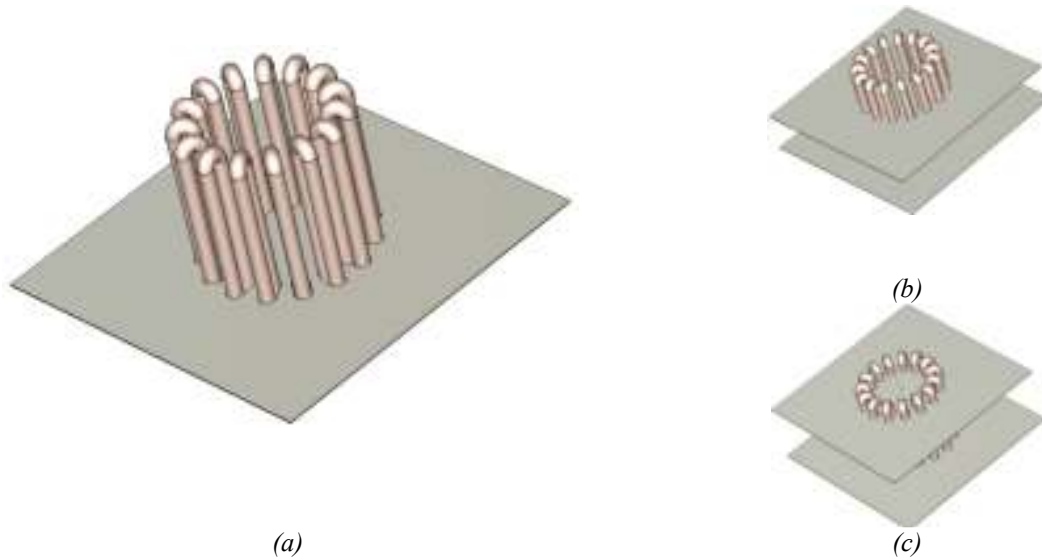
Figure 3.51– The simulation designs. (a) Primary design with 115 mm CFL height. (b) Second design with 54 mm CFL height. (c) Third design with 15 mm CFL height.

However to redo the fabrication process will take some extra time and cost. As a result, by adding another ground plane as shown in Figure 3.51 (b) and 3.51 (c), the height of antenna element can be reduced and its performance can be analyzed. These two new arrangements represent a compact version of RRA with reduced height which is possible to be fabricated.

Prior to antenna realization, several simulations have been performed to study the effect of adding second layer of the ground plane. A comparison has been conducted between two cases; 1) a single layer, and 2) two layers of ground plane both with identical element height. The results have proved that by adding extra layer of ground plane, antenna radiation patterns are identical for each case in both H- and E- planes. In conclusion, the compact version of RRA with reduced element height can be analyzed by changing its element height with the aid of second layer of the ground plane. The photographs of the second ground plane are shown in Figure 3.52.

(a)   *(b)*

(c)   *(d)*

Figure 3.52– Photograph of the secondary ground plane and its equivalent RRA. (a)-(b) The h is 54 mm with the inserted secondary ground plane. (c)-(d) The h is 15 mm with the inserted second layer of the ground plane.

The first RRA prototype is realized using a set of U-shaped CFLs with the base-to-base length is 152 mm (total height from top to bottom). Its technical data are listed in Appendix 3.3. The second design is realized by adding extra ground plane and the resulting height of element is 54 mm which represent the height of other U-shaped CFLs with the base-to-base length equivalent to 92 mm that is available in the market. Its technical data are listed in Appendix 3.4. The third design was purposely realized to investigate the RRA performance if its element's height is lesser than its resonating element.

3.2.6 Results and analysis of the fabricated round reflector antenna (RRA)

This part presents numerous set of simulation and measurement results of the designed RRA. The effects of surrounding dielectric tubes on monopole antenna radiation patterns are presented in the first part of this section. Plasma window is the main factor to shape an incoming beam, thus its effect are also discussed with three different element's heights. Finally, scanning capability of RRA with 9 activated elements is presented. The results are given for the three element heights (115 mm, 54 mm 15 mm).

3.2.6.1   Effect of surrounding dielectric tubes on monopole antenna radiation pattern

In order to observe the effect of dielectric tubes on radiation pattern of the monopole antenna, the design model has been simulated and measured for two configurations; a) monopole antenna without dielectric tubes, and b) monopole antenna surrounded by

dielectric tubes (plasma OFF) as previously shown in Figure 3.47 (a). For the configuration with 115 mm dielectric tubes, the absent of plasma leaves argon gas inside the tubes. The simulated and measured radiation patterns for both cases are then compared. The results show quite similar radiation patterns for both cases that conclude the existence of dielectric tube can be neglected. Figure 3.53 shows the simulated and measured normalized radiation patterns in the H- and E- planes for the both configurations.
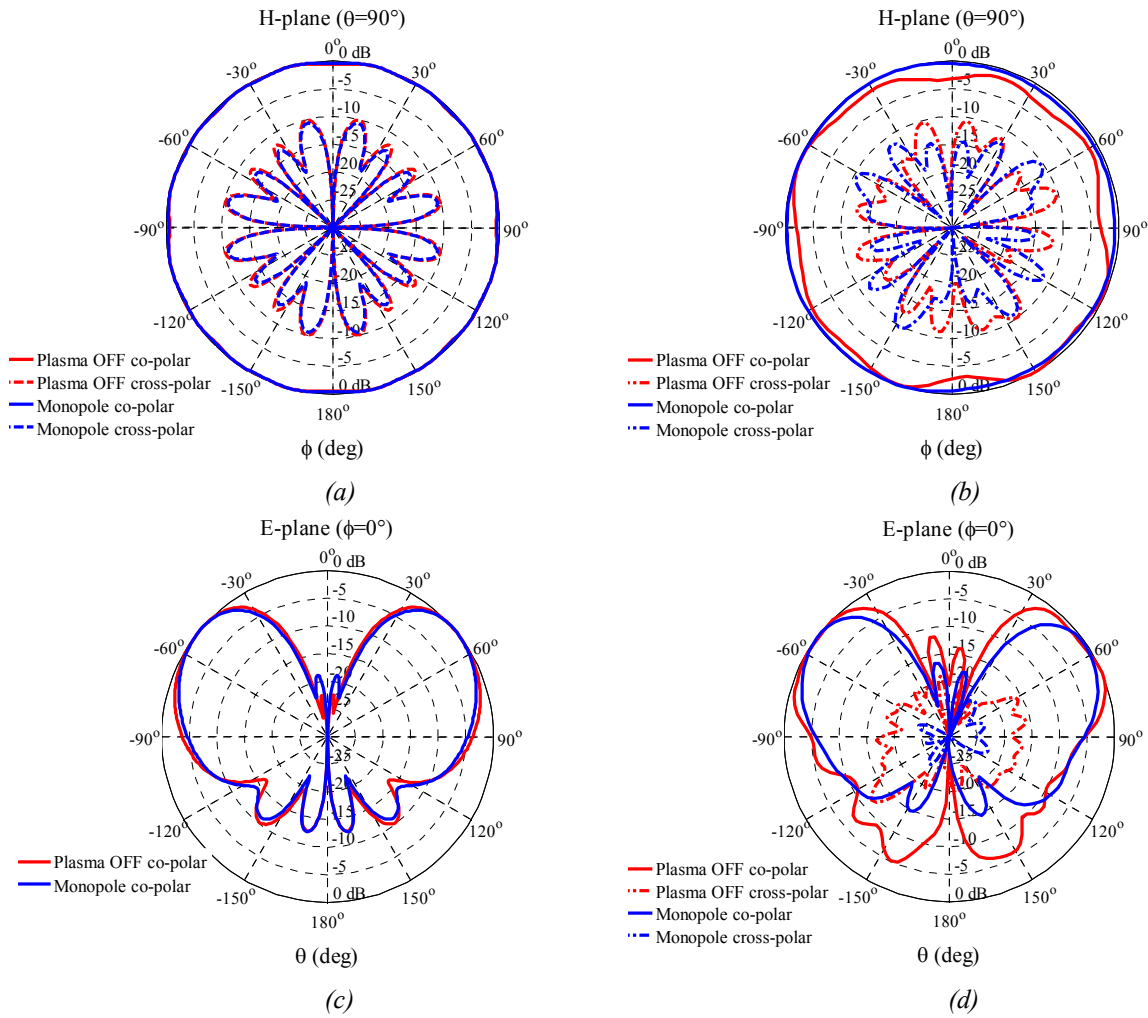
Figure 3.53 – Comparison of the normalized radiation patterns of a monopole antenna for two antenna configurations (monopole antenna and monopole antenna surrounded by dielectric tubes), E_θ and E_ϕ components at 2.4 GHz. (a) Simulated H-plane radiation patterns. (b) Measured H-plane radiation patterns. (c) Simulated E-plane radiation patterns. (d) Measured E-plane radiation patterns.

The simulated cross polarization levels in the E-plane for the both configurations are below than -25 dB. As a result, they are not able to be seen in Figure 3.53 (c). During the measurement for the configuration with surrounding dielectric tubes, a set of wires to energize the CFLs are always there, therefore having some effect on the back radiation pattern. However the effect is negligible since it does not degrade the main

lobe as can be seen in Figure 3.53 (d) or even in the H-plane radiation patterns depicted in Figure 3.53 (b).

The reflection coefficients are almost similar for both cases as shown in Figure 3.54 (a) and 3.54 (b). Both configurations are matched with reflection coefficient below than -10 dB at operating frequency.
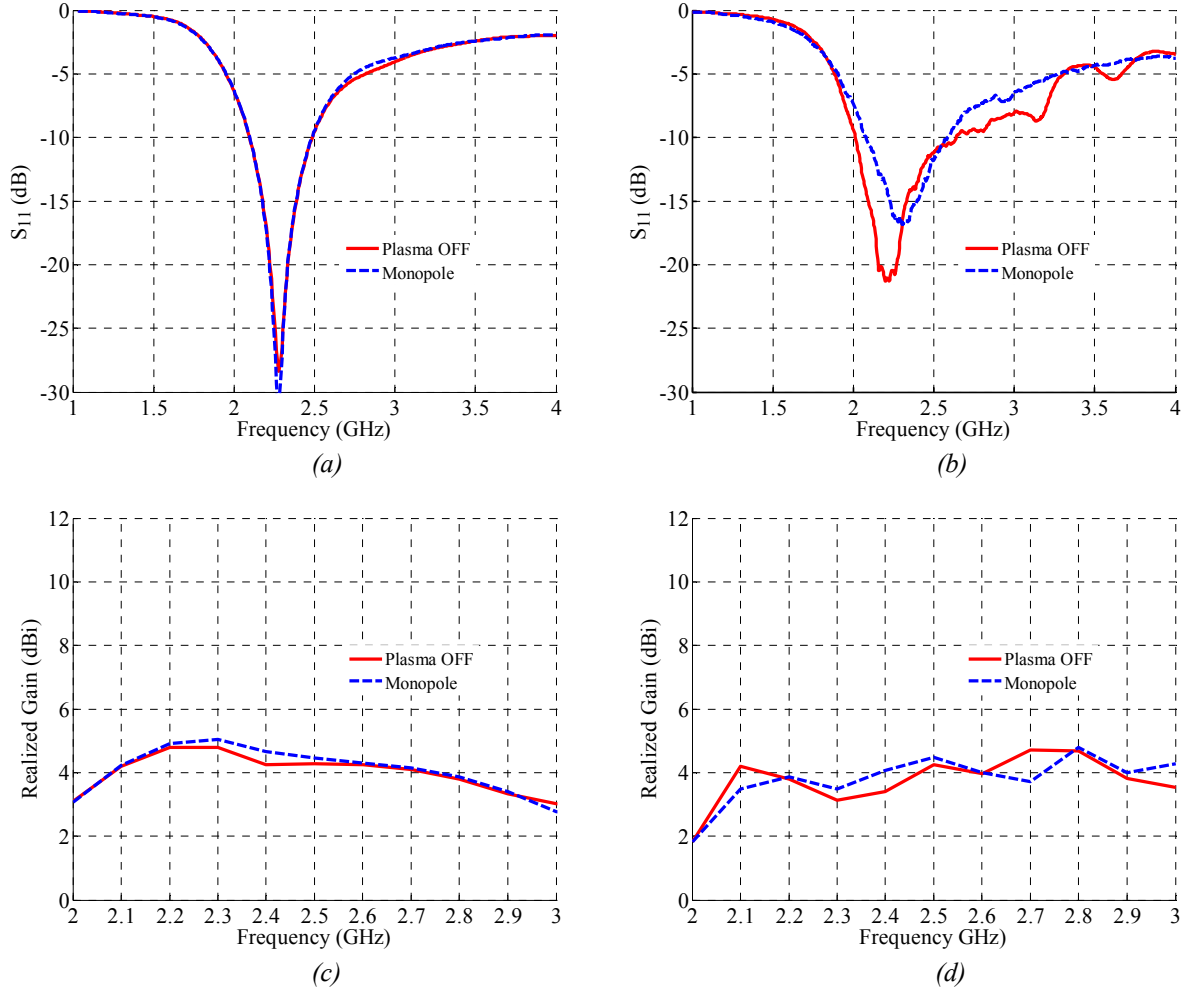
Figure 3.54 – Monopole antenna performances with (plasma OFF) and without the presence of dielectric tubes. (a) Magnitude of simulated reflection coefficients, S_{11}. (b) Magnitude of measured reflection coefficients, S_{11}. (c) Simulated gains. (d) Measured gains.

The gain of the monopole antenna is also compared for the two configurations as shown in Figure 3.54 (c) and 3.54 (d), for the simulation and measurement respectively. There is no much reduction in gain with the presence of the surrounding dielectric tubes for both configurations either in simulation or measurement.

The results again confirm that, the presence of dielectric tubes surrounding the monopole antenna has no significant effects to the reflection coefficient. Therefore, it is possible to construct reconfigurable reflector antenna by only activate and de-activate the plasma elements without having to worry about the surrounding dielectric tubes.

3.2.6.2   Beam shaping of RRA by varying plasma window

Several simulations have been performed to find good radiation patterns in the H- and E- planes with different number of elements activated at one time as the beam profiles of the reflected signal can be shaped by varying the size of plasma window. This can be realized by activating arbitrary adjacent elements. In this study, three configurations setup have been identified. The configuration is 7-, the second is 9- and the third configuration is 11-elements activated. In this investigation, the 7-elements corresponds to the widest plasma window while 11-elements represents the narrowest plasma window. Figure 3.55 illustrates these three configurations.
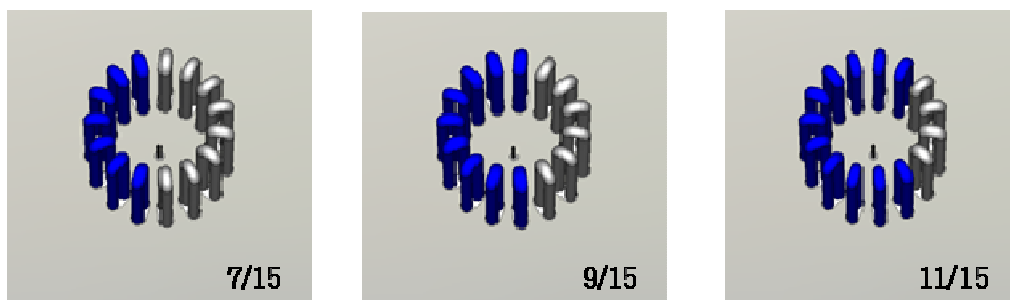
Figure 3.55 – Number of de-activated elements (grey color) represents the size of plasma window. In this investigation, the widest window is with 8 de-activated elements and 7 activated elements (blue color) while the narrowest window is with 4 de-activated elements. (7/15 represents 7 activated elements out of 15 total elements).

From the simulation results, it is better to anticipate that by narrowing the plasma window, the beam will be more focus and will lead to high directivity which allows longer communication distance and vice versa. The variation of radiation patterns for different plasma window's sizes in the H- and E- planes are presented in the following subsections. The antenna performances with regard to its configuration are also discussed accordingly.

3.2.6.2.1   Beam shaping of RRA with element height, *h* equals 115 mm

The variation of radiation patterns for different size of plasma windows in the H- plane is shown in Figure 3.56 while the simulated and measured antenna gains are shown in Figure 3.57 (a) and 3.57 (b), respectively. Let's take a look at antenna radiation patterns; a wider beam at broadside direction is observed when 7 elements are activated. The gain tends to drop from 9 dBi (9-elements configuration) to 6.8 dBi due the broadening radiation effect. When the number of elements is increased to 11, the gain also decreased to 7.6 dBi. However this is due to the narrowing effect of plasma

window leading to the diffraction of electromagnetic wave and hence reduces the gain. The -3 dB beamwidths are similar for the three configurations. From these three patterns, one can see with 9-elements configuration the radiation pattern is at optimum. The beam is more focused while the side lobe and the back radiation are reduced, giving the highest gain.

Albeit the 11-elements configuration has comparative beam at broadside direction, its back radiation is much higher. Thus the gain of this configuration is lower than 9-elements configuration. Therefore for scanning validation in the next section, the 9-elements configuration was adopted. It is important mentioning that both simulation and experimental results have cross polarization below than -10 dB and their front to back ratio (f/b) is more than 10 dB for the three configurations discussed here. The E-plane radiation patterns are shown in Figure 3.56 (c) and 3.56 (d). The maximum gains occur at elevation angle between 29° and 30° for all configurations.
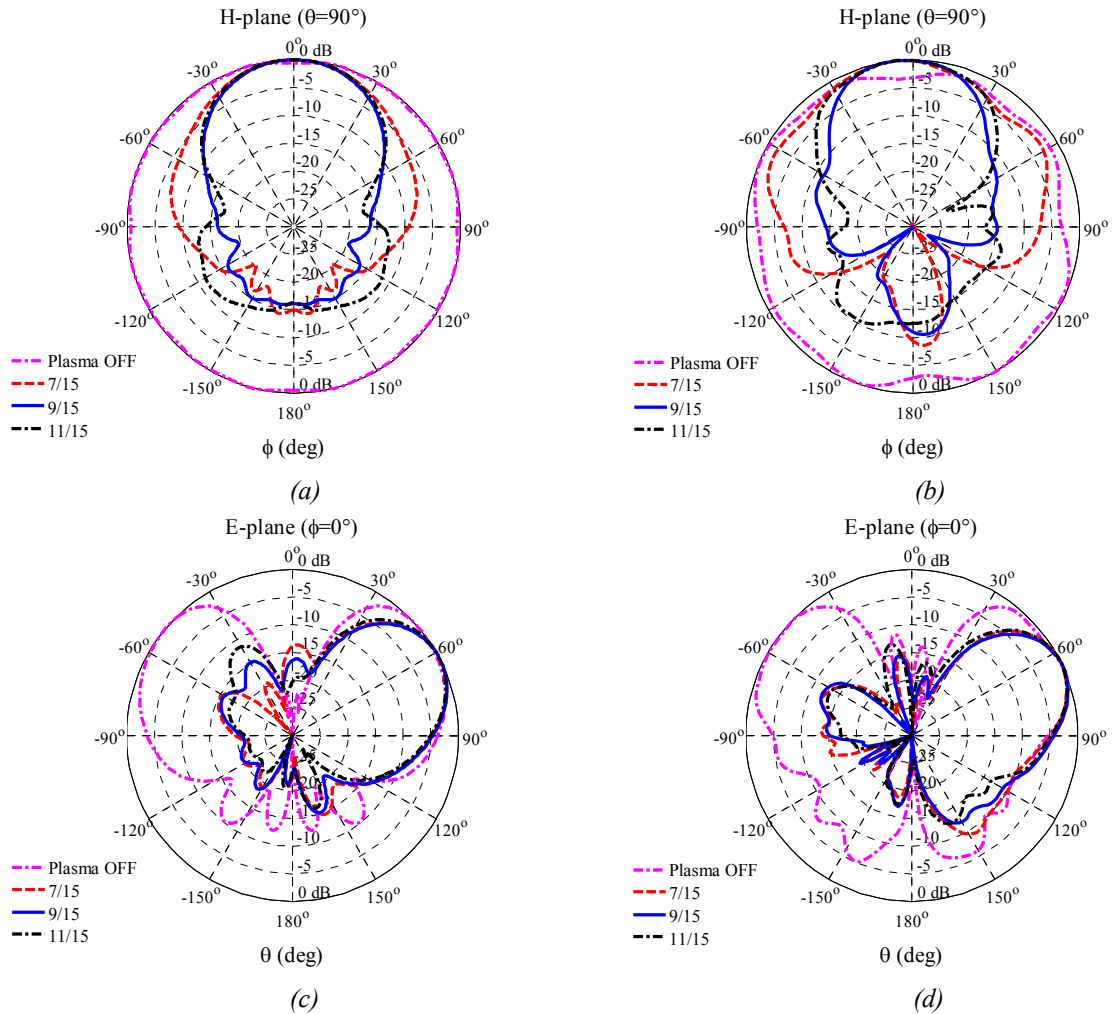
Figure 3.56 – Normalized radiation patterns, E_θ components at 2.4 GHz. (a) Simulated H-plane radiation patterns. (b) Measured H-plane radiation patterns. (c) Simulated E-plane radiation patterns. (d) Measured E-plane radiation patterns.

The measured gain with 9 elements activated at 2.4 GHz is 9 dBi which is 1 dB lower than its simulation one.
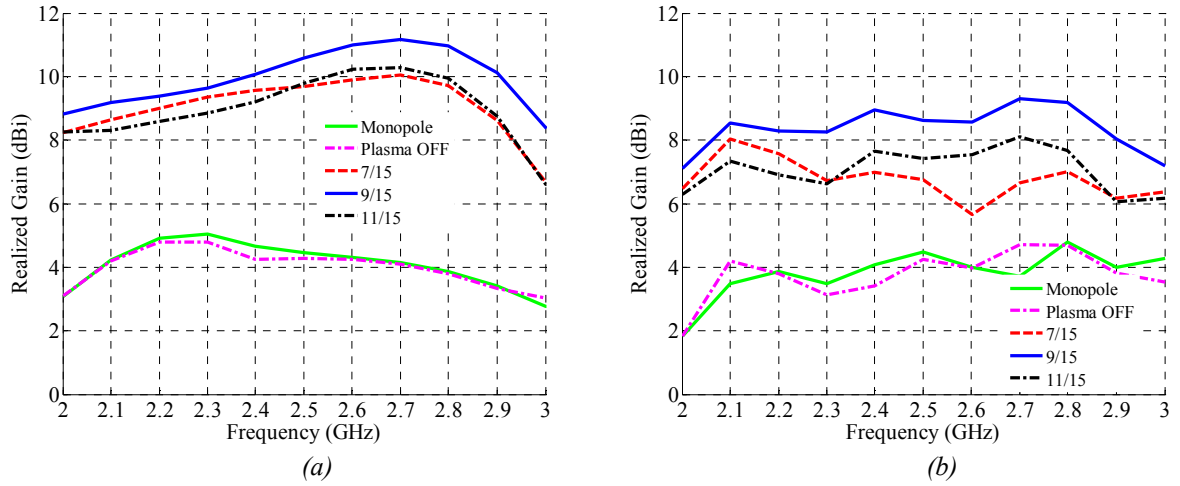
Figure 3.57 – *Antenna gains comparison. (a) Simulated. (b) Measured.*

The antenna reflection coefficients are shown in Figure 3.58 for the three configurations. For 7- and 9- elements configurations, the S_{11} are below than -10 dB for a wide bandwidth. Overall, both measured and simulated results are in good agreements. The ripples seen in the measured reflection coefficients are due to the striation effect of the plasma. This effect will not be seen if the sensitivity of the sampling frequency of network analyzer is reduced.
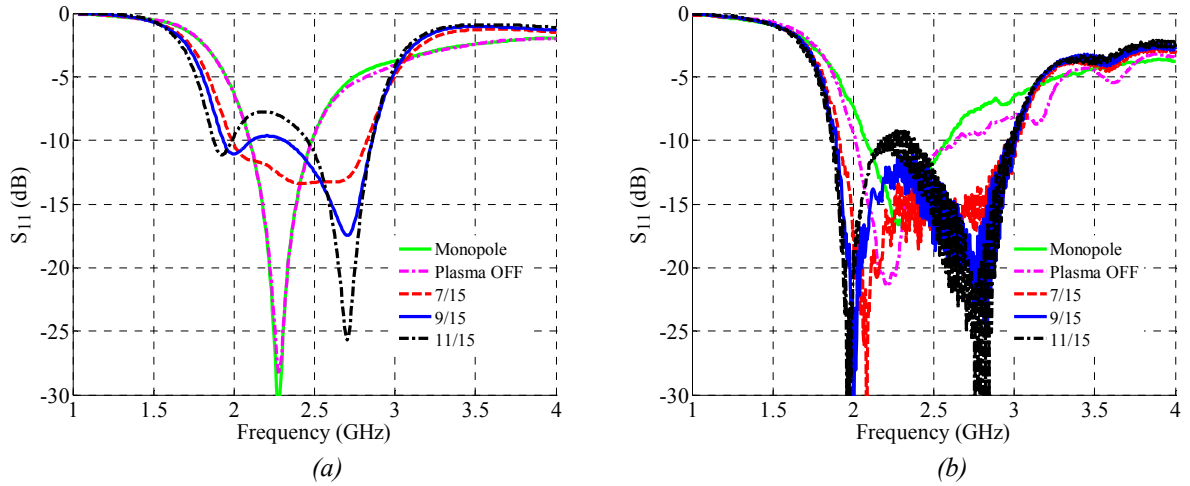
Figure 3.58 – Comparison of magnitude of reflection coefficients, S_{11}. (a) Simulated. (b) Measured.

3.2.6.2.2   Beam shaping of RRA with element height, *h* equals 54 mm

For the implementation of case with 54 mm height CFL, a second layer ground plane is inserted from the top of the antenna as illustrated previously in Figure 3.50 (b). The second layer is fixed to the first ground plane layer using a set of poly legs and a central monopole antenna is attached on it. There is no electrical connection between the first and second ground planes. The procedures of varying the plasma window are the same as the one applied for the case of *h* equals 115 mm. The measurement and simulation results are given in Figure 3.59 and Figure 3.60.

(a)

(b)

(c)

(d)

Figure 3.59 – Measured and simulated radiation patterns, E_θ components at 2.4 GHz (h=54 mm). (a) Simulated H-plane radiation patterns. (b) Measured H-plane radiation patterns. (c) Simulated E-plane radiation patterns. (d) Measured E-plane radiation patterns.

There are good agreements between simulation and measurement results as it can be seen in Figure 3.59. If we compared the measured H-plane radiation patterns with the case of *h* equals 115 mm, there are some improvements for the back radiation, however

both performances are acceptable since the values are lesser than -10 dB. Moreover, the half power beamwidths do not have any significant dissimilarity.

The antenna reflection coefficients and its gains are shown in Figure 3.60 for the three configurations. For the 11-elements configuration the S_{11} is slightly higher than -10 dB however for 7- and 9- elements configurations, the S_{11} are below than -10 dB and offer wide operating bandwidth. When the plasma is de-activated (OFF), its measured and simulated reflection coefficient patterns are alike. A similar pattern of gains are shown in both simulated and measured results as depicted in Figure 3.60 (c) and 3.60 (d). The maximum simulated and measured gains of the 9-elements configuration are 9.6 dBi and 9.2 dBi respectively. This is 0.2 dB higher than measured gain with the case of *h* equals 115 mm. Overall, both measured and simulated results are in good agreements.

Figure 3.60 – Antenna performances (h=54 mm). (a) Magnitude of simulated reflection coefficients, S_{11}. (b) Magnitude of measured reflection coefficients, S_{11}. (c) Simulated gains. (d) Measured gains.

3.2.6.2.3 Beam shaping of RRA with element height, *h* equals 15 mm

For the third case, the *h* is equivalent to 15 mm. To realize it, a second layer of ground plane is needed to be fixed to the primary ground plane with the aid of poly legs so that the corresponding height of elements is now 15 mm. The similar methods of varying plasma windows are applied. The simulated and measurement radiation pattern results are shown in Figure 3.61. The effects of dielectric tube (plasma OFF) on monopole radiation pattern are also included in Figure 3.61.
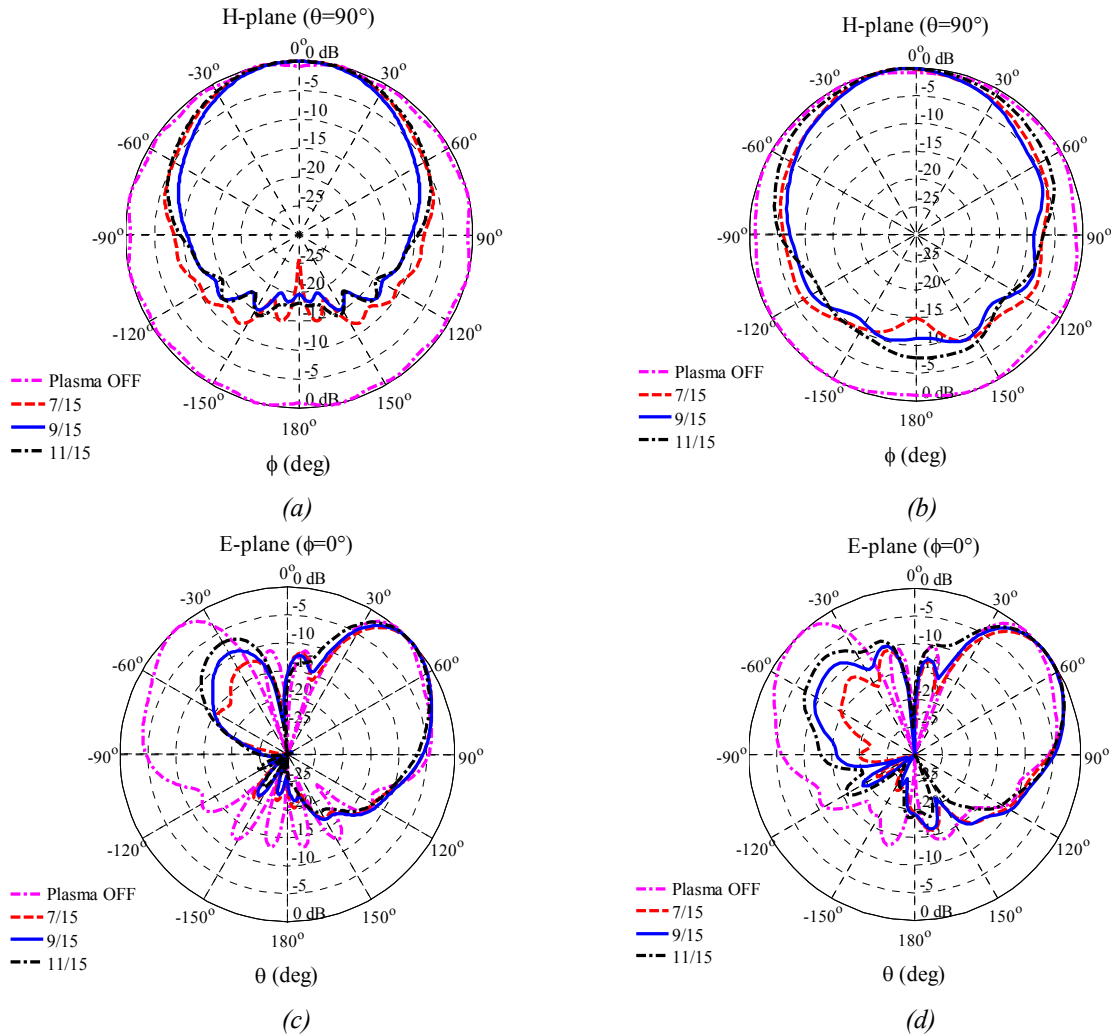
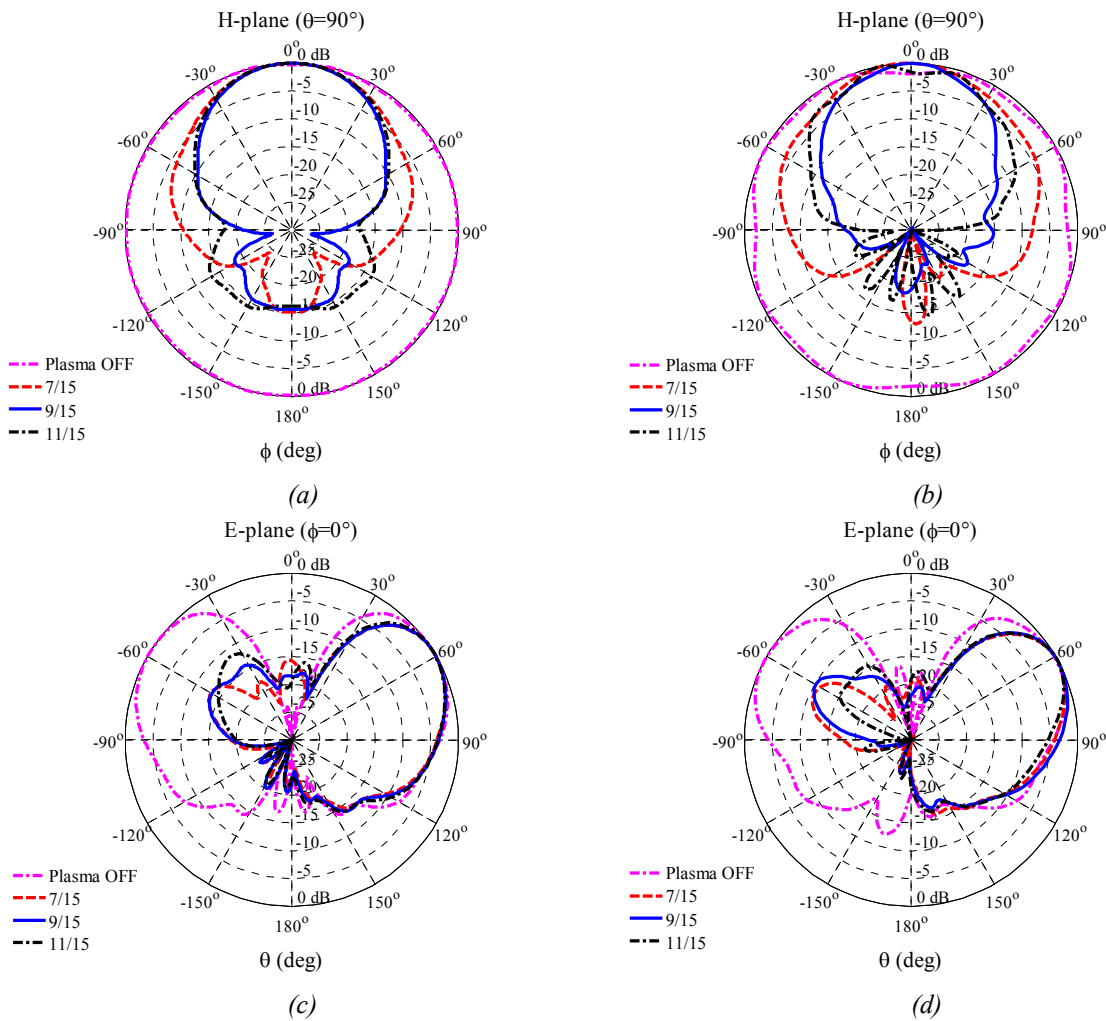*Figure 3.61 – Measured and simulated radiation patterns, E_θ components at 2.4 GHz (h=15 mm). (a) Simulated H-plane radiation patterns. (b) Measured H-plane radiation patterns. (c) Simulated E-plane radiation patterns (d) Measured E-plane radiation patterns.*

From the Figure 3.61, there are good agreements between simulated and measured radiation patterns. However, with further decreasing elements height below than resonating monopole antenna, the broadside beamwidth becomes wider for the 7-, 9-, and 11- elements configurations thus reducing the antenna focusing properties. Furthermore, with this focusing degradation, the antenna gains are now lesser than 8 dBi

if compared to the previous cases (*h*=115 mm and *h* = 54 mm). The antenna reflection coefficients and gains are depicted in Figure 3.62. All antenna configurations are matched at 2.4 GHz and good agreements between simulated and measured results can be seen in Figure 3.62.

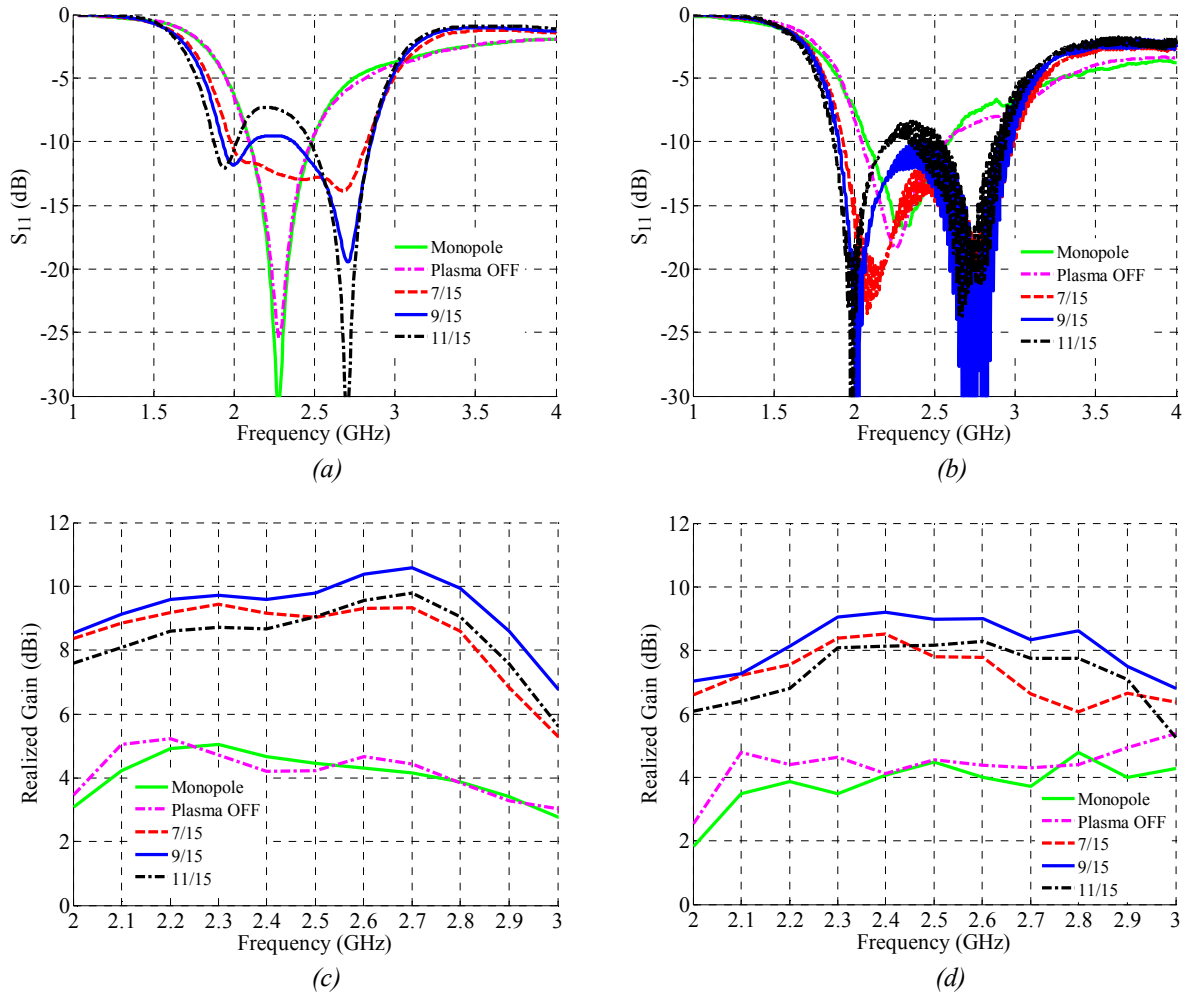*(a)*   *(b)*

(c)   *(d)*
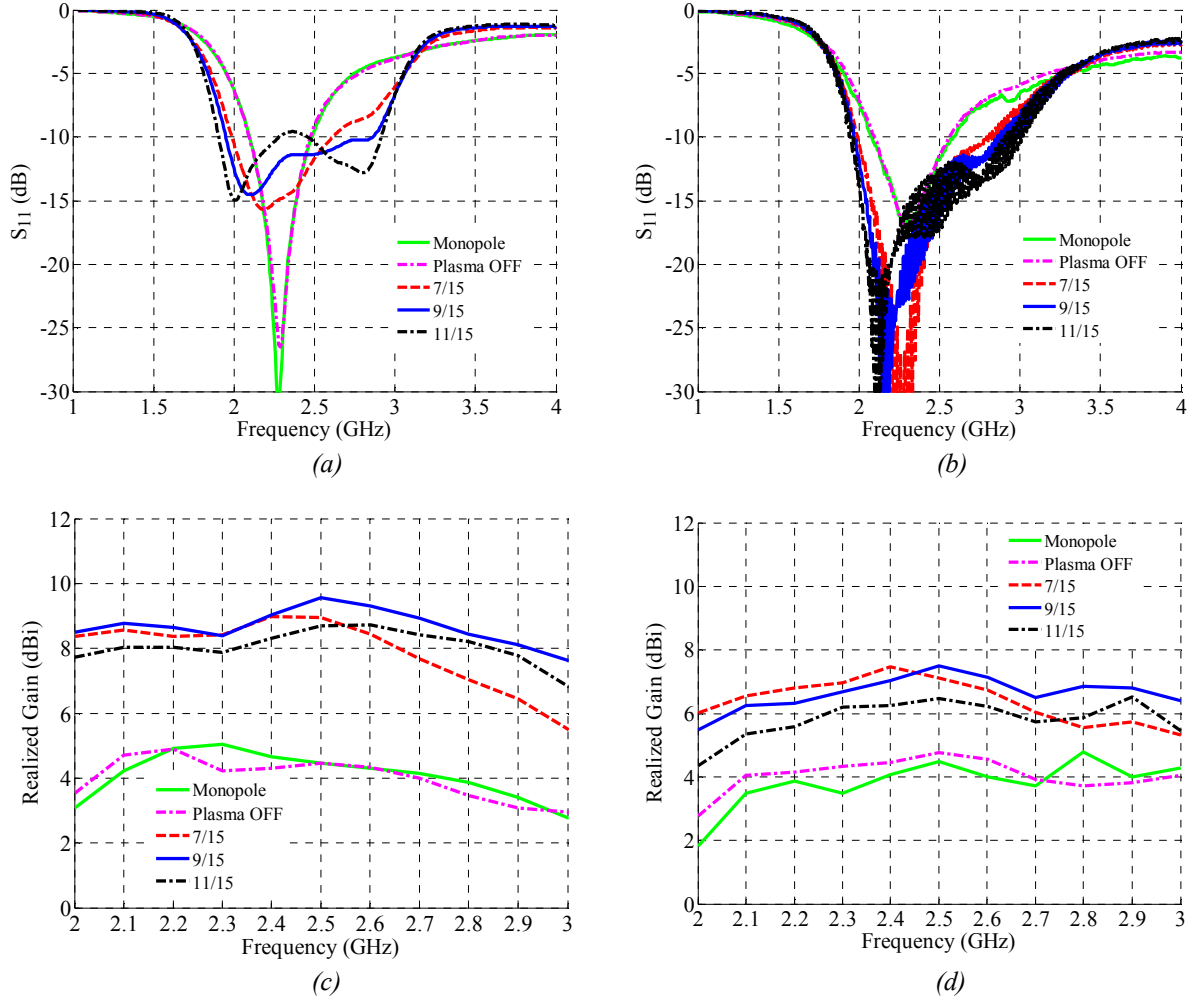
Figure 3.62 – Antenna performances (h = 15 mm). (a) Magnitude of simulated reflection coefficients, S_{11}. (b) Magnitude of measured reflection coefficients, S_{11}. (c) Simulated gains. (d) Measured gains.

3.2.6.3   Beam scanning of RRA

In order to steer a beam from 0° to 360°, only 9 elements need to be activated (switched ON) while the rest remains de-activated (OFF state). To ease the scanning process, each of the elements is numbered by its location in anti-clockwise direction as shown in Figure 3.50. Element number 1 is always at 180° from *x*-direction on the reference plane. The smallest scanning step is 48°, thus to move a main beam from 0° to 48°, the next 9 elements is counted from the third element (element number 3) in the 0° configuration. This sequence must be followed to move the main beam from 48° to 96°

and up to 360°. Basically, the first element is counted after the second element in the previous configuration. The ON-OFF sequences to scan are made based on the switching setting scheme listed in Table 3.3 which has been explained in the earlier section (switching scheme).

3.2.6.3.1   Beam scanning of RRA with element height, *h* equals 115 mm

Figure 3.63 shows simulated and measured scanning radiation patterns in the H-plane. The simulated and measured cross polarization radiation patterns are shown in Figure 3.63 (c) and Figure 3.63 (d) respectively. The front to back ratio (f/b) are always more than 10 dB in the simulations as well as in the measurements. The beam can be directed at desired direction by switching ON the appropriate numbers of adjacent elements. Figure 3.63 (a) and Figure 3.63 (b) can be easily compared showing that the simulated and measured results are comparable to each other. The simulated HPBW is ± 30° whereas the measured HPBW is ± 27°.

(a)

(b)

(c)

(d)
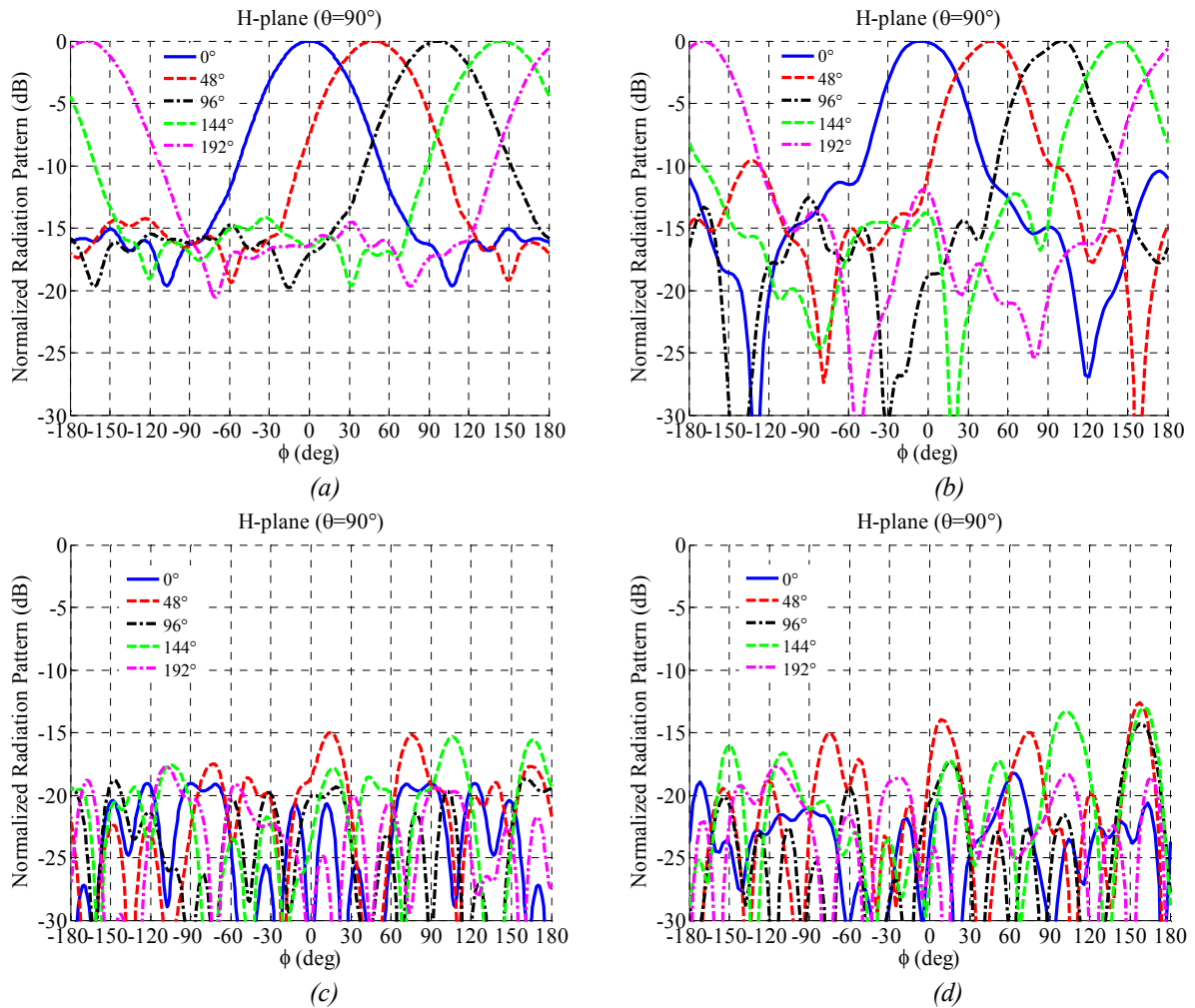
Figure 3.63 – Normalized H-plane scanning radiation patterns at 2.4 GHz with h equals 115 mm. (a) Simulated co-polarization, E_θ component. (b) Measured co-polarization, E_θ component. (c) Simulated cross-polarization, E_ϕ component. (d) Measured cross-polarization, E_ϕ component.

For the antenna performances, because of the 9-elements configuration is implemented for the scanning, the highest measured gain remains at 9 dBi. The simulated and measured scanning gains are shown in Figure 3.64 (a) and 3.64 (b) correspondingly. The patterns are quite similar for both simulated and measured gains. The simulated bandwidths below than -10 dB remain wide (>1 GHz) throughout the scanning as well as measurements. These scenarios are shown in Figure 3.64 (c) and in Figure 3.64 (d).

(a)

(b)

(c)

(d)

Figure 3.64 – Antenna performances (h = 115 mm). (a)Simulated gains. (b) Measured gains. (c) Magnitude of simulated reflection coefficients, S_{11}. (d) Magnitude of measured reflection coefficients, S_{11}.

3.2.6.3.2   Beam scanning of RRA with element height, *h* equals 54 mm

The similar scanning scheme setting was applied to this case. A second layer of ground plane is used to reduce the element's height to 54 mm. The simulated and measured radiation patterns in the H-plane are shown in Figure 3.65 (a) and Figure 3.65 (b) respectively. The cross polarization radiation patterns are demonstrated in Figure 3.65 (c) for the simulation and in Figure 3.65 (d) for the measurement.

Figure 3.65 – Normalized H-plane scanning radiation patterns at 2.4 GHz with h equals 54 mm. (a) Simulated co-polarization, E_θ component. (b) Measured co-polarization, E_θ component. (c) Simulated cross-polarization, E_ϕ component. (d) Measured cross-polarization, E_ϕ component.

The measured HPBWs are similar to those achieved in the previous case (*h* = 115 mm) and both simulated and measured radiation patterns are very analogous to each other. The side lobe level (SLL) of this case is much better than in earlier case but both performances are below than -10 dB which is more than enough. The cross polarization components remain below than -15 dB for simulation as well as measurement.

The maximum scanning gain is measured at 9.5 dBi which is 0.3 dB lower than its computed gain. This measured gain is 0.5 dB higher than those measured in previous case (*h*=115 mm) which is attributed to the improvement at the back radiation pattern so that more energy are reflected in the broadside direction. Similarity in patterns can be observed for both simulated and measured gain and these patterns are given in Figure 3.66 (a) and 3.66 (b) respectively. As those achieved in previous case, measured reflection coefficients remain wide for both simulation and measurement. These patterns can be seen in Figure 3.66 (c) and Figure 3.66 (d), respectively.
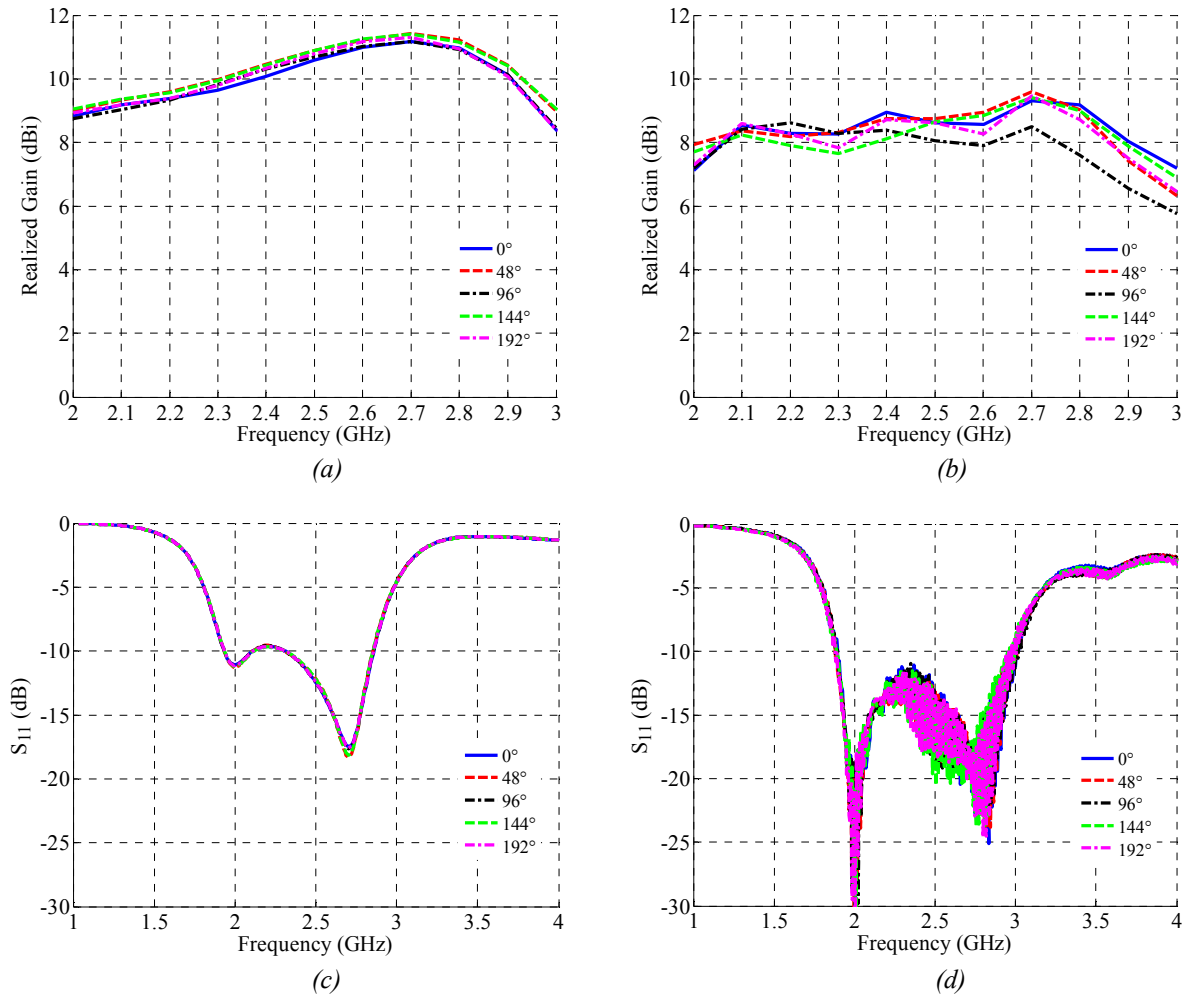

Figure 3.66 – Antenna performances (h = 54 mm). (a)Simulated gains. (b) Measured gains. (c) Magnitude of simulated reflection coefficients, S_{11}. (d) Magnitude of measured reflection coefficients, S_{11}.

3.2.6.3.3   Beam scanning of RRA with element height, *h* equals 15 mm

As the antenna element's height is further reduced to 15 mm, the antenna performances are also seemed to degrade. This circumstance occurs for its radiation

patterns especially in the broadside direction. The measured HPBW is more than ± 30° which is wider than those reported for the two previous cases. The measured SLLs are higher than -10 dB which are approximately 2.5 dB shifted if compared to its computed SLLs. However, the cross polarization components stay below than -10 dB for both computed and measured cross polarizations. The comparison of radiation patterns for co- and cross- polarizations components in the H-plane for computed and measured patterns are given in Figure 3.67.
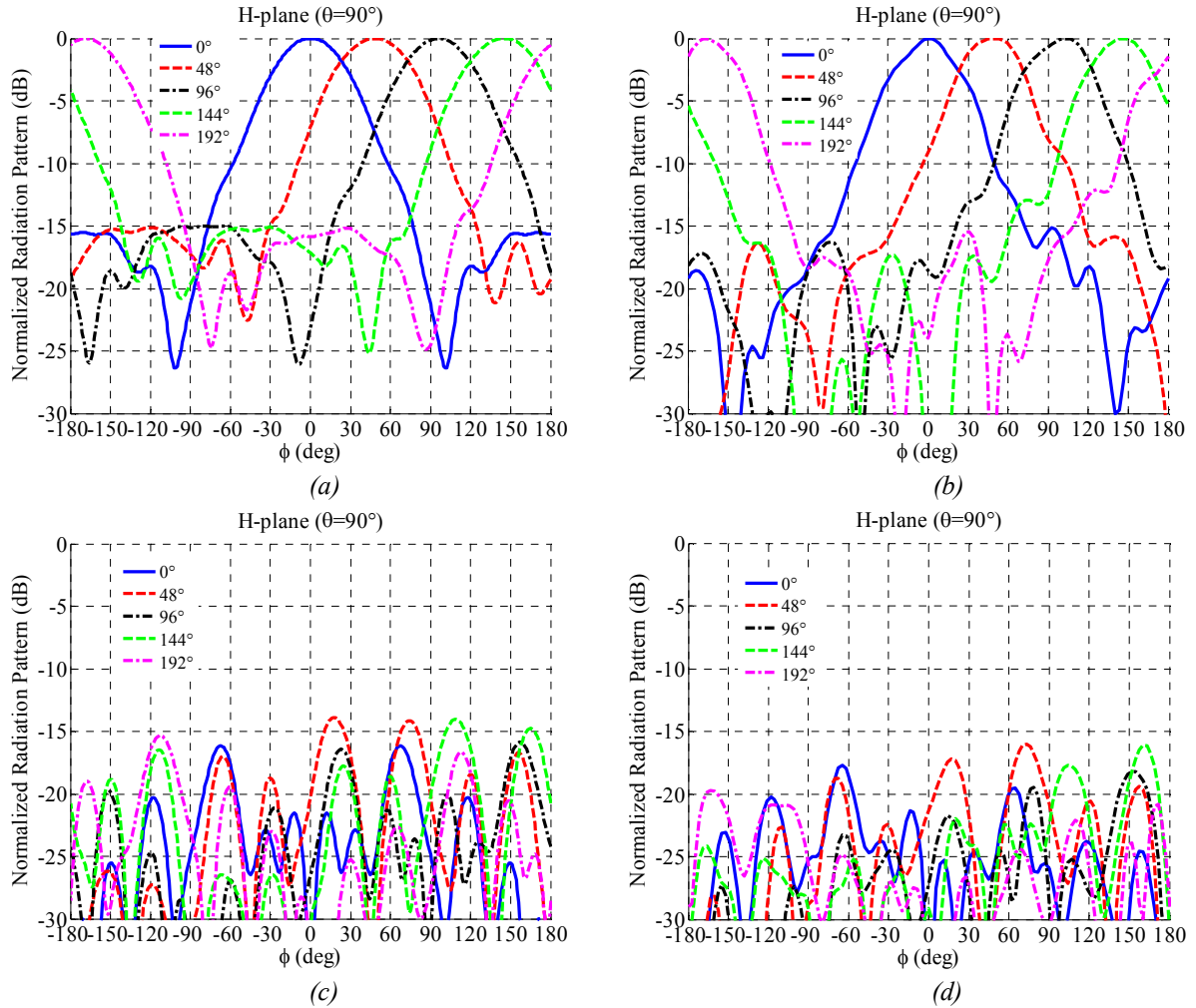

(a)   *(b)*

(c)   *(d)*
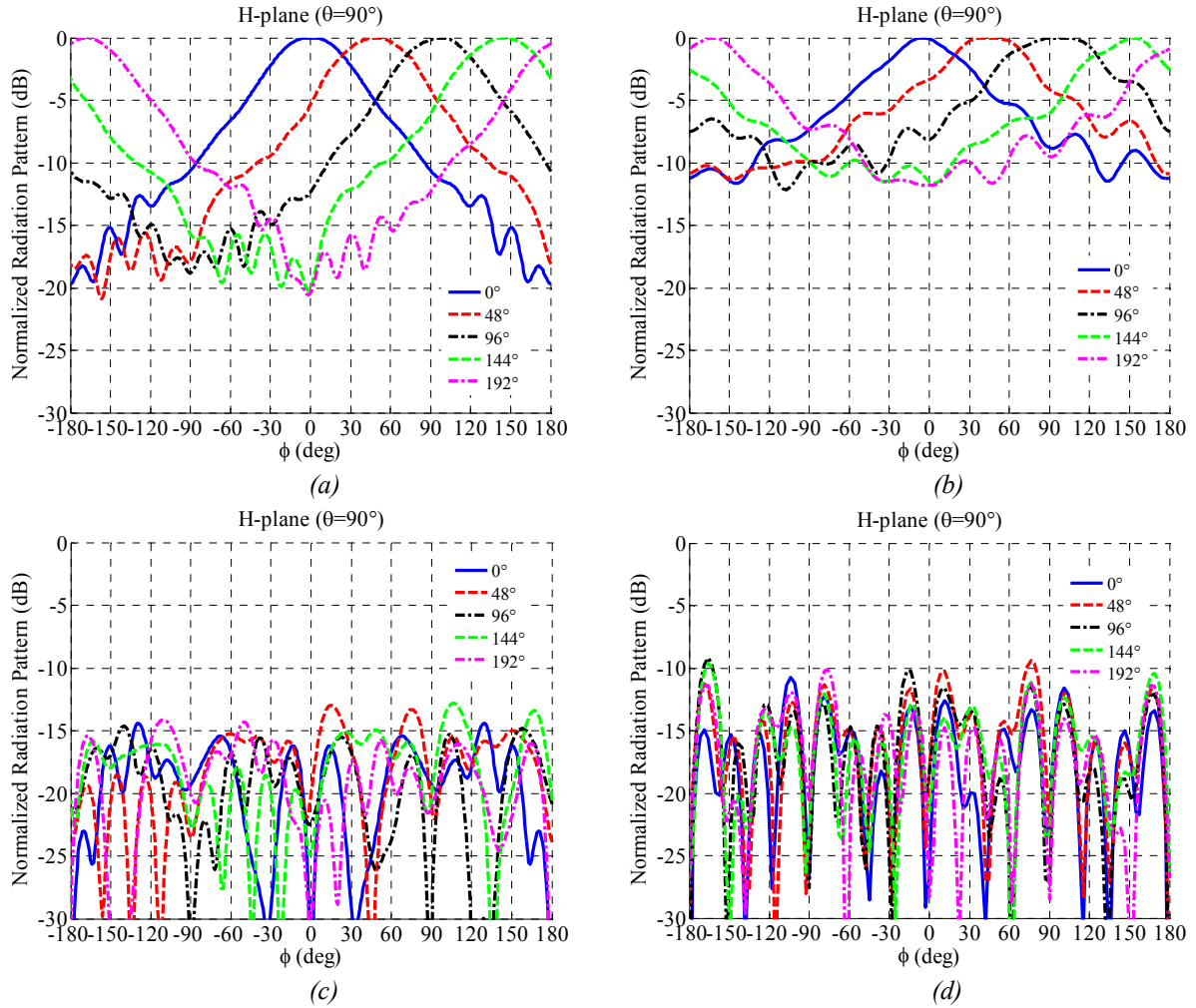
Figure 3.67 – Normalized H-plane scanning radiation patterns at 2.4 GHz with h equals 15 mm. (a) Simulated co-polarization, E_θ component. (b) Measured co-polarization, E_θ component. (c) Simulated cross-polarization, E_ϕ component. (d) Measured cross-polarization, E_ϕ component.

The antenna maximum scanning gain is measured at 8 dBi which is 1.5 dB lower than its computed version. This is due to the degrading of its side lobe level and front to back ratio performances. Both computed and measured gain patterns are shown in Figure 3.68 (a) and Figure 3.68 (b), respectively. Since the reflecting elements are shorter than its radiating monopole antenna, the measured reflection coefficients exhibited a similar pattern as its monopole antenna. Both simulated and measured reflection coefficients are matched at 2.4 GHz and offering bandwidths that are slightly

lower than 1 GHz. Figure 3.68 (c) and 3.68 (d) show the simulated and measured reflection coefficients.

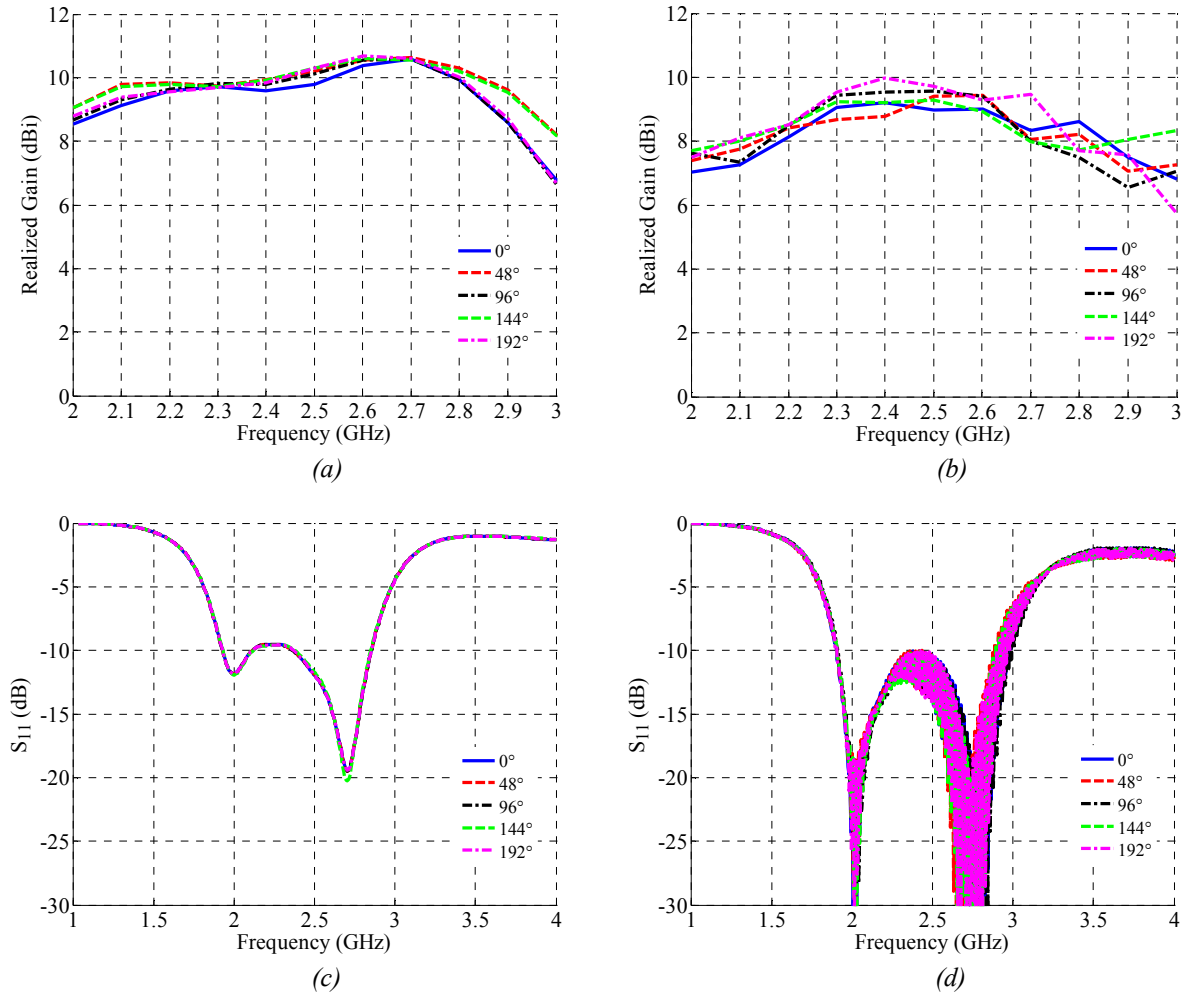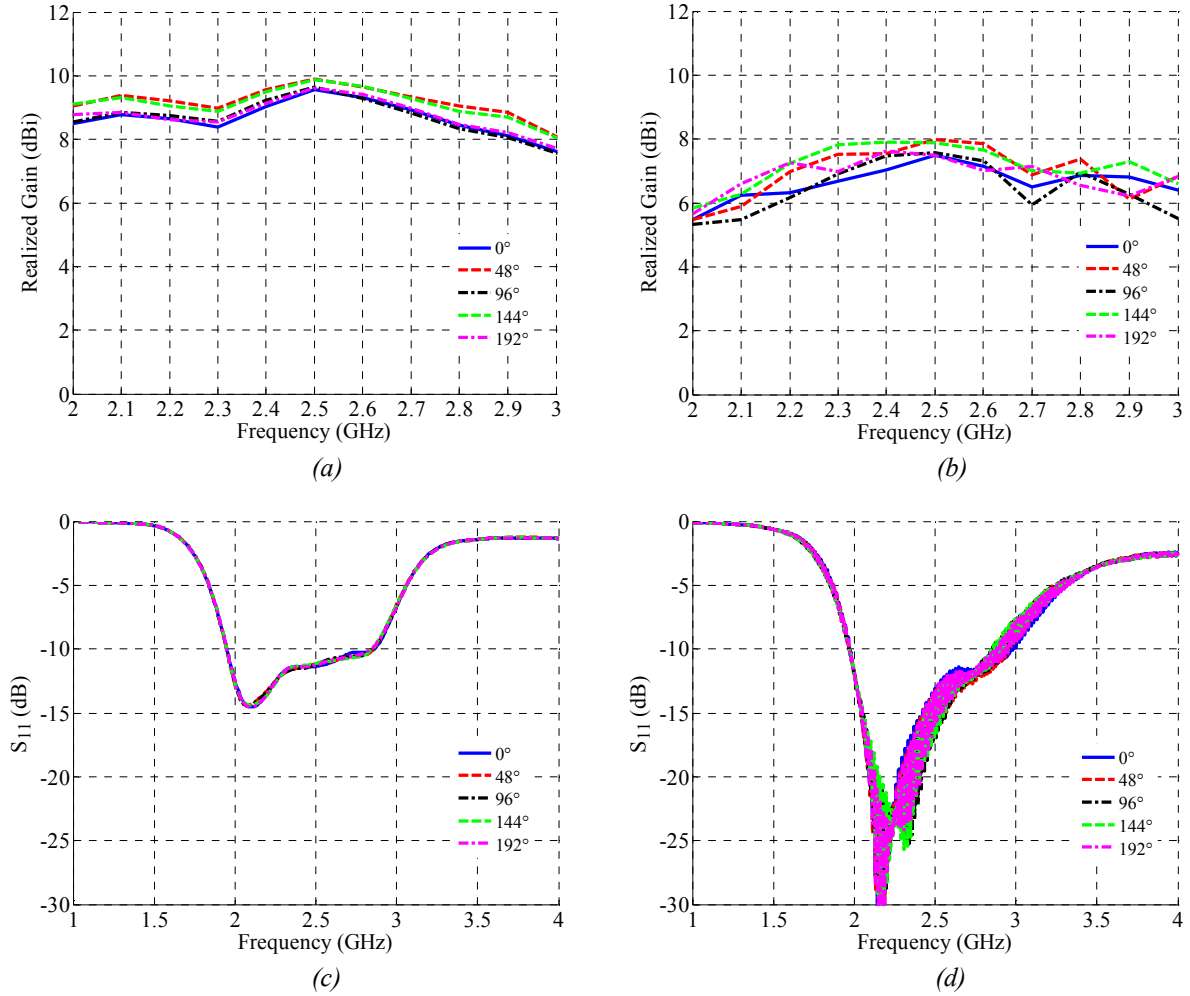*Figure 3.68 – Antenna performances (h = 15 mm). (a)Simulated gains. (b) Measured gains. (c) Magnitude of simulated reflection coefficients, S_{11}. (d) Magnitude of measured reflection coefficients, S_{11}.*

3.2.7 Summary of result analysis of RRA

In the results analysis section, simulated and measured of several configurations of RRA have been explained and discussed thoroughly. The configurations are including three different element heights which are 115 mm, 54 mm, and 15 mm. The idea to change the element height is because it is useful to analyze the possibility of variable size of the RRA since some applications may prefer compact size of antennas. Besides, there are many shapes and sizes of CFLs that are commercially available in the market including a shorter CFL listed in Appendix B which can be employed as antenna elements. Furthermore, by fabricating second layer of ground plane and fixing it to primary ground plane, variable element height can be measured and analyzed without expending more time and cost to fabricate another RRA with different element heights.

Prior to this idea implementation, designs are computed and its results are compared between one layer and two of ground plane with a similar element height. Indeed, there is no difference between the two simulated cases thus allowing the idea to be implemented.

In the beginning of this result analysis section, the effect of surrounding dielectric tube was investigated and by having it to exist while the plasma elements are de-activated, as a result a similar pattern of classical omnidirectional was observed. The results prove that, the surrounding dielectric tubes do not deteriorate the monopole antenna radiation pattern. The radiation patterns of monopole antenna surrounded by dielectric tubes were also presented in order to demonstrate the antenna reconfigurability in every configuration.

One of the reasons of having circular shape of reflector antenna is the huge possibility of having plasma window size that allows beam scanning to be done in many possibility of step size. The plasma window or reflector antenna aperture can be resized by de-activating plasma elements, thus with this arrangement, plasma window can be shaped with the smallest window size of 48° (one de-activated plasma element) and the higher up to more than 270° which is more than what metallic elements could do as proposed in [49]. In this study, only three window sizes were validated with measurement by de-activating several plasma elements which are 8-, 6-, and 4- elements that corresponding to 7-, 9-, and 11- elements configurations. If compared the RRA performances (9-elements configuration, with 9 dBi measured gain at 2.4 GHz and HPBW in the H-plane is 52°) with circular monopole array (CMA) measured in [25] (with measured maximum gain of 10 dBi only occurs at 2.8 GHz and HPBW in the H-plane is 67°), the RRA radiation pattern is comparable and its performances are much better in terms of half power beamwidth and gain.

The results also have proved that, the fabricated RRA are able to do wide scanning which cover up to 360° of scanning area. The measured scanning gain fluctuates between 8.1 dBi and 9 dBi when the main beam is steered from one direction to another. The scanning step can be narrow down with the implementation of smaller separation angle between two adjacent elements and it can be done with the used of plasma element with the smaller radius. The realized RRA discussed here has the smallest scanning step of 24°. However in this investigation, scanning step of 48° is chosen after taking into account of overlapping -3 dB beamwidth. The measured scanning radiation patterns are in good agreements with the simulation ones.

As finale, in this investigation a new design of round reflector antenna (RRA) using commercially available compact fluorescent lamps (CFLs) was proposed, simulated and validated. The fabricated RRA was analyzed with three different elements heights (115 mm, 54 mm, and 15 mm) in which it representing three individual RRA if they are about to be fabricated individually. Since the RRA can provide beam shaping, beam steering and wide scanning, it can be employed to suite many applications.

3.3   Reconfigurable corner-reflector antenna (CRA)

The corner reflector antenna (CRA) was first introduced by John Kraus in early of 1940s [95]. Most of CRA use classical antennas such as dipole as a feeder and two flat sheets intersecting at an angle (known as included angle) as the reflector elements. Some of CRA use a wire grid to reflect signals. The wire grid offers reduction of wind resistance to overcome the disadvantage of flat surface if it mounted in the open space. The angle between these two reflective surfaces will defined the radiation properties. To construct a simple corner reflector antenna, a 90° included angle is adequate. In order to better collimate energy to forward direction, the geometrical shape of the reflector must be modified to reduce radiation in the back and side directions. The smaller included angle will produce high directivity and vice versa. However, the relation between the included angle and the distance between vertex and feed point is opposite. The smaller the angle, the far distance between feed and vertex is needed and thus reducing the reflector aperture.

3.3.1   Antenna specifications of plasma corner reflector antenna

A basic guide to construct a corner reflector antenna with 90° included angle as shown in Figure 3.69 is well documented in [64]. The S, is the distance between the vertex and feed point, the L is the length of reflector, and D_a is the reflector aperture.
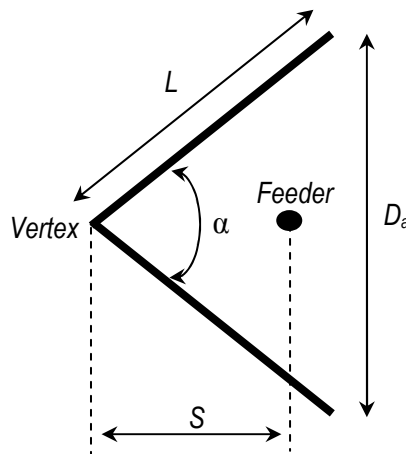

Figure 3.69 – A corner reflector antenna with 90° included angle.

To simplify, the following are the basic guides to construct a CRA.

❖ Spacing between vertex and feeder must be increased as the included angle of the reflector decreases, and vice versa.

❖ For reflectors with infinite sides, the gain increases as the included angle decreases, this however not is true for finite size plates.

❖ The practical minimum value for side surface length, L of corner reflectors (α = 90°) is equivalent to $2S$ [65]. For the case of $\alpha < 90°$, the L must be increased.

❖ The reflector aperture should be in the range of $\lambda < D_a < 2\lambda$.

❖ The vertex to feed point distance must in the range of $\lambda/3 < S < 2\lambda/3$.

❖ If the wires grid are used instead of plane surfaces, the distance, g between two adjacent wires must be in the range of $< \lambda/10$.

In the beginning, ten configurations of corner reflector antenna (CRA) have been simulated for both plasma and metallic cases. The configurations are varied depending on the vertex-to-feed distance, S from 0.1λ to λ. The proposed CRAs are operating at 2.4 GHz. However in this investigation, only two configurations of the CRA will be discussed. The CRAs with the S of 0.5λ and 1.0λ are illustrated in Figure 3.70 and Figure 3.72, respectively.

The CRA elements are made of series of CFLs which are coordinated in V arrangement as shown in Figure 3.70. As the included angle is equal to 90° this CRA is also known as square-CRA [28], [64], [65]. The number of CFL elements used in simulation is depending on the length of the reflecting grids of the reflector, L. This is about twice of the distance between monopole antenna and the vertex, S. The half lambda distance (S=0.5λ) required 10 elements while the lambda distance (S=1.0λ) required 18 elements for both reflector sides. Number of elements used in the simulation has fulfilled minimum requirement of the L [65].

Since the number of CFL elements used in simulation is depending on L and the corresponding S, there were two ground plane sizes used in the simulations; a 2.4λ x 2.4λ ground plane for the distances of 0.6λ and below (Figure 3.70) and a 4λ x 4λ ground plane for the distances of 0.7λ and onwards (Figure 3.72). The S of 0.5λ configuration will produce a single focused beam in the broad side direction and while the S of λ will produce double beam at approximately ± 30° in the H-plane.

Based on Figure 3.70 and Figure 3.72, the geometric scales of the elements are based on the actual size of CFL. The height of each element measured from the ground plane surface is 115 mm, and its diameter is 13 mm leaving 0.5 mm space gap between the CFL surface and the ground plane (to ease the lamp installation). The sizes of both ground planes were set unchanged in all corresponding simulations.
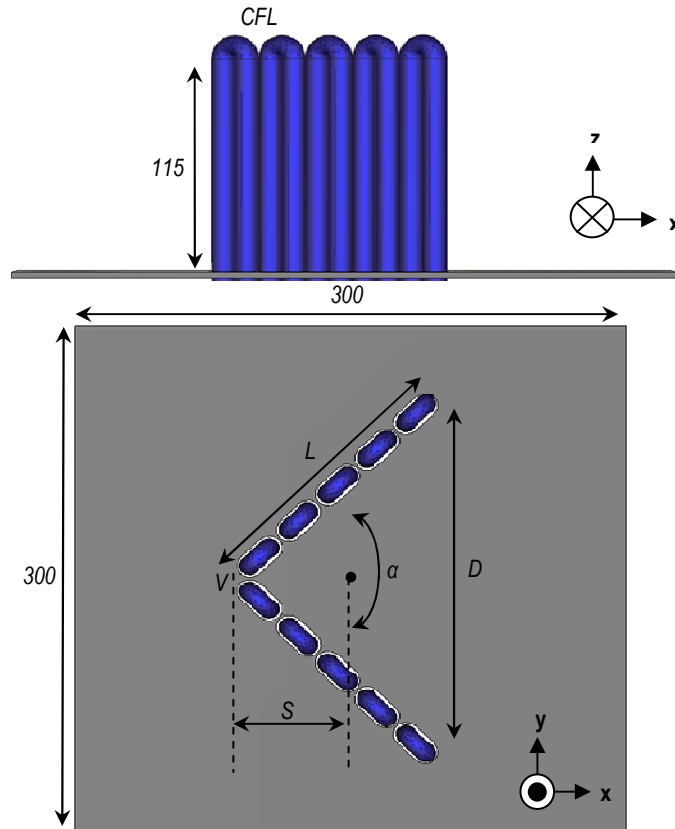
Figure 3.70 – Geometry of CRA with S is 0.5λ and 10 activated plasma elements.

The simulated radiation patterns and antenna performances of 0.5λ CRA configuration are depicted in Figure 3.71. By referring to Figure 3.71 (a) and Figure 3.71 (b), the simulated metal and plasma radiation patterns show a good correlation in the broadside direction and this relation can be seen in the H- and the E- planes.

A broader back radiation is occurred for the case of plasma and this scenario can be observed Figure 3.71 (a), however its back radiation pattern is lower than -10 dB. As can be seen in Figure 3.71 (c), the antennas with metal and plasma cases are matched at 2.4 GHz and the plasma offers wider bandwidth than its counterpart.

Figure 3.71 – Simulated radiation patterns and antenna performances. (a) H-plane. (b) E-plane. (c) Magnitude of reflection coefficients, S_{11}. (d) Gains.

If the plasma elements are in OFF state (de-activated), the resonating monopole antenna will produce a classical omnidirectional pattern with the gain of 5 dBi at 2.4 GHz. This result somehow verifies that the remaining dielectric tubes does not disturbing the monopole radiation pattern. The antenna gain is 5 dB higher than the gain of radiating element whenever the plasma or metal is applied as reflecting element. The plasma gain is about 10 dBi while the metal gain is 2 dB higher than plasma. The gain patterns are shown in Figure 3.71 (d).

For the case of lambda distance (S=1.0λ) with the geometry illustrated in Figure 3.72, two beams or double beam will be produced in the broadside direction. Theoretically, these beams will have it highest peak at ± 30° in the H-plane as computed and shown in Figure 3.73 (a) and 3.73 (b), respectively.
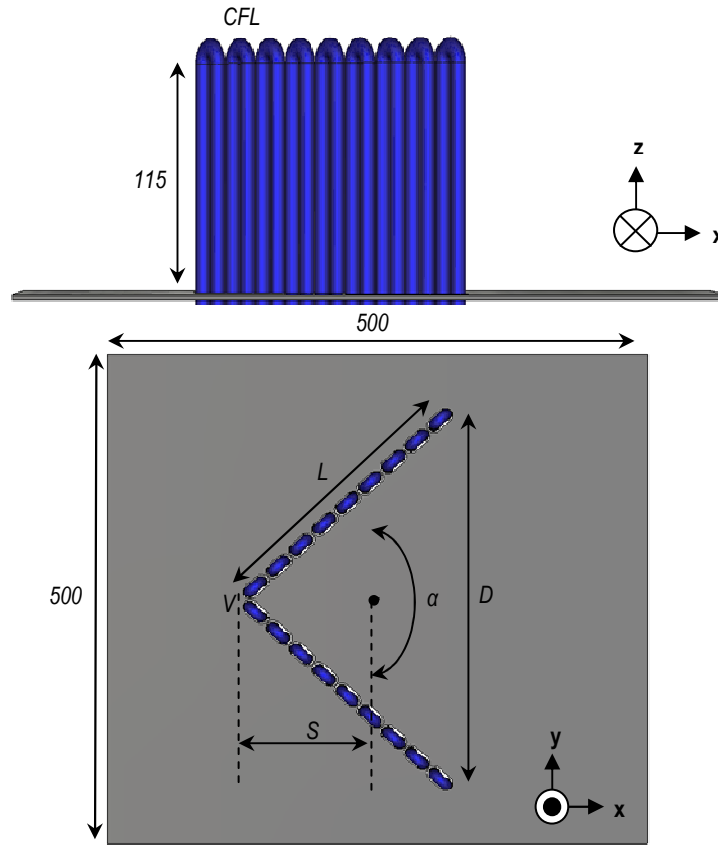
Figure 3.72 – Geometry of CRA with S=λ and 18 activated plasma elements.

These two beams are separated by a null as low as -15 dB. The back radiation is also below than -10 dB however the metal case having 10 dB better than its plasma twin. Once the plasma is de-activated, the antenna will produce omnidirectinal radiation pattern as can be seen in Figure 3.73 (a).
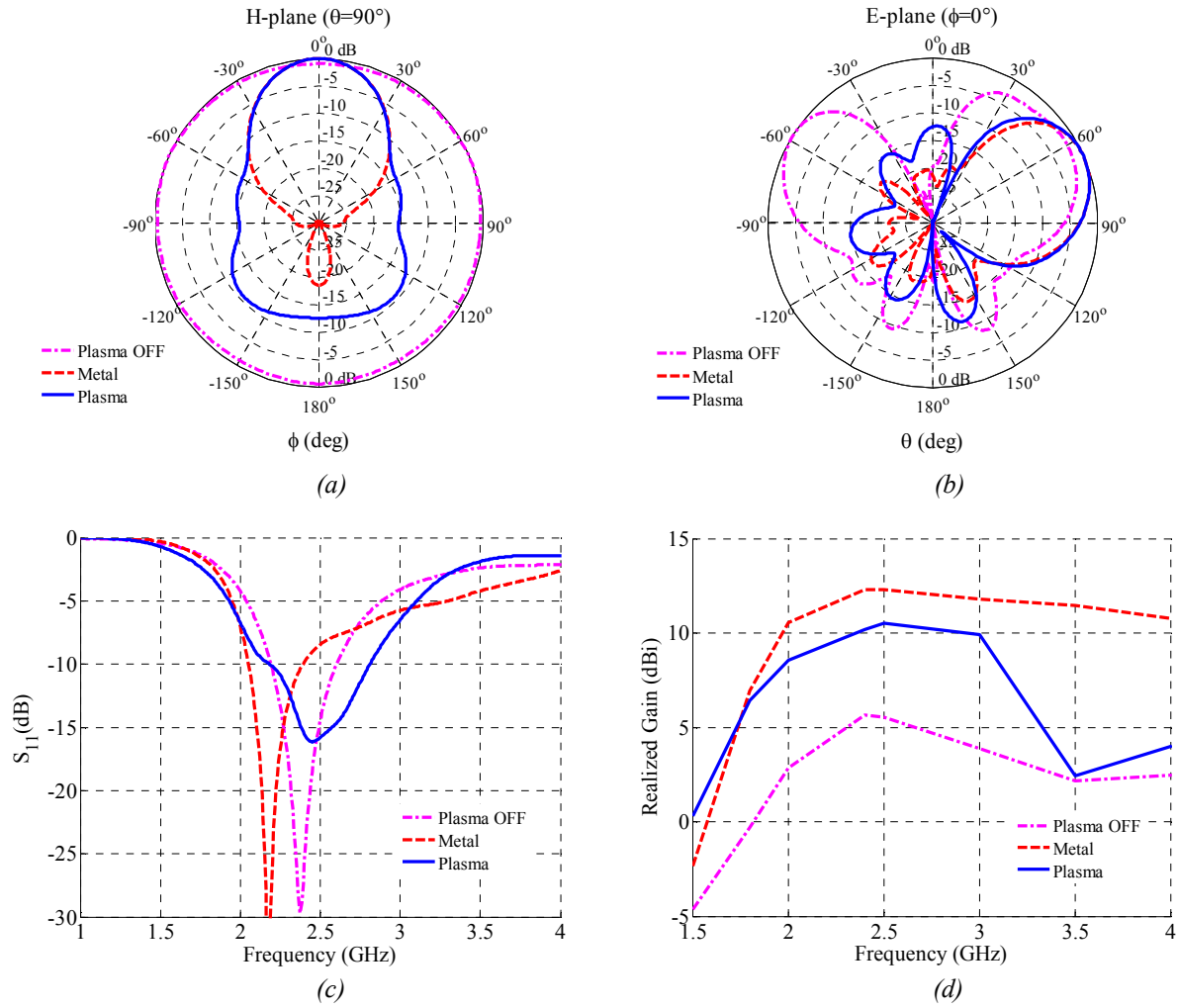

(a)

(b)

(c)

(d)
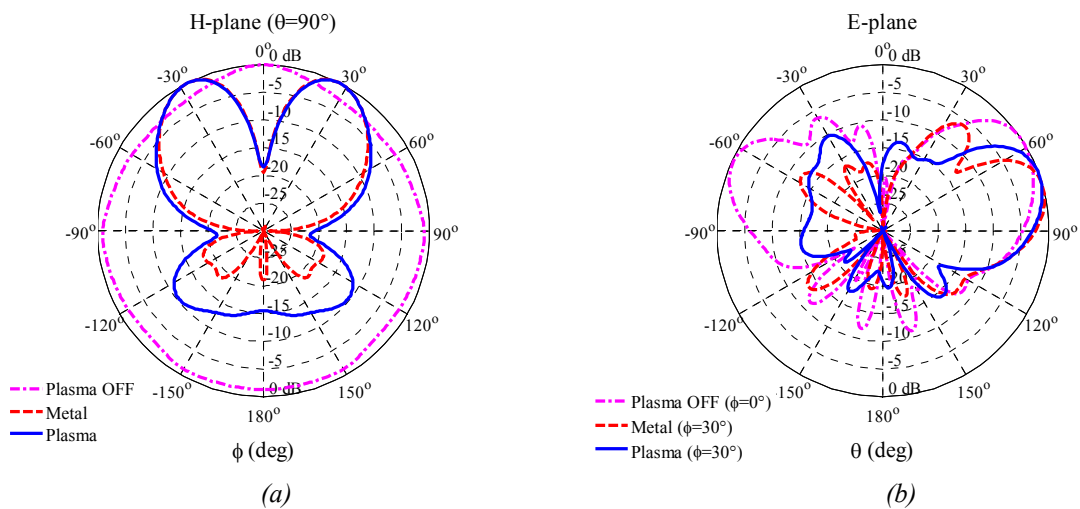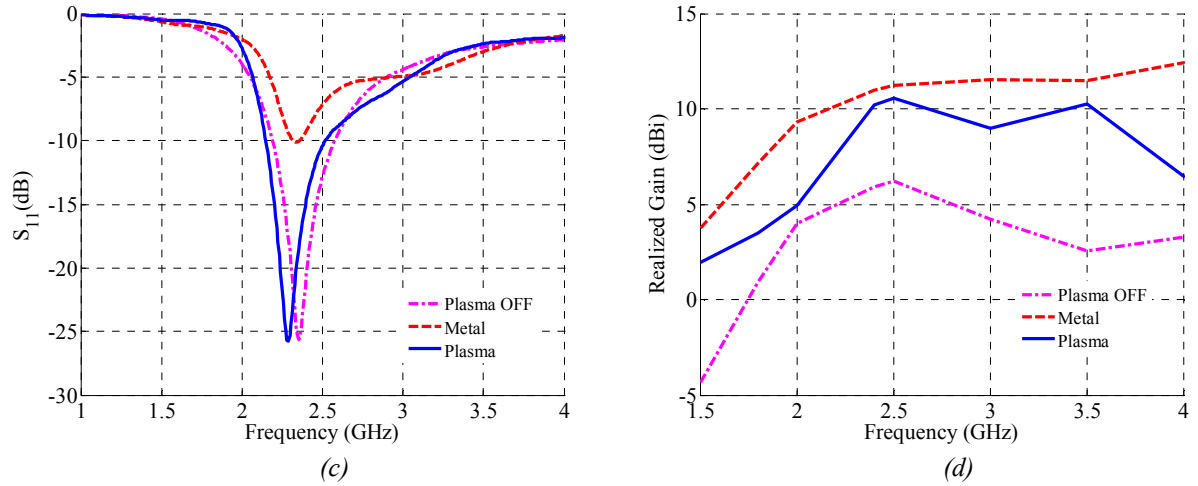
Figure 3.73 – Simulated radiation patterns and antenna performances. (a) H-plane. (b) E-plane. (c) Magnitude of simulated reflection coefficients, S_{11}. (d) Gains.

In term of impedance matching, the metal has poor performance at 2.4 GHz but the plasma reflection coefficient pattern is somehow similar with monopole antenna as if the plasma is de-activated. These matching patterns and performances are shown in Figure 3.73 (c) and Figure 3.73 (d) respectively. Both metal and plasma configurations produce good values of gains at 2.4 GHz.

In general, the number of elements used as reflector is controlled by the value of *S*. As the *S* is increased, the minimum number of element needed to construct CRA is also increased. However, the resulting numbers of required elements from this relation are not yet optimized. Thus, there is still room to obtain an optimum number of required elements which are corresponding to the antenna performances. One way of optimizing it, is by reducing a space gap between two adjacent elements. Figure 3.74 shows the CRA efficiency comparison for metal and plasma cases with similar configurations versus distance between monopole antenna and the vertex, *S*.
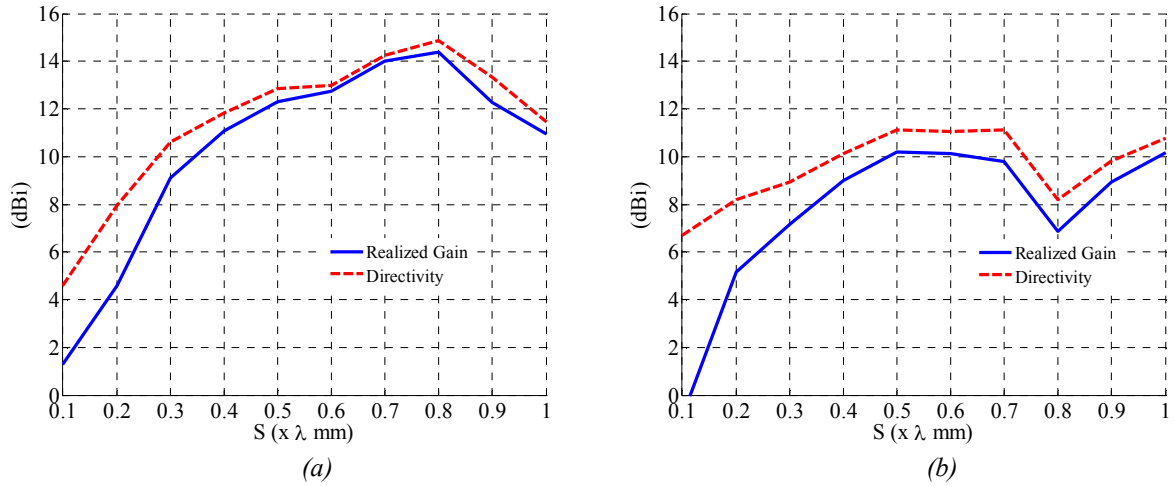
Figure 3.74 – Simulated antenna gain and directivity at 2.4 GHz. (a) Metallic case. (b) Plasma case.

Even though, the gains of metal case are higher than plasma case, the efficiencies of plasma CRA and metal CRA are comparable. Note that in both figures (Figure 3.74 (a) and Figure 3.74 (b)), the difference of gain between metal and plasma at certain distance such as at 0.5λ and λ are between 1 dB to 2 dB. However, the simulated plasma gain at 2.4 GHz is 10 dBi which is about 5 dB more than the gain of monopole antenna and can be considered good in terms of reflecting signal. The resulting number of elements needed to construct CRA with regard to the values of *S* is shown in Figure 3.75. For the case of *S* equals to 0.5λ and 0.6λ the same number of elements required to reflect incoming signal which is 10.
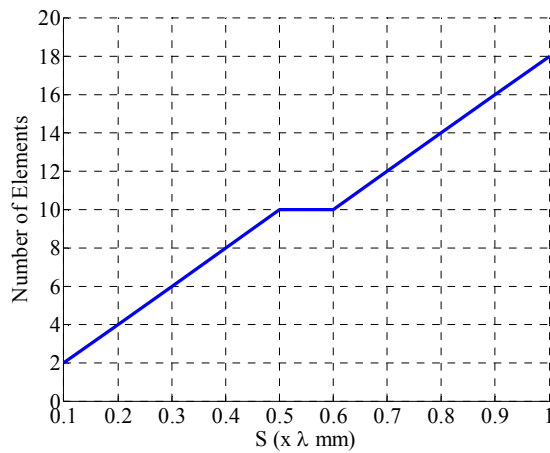
Figure 3.75 – Number of elements required to construct CRA with respect to the S values at 2.4 GHz.

Since plasma can be destroyed in milliseconds and the dielectric tubes do not deteriorate the omnidirectional pattern as shown in previous figures (Figure 3.71 (a), and 3.73 (a)), it is a brilliant idea to combine several CRAs with different *S* values on a single ground plane. Therefore, two or even more CRAs could be combined in a single

ground plane. In this study, instead of having one corner reflector, by combining two or more CRA could add additional beam shaping capability thus minimizing a requirement of more than one antenna in order to provide two different beam shapes.

In this investigation, for the beginning, combination of two CRA on a single ground plane is preferred. Based on Figure 3.74 (b), the efficiency results of plasma suggest that the plasma CRAs work with better efficiency at 0.5λ and 1.0λ if compared to other distances that have been simulated. Therefore, these configurations are chosen to be merged together for the final design.

To the best of our knowledge, the merging possibility makes this design being the first design up to now that combines two CRAs on a single ground plane. The method used for two plasma CRAs to be combined together cannot be applied to other metallic CRAs elsewhere in the world. Therefore, the integration of two CRA on a single finite ground plane is a significant finding to appear from this research work.

3.3.2 Design and optimization of plasma corner reflector antenna

Due to the size of the bottom part of plasma source (CFLs), the CRA with 3.5 mm spacing between elements as anticipated in simulations cannot be realized. This is because the smallest gap between two adjacent CFLs is approximately 5 mm, which is 1.5 mm larger than the ones have been simulated. In real case, the original gap is about 10.73 mm if two elements are put side by side; however by cutting the base of a CFL at both sides, the space between elements can be reduced to 5.73 mm (2.5 mm reduction at the both sides). Note that, with this reduction, the number of elements is now decreased. Figure 3.76 shows photograph of lower part of CFL before and after the cutting process. Thus, to fabricate two CRAs on a single ground plane, a total of 24 elements are needed (including 16 elements for CRA with S is equal to λ and 8 elements for CRA with S equals 0.5λ).

(a) *(b)*
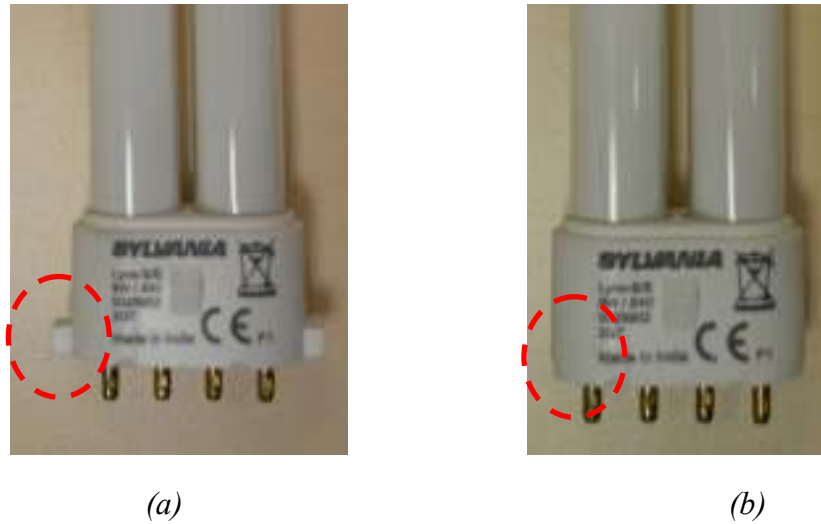
Figure 3.76 – Photograph of the lower part of CFL (red circle) before and after physical modification. (a) Original shape. (b) Modified shape (5 mm of unnecessary parts were removed).

The side view of the optimized ground plane with two reflective elements and a feeder monopole antenna is clearly illustrated in the Figure 3.77.
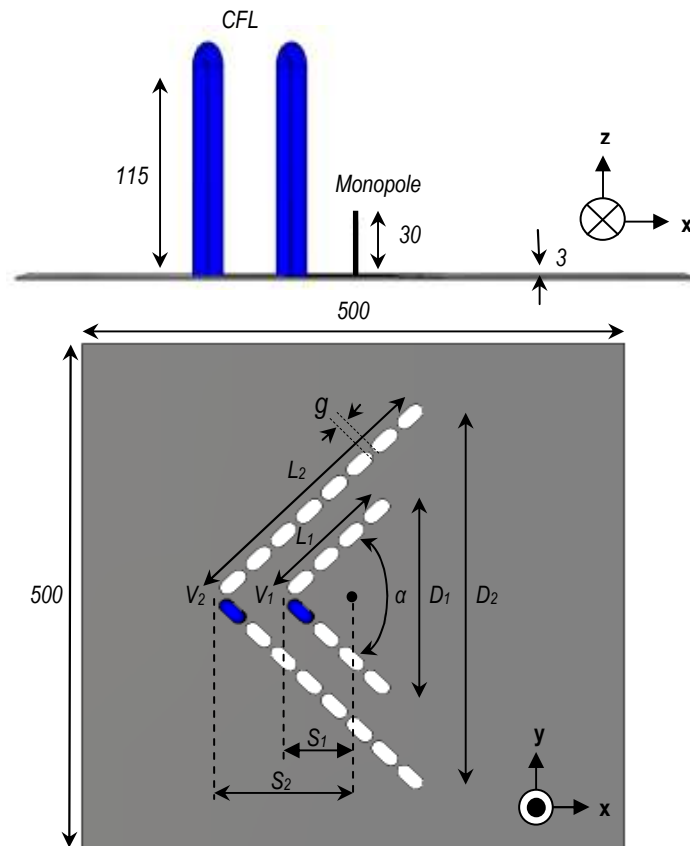
Figure 3.77 – Geometry of optimized ground plane of the CRA with two reflective elements (blue color). A set of 24 holes is required to insert 24 reflective elements (CFL) and a monopole antenna is placed in the center of the ground plane.

120

Sets of holes for CFL insertion are also shown in Figure 3.77 (top view). In the following sections, the primary CRA with the half lambda distance (0.5λ) and the secondary CRA with the lambda distance (λ) will be referred as CRA1 and CRA2, respectively.

In Figure 3.77, only two elements are depicted to show two sets of holes (for the two CRAs) used to insert CFLs from lower part of the ground plane. The CRA1 and CRA2 are separated by 0.5λ between both vertexes (V_1 and V_2). The length of both dihedral corner sides are defined by L_1 and L_2 and with 90° concluded angle, resulting reflector apertures to be D_1 and D_2 as denoted in the figure. The sides length (L_1 and L_2) are about twice of the distance between monopole antenna and the vertex (denoted by S_1 and S_2). The heights of the inserted CFLs are measured 115 mm from the ground plane surface. A central monopole resonating at 2.4 GHz is used to radiate the signal. The ground plane geometry details of the fabricated CRA are summarized in Table 3.4.

Table 3.4 - Optimized CRA specifications.

Ground plane thickness	3 mm
Ground plane size (*w* x *l*)	500 mm x 500 mm
Concluded angle, *α*	90°
L_2	265.3 mm
L_1	133.25 mm
Space gap in a single elements	2 mm
Space gap between elements, *g*	5 mm
D_2	375.19 mm
D_1	188.44 mm
Vertex to center of first elements	12.75 mm
Hole diameter	7 mm
Feed-to-vertex, S_2	125 mm
Feed-to-vertex, S_1	62.5 mm

3.3.3 Fabrication of plasma corner reflector antenna

The realized model was fabricated using 3 mm thick ground plane as shown in Figure 3.78 (a). The power to energize the 9 Watts CFLs is supplied by a set of electronic ballasts with specification of 220-240V, 50-60 Hz. Each of the electronic ballasts is controlled by a small single-pole switch and requires 4 wires to be connected to each of the CFLs. Thus, to realize the prototype, the similar electronic switches and ballasts used to operate RRA in previous section were employed. However in order to operate the CRA, a number of 24 electronic ballasts and 24 switches are required. A monopole antenna (Figure 3.78 (b)) with diameter of 2 mm is connected to the feeding line via a 50Ω SMA female connector.

(a)   *(b)*

Figure 3.78 – CRA prototype. (a) 500 mm x 500 mm ground plane. (b) The 24 plasma elements with a monopole antenna in the center of the ground plane.

3.3.4 Measurement setup of plasma corner reflector antenna

In this section, explanation on the measurements setup of the CRA is carried out. A switching scheme to reflect incoming beam is also discussed.

3.3.4.1 Antenna performance measurement of corner reflector antenna

The antenna performances measurements were conducted using similar setup as performed for RRA in the earliest part. The radiation pattern measurements were performed in a SATIMO 32 anechoic chamber with the peak gain accuracy of ± 0.8 dBi for 1 GHz up to 6 GHz operating frequencies. Photograph of measurement equipments on instrument rack is shown in Figure 3.79 (a). The antenna under test (AUT) is placed on a support fixture as can be seen in Figure 3.79 (b).

(a)   *(b)*
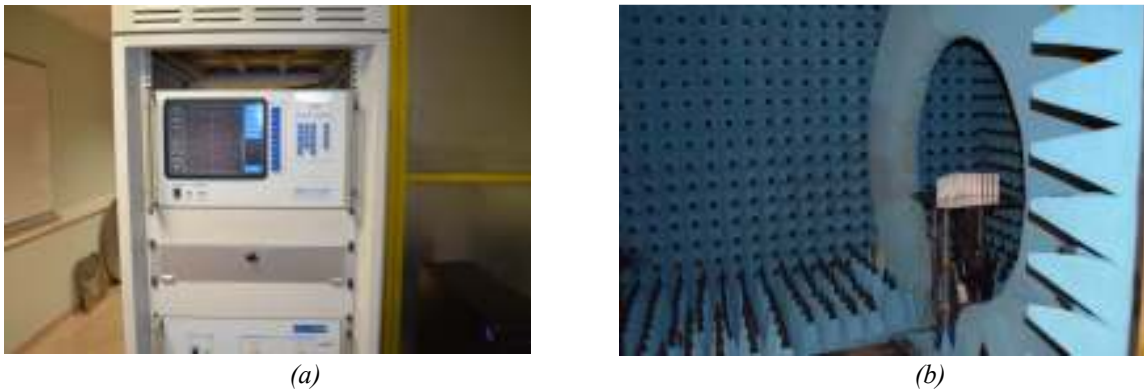
Figure 3.79 – SATIMO Stargate 32. (a) Radiation pattern measurement equipments. (b) A specially made support fixture used to place the CRA.

3.3.4.2 Switching scheme of corner reflector antenna for beam shaping

The antenna prototype uses 24 single-pole electronic switches to control its element state (ON or OFF) in order to shape the main beam. Since each of the elements can be controlled individually, the antenna has huge possibility to shape its beam. Figure 3.80 shows that each of the elements is numbered accordingly to a specific electronic switch.
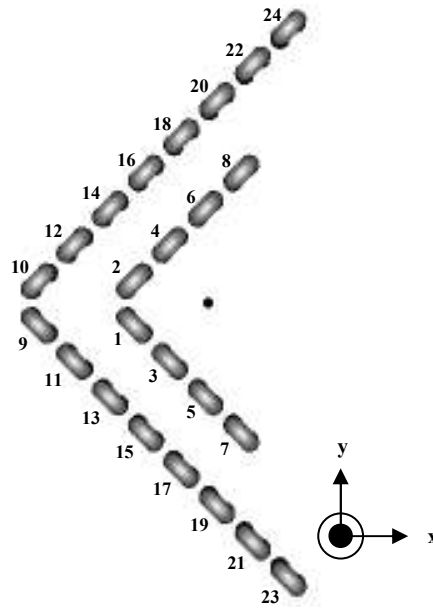
Figure 3.80 – Switching numbering of the CRA for beam shaping.

Generally, a number of activated elements (switched ON) will define the size of reflector aperture, D (denoted by D_1 and D_2 in Figure 3.77) thus controlling the reflected beam profile. In this investigation, there are 8 configurations of with the optimized CRA were measured. The configurations are listed in Table 3.5 along with its corresponding switching setting.

Table 3.5 - Switching setting of fabricated CRA (dark blue color represents activated plasma elements (ON) while light blue color represents de-activated plasma elements (OFF)).

No. of configurations	CRA Configurations	Switched ON Elements	Switched OFF Elements
1		None	All
2		1, 2, 3, 4, 5, 6, 7, and 8	9, 10, 11, 12, 13, 14, 15, 16, 17, 18, 19, 20, 21, 22, 23, and 24

3		9, 10, 11, 12, 13, 14, 15, 16, 17, 18, 19, 20, 21, 22, 23, and 24	1, 2, 3, 4, 5, 6, 7, and 8
4		1, 2, 3, and 4	5, 6, 7, 8, 9, 10, 11, 12, 13, 14, 15, 16, 17, 18, 19, 20, 21, 22, 23, and 24
5		9, 10, 11, 12, 13, 14, 15, 16, 17, 18, 19, and 20	1, 2, 3, 4, 5, 6, 7, 8, 21, 22, 23, and 24
6		9, 10, 11, 12, 13, 14, 15, and 16	1, 2, 3, 4, 5, 6, 7, 8, 17, 18, 19, 20, 21, 22, 23, and 24
7		9, 10, 11, and 12	1, 2, 3, 4, 5, 6, 7, 8, 13, 14, 15, 16, 17, 18, 19, 20, 21, 22, 23, and 24
8		All	None

3.3.5 Design variety of corner reflector antenna

In order to realize CRAs with reduced height, a set of simulation were conducted for 54 mm and 15 mm CFLs' height. Since the realized prototype is made by using 115 mm CFL, another ground plane is needed to reduce the element height with respect to ground plane surface. The height variations of the design were simulated as shown in Figure 3.81. Prior to antenna realization, several simulations have been carried out to study the effect of adding secondary ground plane. A comparison has been conducted between two cases; 1) a single layer, and 2) two layers of ground plane, both with identical elements' height. The results have proved that by adding extra layer of ground plane, antenna radiation patterns are identical for each case (115 mm and 15 mm) in both H- and E- planes. To conclude, the compact version of CRA with reduced height can be analyzed by changing its element height with the aid of secondary layer of the

ground plane. The photographs of the CRA with the primary and secondary ground planes are shown in Figure 3.82.
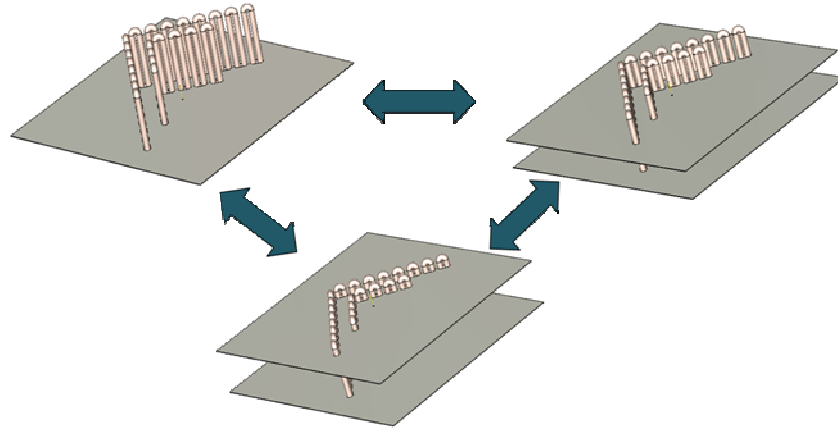
Figure 3.81 – The simulation designs with three element heights (115 mm, 54 mm, and 15 mm) and secondary ground planes.
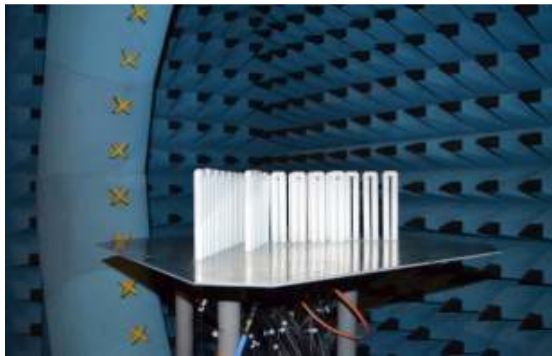
(a)

(b)
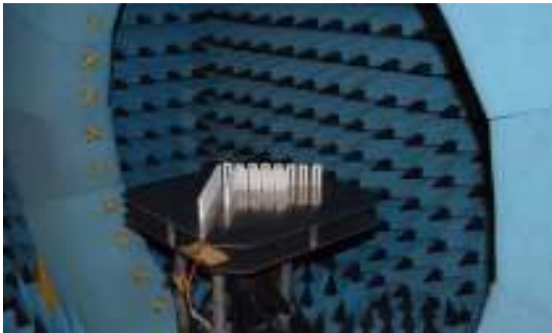
(c)
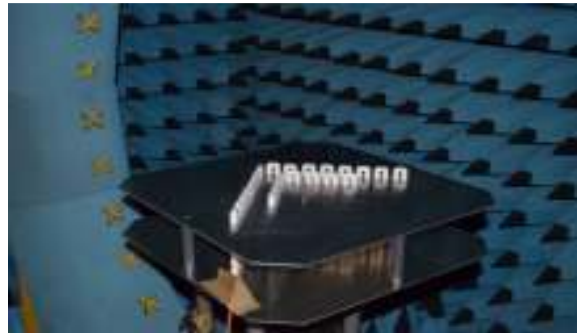
(d)

Figure 3.82 – Photograph of the fabricated CRA with primary and secondary ground plane. (a)-(b) The h is 115 mm. (c) The h is 54 mm with the inserted secondary ground plane.(d) The h is 15 mm with the inserted secondary ground plane.

3.3.6 Results and analysis of corner reflector antenna

This section presents numerous set of simulation and measurement results of the designed CRA. The investigations were focused on three conditions; 1) beam shaping by varying feeder-to-vertex, S, 2) beam shaping by varying reflector side length, L, and 3) beam shaping by activating all elements. Prior to that, a subsection is made dedicated to present the study of effect of dielectric tubes on omnidirectional radiation patterns.

Series of measurements were carried out to validate the simulation results. Implementation of two reflectors on a single ground plane enables single beam and dual beam shapes to be realized just at hands. The single shape can be changed into dual beam shape within split seconds or even microseconds with fast switching scheme. In fact, the fastest time taken to change the beam shape from one to another only depends on the time taken by the plasma to decay [6], [62]. Evolution of the beam shapes are presented in this section, for the H-plane and the E-plane respectively. The antenna reflection coefficients and gains are also included in this section.

3.3.6.1   Effect of dielectric tubes on omnidirectional beam pattern

In this section, the effect of dielectric tubes surrounding a monopole antenna are presented and discussed. The antenna configurations are based configuration number 1 as listed in Table 3.5 is represented in Figure 3.83. The measured and simulated results of the antenna radiation patterns and performances are discussed based on the three element's height; 115 mm, 54 mm and 15 mm respectively. A secondary ground plane has to be used for the cases of element's heights are equal to 54 mm and 15 mm. The secondary ground plane is attached to the primary ground plane by using two sets of four poly legs.
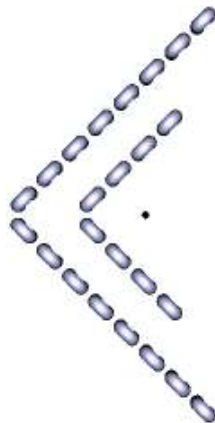
Figure 3.83 – Configuration number 1. CRA1 and CRA2 are switched OFF.

As soon as the monopole in operating mode and all elements are switched OFF, omnidirectional beam shapes were observed in the H-plane as shown in Figure 3.84. Even though the dielectric tube only contains argon gas (with assumption of the thin phosphor layer does not giving any effect on antenna performances), somehow with its arrangement (coordination and height), it could confer trivial effect to the antenna radiation pattern. This can be seen in the H-plane radiation patterns for *h* equals 115 mm. The measured radiation pattern in the H-plane is approximately 5 dB lower at some points than its simulation one. But it differs from the other two heights, which are having good radiation pattern correlations between simulation and measurement. For the E-plane patterns, a satisfactory agreement can be observed between simulation and measurement radiation patterns. Even though the cross polarization patterns are not represented in the figures, their levels are about below than -10 dB in the H- and E - planes, in both simulation and measurement.

Figure 3.84 – Measured and simulated radiation patterns of corner reflector antenna at 2.4 GHz, E_θ component. (a) Simulated H-plane radiation patterns. (b) Measured H-plane radiation patterns. (c) Simulated E-plane radiation patterns. (d) Measured E-plane radiation patterns.

In term of performances, both simulated and measured reflection coefficients are in good agreements and the antenna is matched at 2.4 GHz for three different element's heights. The measured maximum gain at operating frequency for the three different height are 5.4 dBi (*h*=115 mm), 5.7 (*h*=54 mm), and 5.8 (*h*=15 mm) and the corresponding simulated gains are 6 dBi, 6.4 dBi, and 6 dBi, respectively. It is worth to note that, the measured monopole antenna with the same ground plane size is 5.4 dBi which is similar to its computed version. A short conclusion can be made here, by having dielectric tubes unevenly surrounding monopole antenna in V coordination, a slight increment in gain was observed for the three measured CRAs with the three heights. The gain patterns and the reflection coefficients are illustrated in Figure 3.85.
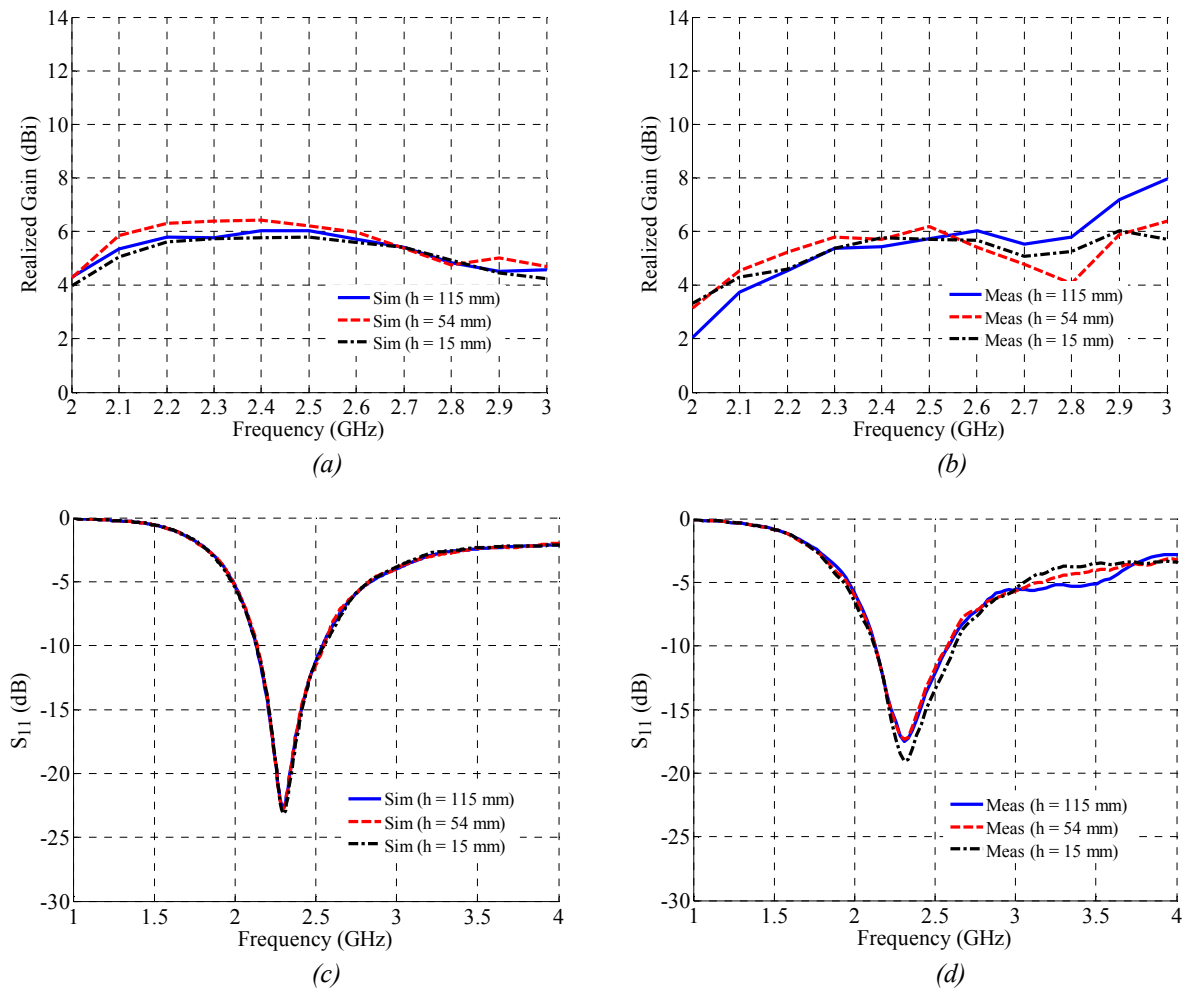
Figure 3.85 – Measured and simulated performance of corner reflector antenna at 2.4 GHz. (a) Simulated gains. (b) Measured gains. (c) Magnitude of simulated reflection coefficient, S_{11}. (d) Magnitude of measured reflection coefficient, S_{11}.

3.3.6.2   Beam shaping by varying feeder-to-vertex distance, *S*

In this section, the CRA radiation patterns and performances when the *S* is varied are discussed. Comparisons of antenna performances and radiation patterns are presented in this section for the three element's heights which are 115 mm, 54 mm, and 15 mm.

3.3.6.2.1   Beam shapes of plasma corner reflector antenna with *S* equals 0.5λ

It is interesting to note that, when the plasma elements of CRA1 are switched ON as depicted in Figure 3.86, the omnidirectional beam patterns are now transformed to more focused beams at the broadside direction.
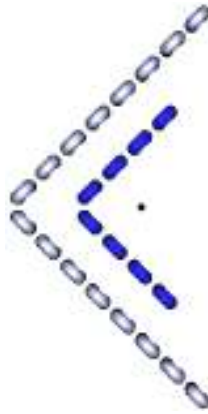
Figure 3.86 – CRA1 is ON (L₁ is 4) and CRA2 is OFF simultaneously (blue color represents activated element).

Good similarities are observed between simulated and measured radiation patterns both in the H- and the E- planes as shown in Figure 3.87. All cases show good front to back ratio and good profile of back radiation patterns. However, for the *h* equals 15 mm the radiation pattern seems to be broader in the broadside direction with increment in the side lobe level. The back radiation profile is somehow much higher and broader than the two other cases but it rather lower than -10 dB. There not much dissimilarity can be observed in the E-plane radiation patterns. Both simulated and measured radiation patterns are similar with the maximum beams are directed at elevation angle of 25°.

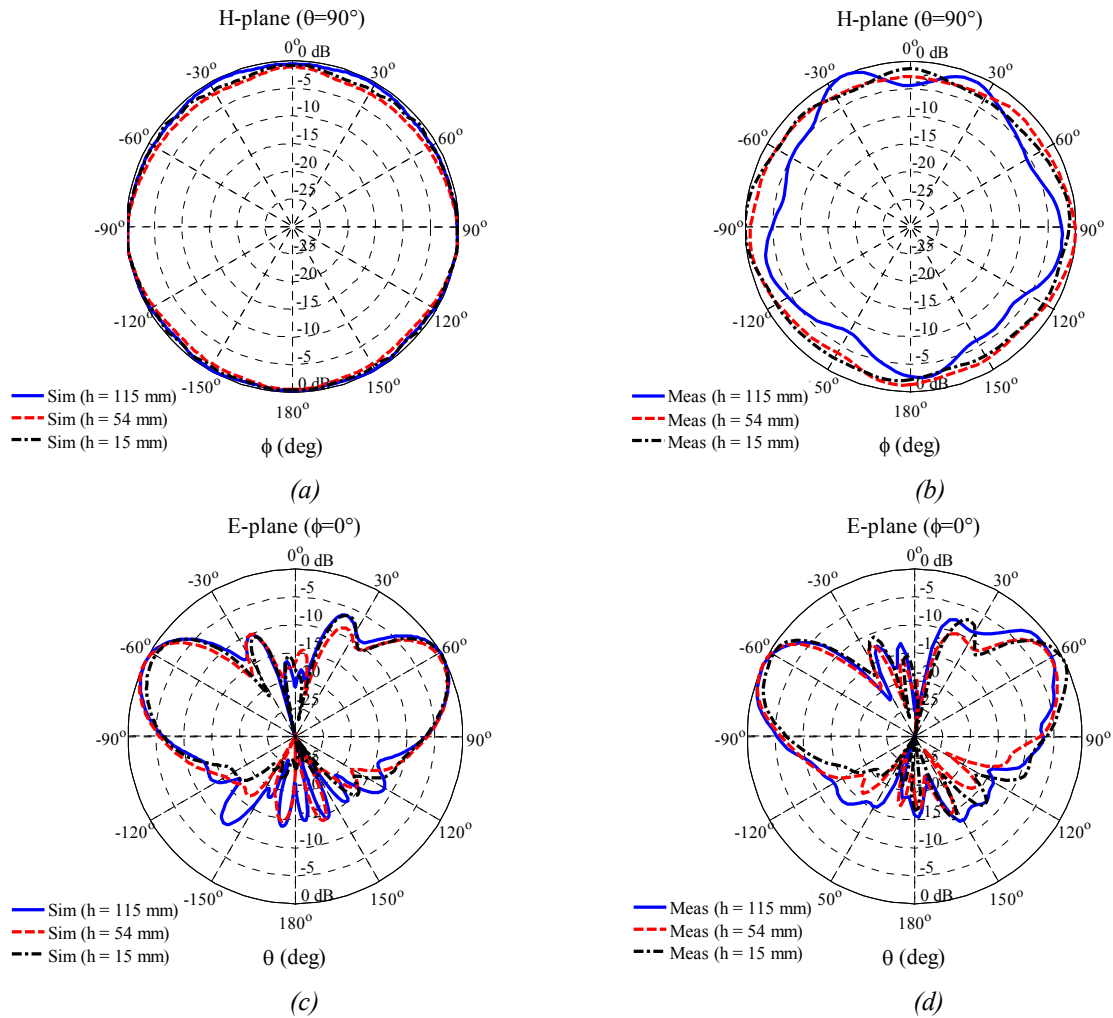*Figure 3.87 – Measured and simulated radiation patterns of CRA1 at 2.4 GHz, E_θ component. (a) Simulated H-plane radiation patterns. (b) Measured H-plane radiation patterns. (c) Simulated E-plane radiation patterns. (d) Measured E-plane radiation patterns.*

Figure 3.88 shows the comparison of simulated and measured gain of the CRA with three different heights. For the case of *h* equals 115 mm, the measured gain is 10.9 dBi and the simulated gain is 11.8 dBi at 2.4 GHz. Both simulation and measurement have more than 5 dB gain if compared to the gain of monopole antenna without or with dielectric tubes (5.4 dBi). The same situation was observed when the CRA is in operating mode for the case of *h* is equal to 54 mm. The measured and simulated gains, 10.8 dBi and 11.3 dBi respectively are a bit lower than the case of 115 mm. Nevertheless, these differences can be neglected since it is too small. The similar procedures were applied for the CRA with *h* is equivalent to 15 mm in order to reflect beam in the broadside direction. However, the antenna radiation pattern and performance are not very encouraging. Even though a good relation between simulation and measurement results can be observed, the CRA with 15 mm of element heights has shown degrading results compared to the two previous cases. The reduction of element height lesser than resonating element may explain these circumstances. The reflection coefficient pattern is more monopole alike and the measured plasma gain only 3 dB

higher than the gain of monopole antenna with the same size of ground plane. This further suggests that, a CRA with this configuration does not efficient in reflecting the omnidirectional beam transmitted by the monopole antenna.

(a)   *(b)*
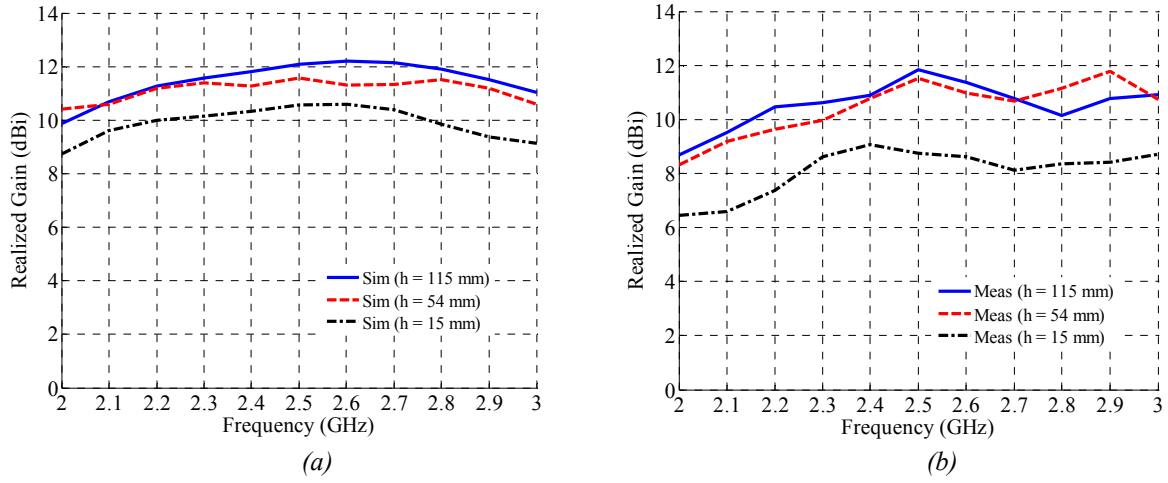
Figure 3.88 – Antenna gains. (a) Simulated (b) Measured.

Once the CRA is in operating mode, the operating bandwidth becomes wider and these scenarios can be viewed in the simulated and measured reflection coefficients as shown in Figure 3.89. This is due to scattering effect that varied the antenna impedance.

(a)   *(b)*
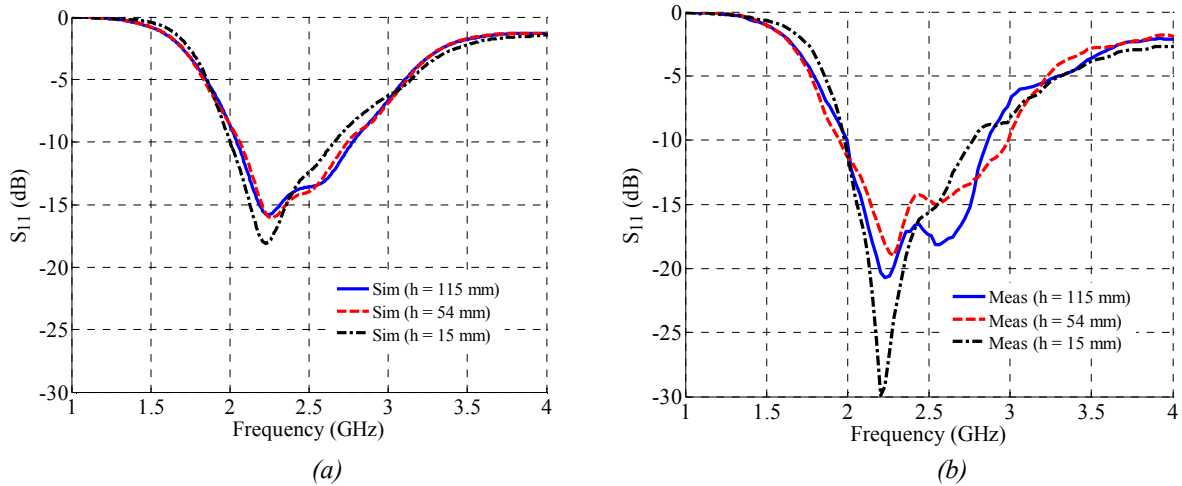
Figure 3.89 – Magnitude of reflection coefficient, S_{11}. (a) Simulated. (b) Measured.

By referring to measured reflection coefficient patterns in Figure 3.89 (b), the CRA offers almost 1 GHz of operating bandwidth especially for the case of *h* equals 54 mm.

3.3.6.2.2 Beam shapes of plasma corner reflector antenna with *S* equals λ

For the case of *S* is equal to λ, CRA2 on the same ground plane is in operating mode while the CRA1 is in OFF mode. This case is measured based on the configuration shown in Figure 3.90. There are 18 activated plasma elements to forward an incoming beam from monopole antenna to forward direction.

Figure 3.90 – CRA2 is ON (L₂ is 8) and CRA1 is OFF at the same time (blue color represents activated element).

Whenever the CRA2 is activated, and at the same time the CRA1 is in OFF mode, the omnidirectional beam radiated by the monopole antenna will be transformed into dual beams in the direction of ϕ is equal to ± 30°. The simulated and measured H-plane radiation patterns are shown in Figure 3.91 (a) and 3.91 (b) respectively. For the case of *h* is 115 mm, the -3 dB beamwidth in the azimuth plane for each of the dual beams is 25° and in the elevation plane, the -3 dB beamwidth is 30° with the maximum beam is directed at θ equals 65°. In the azimuth plane, a null is observed at ϕ equals 0° which is below than -10 dB. The null is somehow similar with a null seen in the simulated result. The same situation occurs when the antenna element's height is reduced to 54 mm. However, the antenna radiation pattern seemed to become broader and producing a poor back radiation profile when the antenna element's height is further reduced to 15 mm. Yet, the double beams remain as those seen in the two cases. The E-plane radiation patterns are represented in Figure 3.91 (c) and in Figure 3.91 (d), for simulation and measurement. These radiation patterns are observed at azimuth angle of 30° which revealing the double beams.
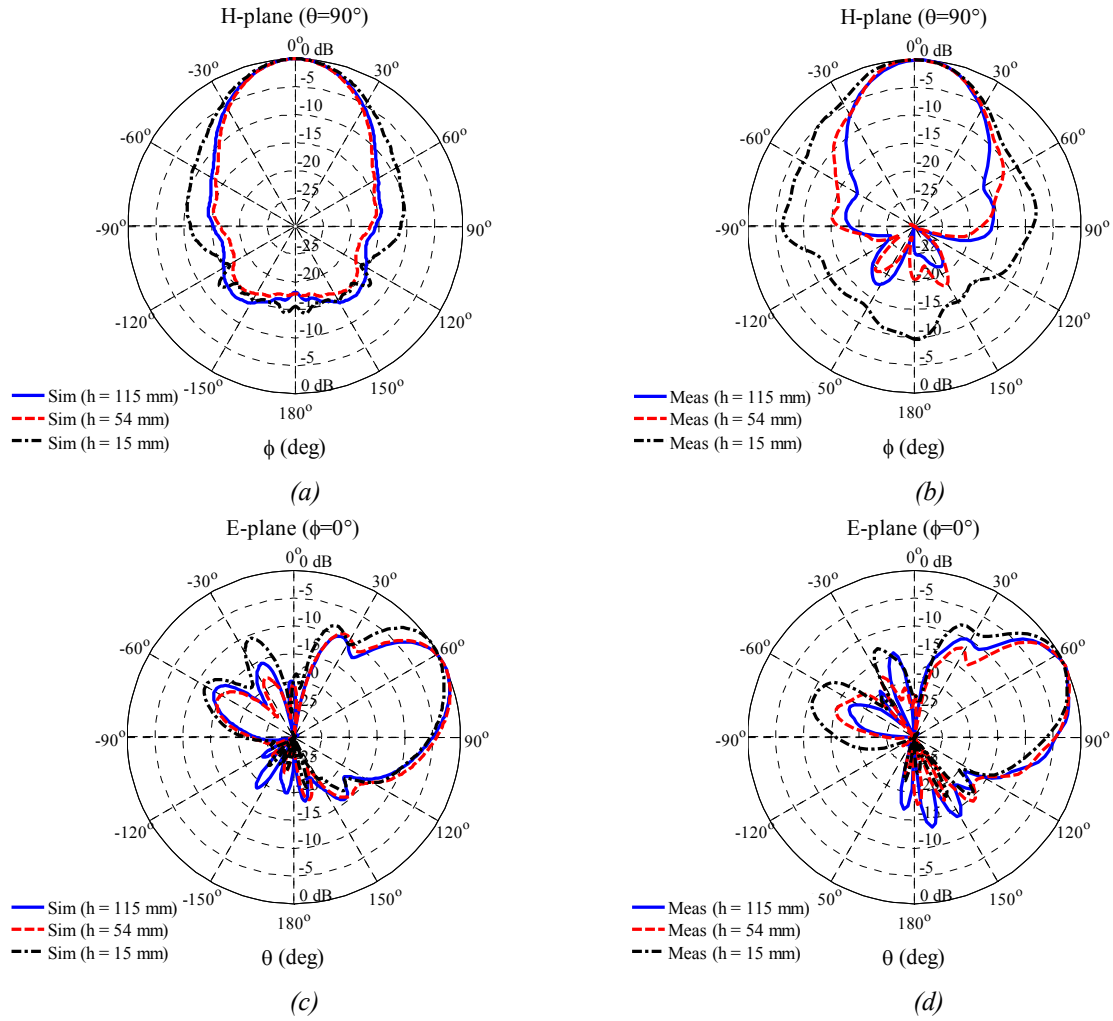
Figure 3.91 – Measured and simulated radiation patterns of CRA2 at 2.4 GHz, E_θ component. (a) Simulated H-plane radiation patterns. (b) Measured H-plane radiation patterns. (c) Simulated E-plane radiation patterns. (d) Measured E-plane radiation patterns.

It is good to highlight that, in all cases, the cross polarization remains below -15 dB. The front to back ratio is higher than 10 dB for all cases except for the measured one with *h* equals 15 mm. On the whole, each of the measured results is in a good agreement with its corresponding simulated result.

The CRA performances can be evaluated by looking to its reflection coefficient (S_{11}) and antenna gain as can be seen in Figure 3.92 and Figure 3.93, respectively. By comparing simulated and measured reflection coefficients, there is a significant correlation between them and indeed, all CRA configurations are matched at 2.4 GHz. It is worth to note that, the CRA2 is matched for a bandwidth of more than 0.5 GHz.
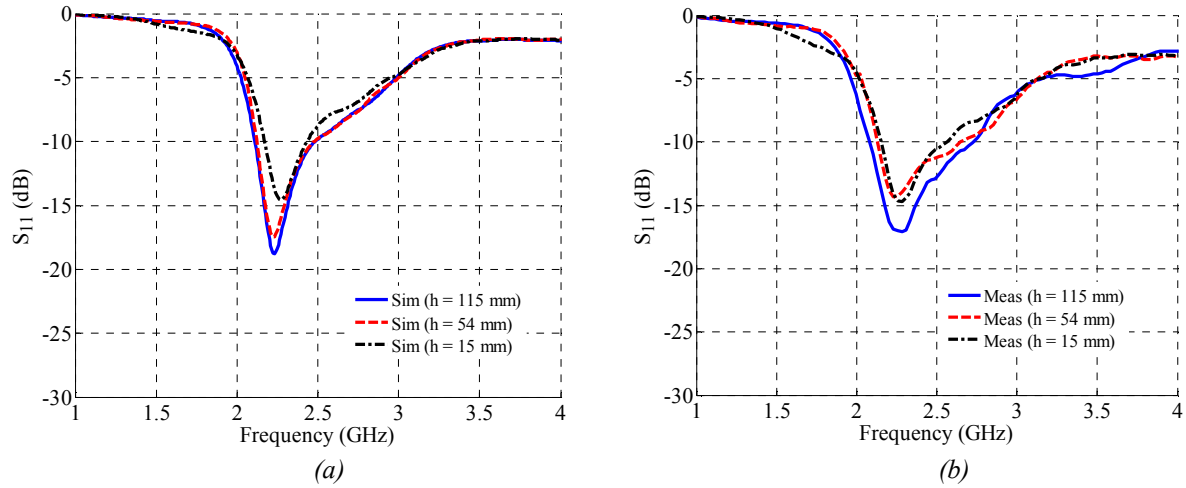
Figure 3.92 – Magnitude of reflection coefficient, S_{11}. (a) Simulated. (b) Measured.

The antenna gain patterns are analogous between simulated and measured gains as represented in Figure 3.93. The maximum gains are 10.5 dBi, 10.2 dBi, and 7.7 dBi for the corresponding 115 mm, 54 mm and 15 mm of element's heights. These gains are approximately 1 dB lower than its corresponding simulated gains.
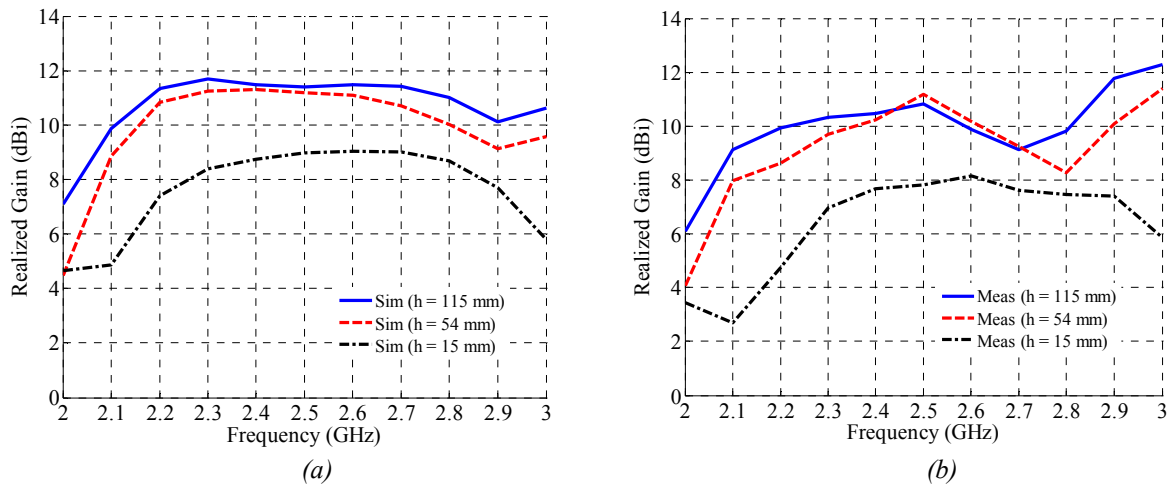
Figure 3.93 – Antenna gains. (a) Simulated. (b) Measured.

3.3.6.3 Beam shaping by varying dihedral reflector side length, *L* with a fixed element height

In this section, CRA radiation patterns and performances for several values of *L* (denoted by L_1 and L_2 in Figure 3.77) are discussed. Since the CRA elements can be individually controlled by electronic switches, the side length of the reflector can be controlled by activating and de-activating plasma elements. Thus the investigation results discussed here are presented in two sections, with the first subsection will discuss

about CRA1 with varying L_1 which consisting of 4 and 2 number of ON elements on one side of the reflector. The second subsection will be focusing on the CRA2 with four L_2 values which are 8, 6, 4 and 2 respectively (number of ON elements on one side of the reflector). Comparisons of antenna performances and radiation patterns are presented in this section for the case of *h* equals 115 mm.

3.3.6.3.1 Beam shapes of plasma corner reflector antenna with *S* equals 0.5λ and L_1 varies from 4 to 2 ON elements

It is sometimes necessary to have a wider -3 dB beamwidth in order to cater system requirements. For that reasons, the CRA1 was designed to provide variable beam shapes with one fix feeder-to-vertex distance, *S*. The resulting beam profiles are depending on the number of activated elements (the L_1). By changing the value of L_1 the corner reflector antenna aperture will also change accordingly. Thus, in section, the results of two beam shapes of the CRA1 are discussed. Figure 3.94 illustrates two conditions of CRA1 with two different L_1 values; 4 and 2 ON elements on one side of the CRA1.

(a)   *(b)*
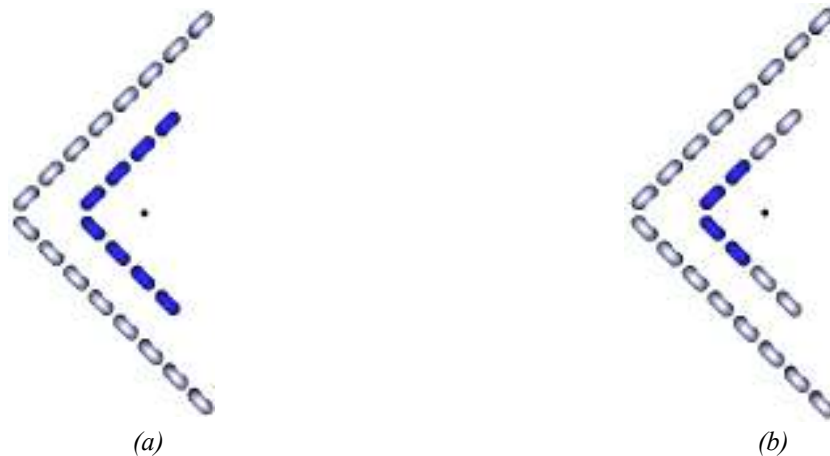
Figure 3.94 – Two configurations of CRA1 (blue color represents activated element). (a) CRA1 is ON (L_1 is 4) and CRA2 is OFF simultaneously. (b) CRA1 is ON (L_1 is 2) whilst CRA2 is OFF.

As a rule of thumb, whenever the L_1 is reduced, the aperture of CRA1 will also trim down. For the case of L_1 is equivalent to 2, the resulting side length does not obeying the minimum value of *L* (*L=2S*) required for square-corner reflectors. As a result a wider beam shape in the broadside direction will be produced. This behavior can be observed in Figure 3.95 for the H- and E- planes radiation pattern, for the L_1 equals 2 and 4 activated elements.
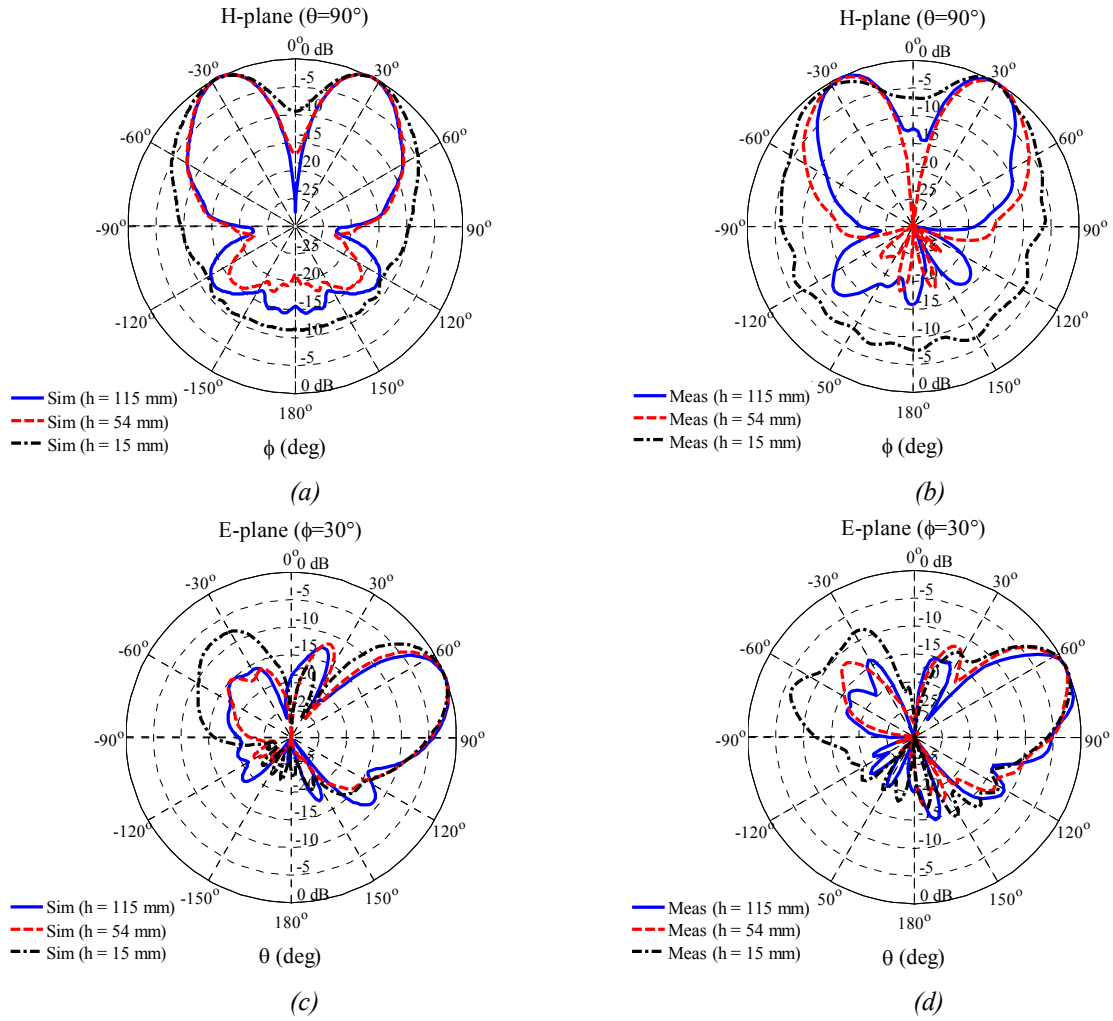
Figure 3.95 – Measured and simulated radiation patterns of CRA1with variable L at 2.4 GHz, E_θ component. (a) Simulated H-plane radiation patterns. (b) Measured H-plane radiation patterns. (c) Simulated E-plane radiation patterns. (d) Measured E-plane radiation patterns.

The measured HPBW are ± 50° (L_1=2) and ± 20° (L_1=4) and the simulated HPBW for L_1 equals 2 is slightly wider (± 55°) than its measured case, however for the case of L is 4, the same HPBW (± 20°) as measured case is noticed. Even though the broadside beamwidth profile is changed when the L_1 is reduced to 2 activated elements, the elevation beam profiles are in some way similar for the two cases. These conditions are shown in Figure 3.95 (c) and 3.95 (d). Certainly, a reduction of gain will occur once the beamwidth gets wider. This situation is proven as shown in Figure 3.96 (a) and 3.96 (b). The measured gain at 2.4 GHz is reduced from 10.9 dBi to 8.3 dBi corresponding to the lessening of L_1. It is about 3.6 dB reduction of gain occurs for the simulation result which is originating at 11.8 dBi. However, the reflection coefficients for the two cases are in a good correlation. The simulated and measured reflection coefficients are showing a similar pattern as can be seen in Figure 3.96 (c) and in Figure 3.96 (d).
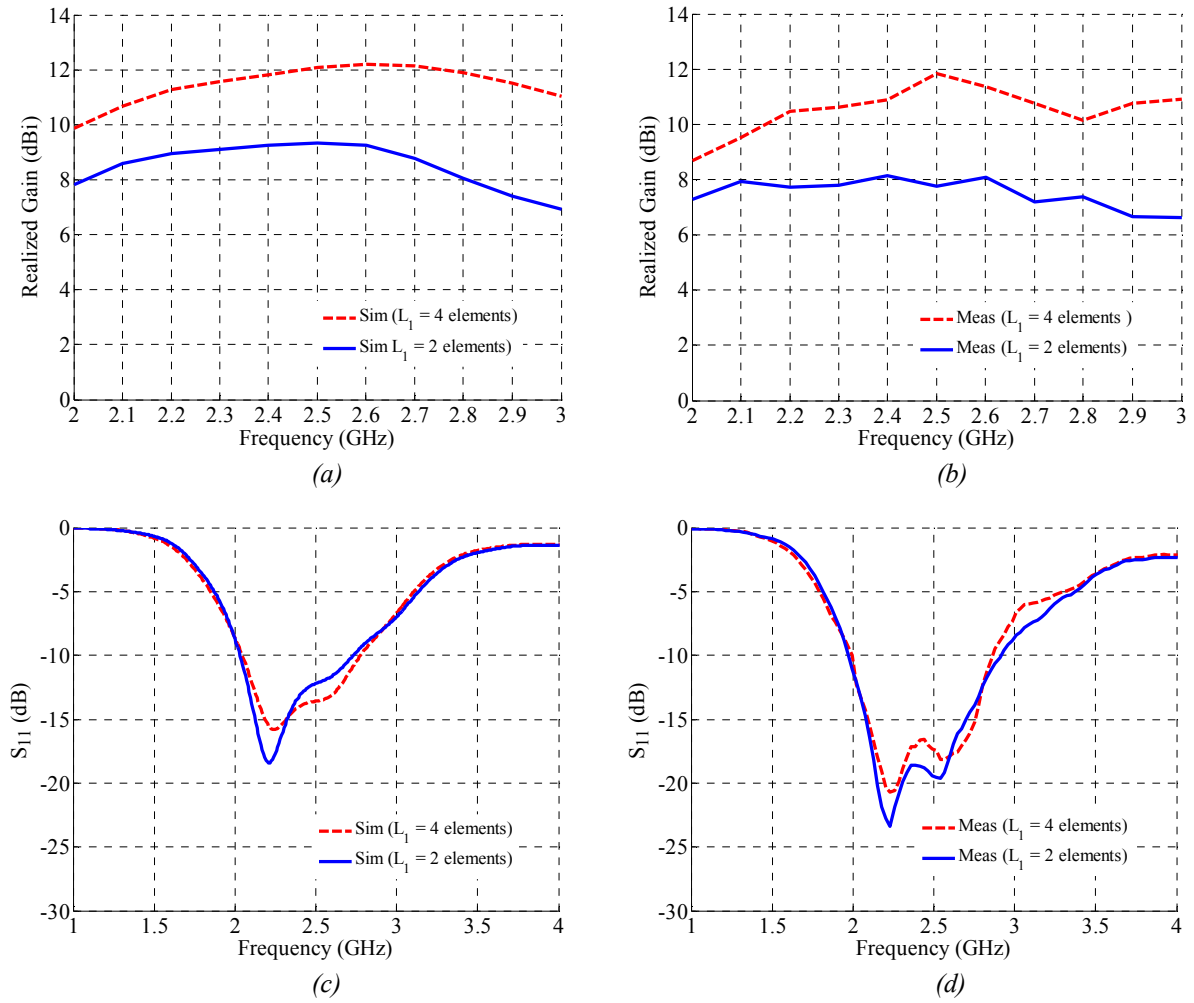
Figure 3.96 – Performances of corner reflector antenna (CRA1) at 2.4 GHz. (a) Simulated realized gains. (b) Measured realized gains. (c) Magnitude of simulated reflection coefficients, S_{11}. (d) Magnitude of measured reflection coefficients, S_{11}.

3.3.6.3.2 Beam shapes of plasma corner reflector antenna with *S* equals λ and L_2 varies from 8 to 2 ON elements

For the case of *S* equals λ, eight possible cases can be measured since each of the dihedral side consists of eight elements that can be controlled individually. For the sake of simplicity, the pattern evolution is observed by de-activating two elements (at each sides of CRA2) at each time for simulation and measurement. Thus, this section compares the results of CRA2 radiation patterns and performances for the value of L_2 equivalent to 8, 6, 4 and 2 activated elements. Figure 3.97 illustrates four configurations of CRA2 for the corresponding L_2 values (8, 6, 4, and 2 ON elements)

(a)   *(b)*

(c)   *(d)*
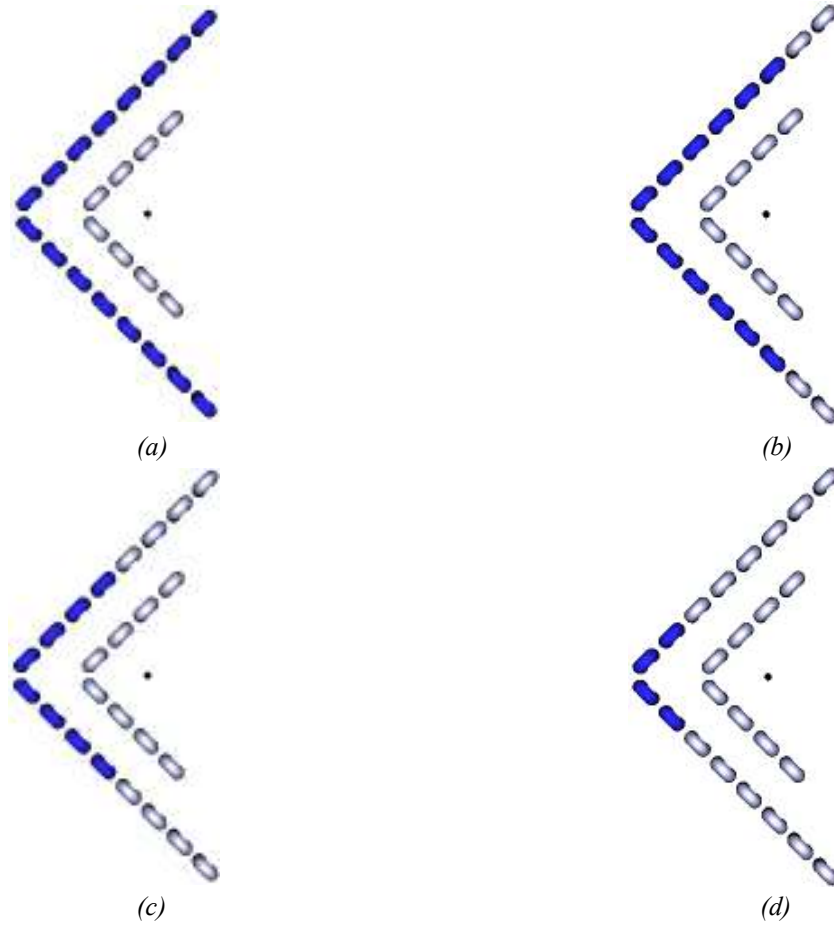
Figure 3.97 – Four configurations of CRA2 (blue color represents activated element). The CRA2 is ON with different values of L_2 whilst CRA1 is OFF. (a) L_2 is 8. (b) L_2 is 6. (c) L_2 is 4. (d) L_2 is 2.

It is noticed in simulations and measurements that, with certain values of L_2, the broadside beam profile will be transformed from dual beams to a single beam. The CRA2 exhibits two beam profiles for the L_2 of 8 and 6 activated elements, and will put on view a single beam profile when the L_2 is minimized to 4 or even 2 activated elements. A null seen when the L_2 is equal to 8 will slowly extinguish when the L_2 is decreasing and thus producing a single beam profile. The drawback of these single beams is the degrading performance in terms of front to back ratio which are less than 10 dB. A cardioids look like pattern is shown by the two single beam profiles. The evolution of the radiation pattern with respect to the varying L_2, is shown in Figure 3.98 (a) (simulation) and 3.98 (b) (measurement) for the H-plane. The maximum beams of the double beams are directed in the ± 30° while the two single beams are directed in the direction of phi is zero in the azimuth plane. All cases are having maximum beams at θ equals 65° in the elevation plane. Figure 3.98 (c) and Figure 3.98 (d) show the pattern evolution in the elevation plane for the simulation and measurement respectively.
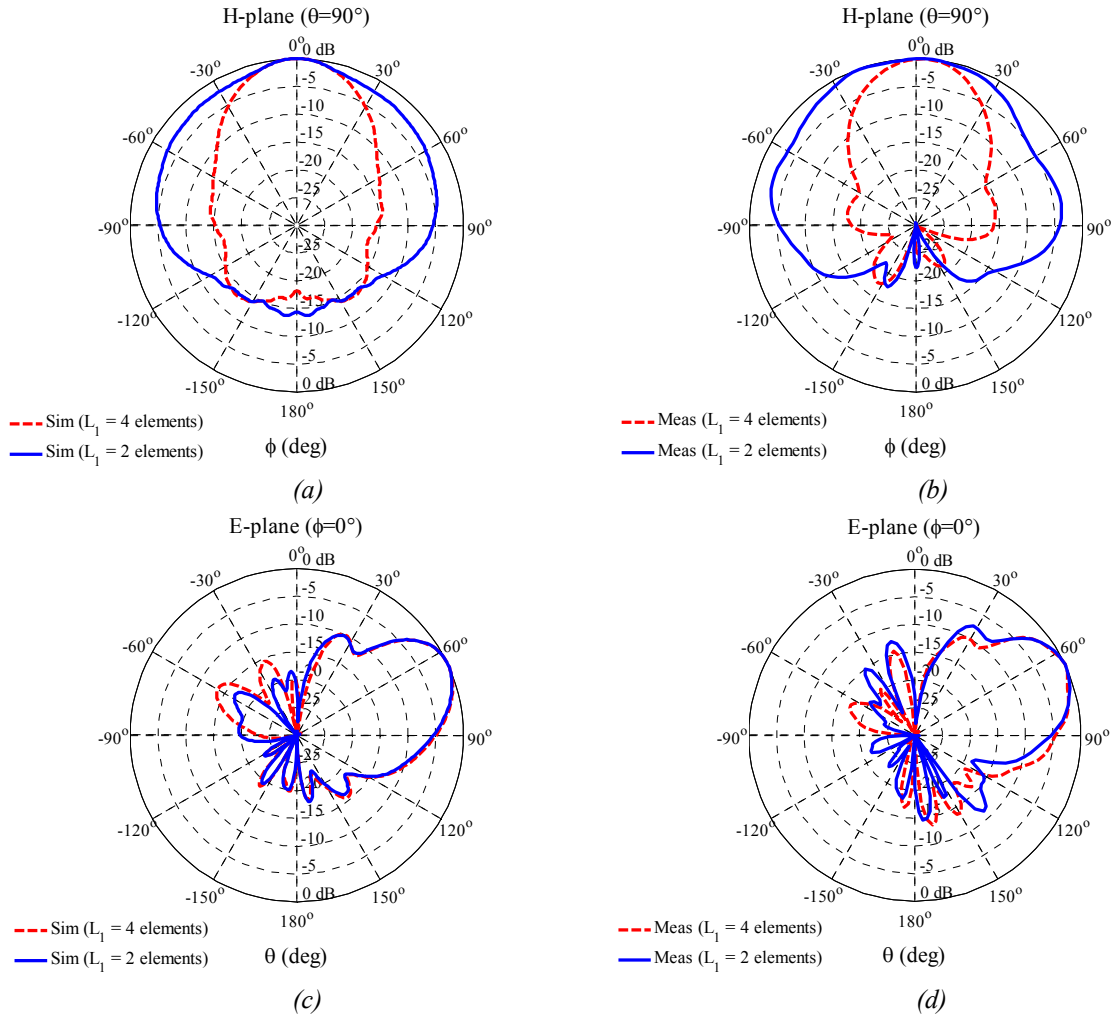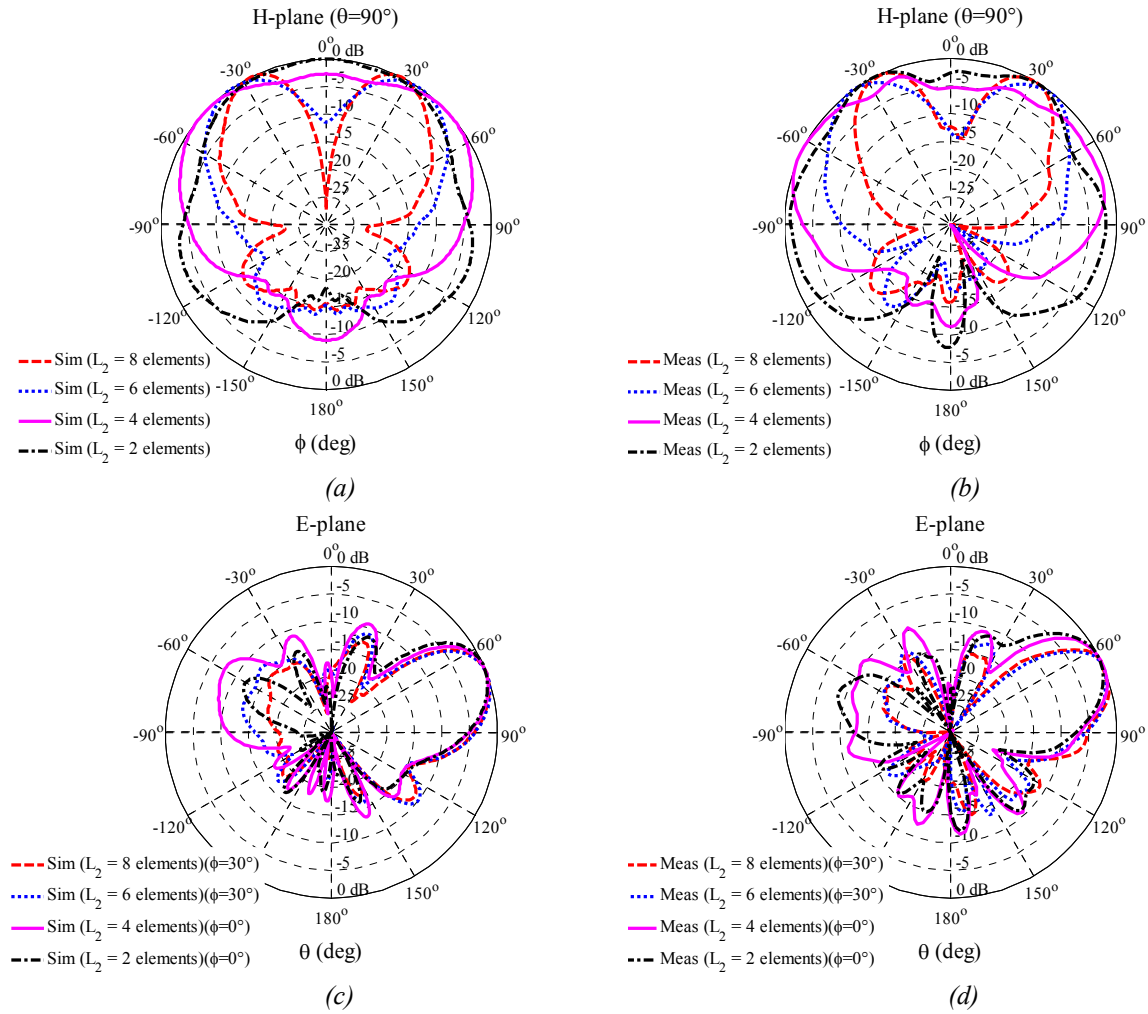
Figure 3.98 – Measured and simulated radiation patterns of CRA2 with variable L_2 at 2.4 GHz, E_θ component. (a) Simulated H-plane radiation patterns. (b) Measured H-plane radiation patterns. (c) Simulated E-plane radiation patterns. (d) Measured E-plane radiation patterns.

The measured and simulated gain patterns are in good agreements. The gains of antenna (Figure 3.99) are decreasing with the lessening of L_2 parameter. The maximum realized gains are 10.5 dBi (a similar gain when L_2 is equal to 8 and 6), 7.8 dBi and 6.9 dBi for the decreasing value of L_2 during measurement. There is 1 - 1.5 dB difference between simulated and measured gains. However, with L_2 is equal to 6 activated elements, the measurement and simulation share the same gain at 10.5 dBi.
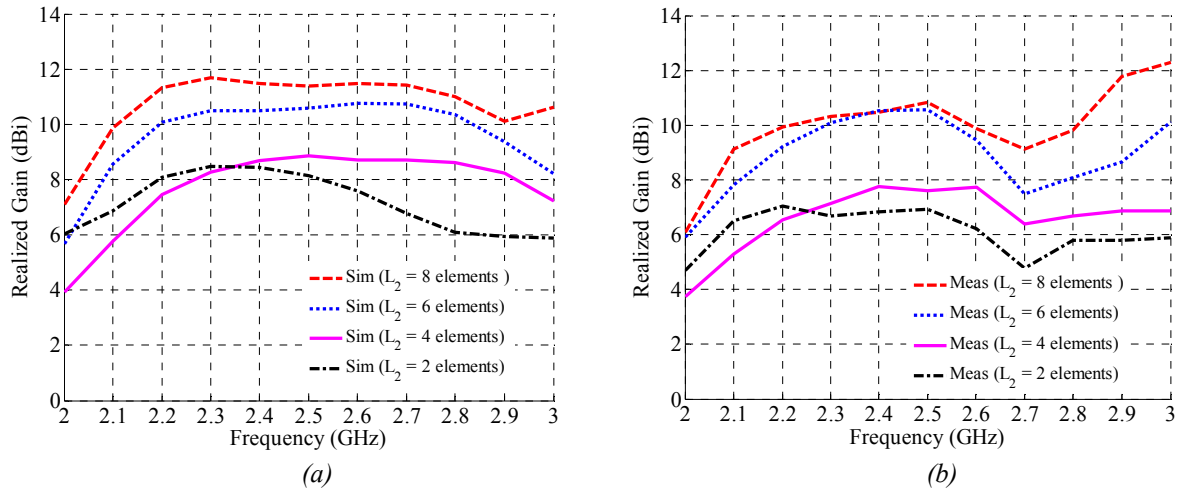
Figure 3.99 – Antenna gains. (a) Simulated. (b) Measured.

The antenna is matched at 2.4 GHz for all value of *L* and this situation can be seen in both measurement and simulation reflection coefficients. The antenna bandwidth performances are depicted in Figure 3.100.
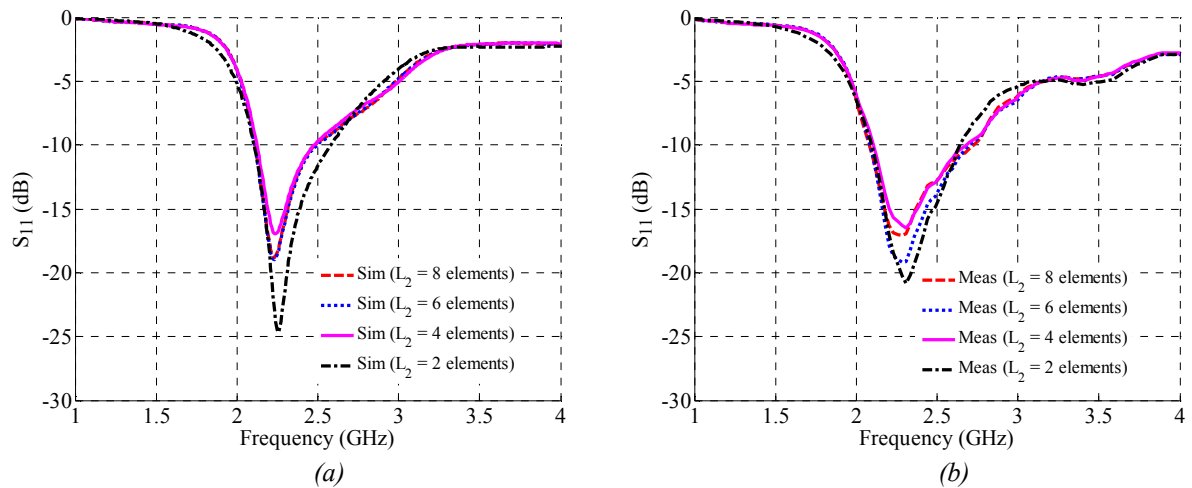
Figure 3.100 –Magnitude of reflection coefficients, S_{11}. (a) Simulated. (b) Measured.

3.3.6.4   Beam shaping by activating all elements

Imagine two classical gridded CRA being integrated on a single ground plane with their vertexes are separated 0.5λ between each other and a monopole is 0.5λ away from the nearest vertex. Up to now, no one has ever integrated metallic CRAs on a single ground plane does leaving this question to be answered by assumptions and computations. However with plasma implementation, this uncommon configuration can be simulated and measured so that it behavior can be studied. The investigation has proved that, the double beams that should emerge with the activated CRA2 is now no

longer seen if the CRA1 is activated at the same time. Figure 3.101 shows the configuration of CRA when CRA1 and CRA2 are activated simultaneously.
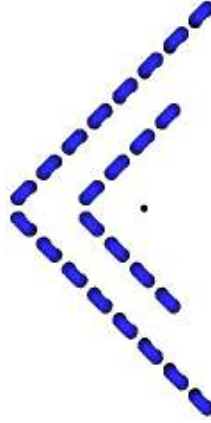
Figure 3.101 – Configuration of CRA when CRA1 and CRA2 are activated at the same time.

The double beams produced by CRA2 are directed to the broadside direction with the aid of CRA1. Therefore by activating CRA1 and CRA2 simultaneously, instead of double beams, a single beam will appear in the broadside direction. The simulated and measured radiation patterns in the H- and E- planes are represented in Figure 3.102.

(a)

(b)

(c)

(d)
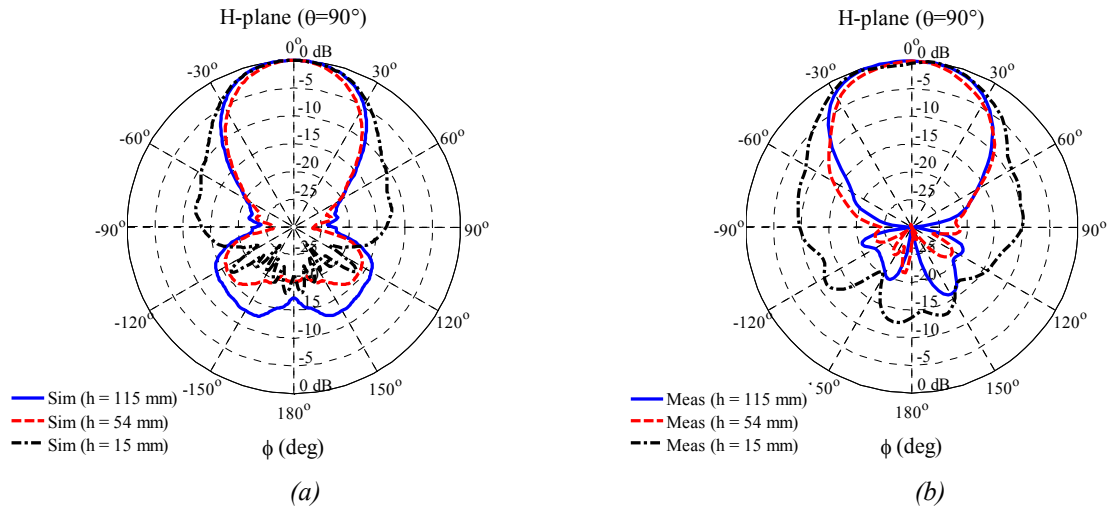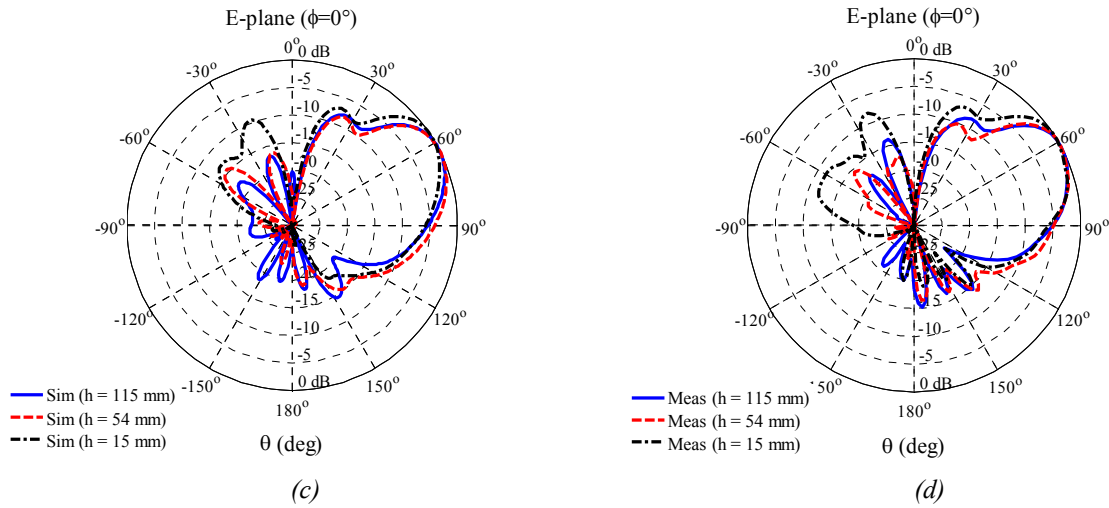
Figure 3.102 – Measured and simulated radiation patterns of CRA1 and CRA2 (activated simultaneously) at 2.4 GHz, E_θ component. (a) Simulated H-plane radiation patterns. (b) Measured H-plane radiation patterns. (c) Simulated E-plane radiation patterns. (d) Measured E-plane radiation patterns.

The only difference of the single beam radiation patterns generated by activating CRA1 and CRA2 simultaneously and the previous case (activating CRA1 solely) is the beamwidth size in the broadside direction. The beamwidth for the case of simultaneously activating CRAs is somehow wider than the case of activating CRA solely. This results lead to the small decreasing in antenna gains as depicted in Figure 3.103. The measured gains are 10.3 dBi for *h* is equals to 115 mm and 54 mm, and 7.9 dBi when the *h* is 15 mm. While the simulated gains are roughly 1 and 2 dB higher and the measured gains (11.3 dBi (115 mm), 11 dBi (54 mm) and 10 dBi (15 mm)). If compared the measured gains in this case with the gains of CRA1 (activated solely for single beam patterns), a 0.5 dB reduction of gain can be seen for the three different element's heights (except for the element's height of 15 mm is having 1 dB difference). This is due to the broadening effect in the broadside direction.
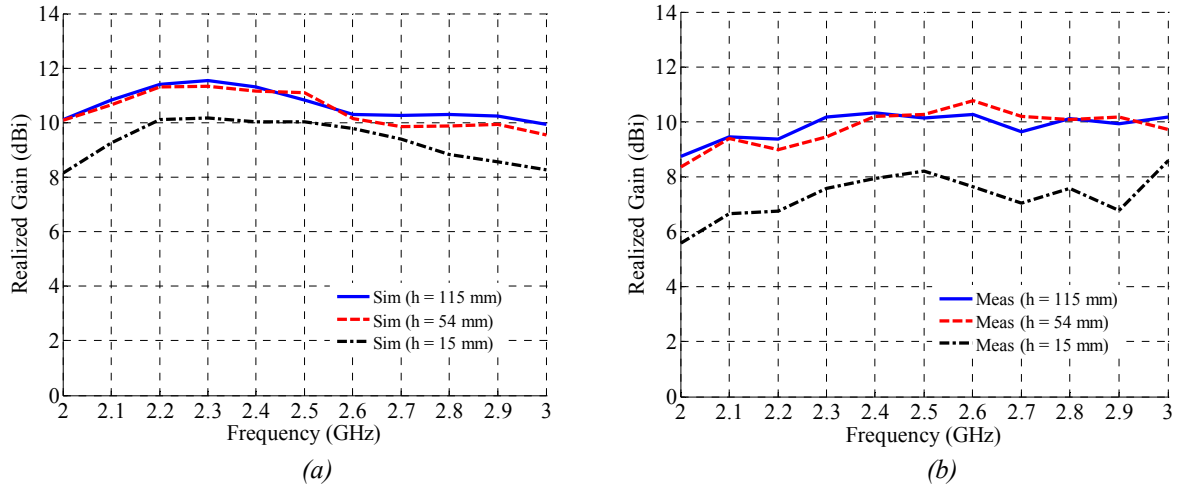
Figure 3.103 – Antenna gains. (a) Simulated. (b) Measured

Both simulated and measured reflection coefficients of the antenna are in good agreements as shown in Figure 3.104. Moreover, these patterns are similar with those seen for the case of activating CRA1 as shown the earliest section. The antenna is matched with 1 GHz bandwidth with two *h* values (115 mm and 54 mm).
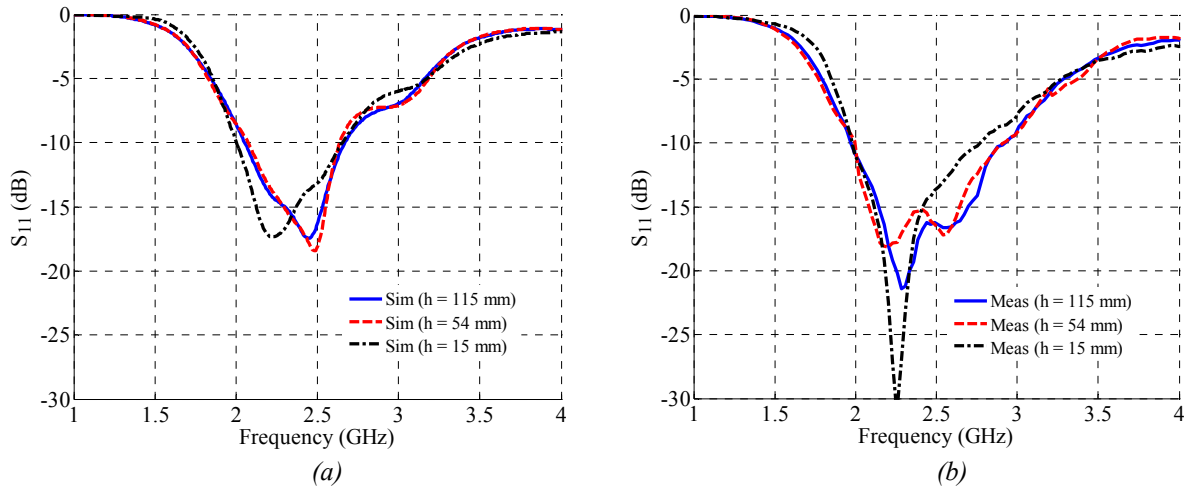
Figure 3.104 – Magnitude of reflection coefficients, S_{11}. (a) Simulated. (b) Measured.

3.3.7 Summary of result analysis of CRA

The third part of this chapter introduces a novel design of CRA that never been introduced before. Two corner reflector antennas (CRA1 and CRA2) are integrated on a single finite ground plane to form a reconfigurable CRA as a whole. The design was undergone optimization procedure in order to find an optimum CRA that uses fewer elements and can produce acceptable radiation pattern and exhibit good microwave performances. The optimized CRA was simulated and measured for several

configurations and the results were discussed thoroughly in the previous sections. This includes four main parts, and the first one is the investigation of the influence of dielectric tube (arranged in V coordination) on ominidirectinal pattern. The simulated and measured results are in satisfactory agreements. Thus, it was proven that, the dielectric tubes used as antenna elements (unused) do not deteriorate the omnidirectinal pattern. However, a small but negligible effect is observed when the height of elements is the maximum.

The second part presents the results of CRA with two values of feeder-to-vertex distance, S which are 0.5λ (CRA1) and λ (CRA2). The CRA1 was proven to produce a single beam in the broadside direction while CRA2 produces dual beams at $\phi \pm 30$ in the azimuth plane. The CRA1 and CRA2 were simulated and measured with three element's heights which are 115 mm, 54 mm and 15 mm. The generated beams demonstrate unique profiles when the element height is changing which could benefit some applications in communication systems. By combining CRA1 and CRA2, and indeed a monopole antenna, the whole system will transform an ominidirectional pattern into a single beam shape or double beam shapes by appropriately activating plasma elements. Moreover, this transformation proves that the CRA can be reconfigured electrically.

The influence of reflector side length (L) on radiation pattern has been discussed in the third subsection. In the investigation, the side length of CRA1 and CRA2 are varied by de-activating two elements at each of reflector's sides. The CRAs produce various beam profiles including a wider -3 dB beamwidth. For the case of CRA2, with a fixed S, double beams can be transformed into single beam by reducing the length of reflector's side accordingly.

In the last part, the effect of activating CRA1 and CRA2 simultaneously has been discussed for simulated and measured cases. This is another way to produce a single beam in the broadside direction without need to de-activate CRA2. However, in practical this configuration will consume more electrical power since all elements are switched ON. This beam profile is somehow similar with the case of activating CRA1 and yet having much wider beam shape in the broadside direction with reduction in gain. This investigation is quite unique because this situation can only be realized by using plasma elements.

As a whole, the fabricated CRA has been proven to work at 2.4 GHz and the CRA can be reconfigured electrically to construct several beam shapes. The CRA also can be fabricated with shorter element height so that the overall antenna size could be reduced without losing too much on its performance.

144

3.4 Conclusion

Although there are considerable amount of literatures have been published for reflector antennas, up to now there is no published paper which deals with plasma reflector antenna realization especially in ISM band frequencies except those in [57], [62], [64]. For this reason, in this chapter the simulated and measured results of a unique round reflector antenna (RRA) and a novel dual dihedral corner-reflector antenna are presented. The RRA offers beam shaping, beam steering and beam scanning capability while the CRA offers beam shaping with three beam shapes. These beams are electrically switchable from one to another. The antennas were simulated, fabricated and finally its performances were validated throughout a series of agile measurements. The quick prove on the antennas reconfigurability were demonstrated through their omnidirectional and beam focusing patterns. The measured reflected radiation patterns are in a good agreement with simulated ones. Most of the measured gains are 5 dB more than the gain of classical monopole antenna with corresponding identical size of finite ground plane. Therefore the plasma model defined in the simulation can be used to analyze the particular CFL for future works. Not to forget, even though not presented here, the cross polarization remains low and front to back ratio (f/b) is more than 10 dB. In addition, it is worth to emphasize that the results in this investigation have confirmed that the dielectric tubes used to enclose plasma have no major effect on a quarter wave antenna radiation pattern at 2.4 GHz. This conclusion is made by taking into account the super thin phosphor layer inside the dielectric tubes. In general, up to now, the fabricated plasma RRA and CRA have been proven that they can offer extra flexibility that cannot be offered by any traditional metal reflector.

References

[1] D. Lee, S. Lee, C. Cheon, Y. Kwon, "A two-dimensional beam scanning antenna array using composite right/left handed leaky-wave antennas," IEEE/MTT-S International Microwave Symposium, pp.1883-1886, 2007.

[2] L. Chui, W. Wu, D. G. Fang, "Printed frequency beam-scanning antenna with flat gain and low sidelobe levels," IEEE Antennas Wireless Propag., Lett., vol. 12, pp. 292-295, 2013.

[3] J. Y. Kim, C. W. Jung, B. Lee, "Reconfigurable beam steering antenna using double loops," AP-S/URSI pp. 1570-1572, 2011.

[4] Y. Yamada, N. Michishita, S. Kamada, "Construction of wide angle beam scanning lens antenna and its applications," Proceeding of the 2009 International Conference on Space Science and Communication, pp. 41-46, Oct. 2009.

[5] O. Lafond, M. Himdi, H. Merlet, P. Lebars, "An active transmitter antenna with beam scanning and beam shaping capability for 60 GHz application," Proceedings of ISAP2012, pp. 263-2666, 2012.

[6] Y. Yang, X. Zhao,"Beam-scanning antennas based on metamaterial planar lens antennas," The 5th European Conference on Antennas and Propagation (EuCAP 2010), pp. 1105-1108, 2010.

[7] M. Kyro, D. Titz, V. M. Kolmonen, S. Ranvier, P. Pons, C. Luxey, P. Vainikainen, "5 x 1 linear antenn array for 60 GHz beam steering applications," The 5th European Conference on Antennas and Propagation (EuCAP 2010), pp. 1258-1262, 2010.

[8] S. Bildik, C. Fritzsch, A. Moessinger, R. Jakoby, "Tuneable liquid crystal reflectarray with rectangular elements," German Microwave Conference, pp. 1-4, 2010.

[9] K. Kitatani, T. Terada, Y. Okamura, "Mechanical beam scanning microstrip crank-line antenna loaded movable dielectric," The 2nd European Conference on Antennas and Propagation (EuCAP 2007), 2007.

[10] C. Chiang, C. C. Tzuang, "Phase-shifterless beam-steering micro-slotline antenna," Elect., Lett., vol. 38, no. 8, pp. 354-355, Apr. 2012.

[11] E. Ojefors, S. Cheng, K. From, I. Skarin, P. Halljorner, A. Rydberg, "Electrically steerable single-layer microstrip traveling wave antenna with varactor diode based phased shifters," IEEE Trans. Antennas Propag., vol. 55, no. 9, pp. 2451-2460, Sept. 2007.

[12] M. T. Ali, M. R. Kamarudin, M. N. Md Tan, T. A. Rahman, "Reconfigurable beam shaping antenna with wilkinson power divider at 5.8 GHz," IEEE International RF and Microwave conference Proceedings, pp. 436-440, Dec. 2008.

[13] Y. G. Kim, T. H. Kim, S. G. Kang, I. G. Choi,"Electronically beam scanning array antenna for 5.8 GHz ISM band application," The proceedings of the 40th European Microwave Conference, pp. 457-460, Sept. 2010.

[14] G. Augustin, Shynu S. V., P. Mohanan, C. K. Aanandan, K. Vasudevan, "Wide band electronically scannable leaky wave antenna for low cost beam steering applications," Proceedings of APMC, 2005.

[15] Z. Lu, X. Yang, "A novel planar beam steering antenna," IEEE International Wireless Symposium (IWS), 2013.

[16] M. Konca, S. Uysal, "Circular multi-directional patch antenna array with selectable beams using a novel feed strcuture and equilateral triangular patches," Mediterranean Microwave Symposium, pp. 440-443, 2010.

[17] N. Din, A. Afzal, J. Tahir, N. Hafeez, "Electronic beam scanning for radar applications," High Capacity Optical Networks and Enabling Technologies (HONET), pp. 355-358, 2011.

[18] M. Adhikari, K. F. Warnick, "Miniature radiation pattern reconfigurable antenna for 2.4 GHz band," IEEE Antennas and Propagation Society International Symposium (APSUSI), pp. 1-4, 2010.

[19] J. C. Ke, C. W. Ling, S. J. Chung, "Implementation of a multi-beam switched parasitic antenna for wireless applications," IEEE Antennas and Propagation Society International Symposium (APS), pp. 3368-3371, 2007.

[20] Z. Li, H. Mopidevi, O. Kaynar, B. A. Cetiner, "Beam-steering antenna based on parasitic layer," Elect., Lett., Vol. 48, no. 2, Jan. 2012.

[21] M. R. Islam, M Ali, "A 900 MHz beam steering parasitic antenna array for wearable wireless applications," IEEE Trans., Antennas Propag., vol. 61, no. 9, pp. 4520-4527, Sept. 2013.

[22] S. Ha, C. W. Jung, "Single patch beam steering antenna with U-slot for wearable fabric applications," IEEE Antennas and Propagation Society International Symposium (AP-S/URSI), pp. 1560-1562, 2011.

[23] Md. Rashidul Islam, M. Ali, "Body-wearable beam steering antenna array for 5.2 GHz WLAN applications," The proceedings of International Conf., on Electrical and computer engineering, pp. 447-449, Dec. 2012.

[24] A. Kalis, M. J. Carras, "A sectored phased array for DBF applications," IEEE Trans., Vehicular Technol., vol. 54, no. 6, pp. 1932-1936, Nov. 2005.

[25] S. K. Sharma, L. Shafai, "Beam focusing properties of circular monopole array antenna on a finite ground plane," IEEE Trans., Antennas Propag., vol. 53, no. 10, pp. 3406-3409, Oct. 2005.

[26] M. T. Ali, T. A. Rahman, M. R. Kamarudin, R. Sauleau, M. N. Md Tan, M. F. Jamlos, "Reconfigurable orthogonal antenna array (ROAA) based on separated feeding network," The 5th European Conference on Antennas and Propagation (EuCAP 2010), Apr. 2010.

[27] P. Ratajczak, P. Brachat, J. M. Fargeas, "An adaptive beam steering antenna for mobile communications," IEEE Antennas and Propagation Society International Symposium (APS), pp. 418-421, 2006.

[28] John D. Kraus, "The corner-reflector antenna," Proceeding of the IRE, pp. 513-519, 1940.

[29] Oakley M. Woodward Jr., "A circularly-polarized corner reflector antenna," IRE Trans., Antennas Propag., pp. 290-297, 1957.

[30] T. S. Ng, K. F. Lee, "Theory of corner-reflector antenna with titled dipole," Proceeding of the IEE, vol. 129, pt. H, no. 1, pp. 11-17, Feb. 1982.

[31] N. Okamoto, "Electronic lobe switching by 90° corner reflector antenna with ferrite cylinders", IEEE Trans., on Antennas and Propag., vol. 23, pp. 527-531, 1975.

[32] R. W. Klopfenstein, "Corner reflector antennas with arbitrary dipole orientation and apex angle," IRE Trans., Antennas Propag., pp. 297-305, 1957.

[33] E. F. Harris, "An experimental investigation of the corner-reflector antenna," Proceeding of the IRE, pp. 645-651, 1953.

[34] A. C. Wilson, H. V. Cottony, "Radiation patterns of finite-size corner-reflector antennas," IRE Trans., Antennas Propag., vol. AP-8, no. 2, pp. 144-157, Mar. 1960.

[35] Naoki Inagaki, "Three dimensional corner-reflector antenna," IEEE Trans., Antennas Propag., pp. 580-582, July 1974.

[36] H. M. Elkamchouchi, "Cylindrical and three-dimensional corner reflector antennas," IEEE Trans. on Antennas and Propag., vol. AP-31, No. 3, pp. 451-455, May 1983.

[37] H. M. Elkamchouchi, M. Elrakaiby,"Solution of the three-dimensional corner reflector antenna problems using the method of moments," Proceedings of the 13th National Radio Science Conference, Mar, 1996.

[38] K. Miyata, "Radiation pattern analysis of corner reflector antennas by boundary-element method," IEEE Antennas and Propagation Society International Symposium (AP-S), pp. 371-374, 1989.

[39] A. D. Olver, U. O. Sterr, "Radiation from gridded corner-reflector antennas using FDTD," IEEE Antennas and Propagation Society International Symposium (APS), pp. 1642-1645, 1997.

[40] J. L. Wong, H. E. King, "A wide-band corner-reflector antenna for 240 to 400 MHz," IEEE Trans. on Antennas and Propag., vol. AP-33, No. 8, pp. 891-892, Aug. 1983.

[41] B. M. Duff, O. Tranbarger", A broadband directional corner reflector antenna for borehole applications," IEEE Antennas and Propagation Society International Symposium (AP-S), pp. 278-281, 1989.

[42] N. Okamoto, "Electronic lobe switching by 90° corner reflector antenna with ferrite cylinders," IEEE Trans. on Antennas and Propag., vol. 23, pp. 527-531, 1975.

[43] A. Harmouch, C. El Moucary, M. Ziade, J. Finianos, C. Akkari, S. Ayoub, "Enhancement of directional characteristic of corner reflector antennas using metallic scatters," in Proc. 19th ICT, pp. 1-4, 2012.

[44] B. H. Henin, M. H. Al Sharkawy and A. Z. Elsherbeni, "Enhanced performance of corner reflector antenna using metamaterial cylinders," The 2nd European Conference on Antennas and Propagation (EuCAP 2007), 2007.

[45] K. T. Mathew, J. Jacob, S. Mathew, U. Raveendranath, "Triple corner reflector antenna and its performance in H-plane," Elect., Lett., vol. 32, no. 16, pp. 1342, Aug. 1996.

[46] U. O. Sterr, A. D. Olver and P. J. B. Clarricoats, "Variable beamwidth corner reflector antenna," Electron. Lett., vol. 34, no. 11, pp. 1050-1051, May 1998.

[47] D. C. Chang, B. H. Zeng, J. C. Liu, "Reconfigurable angular diversity antenna with quad corner reflector arrays for 2.4GHz applications," Microw., Antennas Propag., pp. 522-528, 2009.

[48] T. D. Dimousios, S. A. Mitilineos, C. Panagiotou, C. N. Capsalis, "Design of a corner-reflector reactively controlled antenna for maximum directivity and multiple beam forming at 2.4GHz," IEEE Trans., on Antennas and Propag., vol. 59, no. 43, pp. 1132-1136, April 2011.

[49] A. Nesic, Z. Micic, S. Javanovic, I. Radnovic, D. Desic, "Millimeter wave corner reflector antenna array," European Microwave Conference, 2005.

[50] Wallace M. Manheimer, "Plasma reflectors for electronic beam steering in radar systems", IEEE Trans., Plasma Sci., vol. 19, no. 6, pp. 1228-1234, December 1991.

[51] P. Linardakis, G. Borg, N. Martin, "Plasma based lens for microwave beam steering," Elect., Lett., vol. 42, no. 8, Apr. 2006.

[52] J. Mathew, Robert A. Meger, Joseph A. Gregor, Robert E. Pechachek, Richard F. Fernsler, W. M. Manheimer, "Electrically steerable plasma mirror for radar applications," IEEE International Radar Conference, pp. 742-747, 1995.

[53] A. E. Robson, R. L. Morgan, R. A. Meger, "Demonstration of a Plasma Mirror for Microwaves," IEEE Trans. Plasma Sci., vol. 20, no. 6, pp. 1036-1040, Dec. 1992.

[54] J. Mathew, R. A. Meger, J. A. Gregor, D. P. Murphy, R. E. Pechachek, R. F. Fernsler, W. M. Manheimer, "Electronically steerable plasma mirror," IEEE International Symposium on Phased Array Systems and Technology, pp. 58-62, 1996.

[55] J. Mathew, "Electronically steerable plasma mirror based radar - concept and characteristics," IEEE AES Systems Magazine, pp. 38-44, Oct. 1996.

[56] R. A. Meger, R. F. Fernsler, J. A. Gregor, W. Manheimer, J. Mathew, D. P. Murphy, M. C. Myers, R. E. Pechachek, "X-Band microwave beam steering using a plasma mirror," IEEE Aerospace Conference Proceedings, pp. 49-56, 1997.

[57] I. Alexeff, T. Anderson, S. Parameswaran, E. P. Pradeep, J. Hulloli, P. Hulloli, "Experimental and theoretical results with plasma antennas," IEEE Trans., Plasma Sci., vol. 34, no. 2, pp. 166-172, April 2006.

[58] T. Anderson, I. Alexeff, N. Karnam, E. P. Pradeep, N. R. Pulasani, J. Peck, "An operating intelligent plasma antenna," IEEE 34th International Conference on Plasma Science (ICOPS 2007), pp. 353-356, 2007.

[59] I. Alexeff, T. Anderson, E. Farshi, N. Karnam, N. R. Pulasani, "Recent results for plasmas," Phys. Plasmas 15, 057104 (2008).

[60] Theodore Anderson, "Plasma antenna windowing," in Plasma Antennas, Artech House, MA: Norwood, 2011, pp. 53-78.

[61] Theodore Anderson, "Smart plasma antenna," in Plasma Antennas, Artech House, MA: Norwood, 2011, pp. 79-112.

[62] X. P. Wu, J.M. Shi, Z. S. Chen, B. Xu, "A new plasma antenna of beam-forming," Progress In Electromagnetics Research (PIER), vol. 126, pp. 539-553, 2012.

[63] J. P. Rayner, A. P. Whichello, A. D. Cheetham, "Physically characteristics of plasma antennas," IEEE Trans., Plasma Sci., vol. 32, no. 1, pp. 269-281, Feb. 2004.

[64] C. A. Balanis, "Reflector antennas," in Antenna Theory Analysis and Design 3rd Edition, John Wiley & Sons, NJ: Hoboken, 2005, pp. 883-892.

[65] J. D. Kraus, R. J. Marhefka, " Flat sheet, corner and parabolic reflector antennas," in Antennas for All Applications 3rd Edition, McGraw Hill, NY: New York, 2002, pp. 347-374.

Appendix 3.1

![SYLVANIA]

Mini-Lynx Fast-Start

ML FAST-START 827 E27 20W SLV

0035123

Range features

CE

PRODUCT OVERVIEW

Ordering number	0035123
Technology	Compact Fluorescent
Light colour	827 Homelight
Energy class	A
Average life (Rated) (h)	10000
Lamp shape	Stick
Lamp finish	Frosted
Dimmable	No
Cap/Base	E27
Type	Mini-Lynx Fast Start T3 4U Stick
EAN code	5410288351230
CRI (Ra)	80
Colour temperature (K)	2700
Luminous flux (Rated) (lm)	1200
Efficacy (Rated) (lm/w)	60
Watt (Nominal) (W)	20
Equivalent watt (W)	86
Voltage (V)	220-240

TECHNICAL DRAWINGS

E27

27

27

Appendix 3.2

BCC

TCI

Mini reattori elettronici multilampada - multipotenza
Multi-lamp and multi-power mini electronic ballasts
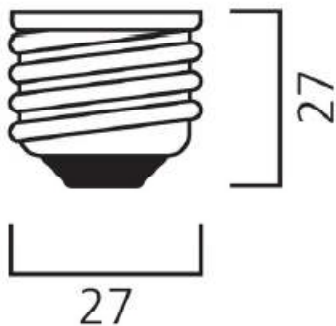
Ballast elettronici / Electronic ballasts

EEI=A2 RoHS CE
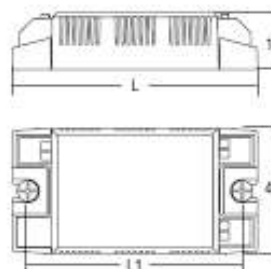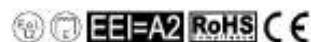
Articolo Article	Codice Code	W	Lampade Lamp	Attacco Cap	Lunghezza Length L	Fissaggio Fixing L1	λ	ta °C	tc °C	Peso Weight gr.	Confezioni Box
BCC 113	137945H13	1x6-8-11-13	T2	W4,3	80	70	0,60 C	-15 +55	75	40	66
BCC 116 +	137945HTC	1x4-6-8-13 1x10 1x5-7-9-11 1x10 1x10-16	T5 T8 TC-S/E TC-D/E TC-DD	G5 G13 2G7 G24q-1 Gr10q	80	70	0,60 C	-15 +55	75	40	66
BCC 117	137940H17TC	1x14-17	PLR	GR14q-1	80	70	0,60 C	-15 +55	80	40	66
BCC 121 +	137948HTC	1x14-21 1x13-18 1x13-18	T5 TC-D/E TC-T/E	G5 G24q-1/2 GX24q-1/2	80	70	0,60 C	-15 +55	80	40	66
BCC 122	137940H22TC	1x22 1x21-28	T-R5 TC-DD	2GX13 Gr10q	80	70	0,60 C	-15 +55	85	40	66
BCC 124 +	137947HTC	1x24 1x14-15-18 1x18-24 1x18-24 1x22	T5 T8 TC-L TC-F T-R5	G5 G13 2G11 2G10 2GX13	80	70	0,60 C	-15 +55	85	40	66
BCC 126 +	137949HTC	1x24 1x24 1x24 1x26 1x26 1x22	T5 TC-L TC-F TC-D/E TC-T/E T-R5	G5 2G11 2G10 G24q-3 GX24q-3 2GX13	80	70	0,60 C	-15 +55	85	40	66

Schema di collegamento a pagina 54 n° 1 - Wiring diagram page 54 n°1

Norme di riferimento
Reference Norms:
EN 61000-3-2
EN 61547
EN 55015
EN 61347-2-3
EN 60598-2-22

Tensione Nominale
Rated Voltage
220 ÷ 240 V

Tensione di utilizzo
Operating range
198 ÷ 264 V

Tensione DC
DC Voltage
176 ÷ 264 V

Frequenza
Frequency
0...50/60 Hz

Potenza
Power
4 ÷ 28 W

- Alimentatore elettronico da incorporare dalle dimensioni compatte.
- Adatto al collegamento con apparecchi di emergenza in base alla EN 60598-2-22.
- Utilizzabile per apparecchi di illuminazione in classe di protezione I e II.
- Dimensioni compatibili con reattore meccanico.
- Morsetti ad innesto rapido.
- Morsetti di entrata e uscita su lati contrapposti.
- Fissaggio dell'alimentatore tramite asole per viti M4.
- Accensione con preriscaldo per aumentare la durata della lampada.
- Protezioni: in caso di disconnessione della lampada (riaccensione con preriscaldo) lampada guasta o a fine vita.
A richiesta disponibile versione senza contenitore (BCC ... OF).

- Compact size electronic ballast to be built-in.
- Suitable for connection to emergency equipment in compliance with EN 60598-2-22.
- It can be used for lighting equipment in protection class I and II.
- Sizes are compatible with mechanical ballast.
- Push-wire connections.
- Input and output terminal blocks on opposite sides.
- Ballast can be secured with slots for screws M4.
- Start with preheating to increase the life of the lamp.
- Protection: in case of disconnection of the lamp (re-start with pre-heating), lamp failure or end of life. Version without housing is available upon request (BCC ... OF).

0,5 - 1,5 □

8,5-9,5

Appendix 3.3

SYLVANIA
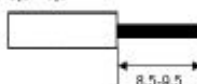
Lynx-SE

SA LYNX-SE 9W/840 2G7 SLV 10

0025902

Range features

- Single-band pin base compact lamp: Suitable for wide range of use
- Suitable for operation on electronic control gear
- Dimmable
- Extremely low profile
- Excellent colour rendering (CRI=85)
- Suitable for emergency lighting
- Dimmable with suitable ballast
- Available in Homelight (2700K), Warm White (3000K) and Cool White (4000K)
- Average rated life: 10900 hours

PRODUCT OVERVIEW

Ordering number	0025902
Technology	Compact Fluorescent
Light colour	840 Cool White
Energy class	A
Average life (Rated) (h)	10000
Lamp shape	Stick
Lamp finish	frosted
Dimmable	YES
Cap/Base	2G7
Type	Lynx SE
EAN code	5410288259024
CRI (Ra)	80
Colour temperature (K)	4000
Luminous flux (Rated) (lm)	600
Efficacy (Rated) (lm/w)	67
Watt (Nominal) (W)	9
Voltage (V)	60

TECHNICAL DRAWINGS
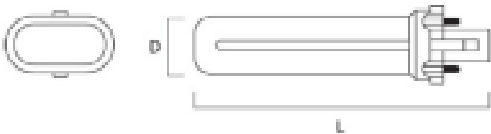
Appendix 3.4

SYLVANIA

Lynx-SE

SA LYNX-SE 5W/840 2G7 SLV 10

0025900

Range features

- Single-bend pin base compact lamp: Suitable for wide range of use
- Suitable for operation on electronic control gear
- Dimmable
- Extremely low profile
- Excellent colour rendering (CRI=85)
- Suitable for emergency lighting
- Dimmable with suitable ballast
- Available in Homelight (2700K), Warm White (3000K) and Cool White (4000K)
- Average rated life: 10000 hours

CE

PRODUCT OVERVIEW

Ordering number	0025900
Technology	Compact Fluorescent
Light colour	840 Cool White
Energy class	A
Average life (Rated) (h)	10000
Lamp shape	Stick
Lamp finish	frosted
Dimmable	YES
Cap/Base	2G7
Type	Lynx SE
EAN code	5410288259000
CRI (Ra)	80
Colour temperature (K)	4000
Luminous flux (Rated) (lm)	265
Efficacy (Rated) (lm/w)	46
Watt (Nominal) (W)	5
Voltage (V)	35

TECHNICAL DRAWINGS

154

Chapter 4

Plasma as radiating element

This chapter aims to discuss and explain the use of plasma as radiating elements. The state of the art of plasma antennas is discussed in the first part of this chapter. The second part is dealing with plasma antenna realization using commercially available U-shaped compact fluorescent lamp (CFL). Further discussions on the prototypes of plasma antennas are elaborated in the third part while the measurement setup is explained in the fourth part. The measurement results are discussed for the two fabricated antennas in terms of their radiation patterns especially on the comparisons between ON and OFF states of plasma in order to validate that the plasma is radiating. Finally, a conclusion is drawn based on the works done and the results of the fabricated plasma antennas.

4.1   Introduction

Plasma has been proven to work as radiator used to transmit radio signal just like metallic materials such as copper wire and copper rods. The plasma radiator is known as plasma antenna. In the earliest of its introduction in communication systems, most of the plasma antennas are meant to operate at lower frequency band typically in UHF and VHF bands. Differ from its metal or copper counterparts, the plasma requires an initial step which is plasma excitation for it to create electrical conductivity so that it can imitate the metallic materials. By having the conductivity, surface wave can propagate along plasma column so that it can be radiated. One of the most important advantages of plasma antenna over metallic antenna is that, plasma antenna can be turn off in microseconds [1], [2]. Thus the plasma antenna exhibits stealth [3] ability because it can be considered not exists in the eyes of radars. Other than that, plasma antenna can be reconfigured to meet varying requirements such as switchable operating frequency and this can be achieved by altering the plasma antenna electrical length accordingly.

4.1.1 State of the arts

Primarily, the working concepts of plasma antennas can be divided into two parts which are the excitation technique and the coupling technique. The technique of excitation is a mean to generate plasma or in other word is referred as a method to ionize gas in dielectric tubes. Several excitation techniques have been discussed previously in Chapter 2. The coupling technique refers to the method to join radio signal onto plasma column. If radio signal is used to excite plasma, there will be an important filtering device in the receiver part which is used to filter out the excitation signal and to allow the receiving signal. In the case of cylindrical plasma antenna, surface wave used to carry information signal propagates along plasma column so that it can be transmitted in the free space [4-7]. The concept of surface wave and its properties are discussed in [8]. It has been studied in many research papers that the plasma characteristics can be altered by changing the input parameters. For example pump power used to ionize the encapsulated gas in dielectric tubes can be varied. By increasing this pump power, plasma density can be increased [9-12] and at the same time improving the electrical conductivity [13]. Essentially, conductivity plays an important role in order for the plasma to behave as good element in radiating radio signals. Conversely for metallic materials, the electrical conductivity is always high (in terms of 10^7 Siemens per meter) and it is not an issue in designing antennas. The following are the example of several ways to increase plasma conductivity.

❖ Pump power - the increment of pump power will lead to higher rate of ionization thus increasing plasma density [1], [4].

❖ Gas pressure - the increment of gas pressure can also increase the ionization rate [10].

The efficiency of cylindrical plasma antenna with respect to pump power has been presented in [11]. The plasma antenna efficiency was compared to its twin copper antenna and the comparison result is shown in Figure 4.1. The efficiency shown in the Figure 4.1 tells that how good the plasma antenna works with respect to the traditional metallic antenna.
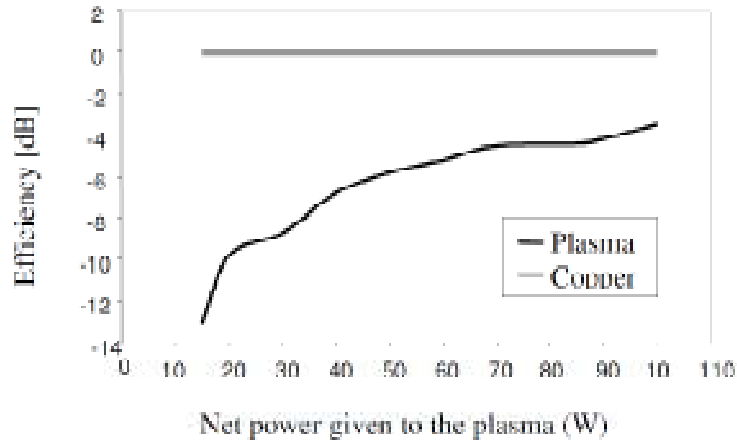
Figure 4.1 – Plasma efficiency as a function of the net pump power [11].

For the copper antenna there was no change in efficiency whenever the pump power in increased to 100 W. This is due to the high conductivity of copper thus it cannot be influenced by the applied power. Differ to copper antenna; plasma antenna is totally depending on the presence of conductivity which is controlled by the pump power. The higher pump power will increase ionization rate thus increasing the conductivity. Regardless what is the pump power applied to plasma column, decreasing patterns in conductivity were observed as the signal propagates along plasma column. These scenarios are illustrated in Figure 4.2.
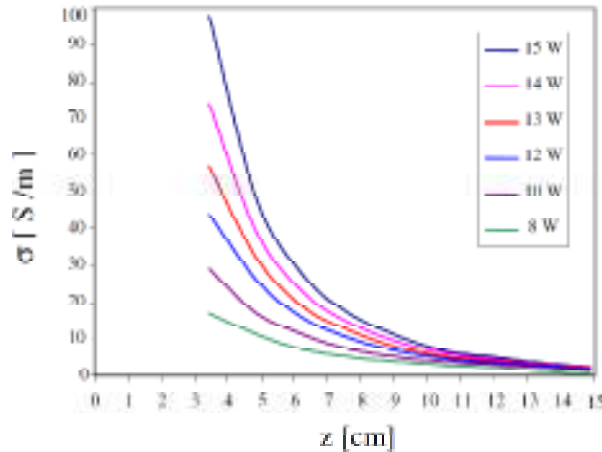
Figure 4.2 – Conductivity of plasma tube versus the axis coordinate, recovered from reflection measurements [11].

Generally, as stated in [14], when an intense field is applied to a point on dielectric tube, the electron density corresponding to the point starts to increase. At the point where it reaches n_D as shown in Figure 4.3, the electromagnetic wave in the form of surface wave starts to propagate along plasma column but its reduces along the way. Indirectly, this phenomenon somehow tells that the conductivity of the plasma column is decreasing in the same manner.
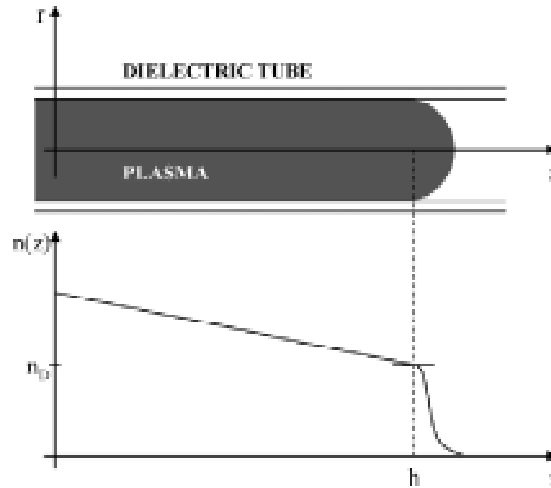
Figure 4.3 – Plasma density with regard its plasma column length [14].

One of a serious discussion on plasma column characteristic was presented in [15]. It was found that when plasma relative permittivity in the range of $0 < \varepsilon_r < 1$, the plasma columns tends to behave like a dielectric and reduces the effective electrical length of the antenna. In the range of $-1 < \varepsilon_r < 0$, where the plasma frequency is higher than the operating frequency, the plasma acts like a lossy conducting medium in the sense that it reflects waves which are incident upon it [15]. To support to these findings, the same agreement was reported in [16]. In [17-19], studies of the regime where plasma works as reflector and absorber have been conducted. It also have been proven that, magnetized plasma with high density is greatly reflects and absorbs microwave signals [17] and to that extend; the rate of collision frequency plays an important role to determine the absorbing characteristic of plasma [18]. Thus, magnetized plasma could be tailored to act either reflector or absorber of microwave signals. Plasma is in the absorbing region when the incoming wave is lesser than collision frequency ($\omega \ll v$) was stated by Stefan A. Maier in his book in [20].

In the following subsections, plasma antenna coupling techniques, type of plasma antenna based on its geometry shapes, and the noise associated with plasma antennas are reviewed.

4.1.1.1   Coupling techniques

In contrast to conventional metallic antennas, it is impossible to make a direct electrical contact with the plasma conductor because the plasma is encapsulated in a dielectric tube. For that reason, it is necessary to use capacitive or inductive coupling to launch surface waves as a way to radiate radio signals. The capacitive coupling is the most favorable coupling technique compared to inductive coupling because it is simple to implement and not causing extra complexity in designing antenna. Moreover, it was introduced and used in many published papers [1], [21-35].

In order for the signal to be transferred to plasma antenna, the capacitive coupling requires only a small portion of cylindrical plasma antenna to be covered by metallic (conductor) materials. The conductor material is well known as coupling sleeve and normally, a copper sheet is preferred to be used. In general the length of the coupling sleeve is approximately 20 mm - 30 mm and it is used for VHF antennas [1], [21], [28], [36]. The Figure 4.4 shows examples of capacitive coupling used in the literatures. A copper sleeve is placed around dielectric tube and connected to a SMA connector.
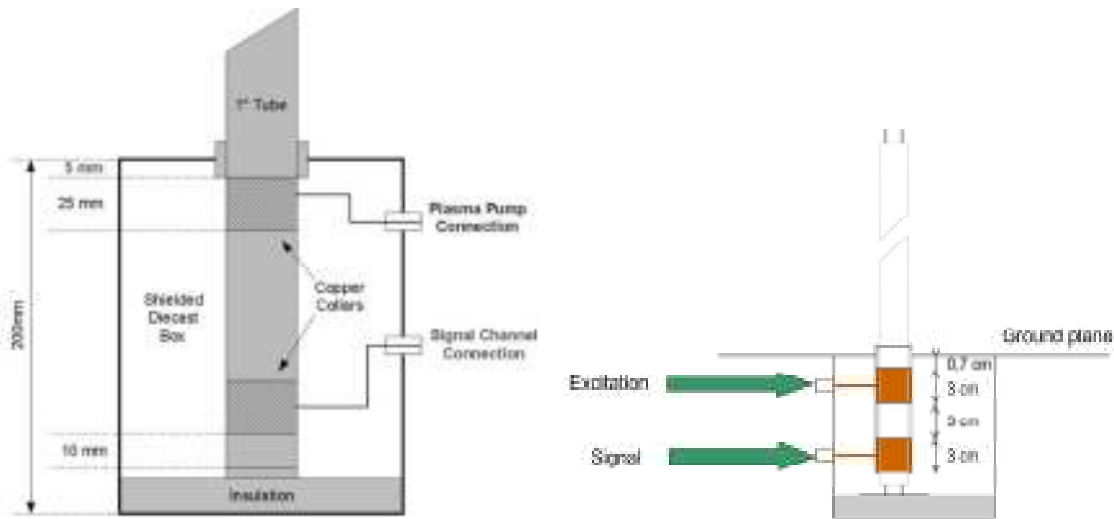
Figure 4.4 – Coupling sleeve in a excitation box. (a) In this case two 25 mm coupling sleeves were employed to excite plasma and to transmit information signal [1]. (b) Two 30 mm coupling sleeves were used to realized plasma antenna [21], [37].

There are two coupling sleeves shown in Figure 4.4, one is used to generate plasma and another one is used to send information signal in the form of surface wave. These two coupling sleeves are connected to two different ports. In this case, it is necessary to have a proper decoupling network since the presence of conductivity could couple the two ports. High conductivity means high coupling between them. A decoupling network was also proposed in [22] to avoid unnecessary coupling between excitation port and useful information signal port. Figure 4.5 shows the measured coupling magnitude between the two ports when the plasma is excited. A copper tube is used to simulate the presence of conductivity. A strong coupling can be seen between exciting port and signal port.

Figure 4.5 – Coupling between the two ports, with plasma (black and thick line) and without (grey and thin line) plasma [22], [36].

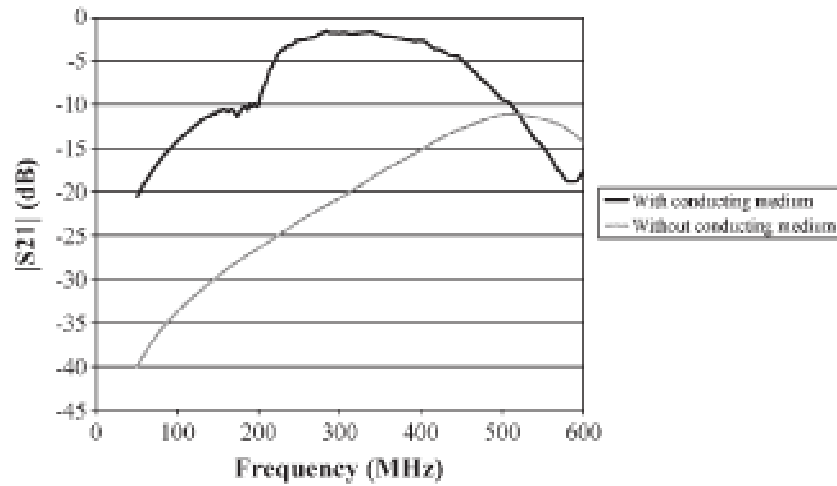In [28], a comparison of different coupling structures was presented with a purpose to find an effective way to transfer the information signal. The comparison was conducted for three coupling structures which are inductive, double inductive and capacitive. The coupling structures are shown in Figure 4.6.
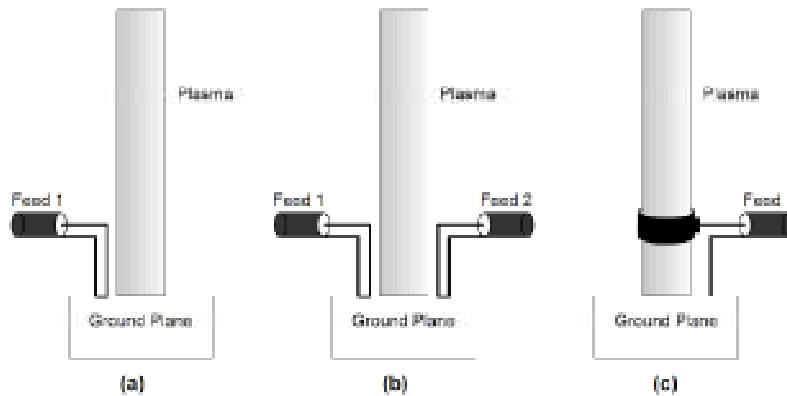
Figure 4.6 – Coupling structures [28]. (a) Inductive coupling; (b) Double inductive coupling. (c) Capacitive coupling.

A similar size of copper tube is used to substitute plasma column for the coupling comparison. The capacitive coupling has significant capacitance in the circuit due to existence of dielectric tube between the coupling sleeve and the plasma, whereas with the inductive coupling option, it is possible that the antenna may not feed effectively off the ground plane. Thus prior to this comparison, a matching network must be included to ensure the maximum available power is transferred to the plasma column. Therefore a block diagram of plasma antenna circuit and measurement system as illustrated in Figure 4.7 was proposed in [28]. A double stub tuner is used to match the network and a signal selection is done by a low pass filter.
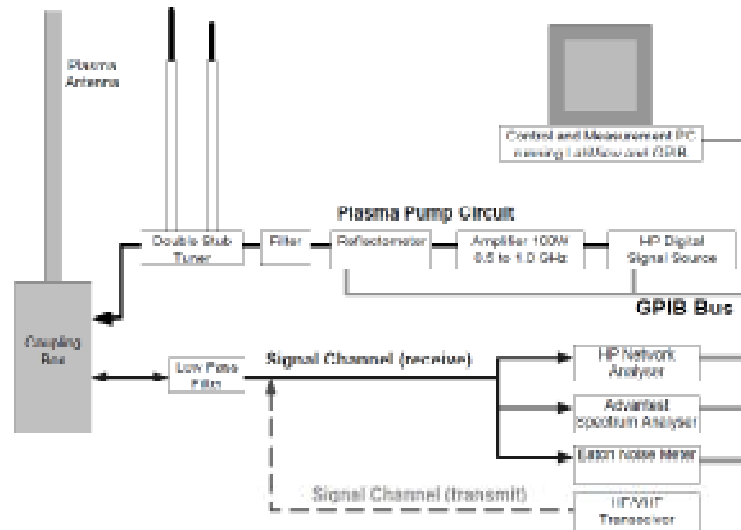
Figure 4.7 – Block diagram of the plasma antenna circuit and measurements systems [28].

The comparison results in term of transmission characteristic (S_{21}) are shown in Figure 4.8. The findings explained that the double inductive is the least effective in coupling RF power into the plasma antenna. The longer inductive and capacitive couplers were found to be more effective than the short ones and these two structures were equally effective. Separation gap between coupling sleeve and the ground plane had a little effect on the transmission characteristic.
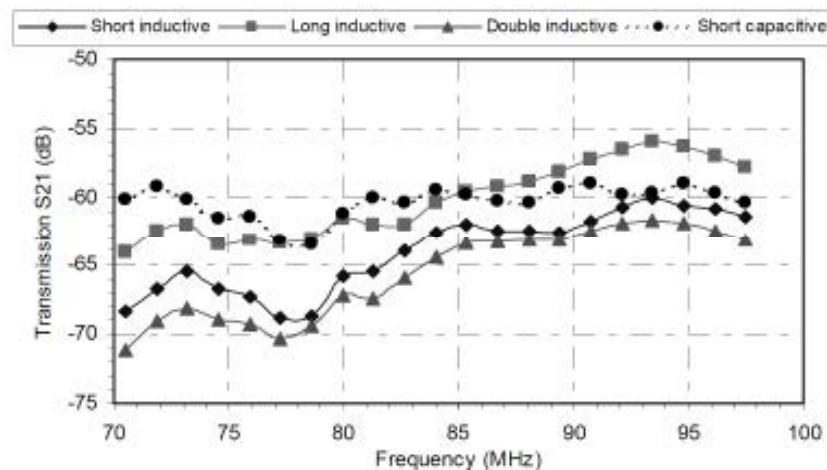
Figure 4.8 – Transmission characteristics (S_{21}) for two type of coupling structures with different configurations [28].

4.1.1.2   Type of plasma antenna based on physical dimension

This section is intended to elaborate several types of plasma antennas based on its physical shapes. These include the home made and the commercially available plasma

sources. The non straight plasma antennas such as helix and whip antennas are also explained in this section. Brief reviews on antenna radiation patterns and performance are also included.

4.1.1.2.1   Cylindrical plasma antennas

A rule of thumb, plasma antenna is uncomplicated to be analyzed if it is in the form of cylindrical shape. As a consequence numerous studies have attempted to explain the plasma characteristics based on this shape [10], [11], [14], [37]. Plasma column does not carry conduction current but a surface wave propagates along the column [6]. Therefore the performance of plasma antenna is totally dependent to the electrical characteristic of the plasma column. It is interesting to study the radiation pattern of plasma antenna as presented in several research papers [26], [28], [30-33], [38]. The limitation of physical experiment apparatus to evaluate plasma characteristics for different plasma structures leads to the usage of numerical simulation in plasma research activities. Therefore, another way to analyze cylindrical plasma antenna radiation pattern is by using FDTD [6], [39], [40].

In 2007 Max Chung et al., have presented in [41] radiation pattern of 60 cm plasma antenna measured at 4.2 GHz. The plasma frequency in the experiment was 8 GHz resulted from other microwave transmission experiment. The plasma antenna was constructed by using a glass tube with 12 mm outer diameter and 10 mm inner diameter and the glass tube is filled with neon (Ne) gas at 2~5 Torr . The geometry and schematic of the plasma antenna are shown in Figure 4.9 (a) and Figure 4.9 (b), respectively. The photograph of the fabricated antenna is shown in Figure 4.9 (c)

On both side of the tube, there are two hollow cathode type cylindrical electrodes used to excite plasma. Two wires for DC bias current are used to connect these electrodes to a high voltage power supply. The communication signal is coupled to the antenna using capacitive a coupling as shown in Figure 4.9 (a). The radiation patterns when the antenna is in vertical position and its corresponding antenna gain are shown in Figure 4.10. The plasma antenna gain is somehow lower than 0 dBi at 4.2 GHz and the increment of gain in upper frequencies could be due to the radiating coupling sleeve.

(a)   *(b)*   *(c)*
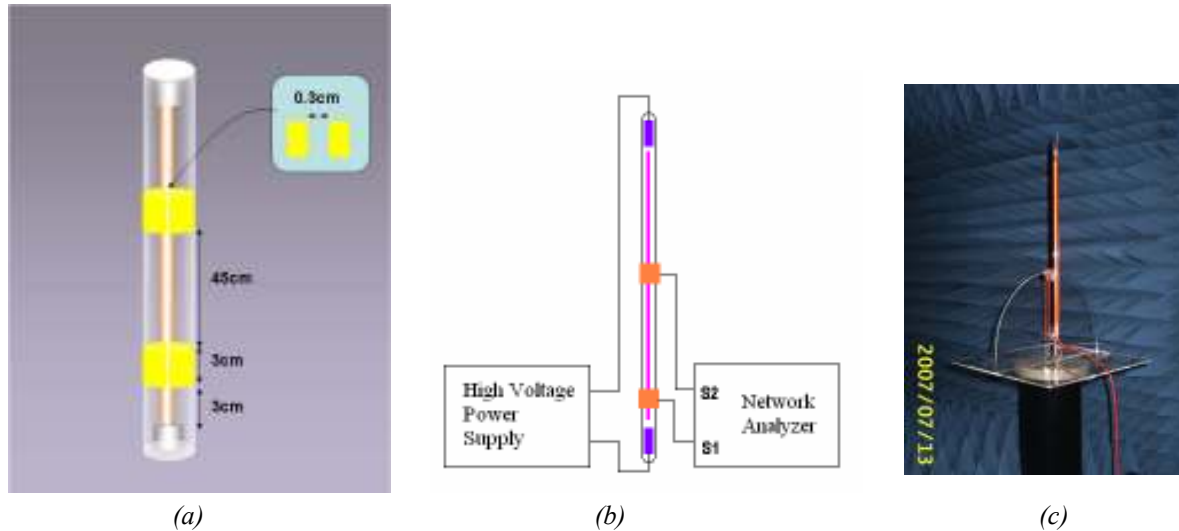
Figure 4.9 – Structure of DC pre-ionized plasma antenna. (a)-(b) Two copper foil are used for signal coupling measurement with two different coupling locations, at the bottom end and at the center of the tube. (c) Photograph of 60 cm plasma antenna [41].

(a)   *(b)*
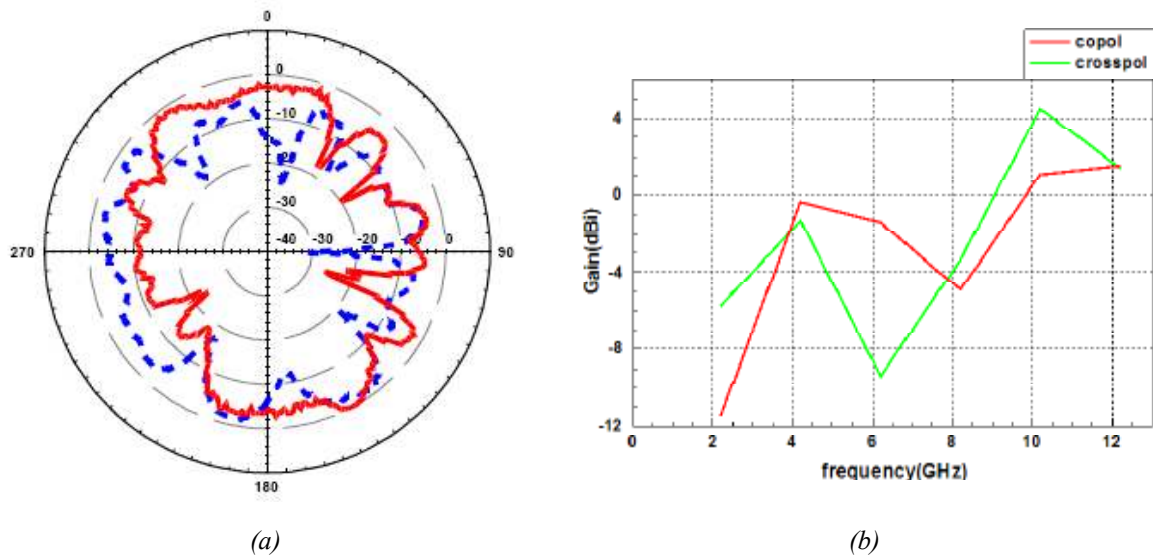
Figure 4.10 – Plasma antenna performances. (a) The E-plane radiation pattern of the 60 cm plasma antenna at 4.2 GHz. (Red curve is the co-polar and blue curve is the cross-polar). (b) Gain [41].

Max Chung et al. later enhance their finding on the effect of different type of low pressure gas in a dielectric tube to its radiation pattern performance. The finding has been reported in [42] with higher operation frequency which is 8.2 GHz and with two different gases which are neon (Ne) and gas combination of argon and mercury vapor (Ar + Hg). Furthermore in [43], with similar objective, plasma antennas were constructed using three noble gases which are neon, argon and xenon. The measured return losses for all antennas made by these gases were reported below -10 dB from 3.4 GHz to 5 GHz.

V. Kumar et al. in [27] have presented the result of radiation pattern of 20 cm plasma column as monopole antenna. The plasma column is made from the

commercially available fluorescent lamps with diameter of 1 cm. An AC discharges was implemented in the experiment with tunable frequencies from 25 Hz to 200 Hz. The experiment setup is shown in Figure 4.11.

(a)   (b)
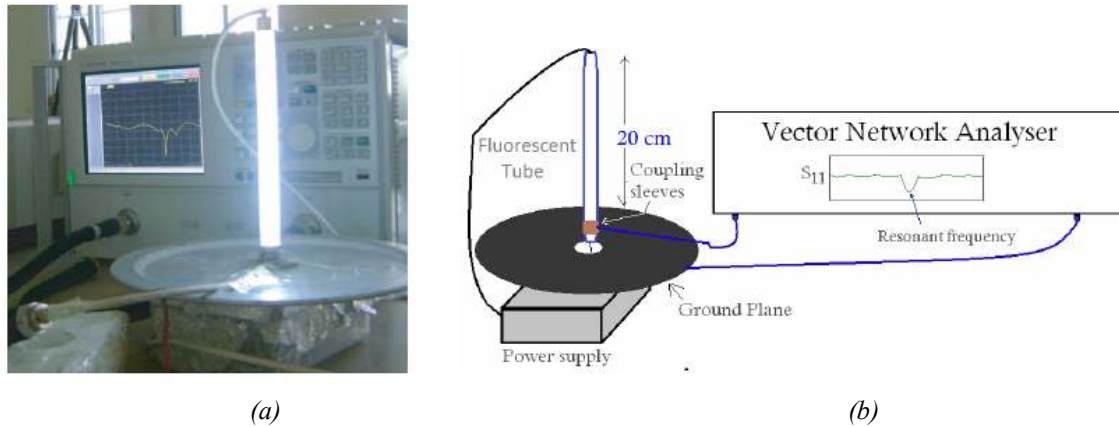
Figure 4.11 – Experimental setup of plasma antenna. (a) Photograph of 20 cm cylindrical plasma antenna. (b) Measurement setup for measuring return loss. [27].

The authors concluded that with higher AC frequency, the measured return loss was at -34 dB and this could lead to better efficiency. The measured co- and cross-polarizations radiation patterns of the plasma antenna in the H-plane are shown in Figure 4.12. It can be seen in Figure 4.12 the co- and cross- polarizations are approximately in the same level for the angle between 0° to 60°. This situation is due to scattering of fields from coaxial cable used to supply power to the upper electrode of the fluorescent tube.
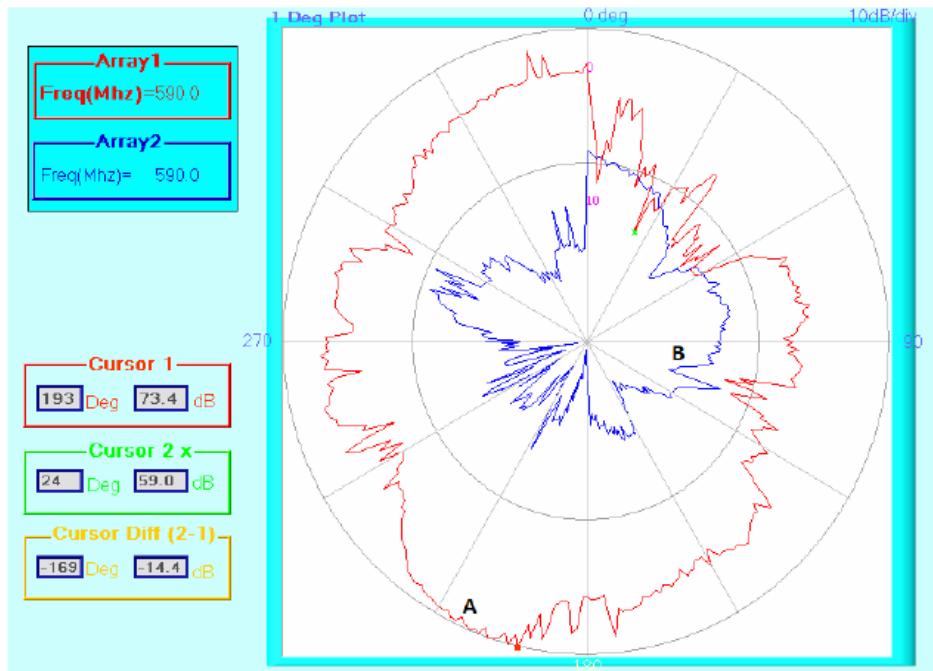
Figure 4.12 – A 20 cm monopole antenna radiation pattern at 590 MHz. Array 1(red line) is the co-polarization and Array 2(blue line) is the cross polarization [27].

In addition, the effect of collision frequency on antenna radiation pattern was studied and presented in [9]. In which the author concluded that, the good conductivity (higher plasma density) of plasma will produce radiation patterns that are closely similar to its metallic antenna counterpart.

4.1.1.2.2   Non-straight structure of plasma antennas

Investigation for plasma antenna radiation pattern for non-straight structures such as triangular monopole and annular plasma antenna have been presented in [44] and in [45], respectively. Both studies have been done for VHF frequency band. The triangular plasma antenna as shown in Figure 4.13 was simulated using HFSS to study the effect of operating frequency, collision frequency and bend angle of triangular shape on its radiation pattern. It has been reported that when the plasma frequency is amply higher than operating frequency and collision frequency is corresponding low, the plasma antenna can operate at similar characteristic with metal antenna.
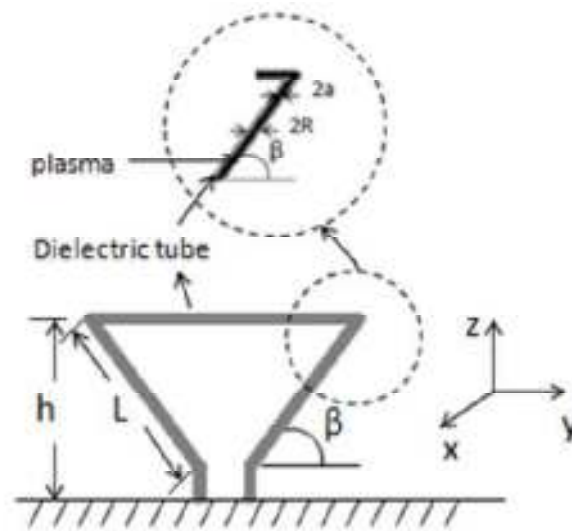
Figure 4.13 – Geometry of the triangular plasma monopole antenna on infinite metal plane [44].

An experiment to study gain and VSWR of plasma antenna using annular fluorescent lamp is presented in [45]. The measurements were conducted with two excitation setup in order to develop plasma inside the fluorescent lamp. The first one was using 220 AC source and for the second one, RF was deployed. The AC and RF source are fed through the electrodes. A 1:4 transmission line transformer is used as balun to connect the RF power generator with a power scale of 40 W to the antenna. The setup is illustrated in Figure 4.14.

165
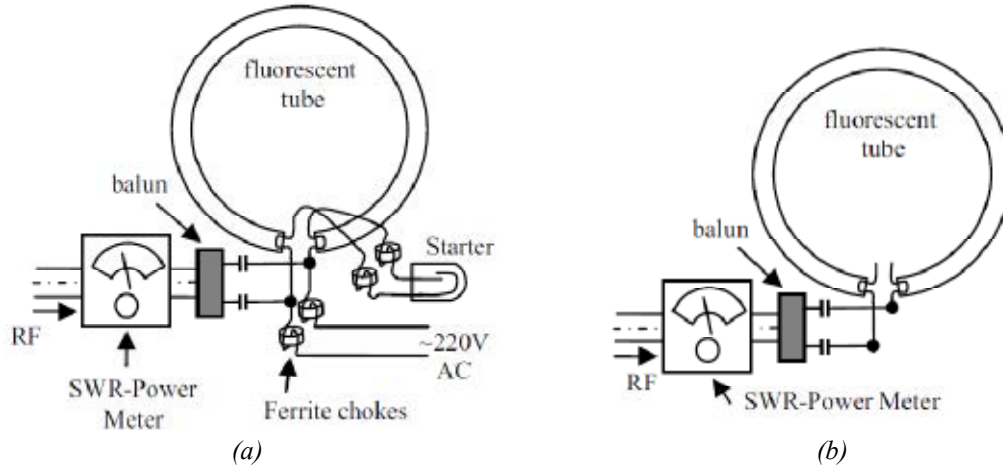
Figure 4.14 – The annular plasma antenna excitation setup. (a) The 220V AC driven plasma antenna. (b) The RF driven plasma antenna [45].

In the measurement, three different resonant frequencies have been observed when comparing to a metal antenna with similar dimension as a reference and by changing excitation method from AC driven to RF driven, see Figure 4.15 (a). The reference antenna resonates at 320 MHz while the RF driven plasma antenna resonates at 290 MHz, 30 MHz lower than the reference. The AC driven antenna was at much lower frequency due to unavoidable leads wires.
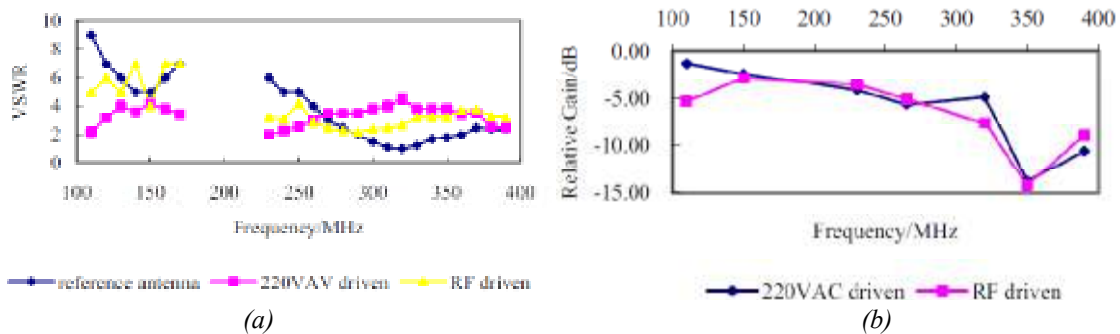
Figure 4.15 – (a) VSWR curves for different antennas. (b) Plasma relative gain to that of the reference antenna [45].

The gain of the two plasma antennas are roughly in the same level and this can be seen in the gain patterns shown in Figure 4.15 (b). The gains of RF and AC driven plasma antennas were at 6.7 dB and 6 dB lower than that of the reference metallic antenna. Overall, the gain at lower frequency band is better than the gain at higher frequency band. The results reported in the paper were solely evaluated without taken into account the effect of balun loss, which the author claimed it was difficult to consider quantitatively.

166

By using numerical method FDTD, plasma whip antenna and plasma helix antenna performances have been reported in [46] and in [47], respectively. The whip antenna structure is shown in Figure 4.16. The plasma whip antenna is made of a glass tube with a relative permittivity of 3.4 and a wall thickness, *t* of 2 mm. The dimension of plasma rectangular cylinder is *d* x *d* x *l* which *d* is equal to 10 mm while the *l* is varying parameter.
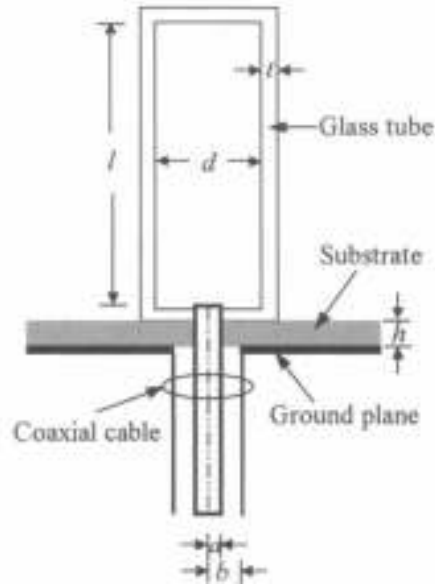
Figure 4.16 – A model of a plasma whip antenna located on dielectric substrate with relative permittivity of 2.35 and the thickness, h is 2 mm [46].

The plasma whip antenna is excited by a coaxial probe with radius of *a* equals 0.5 mm and the *b* is about twice of *a*. The antenna is simulated for different plasma frequencies, collision frequencies and plasma lengths. The results are shown in 4.17 are compared to its identical metal antenna. Based on the results, the resonant frequency is shifted up when the *l* varies from 160 mm to 140 mm. The resonant frequency of the plasma whip antenna also changes when the plasma frequency is increasing from 20 GHz to 40 GHz. This behavior indicates that the operating frequency of plasma can be achieved by controlling plasma density. For the case of varying collision frequency, it was observed that the amplitude of return loss reduces with the increment of collision frequency. This is due to the fact that the conductivity of plasma is also contributed by collision frequency.

(a)

(b)

(c)
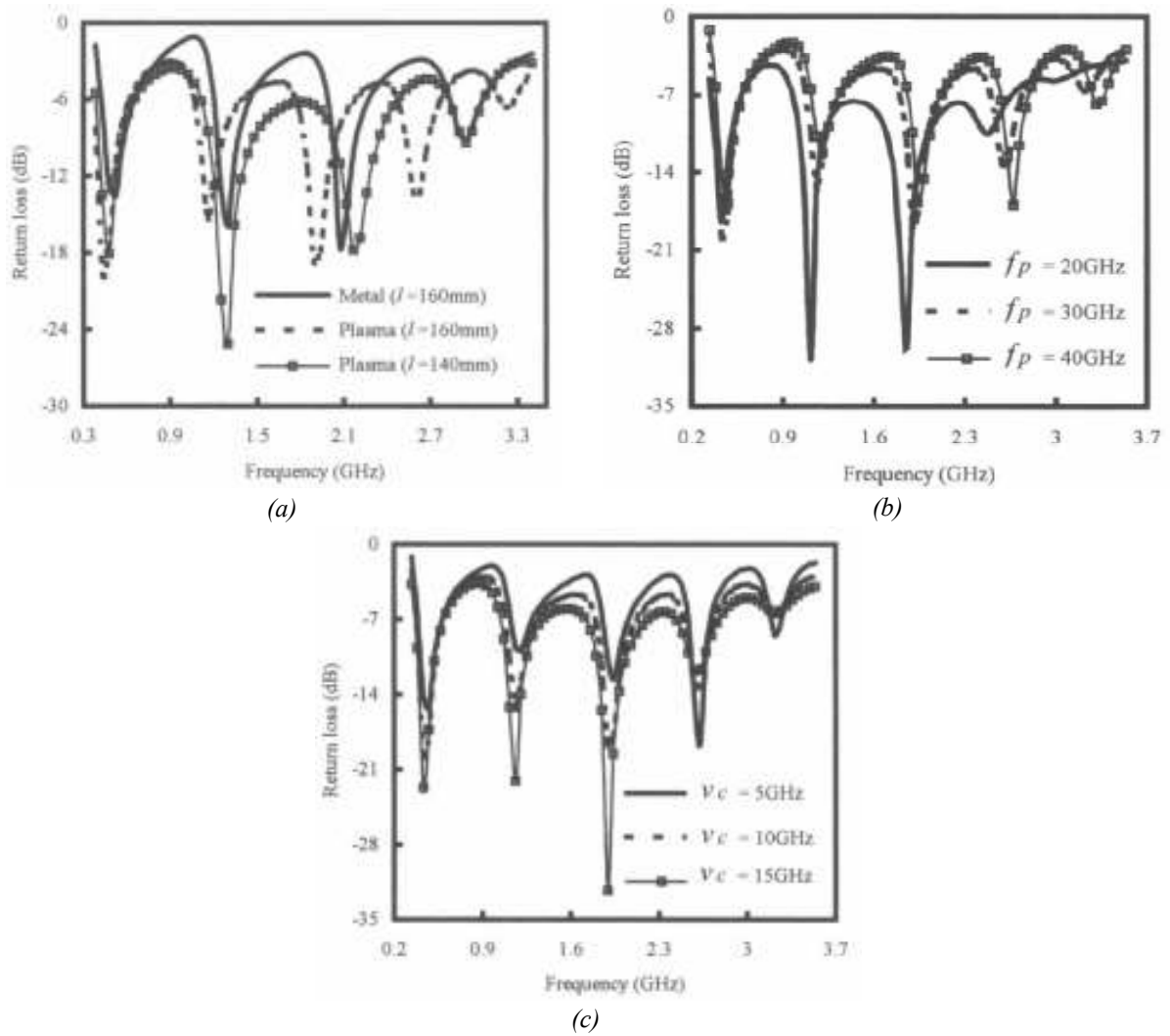
Figure 4.17 – Return loss of plasma whip antenna versus operating frequency for different parameters; (a) length, (b) plasma frequency, (c) collision frequency [46].

In [47], the helix antenna was simulated to study the relation between its radiation pattern and plasma characteristics at 1 GHz for different values of plasma (from 3 GHz up to 300 GHz) and collision (from 5 MHz up to 500 GHz) frequencies. The model of helix antenna is shown in Figure 4.18. The plasma is excited at the joint between the plasma tube and the coaxial line, and the plasma density is assumed uniform along the tube. The helix is chosen to be 19.08 cm in length (L), with 4 turns (N), 9.54 cm in diameter (D) and 5 cm uniform radius for the wire tube. The ground plane diameter is set to 12.5 cm (R). It has been concluded that the plasma will behave like a metal when the plasma frequency is 10 times larger than operating frequency. The radiation patterns of the helix antenna for different operating frequencies are shown in Figure 4.19 whereas for different collision frequencies are depicted in Figure 4.20.

168
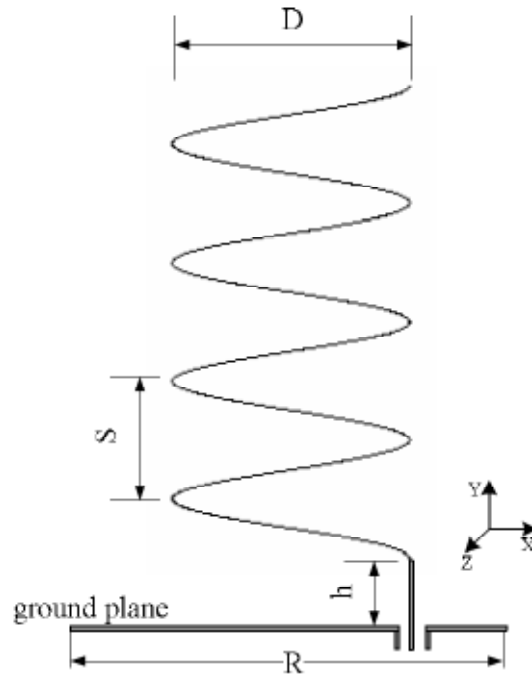
Figure 4.18 – The ideal model of plasma helix antenna. (R =12.5 cm, D = 9.54 cm, h is the length of the coaxial line while S is the length between two turns) [47].

Based on Figure 4.19, the radiation patterns of plasma helix antenna is closer to the radiation pattern of metallic helix antenna when the plasma frequency is larger than the operating frequency.
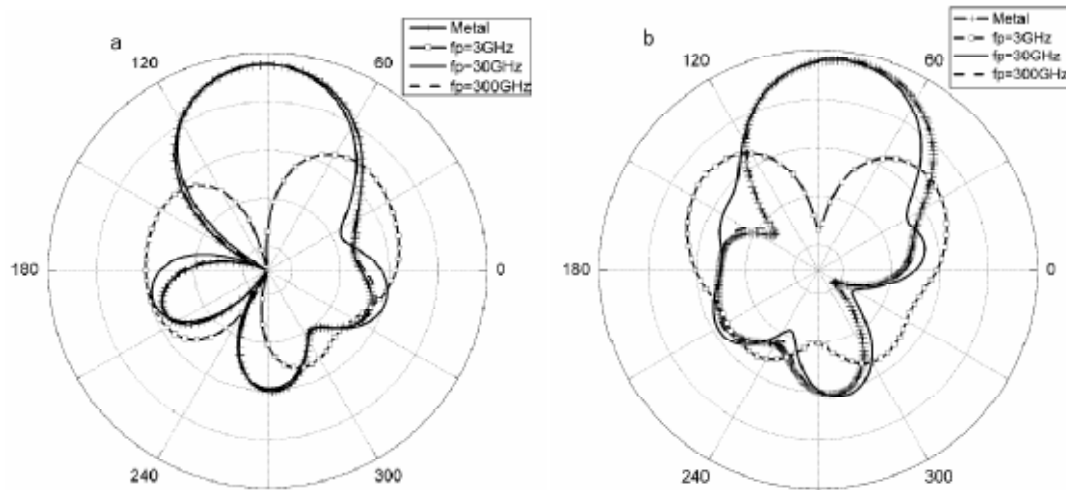
Figure 4.19 – The radiation patterns of plasma helix antenna in horizontal and vertical planes at 1 GHz. The plasma frequency is varied from 3 GHz up to 300 GHz and the collision frequency is fixed at 5 MHz. (a) Horizontal plane. (b) Vertical plane [47].

For the effect of varying plasma collision frequency from 5 MHz to 500 GHz, the radiation pattern of plasma helix antenna is getting closer to its metallic counterpart when the collision frequency is decreasing from high to low value. This behavior can be observed in Figure 4.20.
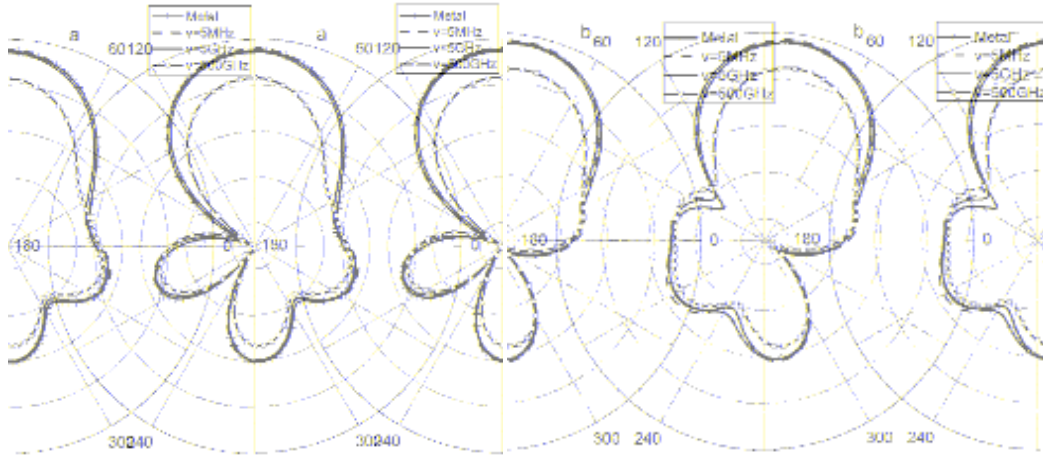
Figure 4.20 – The radiation patterns of plasma helix antenna in horizontal and vertical planes at 1 GHz when the collision frequency is varied from 5 MHz to 500 GHz. The plasma frequency is fixed at 300 GHz. (a) Horizontal plane. (b) Vertical plane [47].

However, the selection of plasma frequency and plasma collision frequency studied in this paper are very high and not realistic. Yet, somehow the paper able to show the variation effect of these two parameters on the antenna's radiation pattern.

4.1.1.3   The associated noise of plasma antennas

Plasmas are well-known sources of noise through to microwave frequencies particularly for DC or main driven AC fluorescent tube. The possible noise sources for a low-pressure gas plasma tube excited by DC or low frequency AC current can be listed as follows [1];

❖ Thermal (Johnson) noise due to random motion of electrons characterized by electron temperature of noise power spectral density, $S_{th} = 4kT_e$ W/Hz

❖ Short Noise due to DC current of spectral density, $S_i = 2eI_{DC}$ A^2/W

❖ Cathode processes including thermionic and secondary emission

❖ Noise in vicinity of the ion plasma frequency

However, many of these noise sources do not occur when the surface wave of plasma tube is used. Only thermal noise and the noise associated with plasma frequency are identified as the main contributors.

In [25] and [26], the investigation of noise associated with plasma antenna was conducted. The experiment aimed to compare the noise level between two excitation techniques which are AC driven plasma antenna and surface wave driven plasma antenna. A metal antenna to transmit and receive signal between 3 - 30 MHz has been used for baseline comparison. The sketch of experiment setup is shown in Figure 4.21.
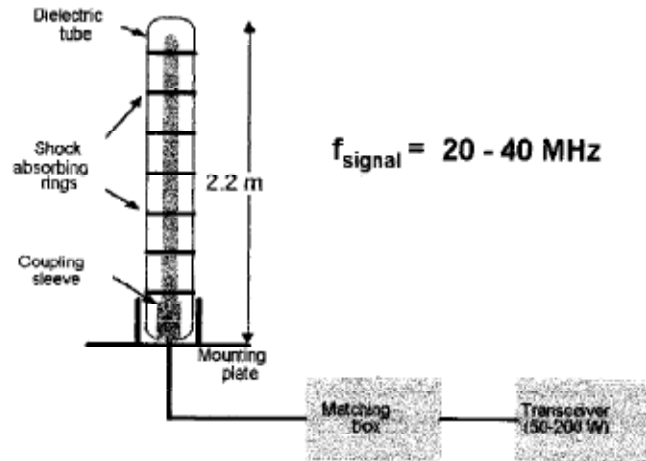
Figure 4.21 – Schematic diagram of surface wave driven plasma antenna [26].

The experiment has been performed to demonstrate that surface wave can form plasma over the frequency range of 3 MHz - 2.5 GHz. The argon gas has been employed at 1 Torr in the experiment. The collision rate, v is 5 x 10^8 s^{-1} and the plasma density is 5 x 10^{17} m^{-3} thus the plasma frequency is almost 6.4 GHz. It has been observed that at 30 MHz, the plasma behaves as a metal with conductivity is equal to 28 S/m ($\sigma = \varepsilon_0 \omega_p{}^2/v$). The following are the three antennas used to receive signals in the frequency range of 0 - 30 MHz.

a) A plasma antenna of length 1.2 m driven by 240 V 50Hz AC applied between electrodes at the ends of the tube. A 60 mm long plasma coupler was employed to detect signals in the HF band for both plasma antennas.

b) A plasma antenna of length 2.2 m, driven by surface wave excitation at 140 MHz. This signal was suitably filtered so as not to appear at the HF port.

c) A metal antenna for baseline comparison.

The measurement results in the form of noise spectra received by the antennas are shown in Figure 4.22. The noise floor of 50 Hz AC driven plasma antenna has noise

levels that are 10 - 30 dB higher across the band. Surface wave driven plasma antenna has shown similar noise spectra with metal antenna.
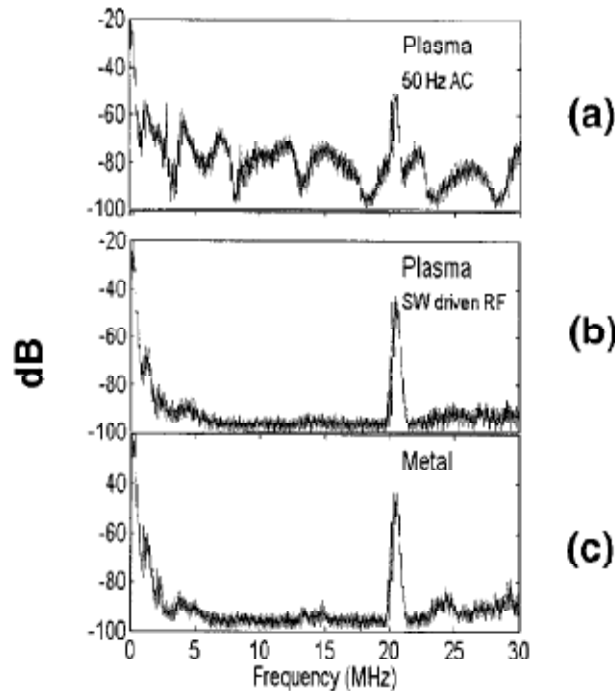
Figure 4.22 – Noise spectra of three antennas. (a) The 50 Hz AC current driven fluorescent tube. (b) A surface wave driven plasma antenna. (c) A metal antenna. [25].

However this noise measurement was not an absolute noise measurement because there was a considerable background noise in the laboratory. Besides, the author highlighted that the experimental technique is severely limited by the noise floor of the spectrum analyzer.

4.1.1.4   Summary

Several published papers were focused on experimental approach where plasma antennas characteristics were examined experimentally. Generally, a cylindrical plasma antenna is the easier plasma source to be used. But, very few papers reported on other shapes of plasma antenna. Since plasma antenna performances are totally dependent on the plasma antenna parameters, the conducted experiments only valid for the particular shapes of antenna. Therefore it is very important to self-experimenting various shapes of plasma antennas in order to understand and to conclude its behavior.

The limitation of physical experiment apparatus to evaluate plasma characteristics for different plasma structures leads to the usage of numerical simulation in plasma research activities. Most of existing plasma structures is not experimental friendly since

its serve different purposes. Therefore this numerical simulation serves as a tool to evaluate the potentials of plasma antennas at low cost and to provide flexibility of choosing verities of geometrical properties. Many papers have reported numerical simulation for a few plasma structures to study their characteristics such as radiation pattern and gain. In fact the definitions and assumptions made are different between one research papers to another. The researches mainly done based on different benchmarks such magnetic field intensity, collision frequency, type of low pressure gas and tube size. This approach basically is based on direct integration (DI) and recursive convolution (RC) methods which have been integrated to be Finite-difference Time-domain (FDTD).

The noise associates with plasma antenna basically are coming from the excitation technique used and very minor on the plasma itself. It was studied that, surface wave driven plasma antenna exhibit good noise performance with respect to its metallic counterpart. However, to come with this approach extra circuits such as filtering and decoupling are essential. As a result, it increases the complexity of the whole antenna circuit. Differ to this approach, even though AC driven plasma antenna is a little bit noisy if compared to surface wave driven plasma antenna, yet the noise level is below than -40 dB as presented in [25]. Moreover, the AC driven plasma antenna is simpler in design and very practical since the whole circuit does not need filtering or decoupling circuits to separate two different signals (excitation and information signals). Thus, with the used of AC supply may help researcher to rapid design and experimenting plasma antennas.

4.2 The realization of plasma antenna using U-shaped compact fluorescent lamp

The measured plasma antennas in this chapter are different to the ones discussed and presented in literatures. The plasma antenna introduced in this chapter was constructed using U-shaped CFL and it was excited using AC supply. The antenna specification is explained in this section.

The plasma antenna is made of a commercially available U-shaped CFL that works as radiating element in this study. In contrast to the coupling sleeves proposed in the literatures, the coupling sleeve in this study is placed underneath ground plane and it is not enclosed by metallic or absorber box. By placing it below the ground plane, the radiation of coupling sleeve in the upper part of ground plane would be reduced if the plasma is in de-activated mode. Small radiation in the upper part of ground plane is expected because of the existence of hole which is used to insert the CFL may allow signal to pass through.

There are two cases were investigated for the plasma as radiating element using a similar type and dimensions of plasma source (CFL). The dimensions of two fabricated plasma antennas are illustrated in Figure 4.23 and Figure 4.24, respectively. The similar type of plasma source as in Appendix 3.3 was employed as radiating element. The difference between these antennas is on its height (measured from the ground plane surface) and the existence of extra part of plasma source just under coupling sleeve.

The Figure 4.23 shows the dimensions of plasma antenna with the antenna height equals 35.7 mm whereas the Figure 4.24 shows the plasma antenna dimension when the antenna height is increased to 77 mm. The coupling sleeves are remained at the same position with respect to the bottom of ground plane for these two antennas. Consequently, with the height of 35.7 mm there is about 41.3 mm extra part of plasma source which is exposed just below the coupling sleeve. The antennas dimensions are summarized in Table 4.1.

Figure 4.23 – Plasma antenna. (a) An overview of plasma antenna. (b) The side view of plasma antenna revealing the coupling part and the extra part of plasma source just below the copper sleeve. (c) The bottom view of plasma antenna showing the dielectric support. (Unit in mm).

For the purpose of fabrication, the copper connector length is set to 17.5 mm with an intention of providing a space to solder the copper connector with the copper sleeve. In

order to hold the plasma source (CFL) in the fix position, a dielectric cube was attached to the bottom part of the ground plane so that a CFL cradle support (to clip and hold the lamp) can be fixed onto it. The dielectric support is made of cestilene HD 500 with a relative permittivity is equal to 2.4.
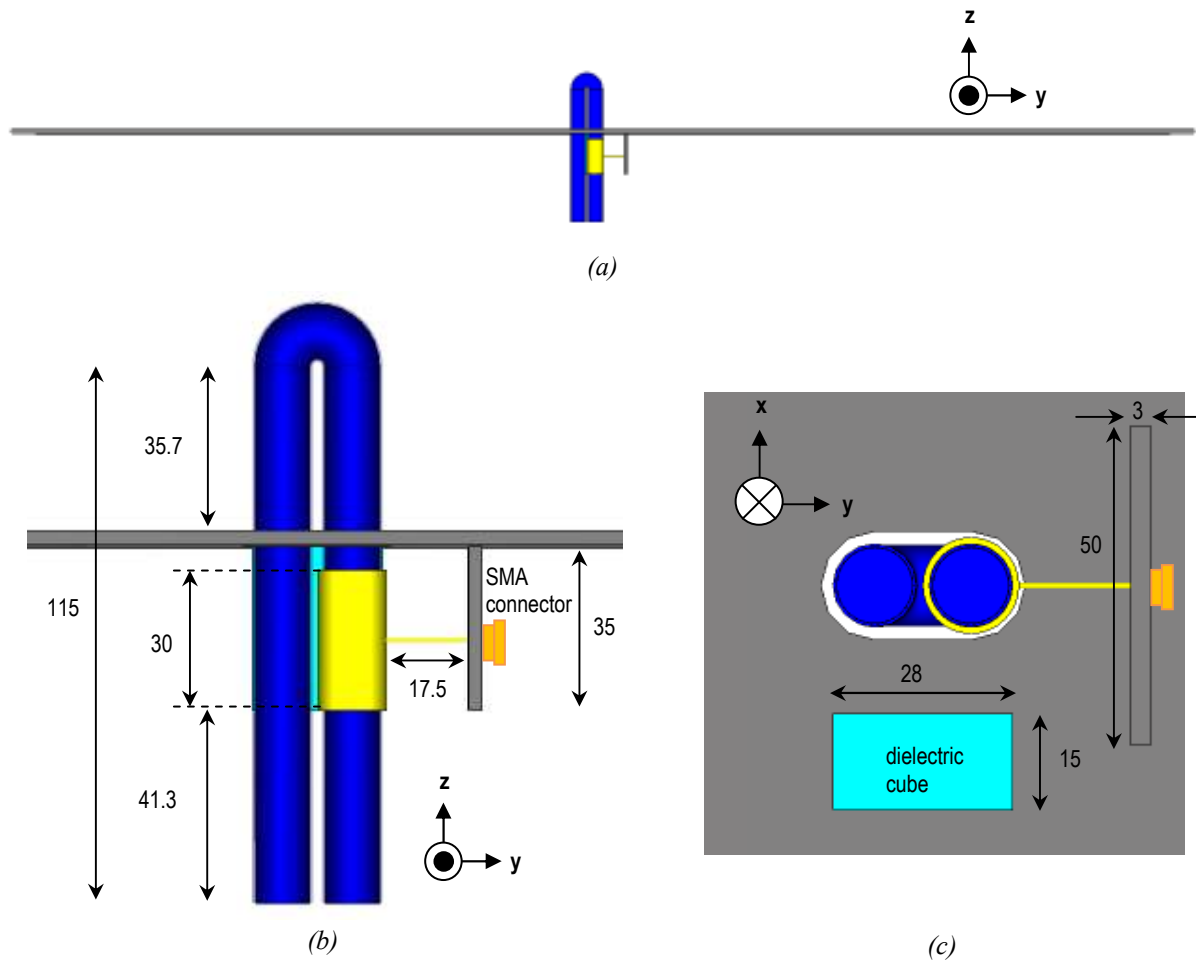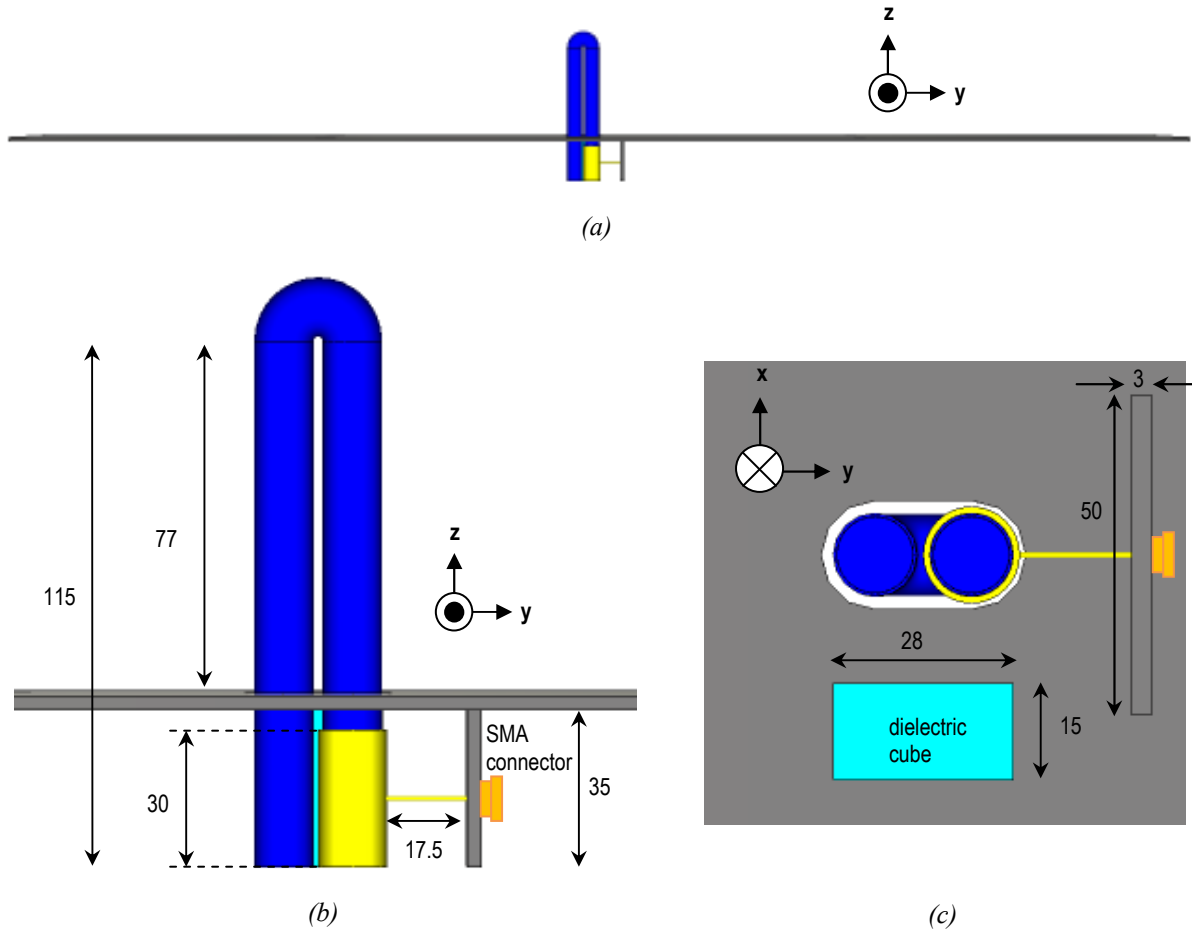

Figure 4.24 – Plasma antenna. (a) An overview of plasma antenna. (b) The side view of plasma antenna revealing the coupling part. (c) The bottom view of plasma antenna showing the dielectric support. (Unit in mm).

Table 4.1- The dimensions of fabricated plasma antennas.

Ground plane thickness, gnd_t	3 mm	
Ground plane size	1000 mm x 1000 mm	
Metal support thickness, l_{ms}	3 mm	
Space gap between coupling sleeve and the bottom of ground plane, g	5 mm	
Antenna height, $h_{radiate}$	35.7 mm	77 mm
Antenna height under coupling sleeve, h_{base}	41.3 mm	0 mm
Coupling sleeve height, h_{sleeve}	30 mm	
Copper connector, l_c	17.5 mm	
Metal support height, h_{ms}	35 mm	
Metal support width, w_{ms}	50 mm	

4.3   Prototype of plasma antenna

The prototype model of plasma antennas were fabricated on 3 mm thick ground plane based on the geometry given in Table 4.1. Excitation power to energize the 9 Watts CFLs is supplied by an electronic ballast that is controlled by a small single-pole switch. There is a set of four wires to be connected to the CFL and these wires are connected to the CFL pins using connector boxes. The photograph of the electronic ballast and the connector boxes are shown in Figure 4.25.

(a)   *(b)*
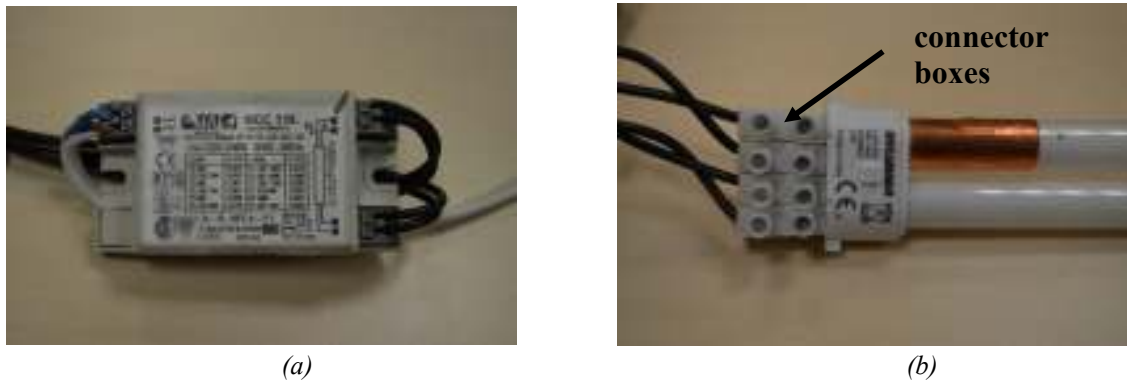
Figure 4.25 – Electrical apparatus to energize the plasma source (CFL). (a) An electronic ballast with specification of 220-240 V, 50-60 Hz.   (b) A set of four connector boxes used to link the CFL pins and the wires.

For the coupling sleeve, a copper scotch of 30 mm x 41 mm was used. This copper scotch is meant to enclose the lower part of dielectric tube so that it can be used to transfer information signal onto plasma once the plasma is formed. The copper sleeve is shown in Figure 4.26.
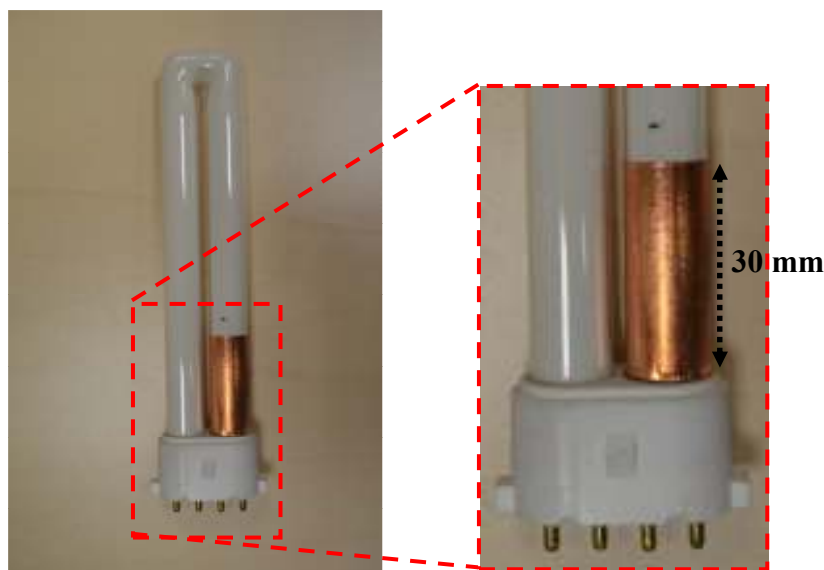
Figure 4.26 – Coupling sleeve made of copper scotch with a dimension of 30 mm x 41 mm.

A copper rod with a length of 17.5 mm and a diameter of 1.25 mm is used to link the SMA connector and copper sleeve. The connection between copper sleeve and copper rod is strengthened by soldering at the point of connection as shown in Figure 4.27. The electrical connection between them was tested using standard electronic multimeter.

(a)

(b)
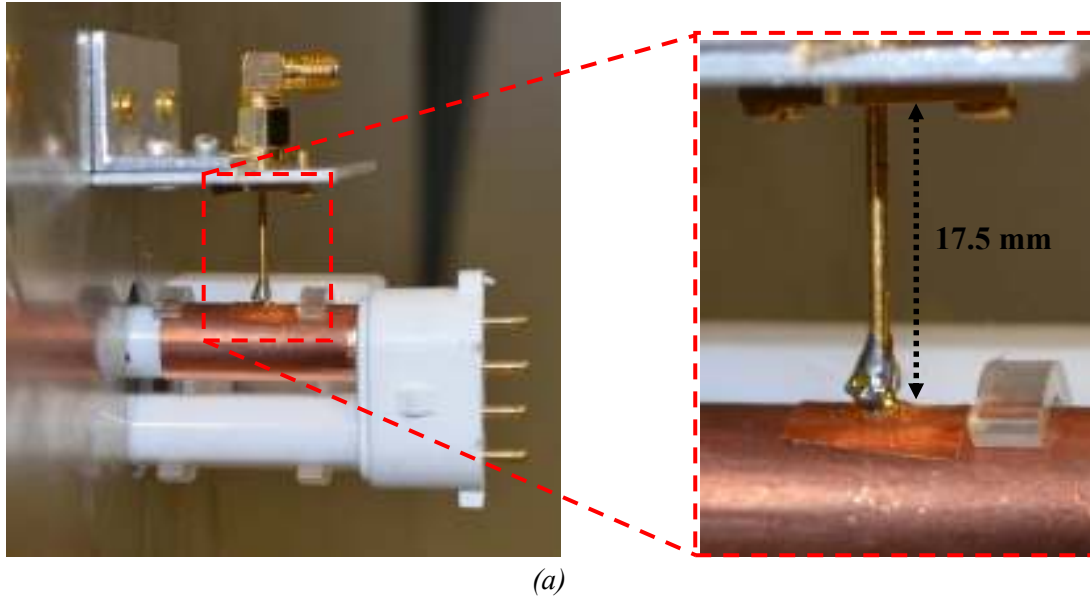
Figure 4.27 – Photographs of lower parts of the fabricated plasma antennas. (a) Plasma antenna with $h_{radiate}$ =77 mm. The inset shows a copper rod (17.5 mm) used to connect the SMA jack and copper sleeve. (b) Plasma antenna with $h_{radiate}$ =35.7 mm.

It easy to see from the photographs in Figure 4.27 that the environments of the bottom part of plasma source (CFL) are not the same for the two fabricated plasma antennas.

The dielectric cube made of cestilene HD 500 used to place the cradle support so that it can hold the CFL in fixed position is shown in Figure 4.28. The specification of the cestilene HD 500 and the cradle support are listed in Appendix 4.1 and Appendix 4.2.
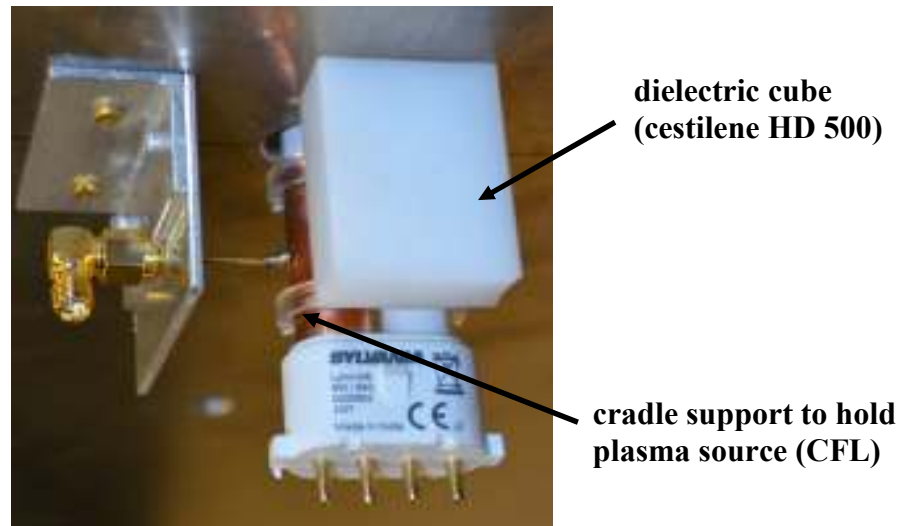
Figure 4.28 – Photograph of the dielectric cube used to place cradle support.

The coupling part of plasma antenna underneath its ground plane was leaving uncover. Therefore radiation patterns caused by the coupling part can be observed for the two antennas. Furthermore, the back radiation for two different cases of plasma antenna heights can also be compared.

4.4 Measurement setup of plasma antenna

The antenna input impedance measurements were conducted using similar setup as those explained in Chapter 3. These measurements were conducted in a small anechoic chamber. For the radiation pattern measurements, a SATIMO 32 anechoic chamber was employed. Photographs of plasma antenna in the SATIMO 32 anechoic chamber are depicted in Figure 4.29. The antenna under test (AUT) is placed on a support fixture as can be seen in Figure 4.29 (a). Figure 4.29 (b) shows the plasma antennas is in operating mode while the Figure 4.29 (c) and Figure 4.29 (d) show photographs underneath ground plane.

The radiation pattern measurements were carried out for wide range of frequency which is from 400 MHz up to 2 GHz, for the two plasma antennas because it was difficult to anticipate the good working frequency of these antennas. Since these two antennas shared the same ground plane, the measurements were conducted one by one. Once the first antenna was measured, it was detached from the ground so that the second antenna (CFL) can be inserted from the bottom of the ground plane. The same procedures (connection between copper sleeve and copper connector is strengthened by soldering) were repeated to ensure there is an electrical connectivity between copper connector and coupling sleeve.

(a)

(b)

(c)

(d)
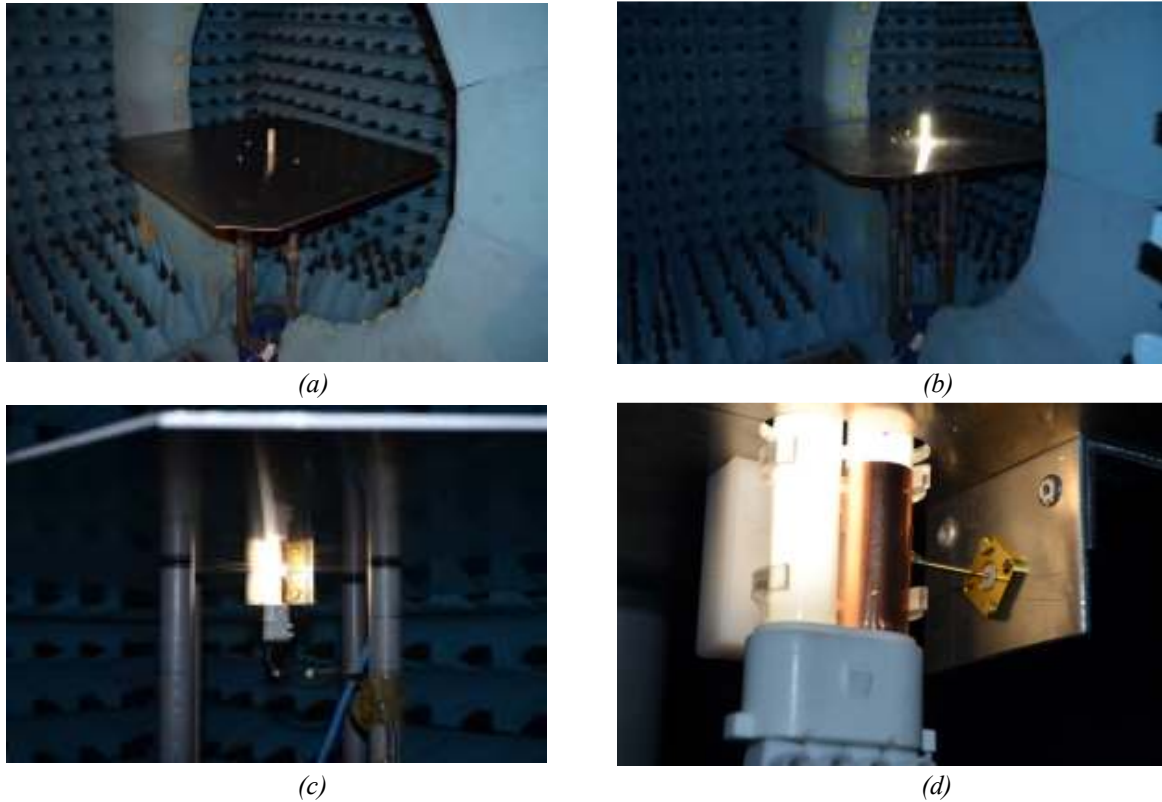
Figure 4.29 – Photograph of plasma antenna in the SATIMO 32 anechoic chamber ($h_{radiate}$ = 77 mm). (a) The plasma antenna in de-activated mode. (b) Plasma antenna in activated mode. (c) - (d) The lower part of plasma during activated mode.

4.5   Measurement results of plasma antenna

This section is discussing about radiation pattern of the two fabricated plasma antennas ($h_{radiate}$ = 35.7 mm and $h_{radiate}$ = 77 mm). The radiation patterns are presented only for two frequencies which are 900 MHz and 450 MHz in this section for easier reading. The radiation patterns for other frequencies, reflection coefficients and antenna gains are included in Appendix 4.3 and Appendix 4.4

4.5.1 Radiation pattern of plasma antenna with $h_{radiate}$ equals 35.7 mm

The measured radiation patterns of plasma antenna with antenna's height of 35.7 mm at 900 MHz are shown in Figure 4.30. The patterns are compared for the OFF and ON cases.

Figure 4.30 – Normalized measured radiation patterns, E_θ and E_ϕ components at 900 MHz. (a)-(b) Co-polarization in the H- and E-planes respectively. (c)-(d) Cross-polarization in the H- and E- planes respectively.

From Figure 4.30 (a) and Figure 4.30 (b), when the plasma is activated, the antenna seems to radiate since there is a large difference between OFF and ON states which is about 15 dB (in the maximum direction). The small radiation seen in the H-plane when the plasma antenna is OFF state is due to the radiating coupling sleeve placed beneath the ground plane. The signal from the copper sleeve radiates through a space that exists between the dielectric tube and the ground plane. A significant back radiation seen in the E-plane is due to the feeding part, in which the copper sleeve and copper rod are also radiate at 900 MHz even though the plasma antenna is de-activated. The cross polarization patterns in the H-plane are below than -15 dB as depicted in Figure 4.30 (c). In the E-plane, the cross polarization patterns are below than -10 dB with small part of the OFF state pattern is slightly higher than -10 dB, as shown in Figure 4.30 (d).

To confirm that the high back radiation pattern occurred at 900 MHz is contributed by the feeding part; the same antenna was measured at 450 MHz. The antenna radiation patterns when the plasma is ON and OFF states at 450 MHz are shown in Figure 4.31.
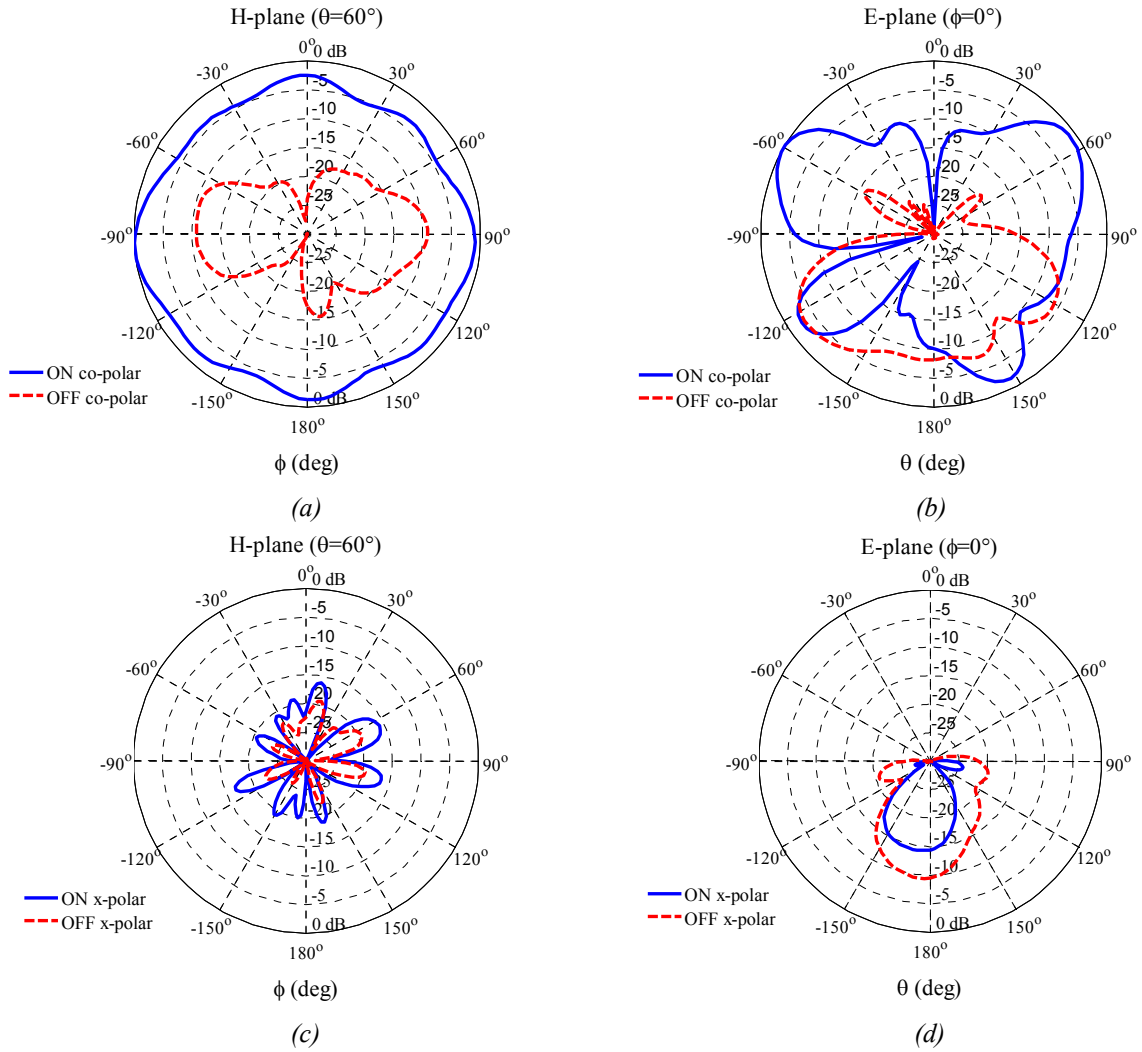
Figure 4.31 – Normalized measured radiation patterns, E_θ and E_ϕ components at 450 MHz. (a)-(b) Co-polarization in the H- and E-planes respectively. (c)-(d) Cross-polarization in the H- and E- planes respectively

There are significant differences which can be seen between ON and OFF states of plasma antenna in the H- and E- planes in Figure 4.31 (a) and 4.31 (b), respectively. These scenarios again confirm that the plasma antenna is radiating at 450 MHz. Moreover the back radiation pattern in the E-plane which is below than -15 dB can be used to prove and explain that the high back radiation seen in Figure 4.30 (b) is due to the feeding part. The cross polarization radiation patterns of this plasma antenna are below than -10 dB in the two principal planes. Other than that, this plasma antenna configuration that comes with an extra part of plasma source exposed just below the coupling sleeve as shown in Figure 4.27 (b), is also radiating in the lower direction (lower part of ground plane) when the plasma is activated.

181

4.5.2 Radiation pattern of plasma antenna with $h_{radiate}$ equals 77 mm

The radiation patterns of plasma antenna with antenna's height equals 77 mm are represented in Figure 4.32 for 900 MHz and in Figure 4.33 for 450 MHz respectively.
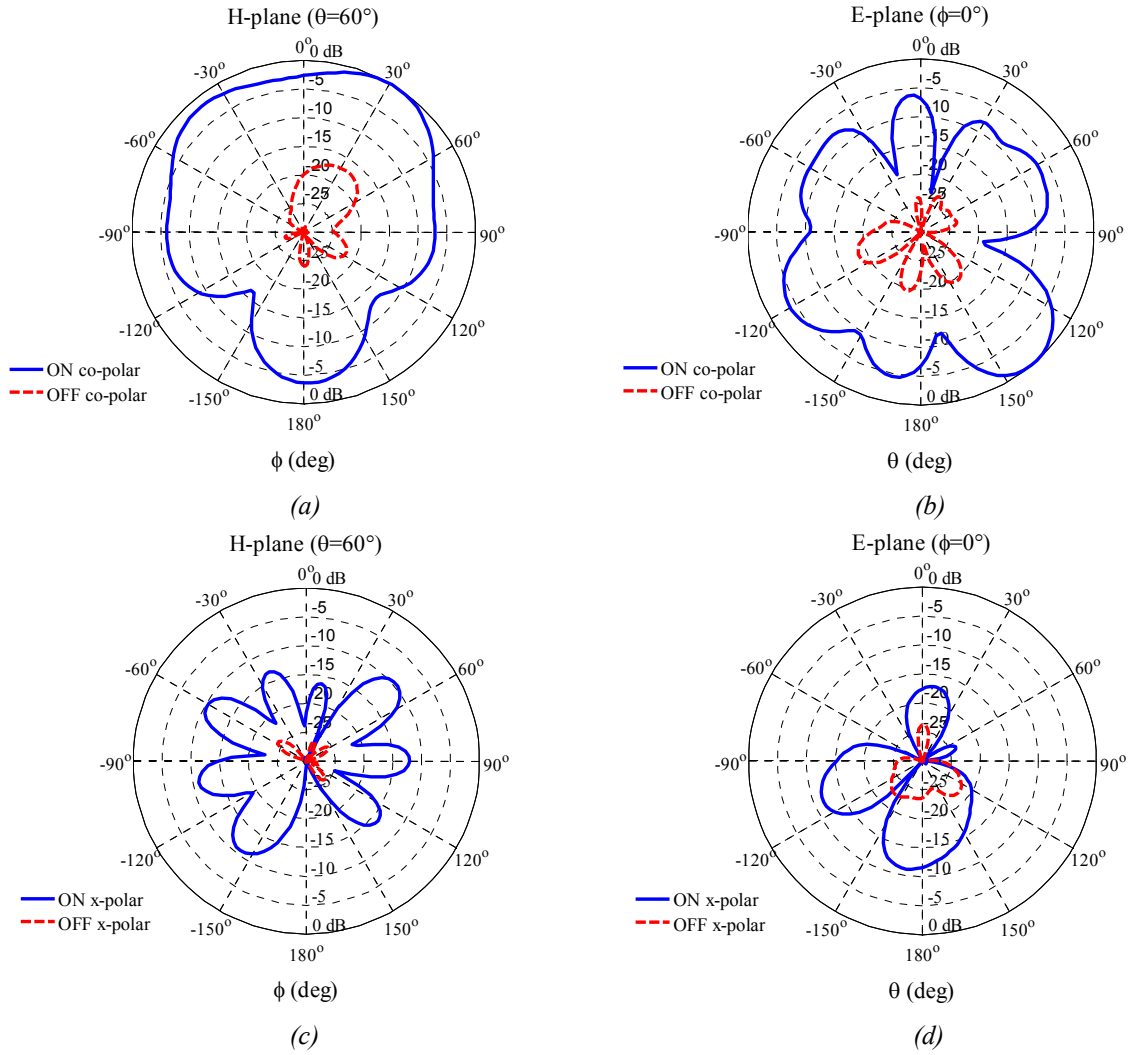

Figure 4.32 – Normalized measured radiation patterns, E_θ and E_ϕ components at 900 MHz. (a)-(b) Co-polarization in the H- and E-planes respectively. (c)-(d) Cross-polarization in the H- and E- planes respectively.

The plasma antenna is radiating at 900 MHz since there is coherent difference between ON and OFF plasma states. The difference is more than 10 dB can be seen in the maximum direction as shown in Figure 4.32 (a) and 4.32 (b). However, back radiations for ON and OFF plasma states are significantly high and this may be due to the antenna feeding part as proved in the previous case. The antenna cross polarization radiation patterns are below than -15 dB in the H-plane and below than -8 dB in the E-plane.

For further investigations, the same antenna was measured at 450 MHz. However, the measurement results in Figure 4.33 show that the antenna is not efficient in radiating signal at 450 MHz (the antenna configuration is illustrated in Figure 4.24 and Figure 4.27 (a)).
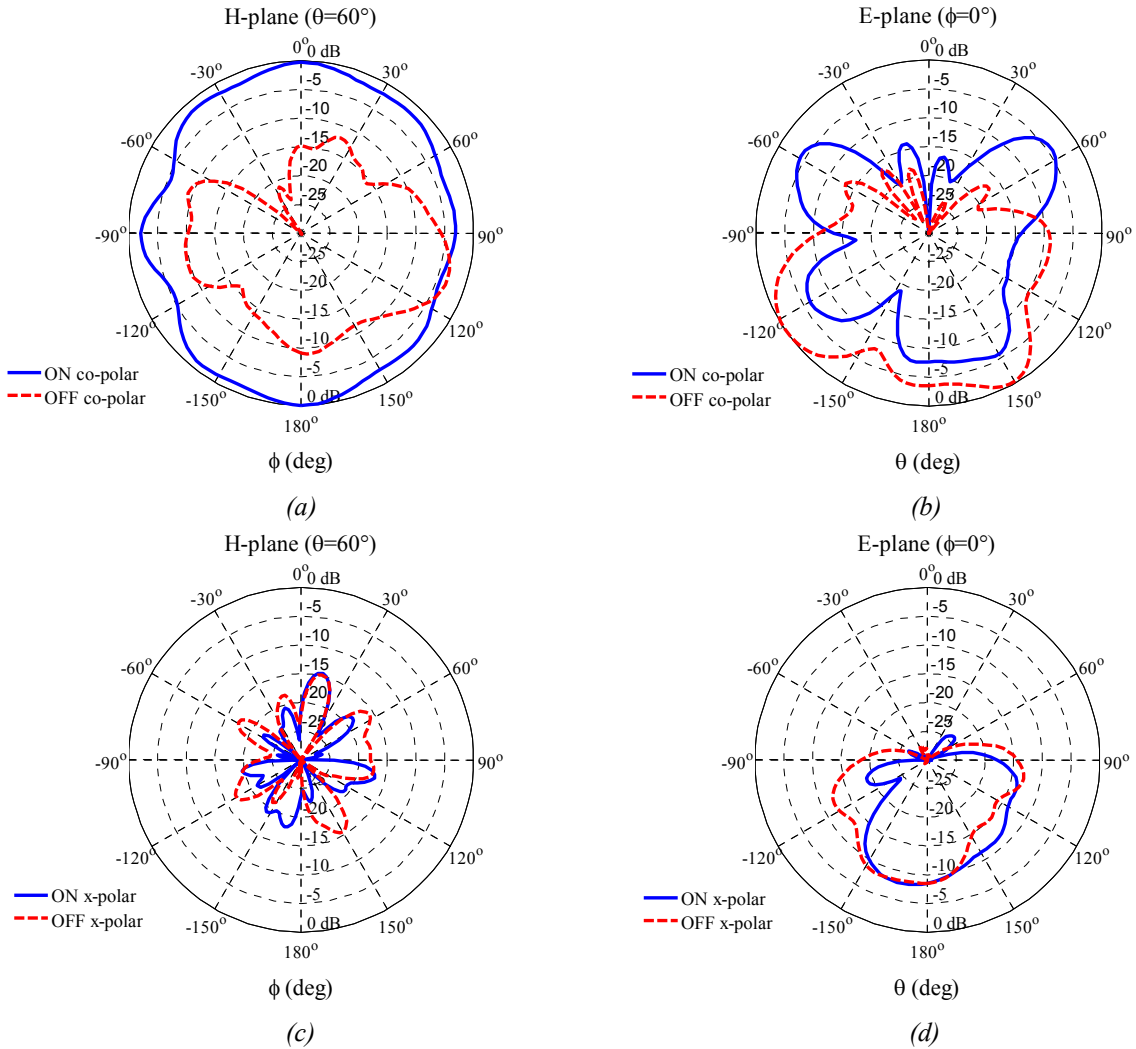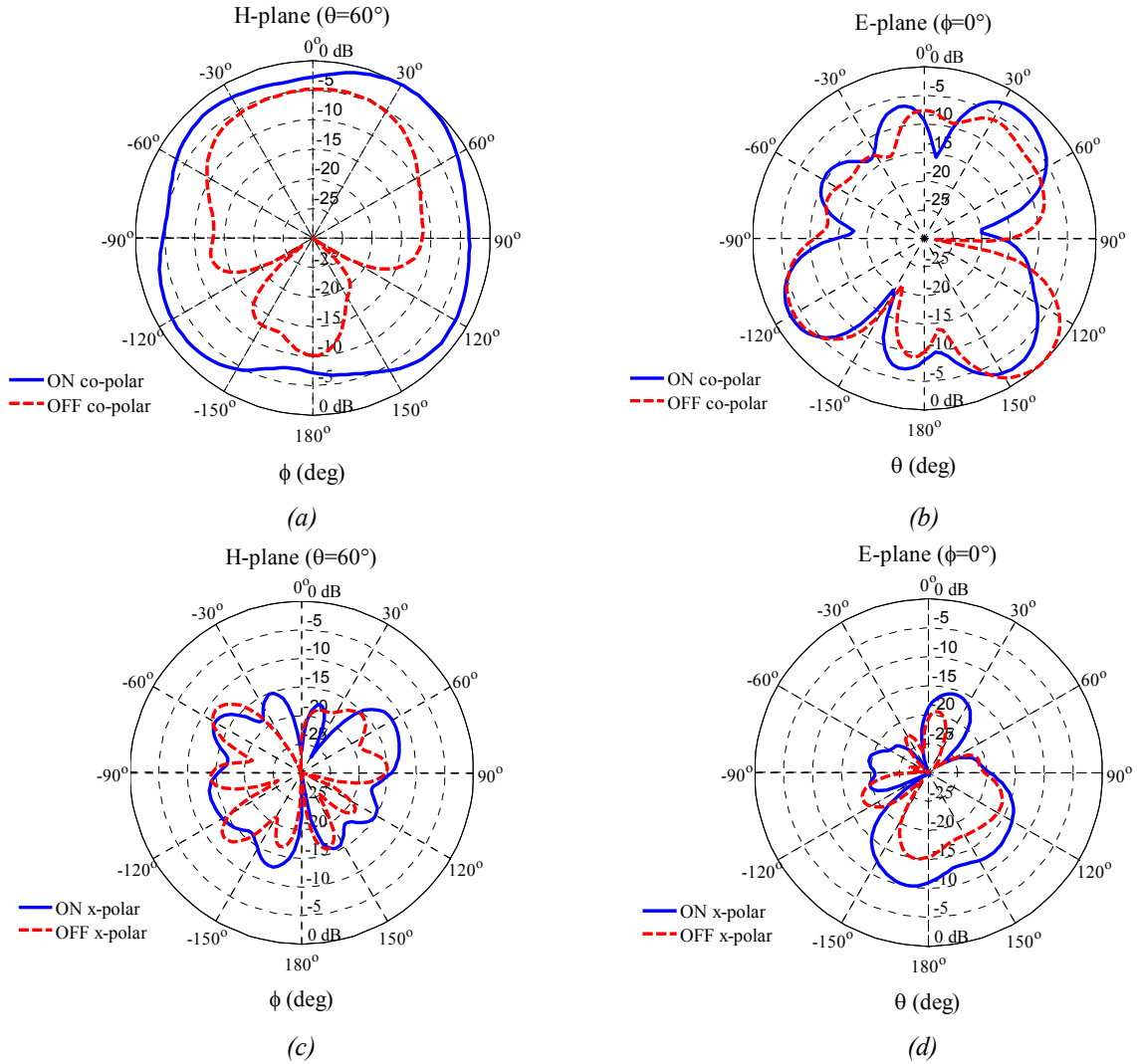

Figure 4.33 – Normalized measured radiation patterns, E_θ and E_ϕ components at 450 MHz. (a)-(b) Co-polarization in the H- and E-planes respectively. (c)-(d) Cross-polarization in the H- and E- planes respectively

Although the normalized radiation pattern in the H-plane (plasma ON state) is somehow similar to omnidirectional pattern and the cross polarization radiation patterns in the both planes are below than -10 dB (Figure 4.33 (c) and Figure 4.33 (d)), the radiation pattern in E-plane tells that the antenna is not an efficient radiator because there is no noteworthy difference between ON and OFF as can be seen in Figure 4.33 (b). The broad back radiation patterns seen in Figure 4.33 (b) were caused by the feeding part of the antenna.

4.6   Conclusion

Based on the measurement results, it can be concluded that, the compact fluorescent lamp (CFL) with an AC excitation can be used to radiate radio signals. Two plasma antennas ($h_{radiate}$ = 35.7 mm and $h_{radiate}$ = 77 mm) were fabricated and measured at 900 MHz and 450 MHz. At 900 MHz both antennas were observed to radiate since there are noteworthy difference on antenna radiation patterns between ON and OFF states of plasma. However, at 450 MHz only plasma antenna with $h_{radiate}$ equals 35.7 mm exhibits significant radiation pattern between ON and OFF states, whereas the plasma antenna with $h_{radiate}$ is equal to 77 mm does not working as an efficient radiator. The reason of this situation is due to the DC feeding part and the close proximity distance between AC feeding line and the copper sleeve. When the height of the antenna, $h_{radiate}$ is increased from 35.7 mm to 77 mm, the coupling sleeve has to be placed in the close proximity with the bottom part of CFL which is used to connect to the AC supply (Figure 4.27 (a)). Thus, this situation may induce unintended interaction between feeding part of the antenna and the AC feeding line which could prevent the element to work as a radiator. Furthermore, the bottom part of CFL behaves as black box in this situation and its interaction towards feeding part is hard to anticipate.

Broad back radiations were seen when the two plasma antennas in the de-activating mode at 900 MHz. The cause of these behaviors was investigated and it was found that at 450 MHz ($h_{radiate}$ = 35.7 mm) when the plasma is OFF, the back radiation is lower than -15 dB. Therefore, it can be concluded that the broad back radiation seen at 900 MHz is caused by the DC feeding elements which consists of coupling sleeve and copper rod. The back radiation contributed by the copper rod can be reduced by optimizing the rod's length.

The radiation patterns of the two plasma antennas measured from 450 MHz to 900 MHz are quite similar to the radiation pattern of classical dipole antenna. If the antenna is meant to work as monopole antenna, the feeding part that is located underneath the ground plane has to be covered by an absorber. However, the existing loss due to the feeding part is still contributing to the plasma antenna performance. Thus a further study to optimize feeding system of the plasma antenna is very essential for future work.

References

[1]   J. P. Rayner, A. P. Whichello, A. D. Cheetham, "Physically characteristics of plasma antennas," IEEE Trans., Plasma Sci., vol. 32, no. 1, pp. 269-281, Feb 2004.

[2]   T. Anderson, I. Alexeff, N. Karnam, E. P. Pradeep, N. R. Pulasani, J. Peck, "An operating intelligent plasma antenna," IEEE 34th International Conference on Plasma Science (ICOPS 2007), pp. 353-356, 2007.

[3]   I. Alexeff, T. Anderson, S. Parameswaran, E. P. Pradeep, J. Hulloli, P. Hulloli, "Experimental and theoretical results with plasma antennas," IEEE Trans., Plasma Sci., vol. 34, no. 2, pp. 166-172, April 2006.

[4]   D. Qian, D. Jun, G. Chen-Jiang, S. Lei, "On characteristics of a plasma column antenna," The International Conference on Microwave and Millimeter Wave Technology (ICMMT 2008), 2008.

[5]   H. Q. Ye, M. Goa, C. J. Tang, "Radiation theory of the plasma antenna," IEEE Trans., Antennas Propag., vol. 59, no. 5, pp. 1497-1502, May 2011.

[6]   Y. Lee, S. Ganguly, "FDTD analysis of a plasma column antenna," IEEE Antennas and Propagation Society International Symposium, pp. 430-433, 2005.

[7]   Y. Liu, C. Tang, X. Xu, "Rigid method for dispersion relation of plasma antenna," The Second International Conference on Mechanic Automation and Control Engineering (MACE), pp. 1590-1593, 2011.

[8]   Francis J. Zuck, "Surface-wave antennas," in Antenna Engineering Handbook, McGraw Hill, NY: New York, 2007, pp. 1-32.

[9]   W. Jiayin, S. Jiaming, W. Jiachun, X. Bo, "Study of the radiation pattern of unipole plasma antenna," The 7th International Symposium on Antennas, Propagation, & EM Theory (ISAPE 06), 2006.

[10]   P. Russo, G. Cerri, E. Vecchioni, "Self-consistent model for the characterization of plasma ignition by propagation of an electromagnetic wave to be used for plasma antennas design," IET Microwaves, Antennas & propagation, vol. 4, iss. 12, pp. 2256-2264, 2010.

[11]   G. Cerri, V. Mariani Primiani, P. Russo, E. Vecchioni, "FDTD approach for the characterization of electromagnetic wave propagation in plasma for application to plasma antennas," The 2nd European Conference on Antennas and Propagation (EuCAP 2007), 2007.

[12]   G. Cerri, P. Russo, E. Vecchioni, "A self-consistent FDTD model of plasma antennas," The 5th European Conference on Antennas and Propagation (EuCAP 2010), 2010.

[13]   G. Cerri, P. Russo, E. Vecchioni, "Electromagnetic characterization of plasma antennas," The 3rd European Conference on Antennas and Propagation (EuCAP 2008), 2008.

[14]   P. Russo, G. Cerri, R. De Leo, E. Vecchioni, "Self-consistent analysis of cylindrical plasma antenna," IEEE Trans., Antennas Propag., vol. 59, no. 5, pp.1503-1511, May 2011.

[15]   C. Ting, B. Roa, W. A. Saxton, "Theoretical and experimental study of a finite cylindrical antenna in a plasma column," IEEE Trans., Antennas Propag., vol. AP-16, no. 2, pp. 246-255, March 1968.

[16]   I. L. Morrow, J. R. James, "Fundamental limitations on excitation of a surface wave on a plasma column," IEEE Antenna and Propagation Society International Symposium, pp. 272-275, 2002.

[17] M. Laroussi, J. R. Roth, "Numerical calculation of the reflection, absorption, and transmission ofm by a nonuniform plasma slab," IEEE Trans., Plasma Sci., vol. 21, no. 4, pp. 366-372, August 1993.

[18] D. L. Tang, A. P. Sun, X. M. Qui, Paul K. Chu, "Interaction of electromagnetic waves with a magnetized nonuniform plasma slab," IEEE Trans., Plasma Sci., vol. 31, no. 3, pp. 405-410, June 2003.

[19] Y. Yi, S. D. Lin, "The reflection, transmission, and absorption of microwave in nonuniform plasma," Asia-pacific Conference on Environmental Electromagnetics (CEEM 2003), pp. 518-522, Nov. 2003.

[20] Stefan A. Maier, "Electromagnetic of metals," in Plasmonics : Fundamentals and Applications, Springer, Bath: The UK, 2007, pp. 12-13.

[21] G. Cerri, R. De Leo, V. Mariani Primiani, P. Russo, "Plasma antenna characterization," The 18th International Conference on Applied Electromagnetics and Communications (ICECom 2005), 2005.

[22] G. Cerri, R. De Leo, V. Mariani Primiani, P. Russo, "Measurement of the properties of a plasma column used as a radiating element," IEEE Trans., Instrum., Meas., vol. 57, no. 2, pp. 242-247, Feb. 2008.

[23] Ovsyanikov V. V., Reznichenko I. A., Ol'shevs'kiy A. L., Popel' V.M., Rodin K. V., and Romanenko Y. D., "Wideband properties of new antenna made of cold plasma," The 4th International Conference on Ultrawideband and Ultrashort Impulse Signals, (UWBUSIS 2008), pp.77-79, 2008.

[24] P. Russo, V. Mariani Primiani, G. Cerri, R. De Leo, E. Vecchioni, "Experimental characterization of a surfaguide fed plasma antenna," IEEE Trans., Antennas Propag., vol. 59, no. 2, pp. 425-433, Feb. 2011.

[25] G. G. Borg, J. H. Harris, N. M. Martin, D. Thorncraft, R. Miliken, D. G. Miljak, B. Kwan, T. Ng, J. Kircher, "Plasmas as antennas: theory, experiment and applications," Phys., Plasmas, vol. 7, pp. 2198-2202, 2000.

[26] G. G. Borg, J. H. Harris, N. M. Martin, D. Thorncraft, R. Miliken, D. G. Miljak, B. Kwan, T. Ng, J. Kircher, "An investigation of the properties and applications of plasma antennas," Switzerland-Millenium Conference on Antennas and Propagation Davos, April 2000.

[27] V. Kumar, M. Mishra, N. K. Joshi, "Study of a fluorescent tube as plasma antenna," Progress in Electromagnetics Research Letters, vol. 24, pp. 17-26, 2011.

[28] M. Hargreave. J. P. Rayner, A. D. Cheetham, G. N. French. A. P. Whichello, "Coupling power and information to a plasma antenna," Proceeding of the 11th International Congress on Plasma Physics, vol. 669, pp. 388-391, June 2003.

[29] I. Alexeff, T. Anderson, E. Farshi, N. Karnam, N. R. Pulasani, "Recent results of plasma antenna," Phys., Plasmas 15, 057104 (2008).

[30] R. Kumar, D. Bora, "Wireless communication capability of a reconfigurable plasma antenna," J., Appl., Phys. 109, 063303 (2011).

[31] L. Wei, Q. Jinghui, L. Shu, S. Ying, "Analysis and design of plasma monopole antenna," The proceeding of the 6th International ICST Conference and Communications and Networking in China (CHINACOM), pp. 921-924, 2011.

[32] R. Kumar, D. Bora, "Experimental study of parameters of a plasma antenna," Plasma Sci., Technol., vol. 12, no. 5, pp. 592-600, Oct. 2010.

[33] B. Anton, G. Volodymyr, O. Viktor, O. Volodymyr, R. Olexandr, S. Valerii, S. Olga, "Research of antennas made gas plasma on microwave band," The 5th European Conference on Antennas and Propagation (EuCAP 2010), 2010.

[34] R. Kumar, D. Bora, "Experimental investigation of different structures of a radio frequency produced plasma medium," Phys., Plasmas 17, 043503 (2010).

[35] H. M. Zali, M. T. Ali, N. A. Halili, H. Ja'afar, I. Pasya, "Study of monopole plasma antenna using fluorescent tube in wireless transmission experiments," The proceeding of The 1st IEEE International Symposium on Telecommunication Technologies, pp. 52-55, 2012.

[36] G. Cerri, R. De Leo, V. Mariani Primiani, P. Russo, "Measurement of the properties of a plasma column used as a radiating element," Instrument and Measurement Technology Conference (IMTC 2006), pp. 483-486, April 2006.

[37] T. J. Dwyer, J. R. Greig , D. P. Murphy, J. M. Perin, R. E. Pechachek, M. Raleigh, "On the feasibility of using atmospheric discharge plasma as an RF antenna," IEEE Trans., Antennas Propag., vol. AP-32, no. 2, pp. 141-146, Feb. 1984.

[38] J. Sun, Y. Xie, Y. Xu, "Progress of UHF/VHF plasma antenna research," The proceeding of The 10th International Symposium Propagation & EM Theory (ISAPE), pp. 23-25, 2012.

[39] X. Li, F. Luo, B. Hu, "FDTD analysis of radiation pattern performance of cylindrical plasma antenna", IEEE Antennas Wireless Propag., Lett., vol. 8, pp. 756-758, 2009.

[40] X. Li, B. Hu, "FDTD analysis of a magneto-plasma antenna with uniform of nonuniform distribution," IEEE Antennas Wireless Propag., Lett., vol. 9, pp. 175-178, 2010.

[41] M. Chung, W. Chen, B. Huang, C. Chang, K. Ku, Y. Yu, T. Suen, "Capacitive coupling return loss of a new pre-ionized monopole plasma antenna," IEEE Region 10 Conference (TENCON 2007), 2007.

[42] M. Chung, W.Chen, Y.Yu, Z. Y. Liou, "Properties of DC-biased plasma antenna," International Conference on Microwave and Millimeter Wave Technology (ICMMT 2008), 2008.

[43] N. A. Halili, M. T. Ali, H. M. Zali, H. Ja'afar, I. Pasya, "A study on plasma antenna characteristics with different gases," The proceeding of The 1st IEEE International Symposium on Telecommunication Technologies, pp. 56-59, 2012.

[44] F. Etesami, F. Mohajeri, "On radiation characteristics of a plasma triangular monopole antenna," The 19th Iranian Conference Electrical Engineering (ICEE), 2011.

[45] Z. Longgen, C. Lihiu, Z. Zhigang, "Study on the gain of plasma antenna," The 8th International Symposium on Antenna, Propagation and EM Theory, (ISAPE 2008), pp.222-224, 2008.

[46] Z. H. Qian, K. W. Leung, R. S. Chen, D. X. Wang, "FDTD analysis of a plasma whip antenna," IEEE Antennas and Propagation Society International Symposium, pp. 166-169, 2005.

[47] M. Liang, G. Qinggong, "FDTD analysis of a plasma helix antenna," IEEE International Conference on Microwave and Milimeter Wave Technology (ICMMT 2008), 2008.

Appendix 4.1

FICHE TECHNIQUE PRODUIT

ISOSUD PLASTICS

CESTILENE HD 500

APPELLATION CHIMIQUE:	PE HD HMW
MASSE VOLUMIQUE:	0,96
COULEUR:	Noir et blanc
ABSORPTION D'EAU	0

PROPRIÉTÉS THERMIQUES

Points de fusion:	137 ℃
Conductibilité thermique à 23 ℃:	0,40W/(K.m)
Température de fléchissement sous charge méthode A: 1,81 N/mm²:	45 ℃
Température d'utilisation admissible dans l'air:	
Par pointes:	100 ℃
En continu pendant 5 000 heures:	80 ℃
En continu pendant 20 000 heures:	-
Minimum:	-100 ℃
Tenue à la flamme suivant UL 94 (épaisseur 3 mm)	HB

PROPRIÉTÉS MÉCANIQUES à 23 ℃

Coefficient de frottement à sec:	0,15-0,25
Coefficient de frottement lubrifié:	0,05-0,12
Essais de traction:	
Contrainte au seuil d'écoulement / contrainte à la rupture ISO 527:	28 Mpa
Allongement à la rupture ISO 527:	10 %
Module d'élasticité en traction ISO 527:	1350 Mpa
Essais de compression:	
Contrainte pour une déformation nominale de 1 / 2 / 5 %	9 / 15 / 23 Mpa
Résistance aux chocsCharpy-non entaillé IOS 179:	Sans Rupture
Résistance aux chocsCharpy-entaillé ISO 179	105 P KJ / m²
Dureté à la bille ISO 2039-1	45 N / mm²
Dureté Rockwell ISO 2039-2	-

PROPRIÉTÉS ÉLECTRIQUES à 23 ℃

|	
Rigidité diélectrique à secs ISO 60243 :	45 KV /mm
Résistivité transversale à secs ISO 60093 :	> 10^{14} Ohm.cm
Résistivité superficielle à secs ISO 60093 :	> 10^{13} Ohm.cm
Permittivité relative à 100 Hz à secs ISO 60250 :	2,4
Permittivité relative à 1 MHz à secs ISO 60250 :	2,4
Facteur de dispersion tg à 100 Hz à secs ISO 60250 :	0,0002
Facteur de dispersion tg à 1M Hz à secs ISO 60250 :	0,0002
Résistance au cheminement (CTI) ISO 60112 :	600

ISOSUD PLASTICS   18 rue des Frères Lumière 69 680 CHASSIEU
Téléphone: 04.72.79.26.00   Télécopie: 04.78.90.45.53   Guide de choix: www.isosudplastics.com

Ces informations sont données à titre indicatif, elles ne peuvent engager la responsabilité de notre société.
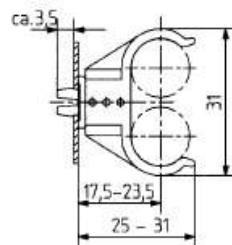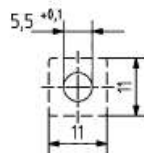
Appendix 4.2

Supports for lamps TC
26.719
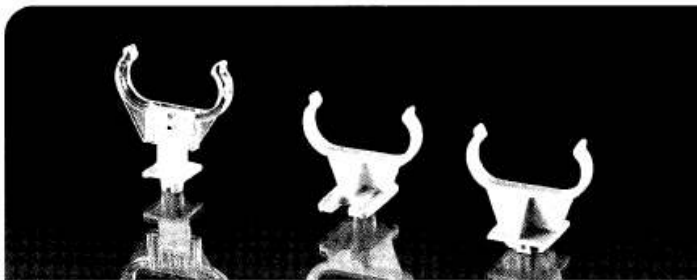
Supports ensure a constant gap between lamp and geartray.
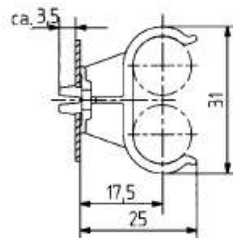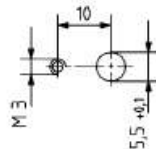
Support material: PC, UV-resistant

0.6 - 1.0

CAD

see pages 300..., 301, 306

		pkg.	wt.	part no.
5,5 +0,1 / 11 / 11 — ca. 3,5 / 31 / 17,5–23,5 / 25 – 31	**cradle support** two pieces, adjustable height 17.5 / 20.5 / 23.5 mm snap in pin: ø 5.5 mm base: white support: transparent	500	1g	**26.719**.U310.50
	Base and support are packed separately.			
10 / M 3 / 5,5 +0,1 — ca. 3,5 / 31 / 17,5 / 25	**cradle support** snap in pin: ø 5.5 mm and screw fixing for screws M 3 DIN 84 white	500	1g	**26.719**.-301.50
10,5 +0,1 / 8,5 +0,1 / 16 / 16 / 16 — ca. 3 / 31 / 17,5 / 25	**cradle support** snap in lug 8.5 x 10.5 mm white	500	1g	**26.719**.-013.50
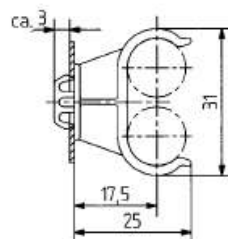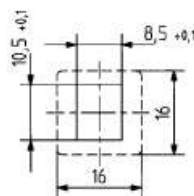
307
1994-1997

189

Appendix 4.3

Radiation patterns of plasma antenna with $h_{radiate}$ equals 35.7 mm

Figure A.4.3. 1 –Normalized measured radiation patterns, E_θ and E_ϕ components at 600 MHz. (a)-(b) Co-polarization in the H- and E-planes respectively. (c)-(d) Cross-polarization in the H- and E- planes respectively.

Figure A.4.3. 2 – Normalized measured radiation patterns, E_θ and E_ϕ components at 700 MHz. (a)-(b) Co-polarization in the H- and E-planes respectively. (c)-(d) Cross-polarization in the H- and E- planes respectively.

(c)   (d)

*Figure A.4.3. 3 – Normalized measured radiation patterns, E_θ and E_ϕ components at 800 MHz.
(a)-(b) Co-polarization in the H- and E-planes respectively. (c)-(d) Cross-polarization in the
H- and E- planes respectively.*

(a)   (b)

*Figure A. 4.4. 4 – (a) Measured magnitude of reflection coefficients, S_{11}. (b) Measured antenna
gains.*

Appendix 4.4

Radiation patterns of plasma antenna with $h_{radiate}$ equals 77 mm
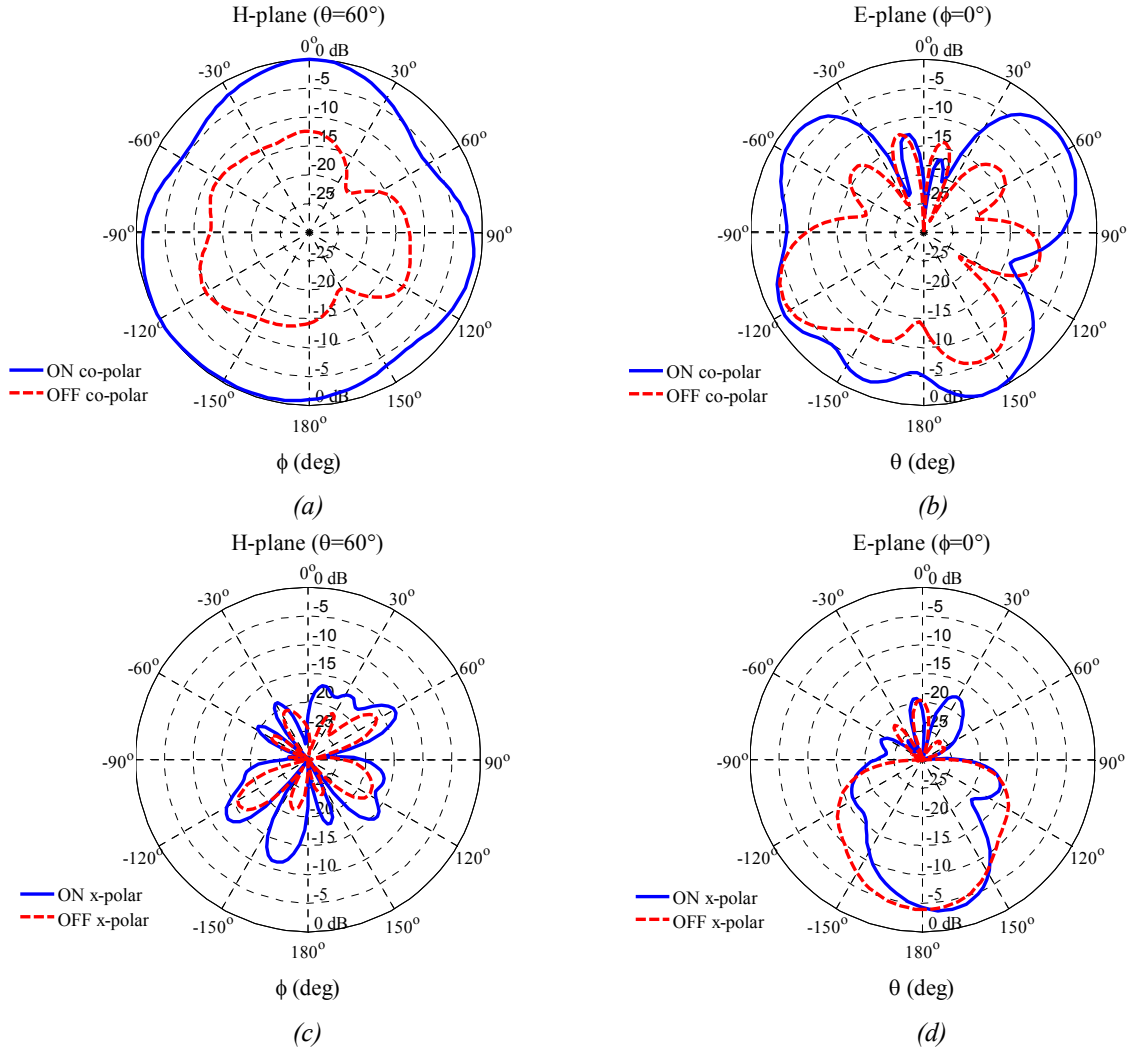

(a)

(b)

(c)

(d)
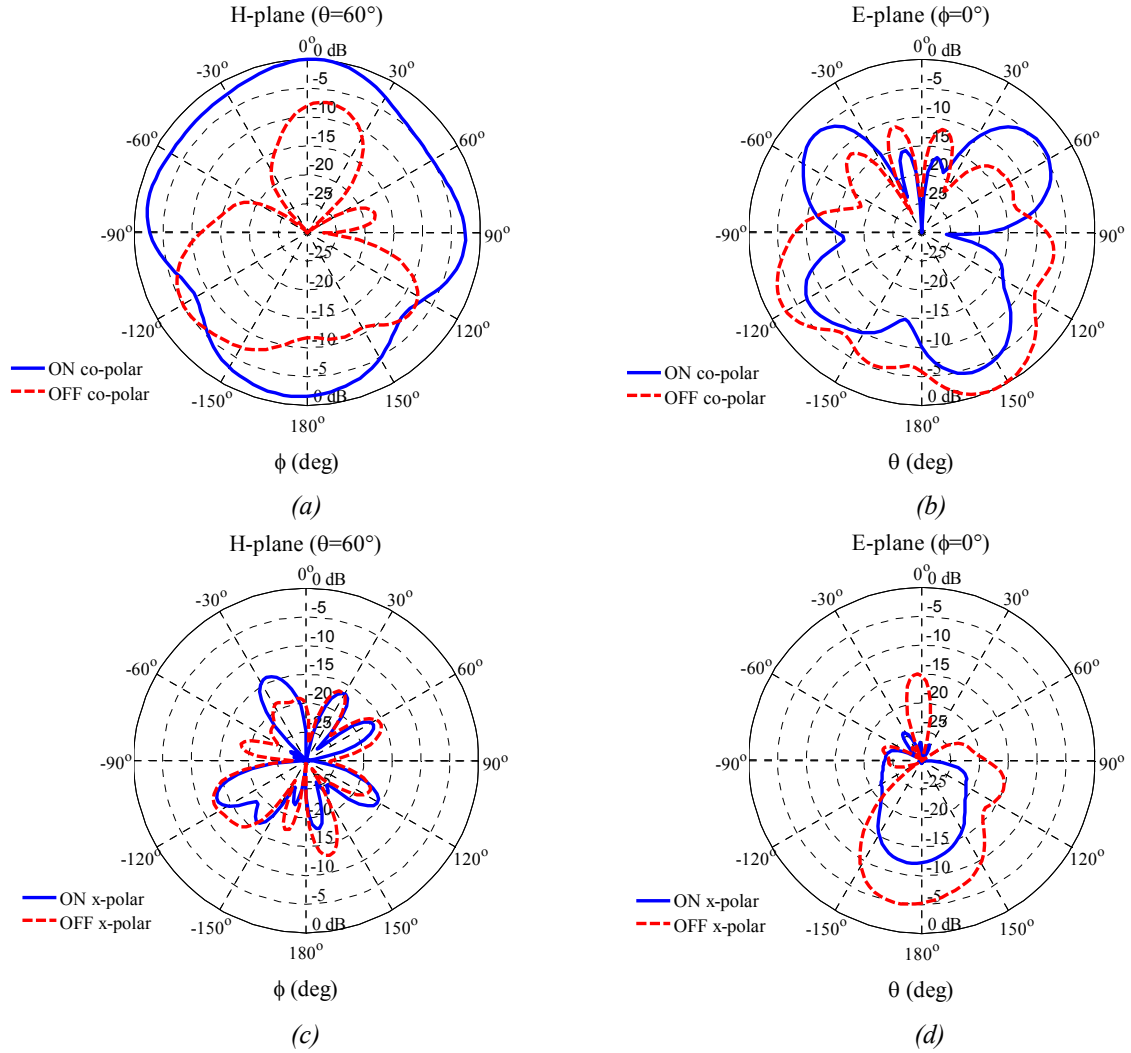
Figure A.4.4. 1 – Normalized measured radiation patterns, E_θ and E_ϕ components at 600 MHz. (a)-(b) Co-polarization in the H- and E-planes respectively. (c)-(d) Cross-polarization in the H- and E- planes respectively.
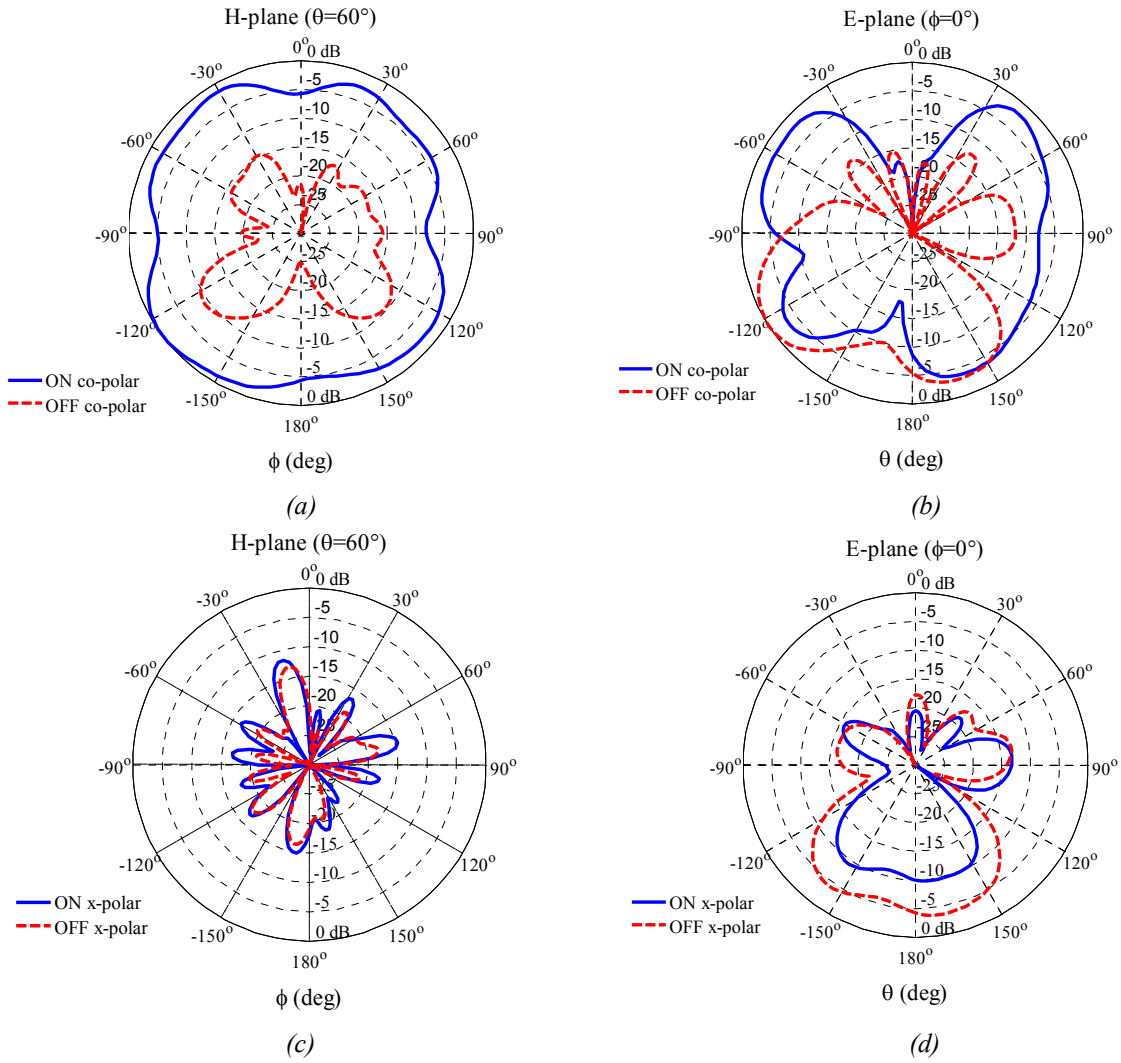
Figure A. 4.4. 2 – Normalized measured radiation patterns, E_θ and E_ϕ components at 700 MHz. (a)-(b) Co-polarization in the H- and E-planes respectively. (c)-(d) Cross-polarization in the H- and E- planes respectively.
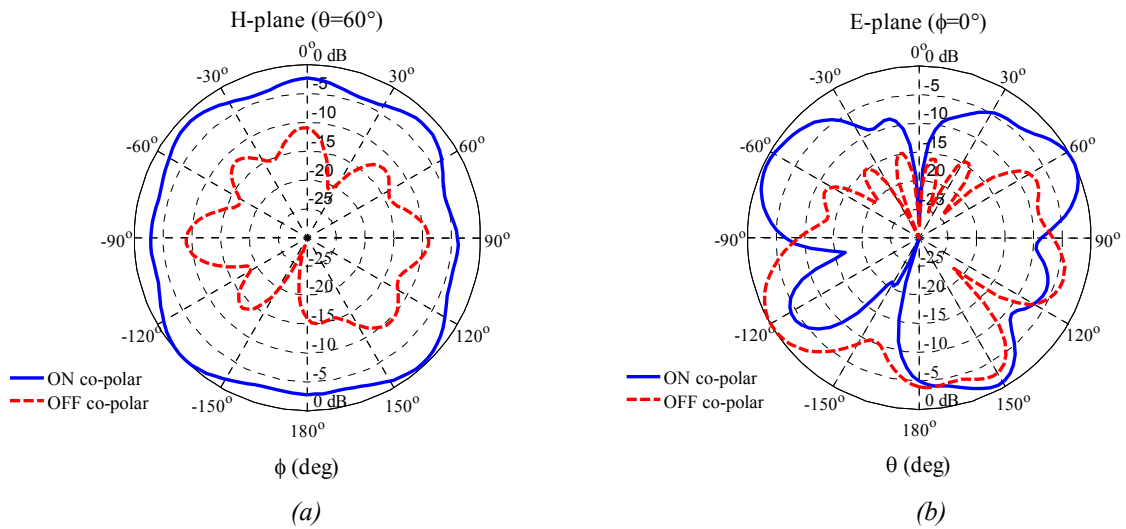
Figure A. 4.4. 3 – Normalized measured radiation patterns, E_θ and E_ϕ components at 800 MHz. (a)-(b) Co-polarization in the H- and E-planes respectively. (c)-(d) Cross-polarization in the H- and E- planes respectively.
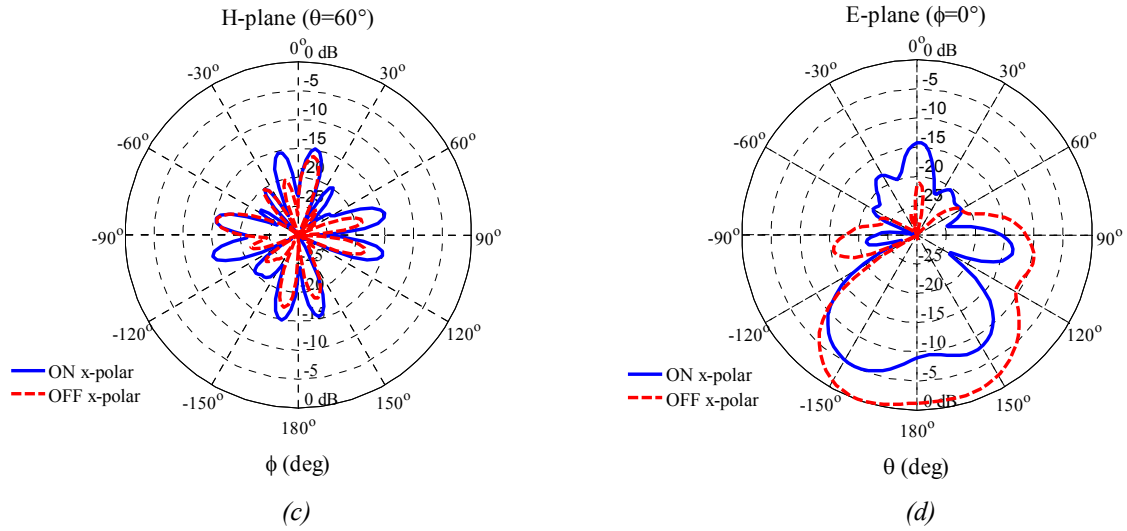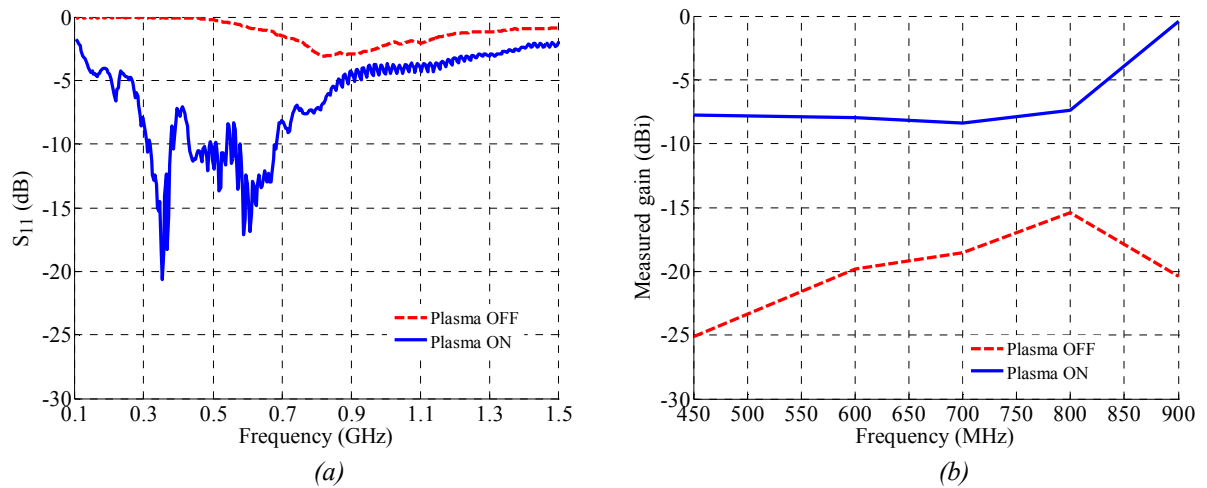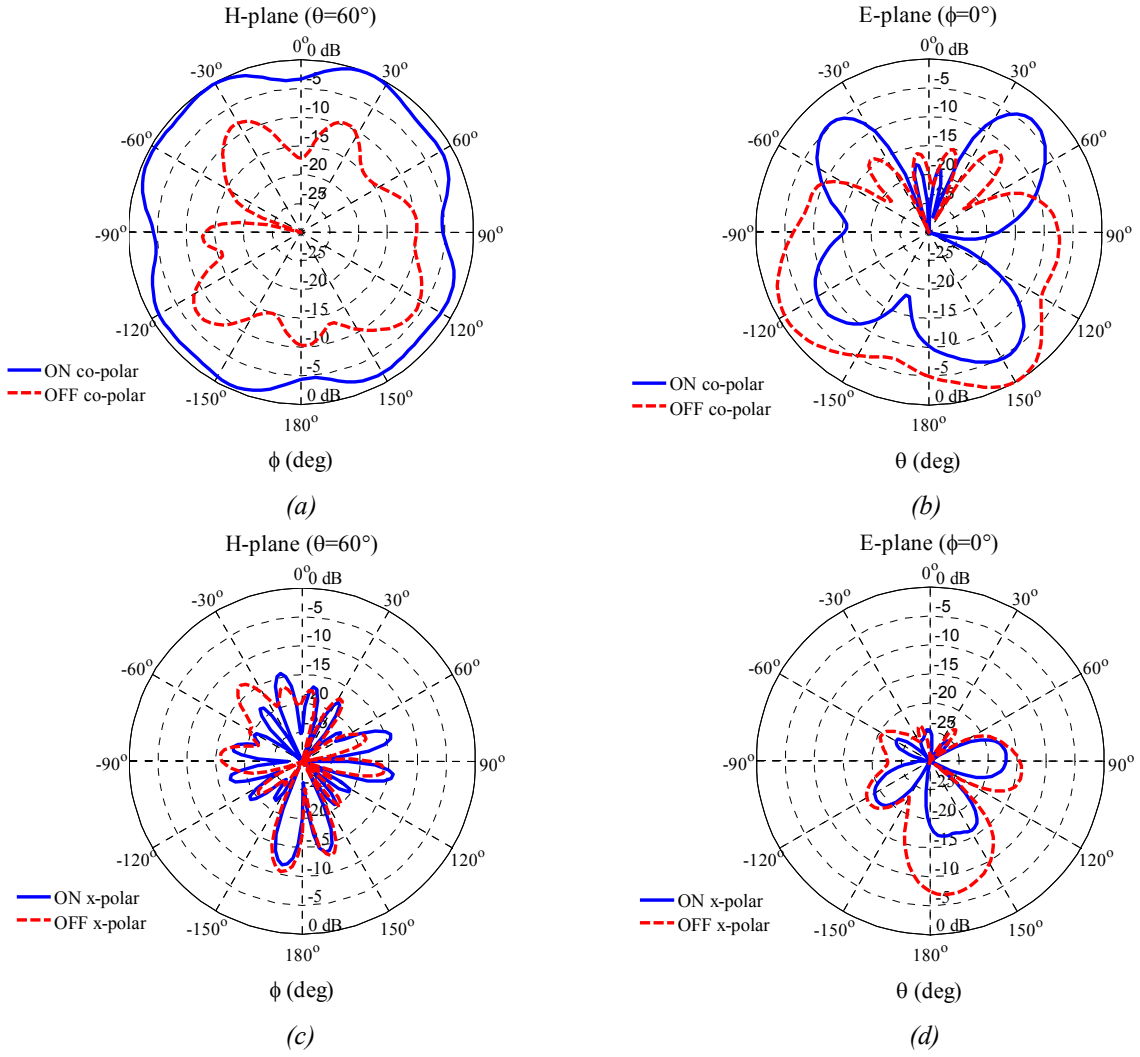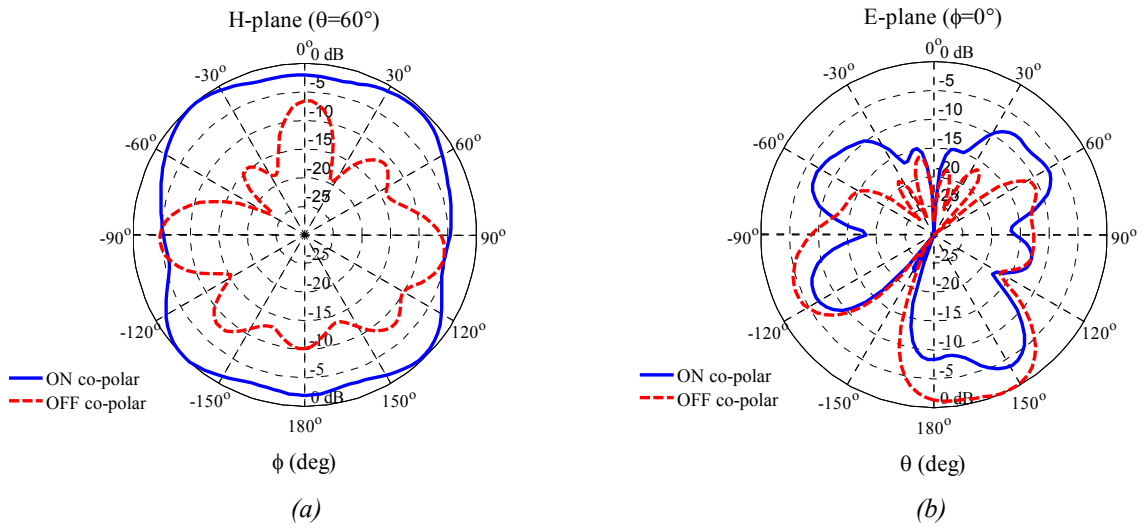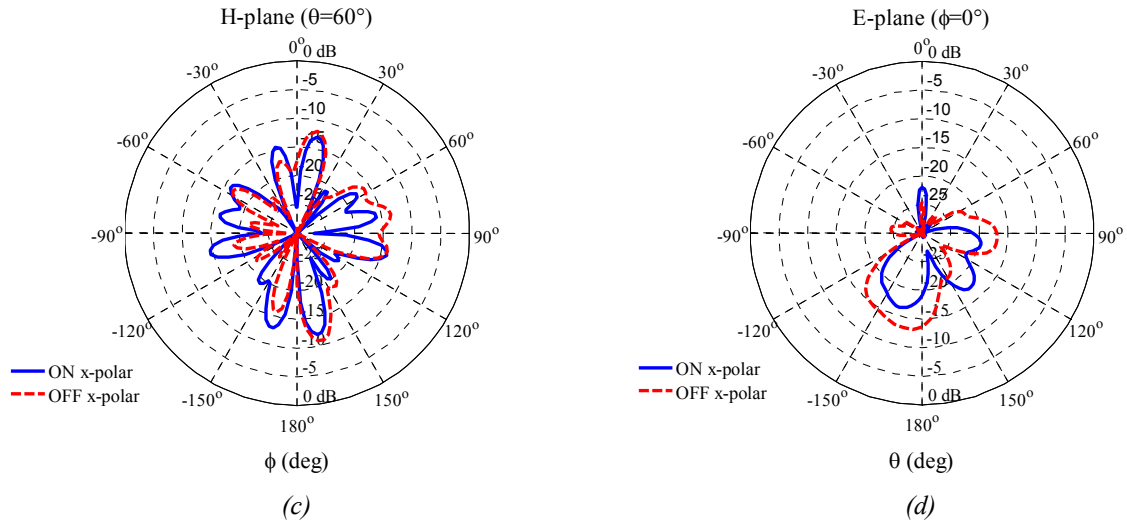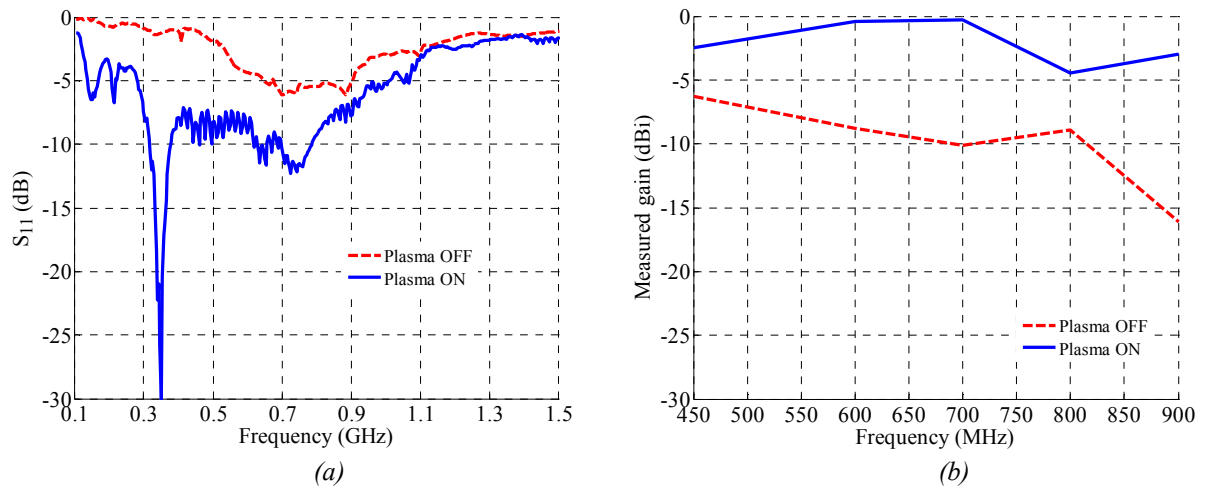

Figure A. 4.4. 4 – (a) Measured magnitude of reflection coefficients, S_{11}. (b) Measured antenna gains.

Chapter 5

Radar cross section (RCS)

This chapter investigates the radar cross section (RCS) of plasma reflector antennas. The basic fundamentals of radar cross section are explained in the first part of this chapter. The second part deals with radar cross section analysis in which the RCS of the well known shapes made of perfect conductor are compared to the simulation results of the similar shapes with the identical dimensions. The excellent agreements from this comparison confirm that the simulation setup and technique used is valid and it can be used for further investigation. In the same section, the simulated RCS of RRA and CRA are presented at 2.4 GHz and 8 GHz. In the third part of this chapter, the measured RCS of the reflector antenna is presented. Finally, a conclusion is drawn based on the simulated and measured findings.

5.1   Introduction

The term of radar is an acronym for Radio Direction And Range. The radar detection ability is measured in terms of radar cross section (RCS). The higher value of RCS means the target object can be easily detected by radar. In general, the strength of detection (the strength of reflections) is depending on the size of the target object, its shape and its electrical parameters such as conductivity and relative permittivity.

Therefore RCS is an important issue in military radar applications. The quest is always to reduce the RCS values so that hostile's radar will not be able to detect the existence of radar targets of its counterpart (such as antennas, fighter jets and ships). Basically there are two ways to reduce the RCS [1]; by appropriately design the radar targets shape and the selection of materials to be used (such as radar absorbing layer material). However it is not easy to come out with less detectable shape since other factors such as aerodynamic specification of complex objects such as fighter jet, missiles or other flying objects are essential. On the other hand, it is a rule of thumb in reducing RCS by taking care of the object's shape such as replacing square corner to round corners, avoid flat and concave surfaces. To optimize the performance of radar target, this rule with the use of right material should be combined. Another way to reduce the RCS is to introduce the secondary scatterers to cancel the "bare" target.

197

5.1.1 Basic type of radar

For the basic comprehension the radar detection and ranging can be divided into three categories of radar such as follows;

a) Bistatic radar [2] - the transmitting and receiving antennas are at different location as viewed from the target. For example the ground transmitter and an airborne receiver or both transmitting and receiving are on the same ground level as suggested in Figure 5.1.

b) Monostatic radar [1], [2] - the transmitting and receiving modules are using the same antenna. This means that, the transmitting and receiving antennas are collocated as viewed from the target.

c) Quasi monostatic radar - the transmitting and receiving antennas are slightly separated but still appear to be at the same location as viewed from the target. For the example transmit and receiving antennas are on the same aircraft.
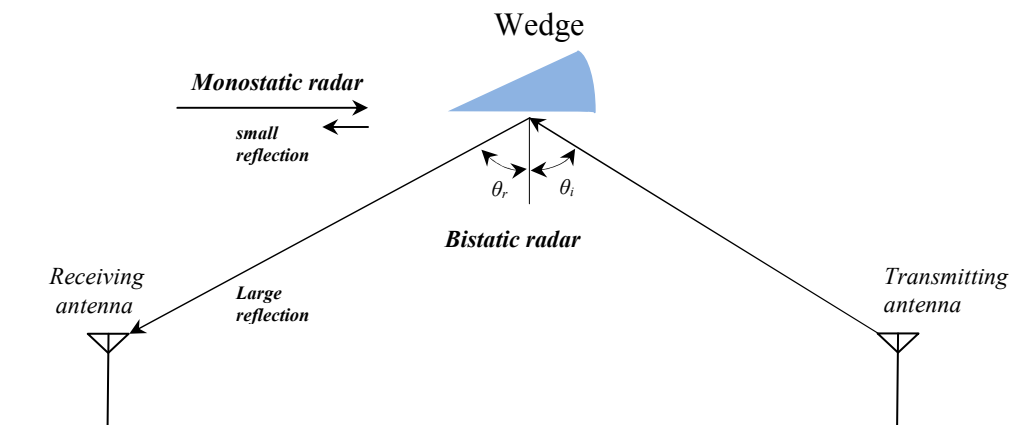
Figure 5.1 – Monostatic and bistatic reflections from wedge. The monostatic reflection from the wedge is small but the bistatic reflection from the flat side of the wedge is large with the angle of reflection is equal to the angle of incidence ($\theta_r = \theta_i$) [2].

These radars can be further classified based on its application purposes. Table 5.1 lists the usage of radars in two main criterions, the civilian and military. Moreover, because of the radar technology advancement, today's cars are likely to be equipped with radar detection system in order to avoid collision.

Table 5.1- List of radar applications for civilian and military usage.

Applications	Users	
	Civilian	Military
Weather detection and avoidance	√	√
Navigation and tracking	√	√
Search and surveillance	√	√
High resolution imaging and mapping	√	√
Proximity fuzes		√
Countermeasures		√
Space flight	√	
Sounding	√	

5.1.2 Definition of Radar Cross Section

The objects that are illuminated by the radar will reflect energy to some extent. Radar cross section (RCS) or echo area of a target which is defined as the area intercepting that amount of power which, when scattered isotropically, produces at the receiver a density which is equal to that scattered by target [1]. The RCS is a parameter denoted by σ, used to characterize the scattering properties of a radar target. It represents the target's size as seen by the radar and has the dimensions of square meters. RCS area is not the same as physical area, but a measure of a target's ability to reflect radar signals in the direction of the receiving antenna. Thus, in general, the RCS of a target is a function of the polarization of the incident wave, the angle of incidence, the angle of observation, the geometry of the target, the electrical properties of the target and the frequency of operation. Therefore, two or more targets with similar physical size may have different RCS values.

For the monostatic radar system, let's start with the power density (W/m^2) radiated by an isotropic antenna is equal to

$$\frac{P_t}{4\pi R^2} \quad Watt/m^2 \tag{5.1}$$

and for a radar, a directive antenna is used to direct the radiated power, P_t in a particular direction of the target. Thus the power density at the target becomes

$$\frac{P_t G}{4\pi R^2} \quad Watt/m^2 \tag{5.2}$$

with the antenna gain, G. By the definition of radar cross section, the target is supposed to reradiate isotropically the power that it has intercepted. As a result, the power density illuminated to the radar is equivalent to

$$\frac{P_t G}{4\pi R^2} \frac{\sigma}{4\pi R^2} \quad Watt/m^2 \tag{5.3}$$

Since the radar having its own maximum effective antenna aperture, A_e, the received power, P_r by the radar is equal to

$$P_r = \frac{P_t G}{4\pi R^2} \frac{\sigma}{4\pi R^2} A_e \quad Watt \tag{5.4}$$

This equation is known as radar equation and from this equation the radar cross section, σ becomes

$$\sigma = \frac{P_r (4\pi R^2)^2}{P_t G A_e} \quad m^2 \tag{5.5}$$

By substituting $A_e = \frac{\lambda^2 G}{4\pi}$ in Eq. 5.5, the RCS equation for monostatic radar is equal to

$$\sigma = \frac{P_r 64\pi^3 R^4}{P_t G^2 \lambda^2} \quad m^2 \tag{5.5}$$

This RCS equation is true for polarization-matched antennas that are aligned for the maximum directional radiation and reception. The RCS of some typical targets are listed in Table 5.2.

Table 5.2 – Typical radar targets and radar cross section values in X band [1].

| Radar targets	RCS	
	m^2	dBsm
Pickup truck	200	23
Automobile	100	20
Jumbo jet airliner	100	20
Commercial jet	40	16
Cabin cruiser boat	10	10
Larger fighter aircraft	6	7.78
Small fighter aircraft	2	3
Adult male	1	0
Conventional winged missile	0.5	-3
Bird	0.01	-20
Insect	0.00001	-50
Advanced tactical fighter	0.000001	-60

5.2   Radar cross section (RCS) analysis

The radar cross section (RCS) of perfectly conducting objects with well known shapes such as sphere, flat plate and cylinder can be easily calculated by assuming the objects are large enough compared to the wavelength. The RCS formulas of these objects are listed in Table 5.3. To note, the RCS of sphere does not depend on the radar frequency (wavelength's size) and it is equivalent to its cross-sectional area.

Table 5.3 – RCS formulas for perfectly conducting objects [2].

Radar targets	RCS (σ)
Sphere, radius *a*	πa^2
Flat plate, are *A*	$\dfrac{4\pi A^2}{\lambda^2}$
Cylinder, radius *a*, length *L*	$\dfrac{2\pi a L^2}{\lambda}$

5.2.1 Simulation of radar cross section for classical case of a sphere and a flat plate

In this section simulations of classical cases for well known shapes (sphere and square flat plate) are presented. The simulations are conducted by using CST software. The dimension of the flat plate is 1000 mm x 1000 mm and the sphere is with radius of 500 mm as illustrated in Figure 5.2.

(a)

(b)
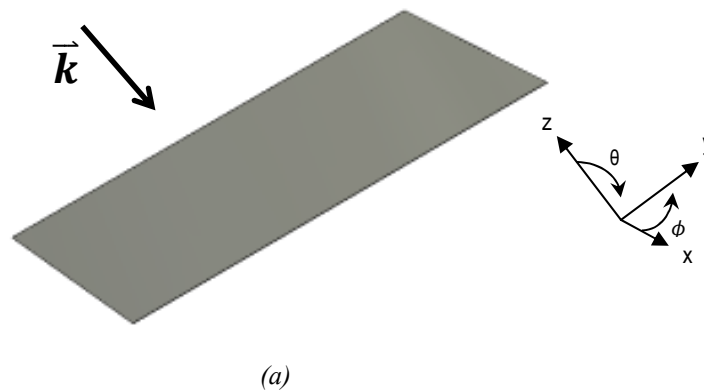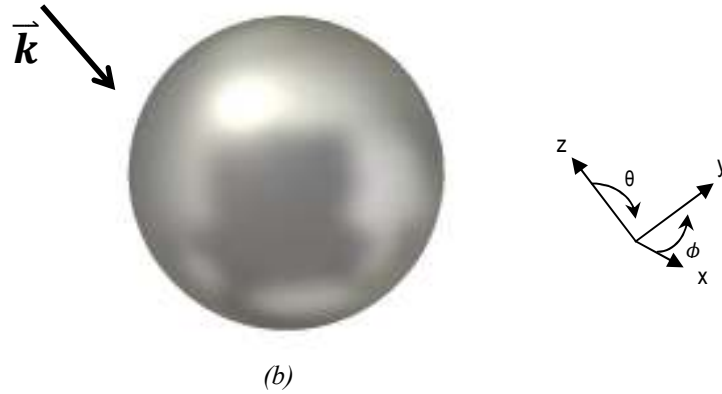
*Figure 5.2 – The well known shapes. (a) Flat plate with dimension of 1000mm x 1000 mm. (b) Sphere with radius of 500 mm. The polarization of electric field, **E** is along x axis.*

A plane wave that is normal to the *x-y* plane is impinged to the objects and the simulated RCS patterns for three frequencies (2.4 GHz, 8 GHz and 10 GHz) are shown in Figure 5.3.

(a)   *(b)*
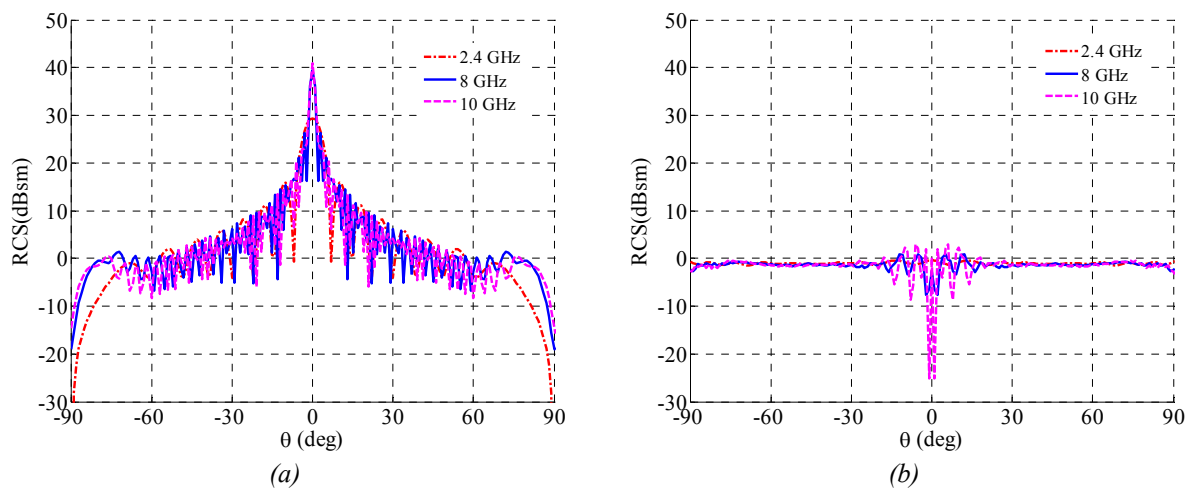
Figure 5.3 – The RCS pattern of metallic objects. (a) PEC square flat plate. (b) PEC sphere.

The comparison between the simulated RCS and the theory (formulas in Table 5.3) are listed in Table 5.4.

Table 5.4 - Comparison between simulated RCS and calculated RCS.

Object	Frequency (GHz)	Calculated (dBsm)	Simulated (dBsm)
Metallic plate	2.4	29	29.3
	8	39.5	39.6
	10	41	40.9
Metallic sphere	2.4	-1.05	-0.4
	8	-1.05	-2.7
	10	-1.05	0.2

The Table 5.4 validates that the simulation setup gives good results compared to the theory and can be used to simulate other cases such as plasma reconfigurable antennas

For further investigations, a set of simulations for plasma objects were conducted. The similar sizes of objects with respect to the metallic objects were employed. In the simulations the plasma frequency is 7 GHz and the neutral collision frequency of plasma is 900 MHz (similar parameters used in Chapter 3). It is good to mention that plasma is a dispersive material and it behavior is depending on the electromagnetic wave impinged on it. At certain frequency typically when the frequency of an incoming wave is more than the plasma frequency, the incoming wave can simply propagates through the plasma objects thus reducing the RCS level. However, this scenario is also tied by the shape of the object. The RCS patterns for plasma flat plate and sphere are shown in Figure 5.4.
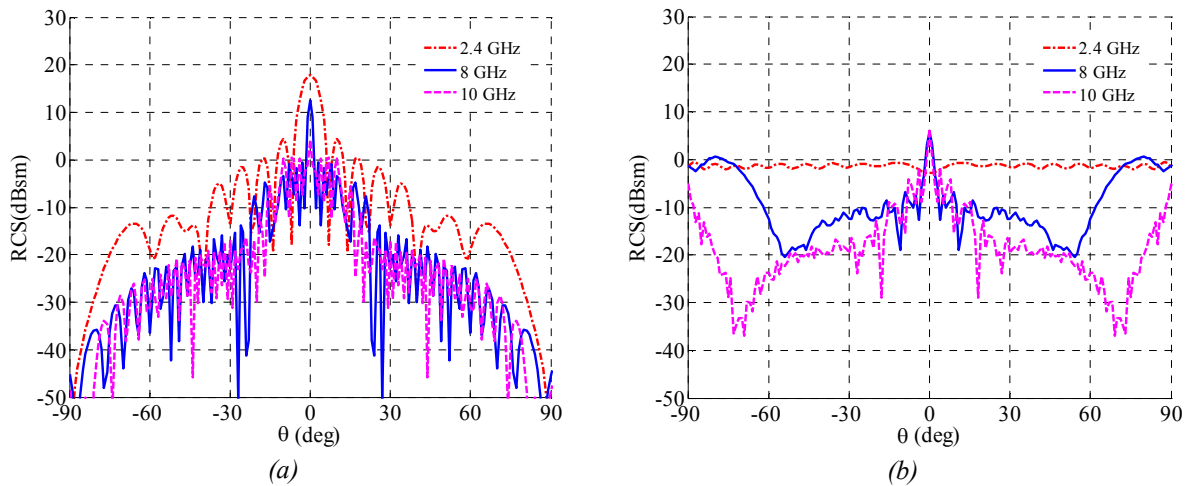
Figure 5.4 – The RCS pattern of plasma objects. (a)Plasma square flat plate. (b) Plasma sphere. (Plasma frequency is 7 GHz).

Based on the simulation results, the RCS of plasma plate can be discussed based on the incoming radar frequencies. At 2.4 GHz the RCS of plasma (17.5 dBsm) is quite the same to it corresponding metallic flat plate because of the plasma acts like a metal at this frequency (radar frequency << plasma frequency). However at 8 GHz (12.5 dBsm) and 10 GHz (4 dBsm), the RCS levels of plasma flat plate are about 20 dB and 30 dB lower than its metallic counterparts because at these frequencies plasma behaves like a lossy dielectric medium.

5.2.2 Simulation of RRA radar cross section

The simulations of RCS of the RRA were performed for two RRA configurations which are the 7- and 9- elements configurations (Chapter 3). A plane wave is applied in the direction of - *x* as shown in Figure 5.5.
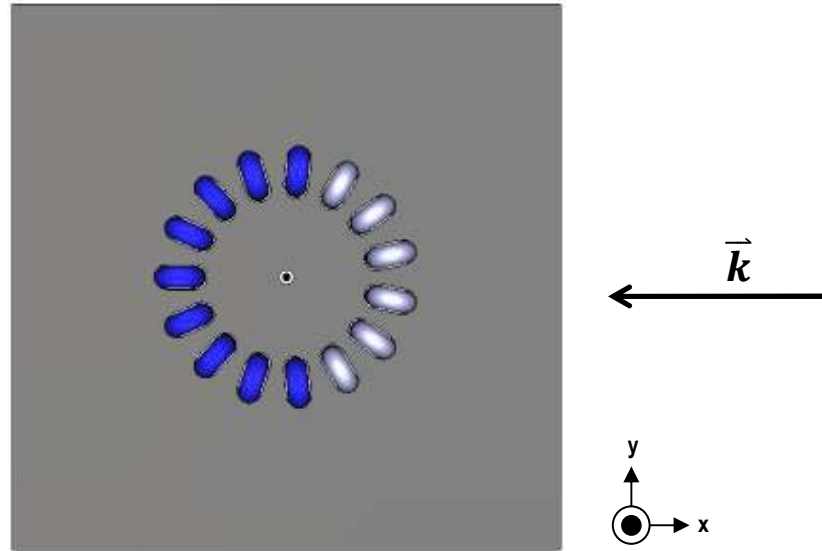
*Figure 5.5 – The RCS simulation of RRA with 9-elements configuration. A plane wave is applied from the x direction and the polarization of electric field, **E** is along z axis. (Dark blue color represents plasma while the light blue represents dielectric tubes filled with air).*

To better compare the RCS of plasma reflector, three RRA conditions were examined. These include when the plasma is in activated mode (ON), de-activated mode (OFF) and also by replacing plasma elements with metallic elements. The ordinary annealed copper was chosen as to replace the plasma. The simulation results of the two configurations (the 7- and 9- elements configuration) are shown in Figure 5.6 and Figure 5.7.
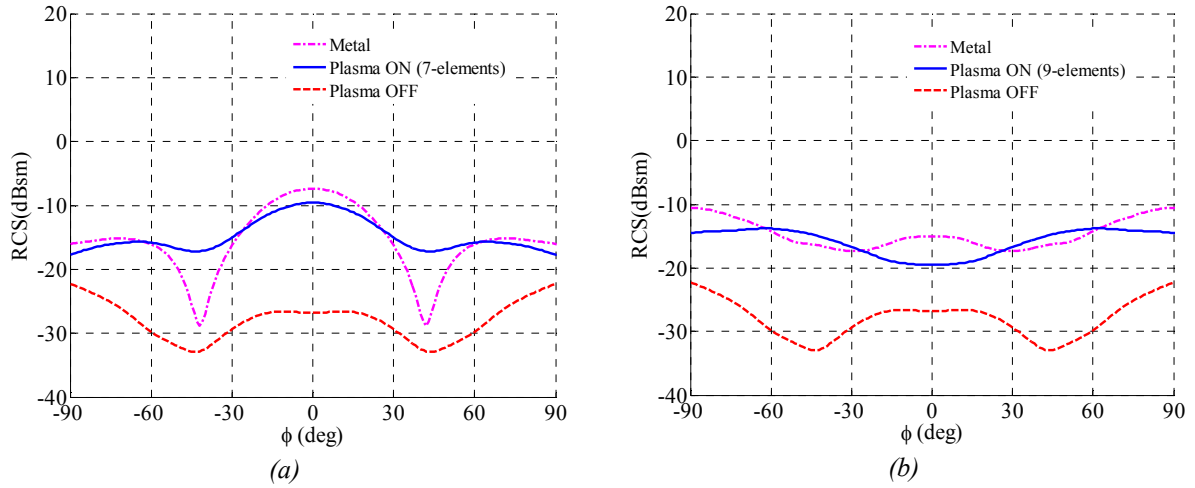
Figure 5.6 – The RCS patterns of the 7- and the 9- elements RRA at 2.4 GHz. (a) The 7-elements RRA. (b) The 9-elements RRA.
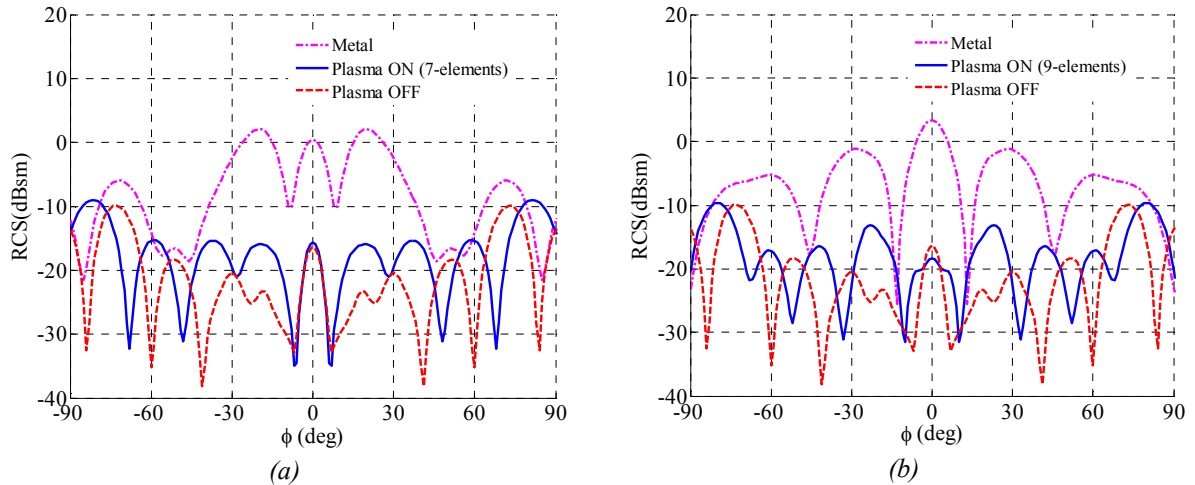
Figure 5.7 – The RCS patterns of the 7- and the 9- elements RRA at 8 GHz. (a) The 7-elements RRA. (b) The 9-elements RRA.

At 2.4 GHz, the maximum RCS of 7-elements RRA (-9.9 dBsm) is 5 dB higher than the maximum RCS of 9-elements RRA (-14.5 dBsm). The arrangement of 7 activated plasma elements may help to sum up the scattering effect caused by the plasma elements that act like a metal thus producing higher RCS level at the radar. However, for the 9 activated plasma elements this situation is different, where the arrangement of the 9-elements may cancel some of the scattering effect so that the corresponding RCS level is lower than the 7-elements configuration. For both configurations, the RCS pattern of metallic RRA (-7.5 dBsm) is somehow similar with its plasma counterpart (-10.5 dBsm). When the plasma is in de-activated mode, the maximum RCS levels of both configurations are the same (-22.5 dBsm) which is more than 10 dB of RCS suppression compared to the two corresponding metallic RRAs. Hence, at 2.4 GHz the de-activated plasma antenna is just like a furtive object if compared to the metal one.

At frequency of 8 GHz, the RCS patterns of activated and de-activated plasma RRAs are comparable and approximately -10 dBsm (-9 dBsm for both ON configurations). If compared the maximum RCS levels of plasma RRAs with its metallic counterparts, there is more than 10 dB reduction in RCS level. Therefore, at 8 GHz, the plasma antenna is hardly to be spotted by radar since it operates stealthily.

5.2.3 Simulation of CRA radar cross section

For the CRA, the RCS simulations were conducted for three configurations (CRA1, CRA2 and simultaneously activating CRA1 and CRA2). The plane wave is coming from the *x* direction as depicted in Figure 5.8.
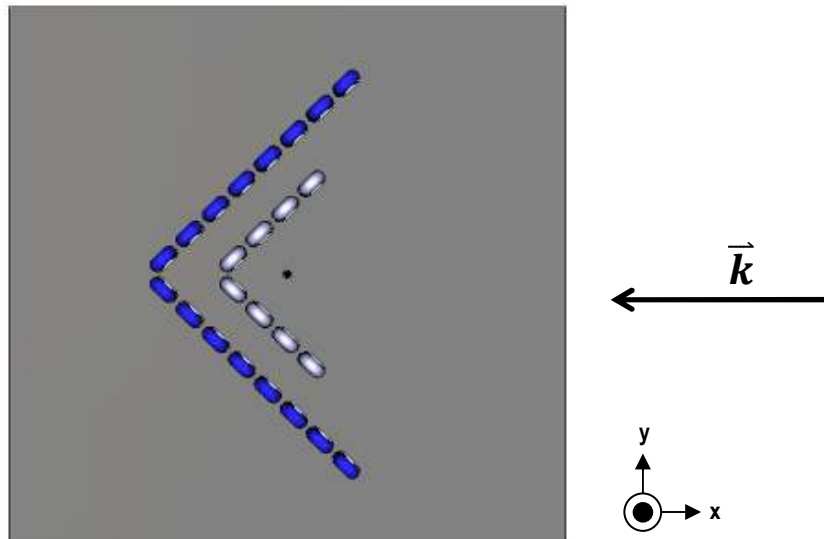
*Figure 5.8 – The activated CRA2 with an incoming plane wave in the direction of –x and the polarization of electric field, **E** is along z axis. (Dark blue color represents plasma while the light blue represents dielectric tubes filled with air).*

The simulation results of RCS patterns for the three CRA configurations represented in Figure 5.9, Figure 5.10 and Figure 5.11, respectively.
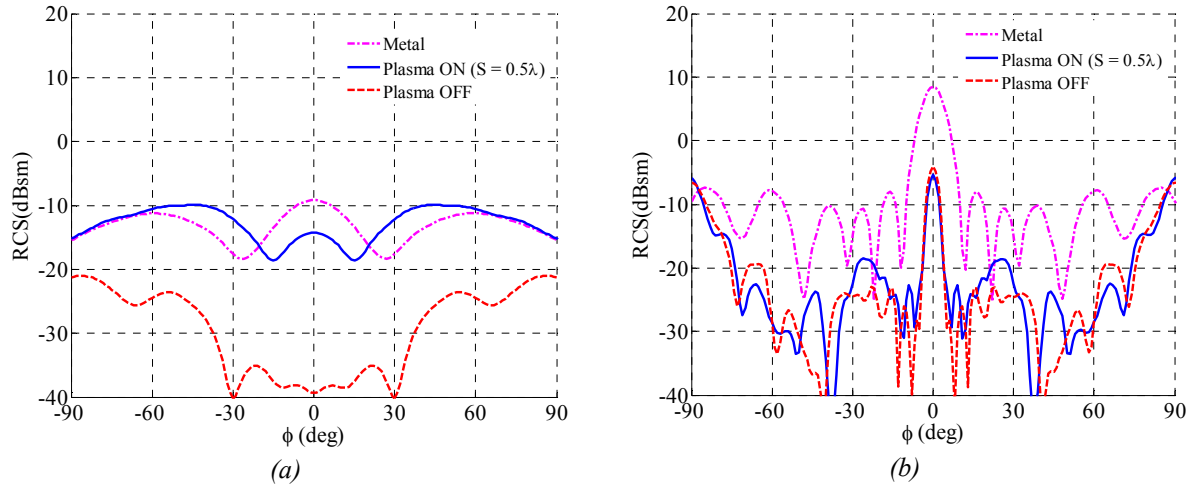
Figure 5.9 – The RCS patterns of activated CRA1. (a) 2.4 GHz. (b) 8 GHz.
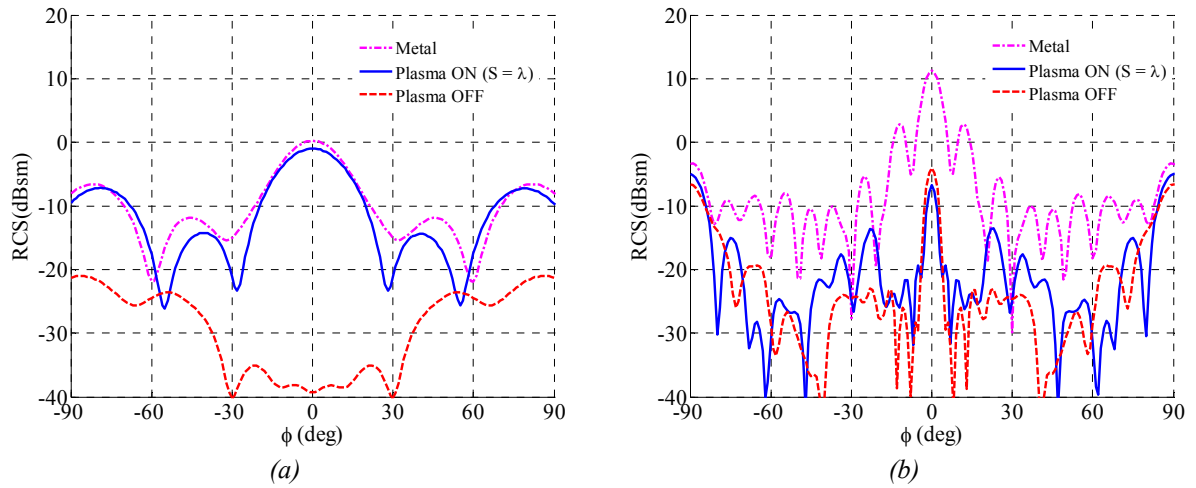

Figure 5.10 – The RCS patterns of activated CRA2. (a) 2.4 GHz. (b) 8 GHz.
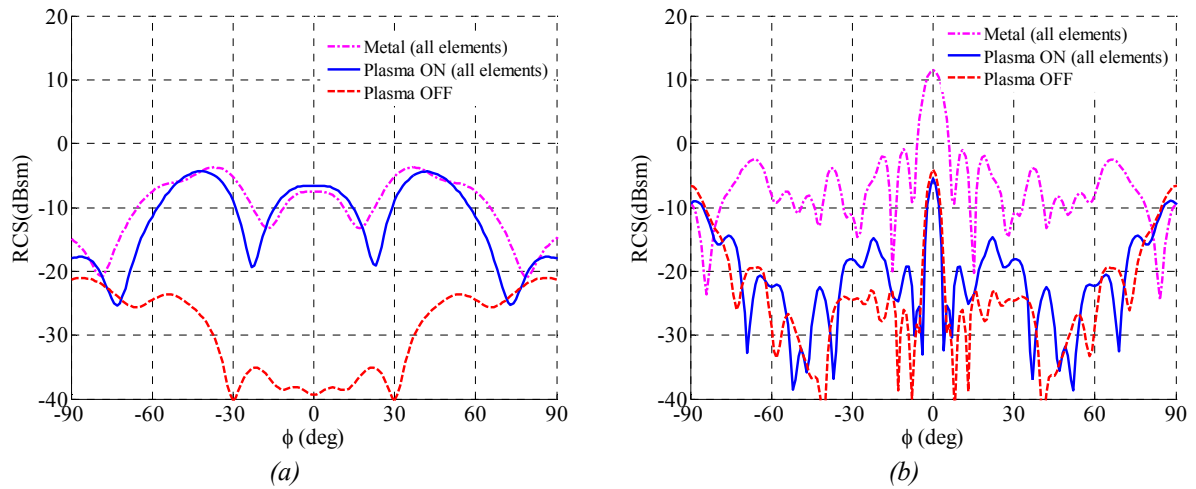

Figure 5.11 – The RCS patterns of simultaneously activated CRA1 and CRA2. (a) 2.4 GHz. (b) 8 GHz.

At 2.4 GHz (for the three configurations), the RCS patterns are somehow similar between plasma CRA and metallic CRA and the maximum RCS levels are below than 0 dBsm and mainly are between -1 dBsm and -10 dBsm. By de-activating the plasma CRA, the maximum RCS is reduced from its respective activated plasma by more than 10 dB as shown in Figure 5.9 (a), Figure 5.10 (a) and Figure 5.11 (a).

If transmitting radar is working at 8 GHz, the activated plasma CRA (CRA1 (-5.5 dBsm), CRA2 (-5 dBsm)) is hardly to be detected if compared to its metallic equivalent (8.5 dBsm and 11.1 dBsm, respectively). Moreover, the de-activated plasma CRA exhibits similar RCS pattern as when the plasma CRA is in activating mode. In general, whether the plasma CRA is operate or not, its corresponding maximum RCS level is far below than it corresponding metallic CRA (>10 dBsm). This is true for all configurations as can be seen in Figure 5.9 (b), Figure 5.10 (b) and Figure 5.11 (b).

5.3 Measurement of radar cross section of reconfigurable reflector antenna

In the beginning of this research work, the radar cross section measurement was conducted in an anechoic chamber for the round reflector antenna (RRA). The measurement setup consists of a network analyzer and a pair of wide band horn antennas with a gain of 10 dBi at 2.4 GHz (refer to Appendix 2.1). The antenna was mounted on a rotator pillar which is located 8.6 meter away from the horn antennas. The rotator can be controlled so that the desired DUT surface can be made facing the horn antenna. The polarization of the horn antennas is similar with the RRA (horizontal-horizontal polarization). This polarization is corresponding to the polarization in simulation. Photographs of the measurement setup are shown in Figure 5.12.

(a)   *(b)*

<center>(c)</center>   <center>(d)</center>
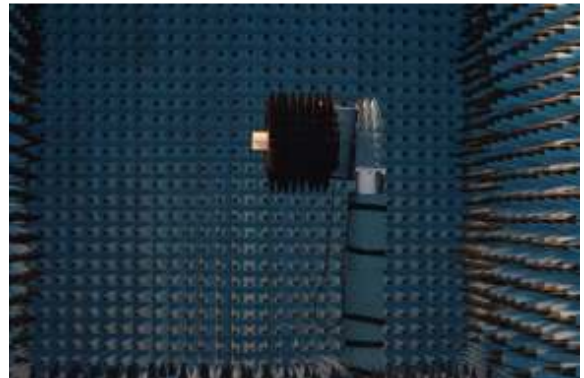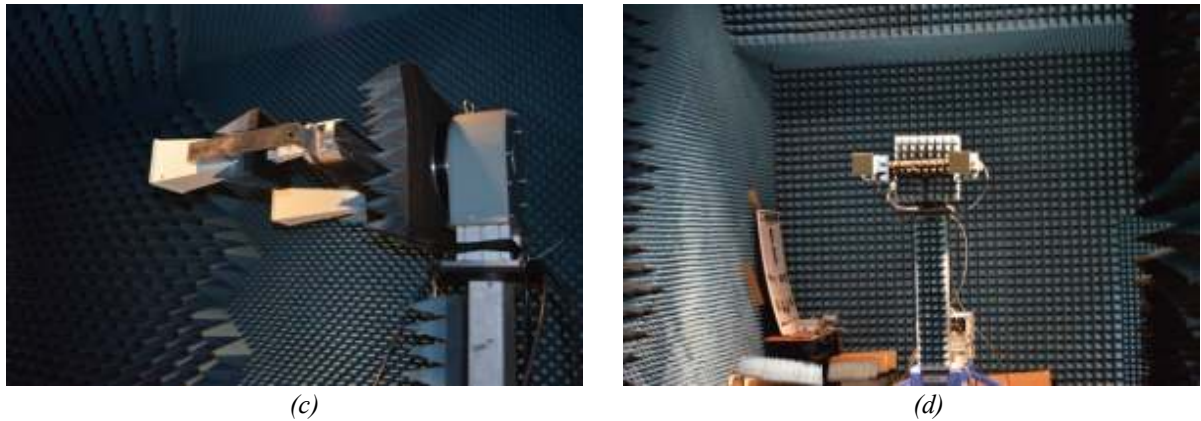
Figure 5.12 – Photograph of RCS measurement setup. (a)-(b) The RRA is mounted on a rotator. (c)-(d) Two wide band horn antennas are place on a tower which is 8.6 a way from the DUT .

In order to get the RCS level of the RRA, the data of measured transmission coefficient (S_{21}) which were gathered from the measurement have to be processed and calculated by using Eq. 5.5.

However, due to the far distance (8.6 meter) between horn antennas and AUT (RRA), the calculated RCS levels yielded from the measurement were not valid. This is because the coupling between the two horn antennas (-56.33 dB) is higher than the anticipated S_{21} (simulation) of the RRA for the similar measurement setup. Furthermore, the measurement is about to measure very low RCS level. As a result, output from the measurement was incorrect since the measurement was measuring signal below than noise level. To overcome this problem which is due to the coupling between horn antennas and the separation distance between transmitter and target, the RCS measurements have been conducted using only one horn antenna as shown in Figure 5.13.

Figure 5.13 – Single horn antenna is being utilized during RCS measurement. The transmitter and the target are separated with a distance of 3.58 meter.

The horn antenna placement in the anechoic chamber is about 3.58 meter from AUTs which is 5.02 meter lesser than the previous measurement setup. The same setup was applied to measure RCS of CRA with the help of controllable mounting rotator. The photographs of the CRA during measurement are shown in Figure 5.14.

<table>
<tr><td>(a)</td><td>(b)</td></tr>
</table>
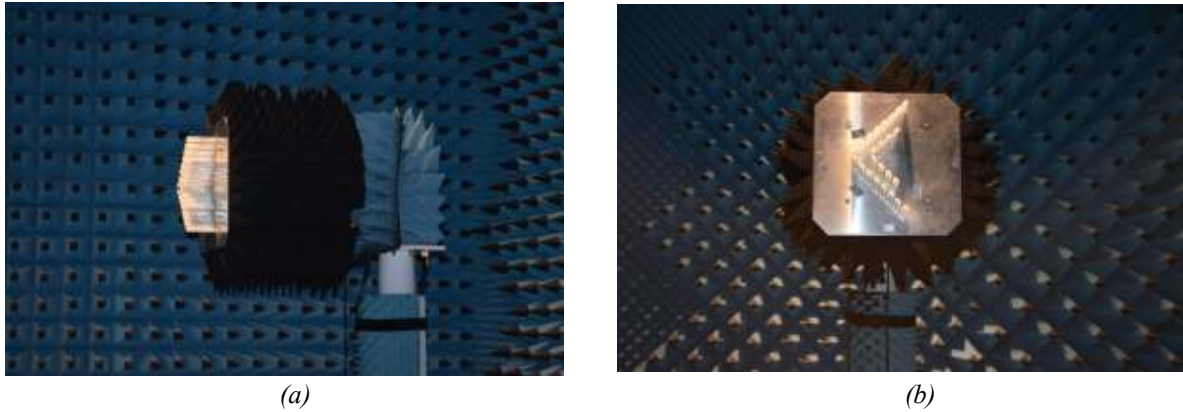
Figure 5.14 –The CRA is mounted on a rotator. (a) The front view of CRA that is direct facing to the transmitter. (b) The side view of the CRA.

In general, the RCS measurement is quite difficult to be conducted because of the existence a lot of unknown parameters. Thus by conducting the measurements and by taking into account factors that could influence the results, the measurements are set to aim an estimation of RCS of the two antennas (RRA and CRA). In order to get the RCS estimation, several measurements need to be conducted so that the data gathered are the desired ones. As a result of these measurements, there are four variables that have been indentified which are horn antenna mismatch, horn antenna transfer function, target and the diffraction in chamber as illustrated in Figure 5.15. The factors due to the horn antenna are independent of rotator angle and the diffraction occur in the chamber is partially independent of the rotator angle which includes the back of the chamber. By knowing the dependency of these parameters with the measurement setup, the data can be translated into information of plasma RCS. The results were processed using Matlab by applying Fourier transform and time gate which was by applying Hanning window.

Figure 5.15 – Radar cross section variables during measurement.

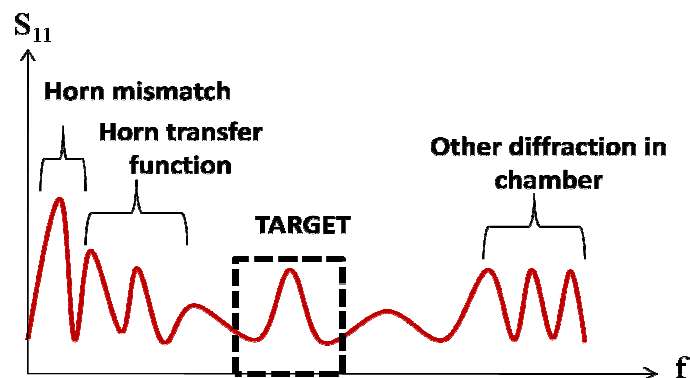The measurement results are depicted in Figure 5.16, where Figure 5.16 (a) is for RRA with 7-elements and Figure 5.16 (b) is for CRA2. Since the results were yielded from real monostatic RCS measurement, the only information that can be compared with simulation is the effect of the presence (ON) and the absence (OFF) of plasma at ϕ equals to 0°. For that reason the estimation of RCS for RRA and CRA2 are 3 dB and 19 dB at comparison point. This is much lower than what have been expected in the simulations. As mention earlier about the difficulties to conduct such measurement, it is adequate to prove that with plasma implementation as antenna element, the RCS can be reduced to certain level with regard to the operating frequency of the radar.
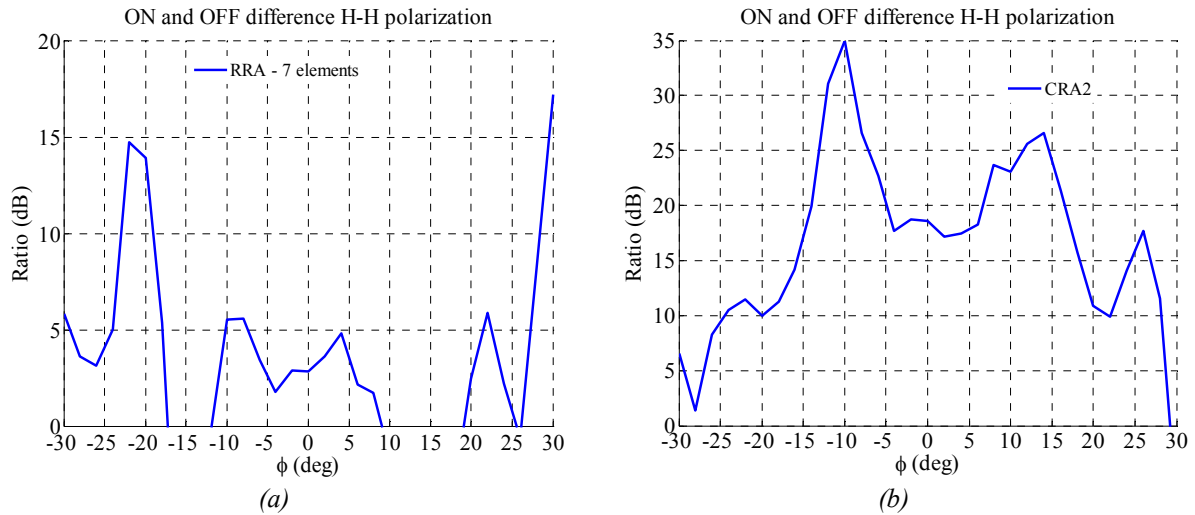
Figure 5.16 – The real monostatic RCS estimation of plasma reflector antennas at 2.4 GHz. (a) RRA with 7 activated elements. (b) CRA2.

5.4 Conclusion

As mentioned in literatures, implementation of plasma as antenna element can lower down the radar cross section. These scenarios have been proven in the simulation results gathered from this study. By replacing metallic elements with plasma elements, the RCS of reflector antennas (RRA and CRA) were seen to improve.

Generally, the RCS performances of plasma reflector antennas are comparable to its metallic counterparts when the radar transmitting at 2.4 GHz. This similarity is due to the plasma itself since it behaves like a metallic one at frequencies lower than plasma frequency. However, when the radar is working within X band frequencies, the maximum RCS of plasma reflector antennas is more than 10 dB below than the maximum RCS of its metallic equivalents. The plasma will allow microwave signal to propagate through it if the incoming microwave signal is higher than plasma frequency. This condition explains the reduction of plasma RCS level and moreover, regardless the plasma antennas are activated or not, the plasma RCS patterns are similar.

In all simulation cases that have been discussed earlier, the maximum RCS level of metallic reflector antennas can be suppressed up to more than 10 dB by de-activating plasma if plasma is used to replace the metallic elements of the reflector antennas. Therefore, the plasma RRA and CRA are barely to be detected by radar since these antennas behave like a furtive object when the plasma is de-activated.

The RCS measurements of RRA and CRA have been conducted with the best capabilities of the lab's facilities. Even though it is quite hard to get the actual RCS of these two antennas because of the nature of the desired signal, the estimation results are adequate enough to prove that the implementation of plasma can suppress the RCS of the particular antenna with regard to its metallic counterparts.

References

[1] C. A. Balanis, "Fundamental parameters of antennas," in Antenna Theory Analysis and Design 3rd Edition, John Wiley & Sons, NJ: Hoboken, 2005, pp. 27-115.

[2] J. D. Kraus, R. J. Marhefka, "Antenna temperature, remote sensing and radar cross section," in Antennas for All Applications 3rd Edition, McGraw Hill, NY: New York, 2002, pp. 401-426.

General conclusion

The implementation of plasma medium in communication systems is very interesting since plasma can be formed and extinguished in milliseconds. Even though, literatures pertaining to the physics of plasma are greatly extensive, only a few papers deal with plasma reflectors and plasma antennas realization especially in ISM band frequencies. Especially in terms of validation of simulation results through measurements.

Therefore in the beginning of this thesis a brief review of plasma as the fourth state of matters has been discussed. The cutoff frequency of plasma is very crucial to define plasma working region and as the plasma complex permittivity is also depending on the cutoff and transmitting frequencies, it is necessary to estimate the values of these two parameters. Several experiments have been conducted to get an approximation of plasma cutoff frequency and the electron-neutral collision frequency. Based on the measurement results the frequencies of 7 GHz and 900 MHz are identified to be plasma frequency and the electron-neutral collision frequency. These parameters values are adequate to represent the actual plasma model.

Two types of plasma reflector antennas have been simulated, fabricated and measured. The first one is RRA and the second one is CRA. The performances of RRA have been validated and it was proven to provide beam shaping and beam scanning capability. The measured radiation patterns are in a good agreement with simulation ones. The measured gain is 5 dB more than the gain of classical monopole antenna with an identical size of finite ground plane. Cross polarization remains low and front to back ratio (f/b) is more than 10 dB. The capability of RRA is exceptional since it can steer its main beam from 0° up to 360°. Moreover, the scanning gain remains the same as the main beam is being moved from one direction to another.

The CRA that has been introduced in this thesis is a novel design since it integrates two corner-reflector antennas on a single ground plane. The CRA offers three beam shapes which are electrically switchable from one shape to another. The CRA was simulated, fabricated and finally its performances were validated throughout a series of agile measurements. The measured reflected radiation patterns are in good agreements with the simulation ones. The measured gains are 5 dB higher than the gain of classical monopole antenna with an identical size of finite ground plane and not to forget the cross polarization remains low and the f/b is more than 10 dB.

The RRA and CRA were measured with different element heights by introducing a second layer ground plane. The objective of this measurement is to verify these reflector performances at three different heights so that it can mimic the compact version of the

RRA and CRA. Indeed, the antennas performances are satisfactory with shorter element height (54 mm). Thus, based on the reflector performances, it was proven that, the RRA and CRA can be fabricated in compact size using commercially available plasma source.

The quick prove of the reflectors reconfigurability was demonstrated through its switchable patterns. Since the measured results are highly comparable to the simulated ones, plasma model defined in the simulation can be used to analyze the particular CFL for other antenna designs. In addition, it is worth to emphasize that the results in the investigation has confirmed that the dielectric tubes used to enclose plasma have no major effect on quarter wave antenna radiation pattern. This conclusion was made by taking into account the super thin phosphor layer inside the dielectric tubes. In general, the fabricated plasma RRA and CRA have demonstrated that it can offer extra flexibility that cannot be offered by any other traditional metallic reflector.

By using the similar plasma source (CFL), two plasma antennas ($h_{radiate}$ = 35.7 mm and $h_{radiate}$ = 77 mm) were fabricated and measured at 900 MHz and 450 MHz. Based on the measurement results, it can be concluded that, the compact fluorescent lamp (CFL) with an AC excitation can be used to radiate radio signals. However, the feeding technique and the location of feeding point play important role in determining plasma antenna performance. The radiation patterns of the two plasma antennas measured from 450 MHz to 900 MHz are quite similar to the radiation pattern of classical dipole antenna. Therefore, if the fabricated antennas are meant to work as monopole antenna, they can be further optimized to exhibit better performance.

As discussed in literatures, implementation of plasma as antenna element can reduce the percentage of metallic materials therefore could minimize the radar cross section. These scenarios have been proven in the simulation results shown in this thesis. By replacing metallic elements with plasma elements, the maximum RCS of reflector antennas (RRA and CRA) were improved. The maximum RCS level of metallic reflector antennas can be reduced to more than 10 dB by de-activating plasma if plasma is used to replace the metallic elements of the reflector antennas. For the higher radar frequency such as in the X band, the RRA and the CRA are barely to be detected when comparing to its respecting metallic reflector antennas.

Perspective and future works

Based on the works done on plasma antennas, the following are some other prospective studies that can be carried out in future:

a) Since the reconfigurable plasma round reflector antenna (RRA) and the plasma corner-reflector antenna (CRA) were proven to work at 2.4 GHz, these antenna can also be designed and optimized to operate at other frequencies such as at GSM frequency band (900 MHz with 890 MHz - 915 MHz uplink frequencies and 935 MHz - 960 MHz downlink frequencies). A new plasma model has to be developed in order to accommodate the loss sensitivity in plasma at lower frequency band.

b) The compact version of CRA and RRA working at 2.4 GHz can also be realized by using smaller compact fluorescent lamps. This is because the measurement results to mimic similar cases reported in this thesis have shown good antenna performances.

c) The novel design of reconfigurable CRA at 2.4GHz can be further enhanced so that the main beam can be switched from 0° to 180°. The preliminary simulation of this design is illustrated in the figure below.
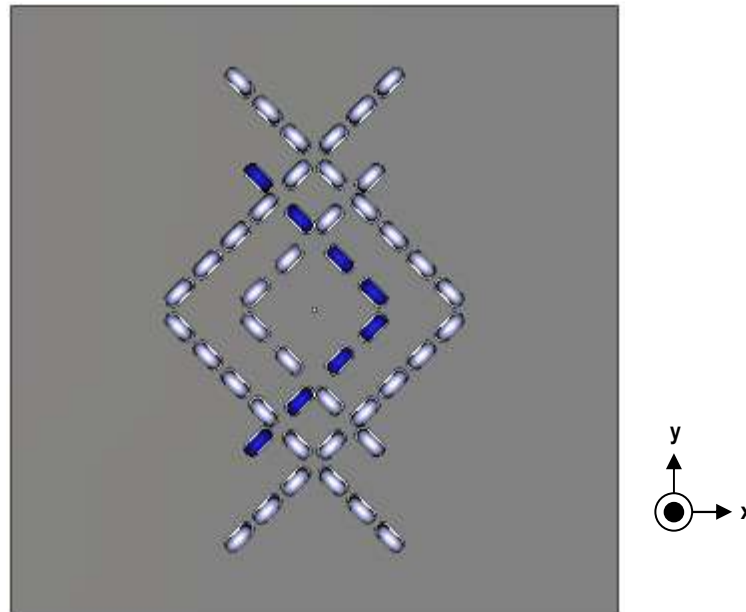
The proposed reconfigurable CRA that can move its main beam direction from 0° to180°. The (Dark blue color represents plasma while the light blue represents dielectric tubes filled with air).

217

d) Based on the research works done on plasma antenna and also the results of fabricated plasma antenna, it can be conclude that, the fabricated plasma antennas in this research works need to undergone an optimization process. A new research work could be brought forward to further analyze the plasma antenna coupling part for the specific plasma source (the CFL used in this study). Especially on the feeding technique in order to transfer the maximum available power to plasma antenna and also on how to reduce the back radiation observed in this study.

List of publications

Peer-reviewed international journals

M. T. Jusoh, O. Lafond, F. Colombel, M. Himdi, "Performance and radiation patterns of a reconfigurable plasma corner-reflector antenna", IEEE Antennas Wireless Propag. Lett., vol. 12, pp. 1137-1140, Sept. 2013.

M. T. Jusoh, O. Lafond, F. Colombel, M. Himdi, "Performance of a reconfigurable reflector antenna with scanning capability using low cost plasma medium," Micro. Opt. Tech. Lett., vol. 55, no. 12, pp. 2869-2874, Dec. 2013.

Peer-reviewed international conferences

M. T. Jusoh, O. Lafond, F. Colombel, M. Himdi, "Scanning capability of reconfigurable plasma reflector antenna," in Proc. 43rd EuMC, pp. 80-83, 2013.

M. T. Jusoh, O. Lafond, F. Colombel, M. Himdi, "Realization of a Dual Dihedral Corner-Reflector Antenna by Using Low Cost Plasma," in Proc. 8th EuCAP, April, 2014.

VU :   VU :

Le Directeur de Thèse   **Le Responsable de l'École**
Doctorale

VU pour autorisation de soutenance

Rennes, le

Le Président de l'Université de Rennes 1

Guy CATHELINEAU

VU après soutenance pour autorisation de publication :

Le Président de Jury,
(Nom et Prénom)

Abstract

Plasma is the 4th state of matter with complex permittivity that can be exploited to give advantages in communication system. Its negative permittivity has been studied in many research papers and it was proven to have similar characteristics as metal material in terms of electrical conductivity. While keeping permeability in the positive region, plasma will respond to electromagnetic waves in the similar manner as metal. Therefore, this thesis aimed to use plasma as an alternative to metal in the construction of reconfigurable antennas. The first part of this thesis is dedicated to characterize a plasma model based on the commercially available plasma source. Since there are many type of plasma source in terms of their electrical properties and physical shapes, it is important to characterize a particular plasma source so that it can be modeled in simulations to construct other types of plasma antennas. The second part presents the realization of plasma reflector antennas. Two types of plasma reflector antennas have been simulated, fabricated and measured at 2.4 GHz. The first one is are round reflector antenna (RRA) and the second one is corner reflector antenna (CRA). The performances of RRA have been validated and it was proven to provide beam shaping and beam scanning capability. The measured radiation patterns are in a good agreement with simulation ones. The capability of RRA is exceptional since it can steer its main beam from 0° up to 360°. Moreover, the scanning gain remains the same as the main beam is being moved from one direction to another. The CRA that has been introduced in this thesis is a novel design since it integrates two corner-reflector antennas on a single ground plane. The CRA offers three beam shapes which are electrically switchable from one shape to another. The CRA was simulated, fabricated and finally its performances were validated throughout a series of agile measurements. The measured reflected radiation patterns are in good agreements with the simulation ones. The measured gains of the RRA and CRA are 5 dB higher than the gain of classical monopole antenna with an identical size of finite ground plane. The fourth part deals with plasma as radio waves radiator. Two plasma antennas using commercially available U-shaped compact fluorescent lamp (CFL) have been fabricated and measured and it was proven that these antennas can be to radiate radio signal. The last part discusses about radar cross section performance of the plasma reflector antennas. The two plasma reflector antennas (RRA and CRA) were tested and measured for their RCS performance.

Keywords : Reconfigurable antenna, plasma antenna, reflector antenna, reconfigurable plasma antenna, reconfigurable reflector antenna

Résumé

Le milieu plasma correspond au $4^{\text{ème}}$ état de la matière présentant une permittivité diélectrique complexe qui peut être exploitée pour les systèmes de communication. Sa permittivité négative a été étudiée dans de nombreux travaux de recherche démontrant que le plasma peut avoir des caractéristiques similaires à celles d'un métal en termes de conductivité électrique. En considérant une perméabilité positive, le plasma peut ainsi réagir de la même manière qu'un métal en présence d'une onde électromagnétique. Cette thèse a pour objectif de démontrer que le plasma est une alternative au métal pour la réalisation d'antennes reconfigurables. La première partie du travail concerne la caractérisation du milieu plasma en utilisant des sources plasma commerciales à savoir des lampes à Néon. Cette caractérisation est primordiale afin de pouvoir ensuite simuler ce type de source. La seconde partie des recherches a concerné la conception et la réalisation d'antennes plasma reconfigurables en rayonnement et ceci à la fréquence de 2.4 GHz. Le premier concept est un réflecteur circulaire et le second un réflecteur à angle droit tous les deux réalisés à partir de différentes lampes à Néon et illuminés par une antenne source monopole. Le réflecteur circulaire permet de dépointer le faisceau d'antennes sur 360° alors que le réflecteur à angle droit permettre de reconfigurer le faisceau rayonnant et de passer d'un faisceau directif à deux faisceaux avec un creux dans l'axe. Ces dispositifs rayonnants innovants basés sur des lampes à Néon ont été validés expérimentalement et les résultats de mesure (S_{11} et rayonnement) sont en bonne adéquation avec les résultats de simulation. Ces deux types d'antennes réflecteurs possèdent également de bons résultats en termes de gain, ce qui valide l'utilisation et la caractérisation des lampes plasma de commerce utilisées. Dans la troisième partie du travail, ce même type de lampe à néon a été utilisé pour concevoir cette fois un élément rayonnant excité par couplage capacitif. La réalisation d'un prototype à permis de démontrer la faisabilité d'une telle source rayonnante. Enfin, la dernière partie des recherches concerne une étude de la Surface Equivalente Radar des antennes réflecteur conçues précédemment. L'étude a démontré que ces antennes réflecteurs plasma présentent des SER largement inférieures lorsqu'elles sont éteintes ainsi qu'à fréquence haute (8 GHz) comparativement à celles d'antennes métalliques équivalentes ce qui en fait des antennes furtives d'un point de vue radar.

Mots clés : Antenne reconfigurable, antenne à plasma, antenne réflecteur, antenne à plasma reconfigurable, antenne réflecteur reconfigurable